EFFECT OF BONDING VARIATION AND COMPONENT COMBINATION ON DYNAMIC CHARACTERISTICS OF COMPOUND SEMI-BONDED CARBON FIBER REINFORCED ELASTOMERIC ISOLATOR (CSB-CFREI)

by

Heshmatollah Adib Natanzi
B.Sc. University of California Berkeley
M. A. Sc., San Jose State University California

A THESIS SUBMITTED IN PARTIAL FULFILLMENT OF

THE REQUIREMENTS FOR THE DEGREE OF

DOCTOR OF PHILOSOPHY

in

THE COLLEGE OF GRADUATE STUDIES

(Civil Engineering)

THE UNIVERSITY OF BRITISH COLUMBIA

(Okanagan)

September 2016

The undersigned certify that they have read, and recommend to the College of Graduate Studies for acceptance, a thesis entitled:

EFFECT OF BONDING VARIATION AND COMPONENT COMBINATION ON DYNAMIC CHARACTERISTICS OF COMPOUND SEMI-BONDED CARBON FIBER REINFORCED ELASTOMERIC ISOLATOR (CSB-CFREI)

submitted by HESHMATOLLAH ADIB NATANZI in partial fulfilment of the

requirements of the degree of

DOCTOR OF PHILOSOPHY

in

THE FACULTY OF GRADUATE STUDIES

(CIVIL ENGINEERING)

Professors: 1-Carlos Ventura Civil Engineering Department UBC-Vancouver
2-Solomon Tesfamariam, School of Engineering UBC-Okanagan

Supervisor, Professor (please print name and faculty/school above the line)

Professors Shahria Alam- School of Engineering UBC-Okanagan

Supervisory Committee Member, Professor (please print name and faculty/school in the line above)

Professor Kasun Hewage-School of Engineering UBC-Okanagan

Supervisory Committee Member, Professor (please print name and faculty/school in the line above)

Professor Keekyoung Kim- School of Engineering UBC- Okanagan

University Examiner, Professor (please print name and faculty/school in the line above)

Professor Reza Kianoush- Civil Engineering Department Ryerson university

External Examiner, Professor (please print name and university in the line above)

September 2016

(Date Submitted to Grad Studies)

Abstract

Over the past thirty years, seismic isolation has been considered a viable earthquake damage mitigation technique and has been implemented to protect new and existing structures. However, due to the high production cost and implementation challenges of conventional seismic isolators, application of this protective technology has been limited to high value buildings with important and sensitive contents. To ensure widespread application of the base isolation systems for ordinary residential and commercial buildings, especially in developing countries, not only the production cost must be reduced, but the implementation efficiency must improve as well. With this intention in this study, a new cost effective Elevated Semi-Bonded Carbon Fiber-Reinforced Elastomeric Isolator (ESB-CFREI) with lower production cost and higher implementation efficiency is designed, manufactured, and tested. The innovative ESB-CFREI undergoes lateral cyclic excitations with a unique deformation mechanism that differs from that of conventional Steel Reinforced Elastomeric Isolators SREI and Bonded and Un-Bonded Carbon Fiber Reinforced Elastomeric Isolators. The ESB-CFREI can be used in isolation as an independent "Component Isolator" or combined with other component isolators to form a CESB-CFREI "Compound Isolator." According to the experimental results, isolators with different bonding levels (BL) are characterized by different overall dynamic characteristics. Depending on component combination configurations, the compound isolators have different average bonding values that result in different damping, effective lateral shear, and axial compression stiffness. Results from experimental tests on different compound isolators demonstrated that change in combination configuration effectively influences the dynamic characteristics of the compound isolator.

Dynamic characteristics of component (ESB-CFREI) and compound isolator (CESB-CFREI) as low-cost seismic isolators were investigated by conducting analytical and experimental studies. The isolator's effective lateral shear and axial compression stiffness along with the isolation efficiency (IE) were defined. The experimental outcome demonstrated the effect of bonding variation on the dynamic characteristics, performance, and efficiency of the ESB-CFREI. The effects of component combination on the dynamic characteristics of the compound isolators were also investigated.

Component material testing to investigate the hyper-elastic behaviour of the isolator's rubber component and long duration excitation tests to study the isolator's durability and performance were conducted as well.

Preface

The Earthquake Engineering Research Facility of the University of British Columbia funded the fabrication of 12 SB-CFERIs test specimens and contributed to the cost of conducting over 200 experimental tests, including the cost of machinery and laboratory technicians. Testing, post processing of the experimental data, and the finite element analysis were conducted by the author under the supervision of the thesis advisors, Professors Carlos Ventura and Solomon Tesfamariam.

A paper describing some of the experimental and analytical studies related to this research was published at the 11th Canadian Conference on Earthquake Engineering 11CCEE. The paper was prepared by me and supervised by Professors Carlos Ventura and Solomon Tesfamariam. The paper was titled "Dynamic Characteristics of Elevated Semi-Bonded Carbon Fiber Reinforced Elastomeric Isolator (ESB-CFREI)" and was co-authored by myself, Carlos Ventura, and Solomon Tesfamariam. I presented it at the conference on July, 2015.

The current thesis contains significant number of pictures, drawings, tables and figures, it is necessary to acknowledge that, all those presented without source reference are drawn, plotted and prepared by the author and belongs to him. For figures from other sources, the copyright permission has been obtained. These figures are mainly in chapter one of the thesis and are cited with the related references.

Table of Contents

List of Tables

List of Figures

List of Abbreviations

AASHTO	American Association of State Highway and Transportation Officials
ASCE	American Society of Civil Engineers
B-CFREI	Bonded Carbon Fiber Reinforced Elastomeric Isolator
B-GFREI	Bonded Glass Fiber Reinforce Elastomeric Isolator
BIS	Base Isolation System
CSB-CFREI	Compound Semi-Bonded Carbon Fiber Reinforced Elastomeric Isolator
FDHD	Force-Displacement Hysteresis Diagram
FEA	Finite Element Analysis
FEM	Finite Element Model
FEMA	Federal Emergency Management Agency
FPS	Friction Pendulum System
LDRB	Low Damping Rubber Bearing
LRB	Lead Rubber Bearing
P-F S	Pure Friction System
R-FBI	Resilient-Friction Base Isolator
SB-CFREI	Semi-Bonded Carbon Fiber Reinforced Elastomeric Isolator
SIS	Seismic Isolation Systems
SREI	Steel Reinforced Elastomeric Isolator
SU-CFREI	Stable Unbonded Carbon Fiber Reinforced Elastomeric Isolator
UB-CFREI	Un-Bonded Carbon Fiber Reinforced Elastomeric Isolator
USGS	U.S. Geological Survey
PL	Pre-Load
NR	Natural Rubber
SSA	Shear Strain Amplitude
ESB-CFREI	Elevated Semi-Bonded Carbon Fiber Reinforced Elastomeric Isolator

Acknowledgements

I would like to express my deepest appreciation and sincere gratitude to my research supervisors, Professor Carlos Ventura and Professor Solomon Tesfamariam, for their interest, support, invaluable guidance, and encouragement throughout this research. I am also extremely grateful to the members of my supervisory committee, Dr. Shahria Alam and Dr. Kasun Hewage, for their valuable comments and advice throughout the course of this research work. I sincerely thank Professor James Kelley from the University of California, Berkeley for inspiring me to explore and grow in the field of seismic isolation technology and for the valuable recommendations and guidance during the isolator's fabrication process and experimental testing.

I would like to thank the technical staff working at the Earthquake Engineering Research Facility of the University of British Columbia (UBC-EERF), in particular Harald Schrempp, the manager of the lab and workshop; Yao Felix, EERF research engineer; and Scott Jackson and John Wong for their technical support and assistance in conducting over 200 tests during the experimental phases of this research. Special thanks to the structural lab machinery technician, Doug Smith, for fabrication and assemblage of the testing machine and the tests equipment set-ups. I also thank Miss Terry Moser, for her assistance during the fabrication of the seismic isolator specimens. My deepest thanks and appreciation to my family, especially my wife for her never-ending care and support during this academic journey, and I also sincerely thank my friends and UBC fellow students for their support and encouragement during the course of this research. Finally, I certainly appreciate the financial support from UBC-EERF for fabrication of the test specimens and the testing machine and related technician cost.

Dedication

This thesis is dedicated to my wife, Peyman, for her understanding, patience, love, and support, and to my son Amir Mohammad and daughter Pardis.

CHAPTER 1: INTRODUCTION TO SEISMIC ISOLATION TECHNOLOGY

Devastating earthquakes, combined with poor construction practices, are a significant cause of human loss of life. The occurrence of destructive, high-magnitude earthquakes in the world results in casualties and financial loss each year. In 1990, for example, there were 18 earthquakes with magnitude of 7 or greater [USGS National Earthquake Information Center], and in just one of those instances—a 7.4 earthquake in Rudbar-Manjil, Iran—the loss of life exceeded 44,000. During the 1999 earthquakes in Turkey, Greece, and Taiwan, more than 90% of low-rise residential buildings suffered damage (Kang et al., 2008). Unfortunately the high seismic zones of the developing world are highly vulnerable and suffer the most. Low-rise, low-importance residential and commercial buildings are predominant in developing regions. These buildings are most vulnerable to earthquake ground motions as they are poorly built and/or lack proper construction technical supervision and are mostly characterized by high fundamental vibration frequencies that, unfortunately, are in the range of most earthquake ground motion predominant frequency content. Priestley et al. (1996) stated that the high damage potential of earthquakes is due to the unfortunate harmony between the fundamental period of vibration of the majority of buildings and the predominant frequency content of the earthquake ground motions.

To protect residential and commercial low-rise buildings and reduce loss of life more effectively, the application of innovative, cost effective seismic protection systems should be considered. The systems must be able to re-tune and shift the natural frequency of these low- to medium-rise buildings away from the earthquakes' predominant ground motion frequency and significantly reduce the seismic demand. Implementation of seismic isolation technology could be the most suitable and effective solution to this problem. Despite remarkable progress in the area of seismic isolation, the application of existing conventional seismic isolation systems has been restricted to important projects with valuable contents. This unfavorable situation is due to numerous deficiencies, but primarily the high production and implementation costs of the conventional seismic isolation system. These deficiencies prevent developing countries from benefitting from seismic isolation technology. The existing deficiencies must be remedied to make application of base isolation as an effective seismic protection technology affordable and practical worldwide.

Base isolation technology offers a reliable and cost-effective strategy for mitigation of seismic damage to structures. The effectiveness of this technology has been demonstrated not only in laboratory research and modeling, but also in the real-world performance of base-isolated structures during past earthquakes. The isolation interface is usually implemented at the base of the building; hence this early, innovative, earthquake resistant design strategy is called *base isolation* or *seismic isolation.* In areas of the world susceptible to earthquakes, it is employed to protecting buildings from earthquake-induced ground motions (Kelly, 1990).

To ensure that structural integrity is maintained, earthquake engineering must consider the most effective design for seismic isolation equipment, such that "on the one hand, it allows for a sufficiently high level of structural decoupling and energy dissipation, and on the other hand provides enough stiffness to prevent excessive deformations or residual offsets" (Bucher, 2009).

The use of support mechanisms to decouple the building from the ground can protect the building from the damaging effect of earthquakes. In the last century a number of variations of this mechanism have been developed, including models that enable the building to move laterally during an earthquake through the use of sand or rollers (Kelly, 1997).

Base isolation design strategies in seismic rehabilitation of ancient monuments and existing structures are most often selected as the optimal retrofitting solutions in terms of reliability and effectiveness. The Los Angeles and Oakland City Hall Buildings located in California, and the Salt Lake City Capitol Building located in Utah are examples of base isolation application in seismic rehabilitation of existing structures.

1.1 Base Isolation System

Rather than increasing the seismic resistance of a building, seismic isolation instead reduces the seismic demand on that building. Proper design and implementation of a base isolation system results in structural elasticity that will successfully endure even during an intense earthquake (Naeim and Kelly, 1999). A base isolation system decouples the building from the earthquake's horizontal ground motion components by providing a flexible interface with low horizontal stiffness between the superstructure and the foundation. Base isolation also provides protection

for nonstructural elements in the building. Figure 1.1 shows a schematic configuration of a building structure system with a base isolation system.

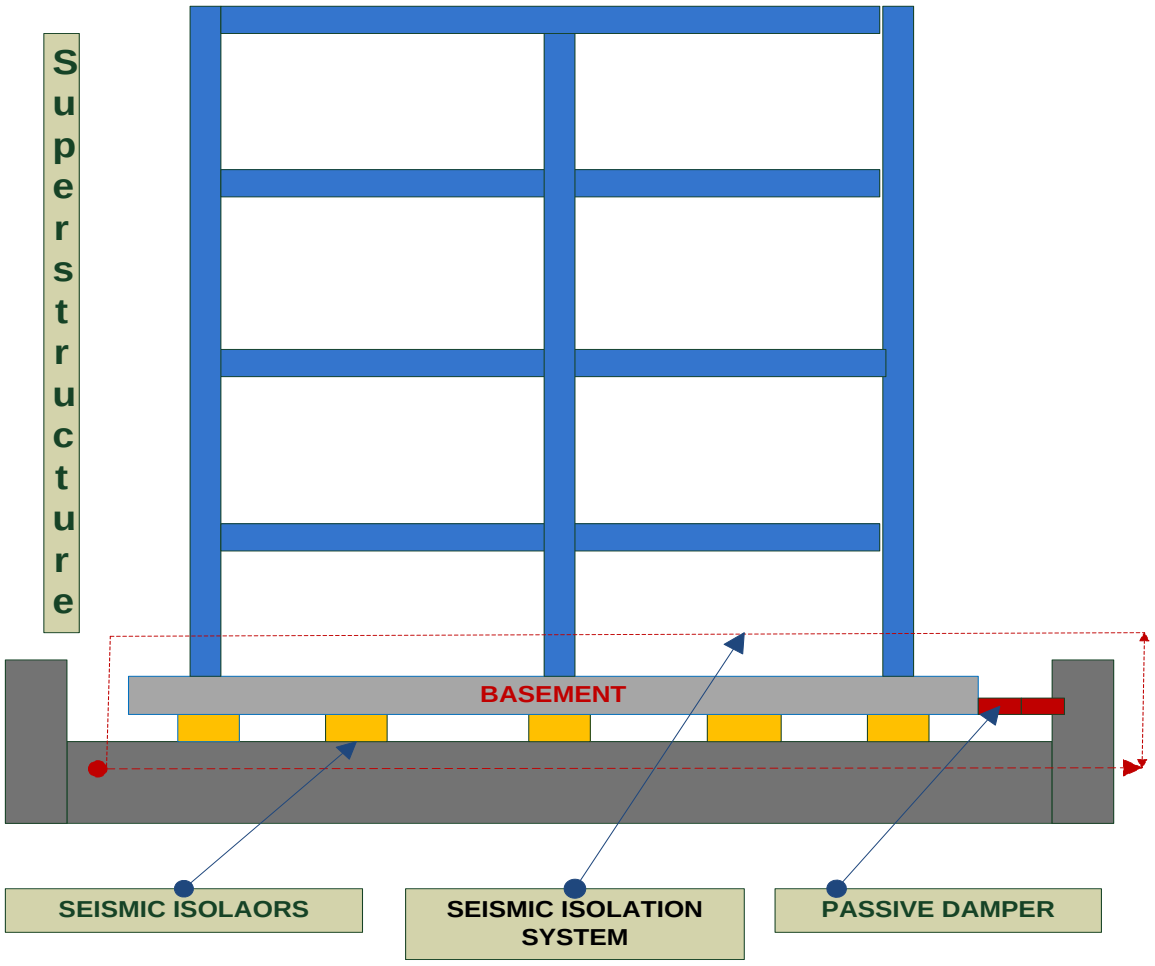

Figure 1.1 Configuration of typical building structure with base isolation system

The following five recent developments are responsible for and effective in shifting the base isolation technology from theory to practical applications (Mayes and Naeim, 2001):

1) High-quality elastomeric pads, also called bearings, designed and produced to support the weight of the building while also being flexible enough to protect it from earthquake forces.

2) Mechanical-energy dissipaters and high-damping elastomers designed and produced to keep displacement across the isolation bearing at levels acceptable for resisting wind and other service loads.
3) Computer software developed and accepted to analyze seismically isolated structures, while including nonlinear material properties and time variances of earthquake forces.
4) Shake table tests with application of the simulated earthquake ground motion time-history.
5) Procedures and provisions developed and accepted to estimate specific earthquake ground motions for different return periods in a specific site.

Seismic isolation may reduce superstructures' maximum structural responses by as much as 80%, and it is more beneficial for rigid buildings (Goda et al., 2009). For a model structure considered in numerical applications, seismic isolation can reduce the expected lifecycle cost by 20%, in comparison to a fixed structure (Goda et al., 2009).

1.2 Background and History of Seismic Isolation Systems

Although the concept of seismic isolation is very ancient, the modern history of base isolation dates back to 1909, when a medical doctor from the northern England city of Scarborough expressed his idea that a building could be seismically protected using a "free joint" and could be built on layers of fine sand, like mica or talc, in order to provide the sliding capability and consequently reduce the seismic-induced forces on the building. This idea is an early example of a seismic resistance design strategy and approach is known as base isolation or seismic isolation (Kelly, 2001).

Seismic isolation has evolved over the last three decades and has become an important practical reality due to the development of multilayer steel reinforced elastomeric bearings. These elastomeric bearings are made by vulcanizing the bond between steel reinforcement plates and rubber sheets. This type of bearing is capable of high vertical stiffness, can support the weight of the building, and is flexible in the horizontal direction. This allows the building to move laterally under strong earthquake ground motion.

Many earthquake-prone regions now employ base isolation to protect important structures from damage. However, a very limited number of demonstration projects have been built using base isolation systems for public housing. These test projects have been completed in countries like China, Indonesia, Chile, and the USA. The goal of these test projects is to provide a suitable and cost-effective base isolation mechanism for use in developing countries located in high seismic zones.

The first use of an elastomeric isolation system to protect structures from earthquake ground motion was in 1969 in Skopje, Republic of Macedonia (in the former Yugoslavia), in an elementary school. This technology was used in a three-story concrete building designed by Swiss engineers; it is isolated by a system known as “full base isolation 3D.” Unlike more recent conventional steel reinforced bearings, the rubber bearings used in this project are completely un-reinforced and will bulge sideways under the weight of the structure. To control the excessive structural movement under wind or low seismic and foot traffic inputs at the base, some foam-glass blocks were used on each side of the rubber bearings as seismic fuses. These fuses are expected to break when seismic shaking exceeds a predefined threshold. Since the vertical and the horizontal stiffness in the implemented base isolation are the same, this building may have high lateral movement due to earthquake-induced motions.

Lead-plug rubber bearings are the most commonly used isolators in the United States, and these elastomeric bearings usually have one or more holes into which lead plugs are inserted. In 1978 the first structure to utilize an isolation system with added damping was the Toetoe Viaduct in the North Island of New Zealand (Skinner et al., 1993). This isolation, called a lead-rubber bearing (LRB) seismic isolator, consists of laminated steel and rubber bearings incorporating a specially formulated high-damping natural rubber, and a lead core for improved energy dissipation. The Foothill Communities Law and Justice Center, built in 1985 in Rancho Cucamonga, California, was the first seismically isolated building in the United States. Located 20 km west of the San Andreas Fault, it is the first base-isolated building in the world to use isolation bearings made of high-damping natural rubber (Kelly, 1997).

1.3 Characteristics and Mechanisms of Different Types of Conventional Seismic Isolators

Base isolation technology has improved greatly over the past 30 years, and it is now considered a mature technology for the protection of human life and property against earthquake damage. A variety of base isolation systems are currently and successfully being used in several countries around the word, and this technology draws significant interest from researchers and inventors in the field. Many new and different types of seismic isolator have been proposed or patented. Although most of these new systems were proven to be impractical and, in some cases, even dangerous to use, the number of new concepts in seismic isolation continues to increase each year. Conventional seismic isolators are either the sliding or the elastomeric type. The elastomer is usually either neoprene or natural rubber. For bearings with a sliding surface, stainless steel or Teflon are typically used. In the following sections a summary of the mechanism and characteristics of the conventional types of seismic isolator most frequently implemented in different countries is presented.

1.4 Elastomeric Seismic Isolator

Elastomeric bearings are more commonly used to introduce flexibility into an isolated structure. Low-damping, natural rubber bearings exhibit essentially linear elastic and linear viscous behaviour to large shear strains (Constantinou and Reinhorn, 2006). The elastomer material used in an isolated building in Skopje in 1906 was low damping natural rubber and completely un-reinforced, so the building weight caused the bearing rubber blocks to bulge up to 25%. This experience showed that elastomeric isolators need reinforcement to increase their vertical stiffness to avoid lateral bulging of the elastomer. The most common type of reinforcement is internal steel plate layers referred to as shims, hot vulcanized with elastomer to form a multilayered and well-laminated seismic bearing (Figure 1. 2). Isolators of this type are categorized as either low-damping and high-damping.

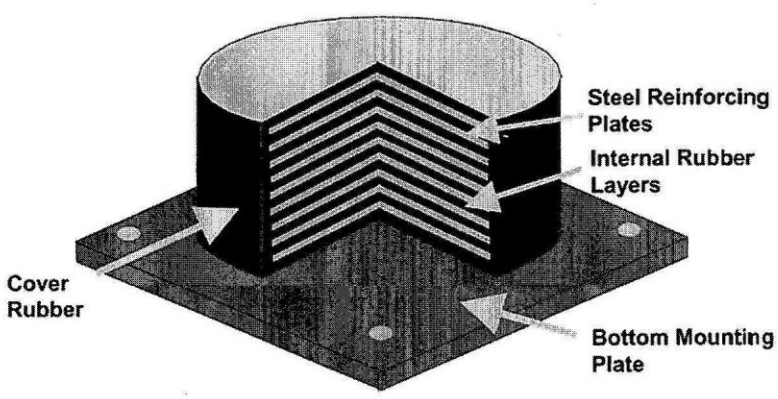

Figure 1.2 Steel Reinforced Elastomeric Seismic Isolator (Primer On Seismic Isolation 2004, courtesy of DIS Inc.)

1.4.1 Low damping Rubber Bearing LDRB

In Japan, low-damping rubber bearings (LDRBs) using natural and/or synthetic rubber are used in combination with supplemental damping devices, such as lead or steel bars and viscous dampers or frictional devices. The isolators have two, thick top and bottom plates as well as a number of thin steel shims. The natural or synthetic rubber is vulcanized, then bonded to the steel plates in a process involving heat and pressure. The steel shims provide a high vertical stiffness and prevent the bulging of the rubber, but they do not effect the horizontal stiffness of the system. This is controlled by the low shear modulus of the elastomer. Although the required flexibility with linear behaviour up to shear strains above 100% is provided by this type of elastomeric bearing, the equivalent viscous damping ratio remains within the range of 2% to 5%, which is not sufficient (Naiem and Kelly, 1999; Priestley et al., 1996).

The LDRBs have the advantage of being easy to manufacture, easy to model, having a process for bonding to steel that is well understood, and having mechanical and dynamic responses that are unaffected by rate of loading, temperature, loading history, and aging. Their only disadvantage is that they require a supplementary damping device.

1.4.2 Lead-plug Bearing (LRB)

Lead–rubber bearings (LRBs) are similar to low-damping rubber bearings (LDRBs), but they contain holes into which one or more lead plugs are inserted. The steel plates in the bearing push

the lead plugs to deform plastically at a flow stress of approximately 10 MPa, and consequently they create a bilinear response in the bearing (Tyler and Robinson, 1984). It is important to have the lead inserted into the hole tightly; to do so, the lead plug should be slightly larger than the hole into which it is inserted. Figure 1.3 shows a typical lead-plug bearing. Since the LRB's effective damping and stiffness depend on the displacement, it is important that the displacement be noted when an LRB damping value is reported. When the lead yields, the lateral stiffness of the bearing is proportional to the lateral stiffness of the rubber. Therefore, lead-plug rubber bearings exhibit a bilinear lateral response. Depending on the diameter of the lead core, damping values of up to 30% can be achieved (Taylor and Igussa, 2004). Since 1982 lead-plug bearings have been tested extensively in New Zealand. These isolation bearings have been employed in a number of buildings, including some that demonstrated satisfactory performance during the 1994 Northridge and the 1995 Kobe earthquakes (Naeim and Kelly, 1999). Figure 1.4 presents the hysteresis force–displacement diagram for different types of elastomeric bearings.

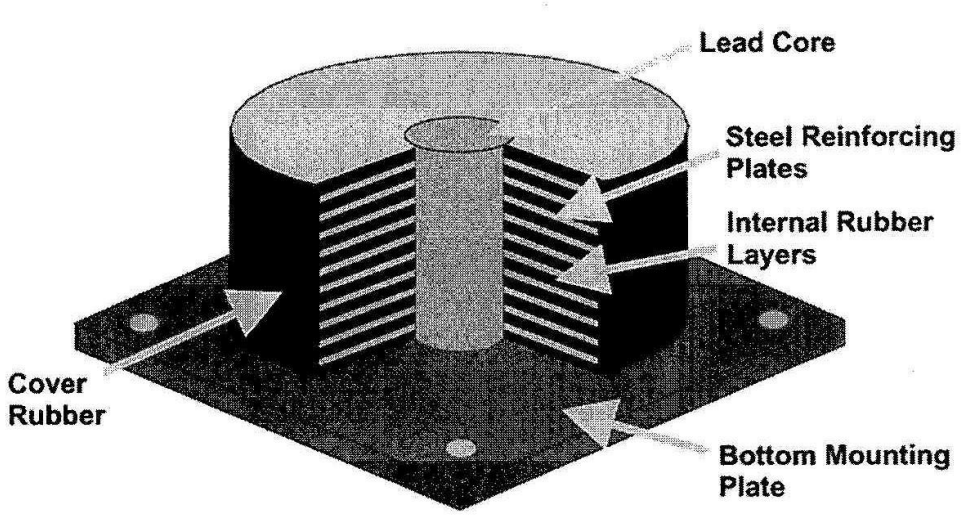

Figure 1.3 Lead-plug elastomeric isolator (Primer on Seismic Isolation 2004, courtesy of DIS Inc.)

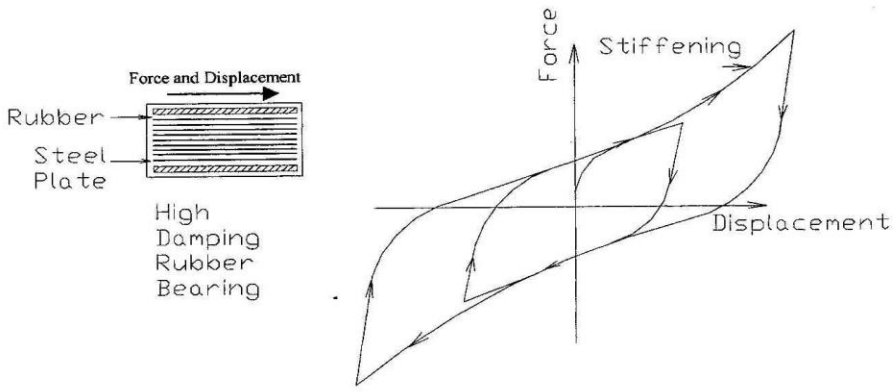

(a)

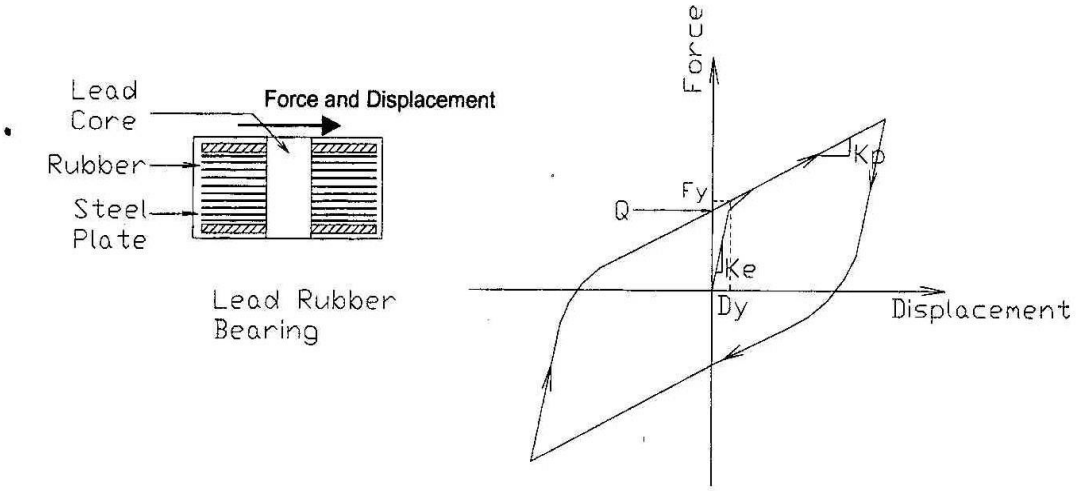

(b)

Figure 1.4 Typical Elastomeric Bearing hysteresis force-displacement diagram, (a) High Damping Steel Reinforced Elastomeric and (b) Lead Rubber Bearing Isolator (Primer on Seismic Isolation 2004)

1.4.3 High-damping Elastomeric Seismic Isolator

In 1982 Malaysian Rubber Producers' Research Association developed high-damping natural or synthetic rubber compounds with sufficient inherent damping to eliminate the need for supplementary damping devices (Derham et al.1985). The damping is increased by adding extra-fine carbon black, oil, or resins, and other fillers. The damping is increased to levels between 10 to 20% of the critical damping, at shear strain amplitude of 100% shear strain range.

High-damping elastomer bearings are more sensitive to temperature and loading rate than low-damped rubber bearings. High-damped rubber bearings are distinguished by their dependence on loading history, although this effect does not manifest in every compound. The first cycle of loading at large shear strain has higher effective stiffness and damping than those of the several cycles that follow. Material characteristics will generally become stable after the third cycle.

The advantage of this type of high-damped laminated bearing is that it combines the required energy dissipation and flexibility phenomenon in a single element, and it is also easy to design and manufacture. These bearings were first used in Foothill Communities law and justice center in Rancho Cucamonga, California, in 1984. In 1995, to study the material performance of the high-damped rubber seismic isolator, two of the isolators were removed from the building and retested. After 12 years of operation the test results showed that the lateral shear stiffness was the same as in the original tests conducted before construction (Clark, 1997).

1.5 Sliding or Friction Type Seismic Isolation System

Sliding or friction type seismic isolators are popular and are implemented to decouple the superstructure from the vibrating foundation by a sliding or frictional interface. These types of seismic isolators are insensitive to earthquake ground acceleration frequency content. The sliding isolators can be used for building structures and bridges. The three advantages of sliding isolators over other conventional types are (1) frictional isolators work well for a wide range of earthquake frequency inputs, (2) because frictional forces take place at the structure base, they are proportional to the mass of the structure, and (3) the sliding isolator's center of mass and center of resistance usually coincide, and consequently the torsional effects due to asymmetry of the structures are diminished.

1.5.1 Pure Friction Seismic Isolator

The simplest type of sliding isolator is called the pure friction (P-F) isolation system. In this system the sliding joint separates the superstructure from the foundation. Layers of sand or rollers in the foundation are an example of a P-F system used for low-rise buildings in China. There has been considerable research work and studies done on P-F (Westermo and Udwadia, 1983; Mostaghel and Tanbakuchi, 1983; Younis and Tadjbakhash, 1984; Jangid, 1996). The advantage of this type of bearing is that it does not increase the natural period of the structure, but rather it limits the shear force transferred into the superstructure. The disadvantage is that it requires a supplemental self-re-centering mechanism to prevent permanent isolation deformation and offset.

1.5.2 Friction Pendulum Systems

FPS is a frictional isolation system that is capable to combines a sliding action and the restoring force by the geometry of the concave plate. The FPS isolator with an articulated slider moves on a stainless steel spherical surface. The coefficient of friction depends on the sliding velocity and the pressure. The effective stiffness of the isolator and the isolation period of the structure are controlled by the radius of the curvature of the concave surface. As the isolator moves over the concave surface the supported mass rises, and this action provides the restoring force for the system. A typical FPS is shown in Figure 1.5.

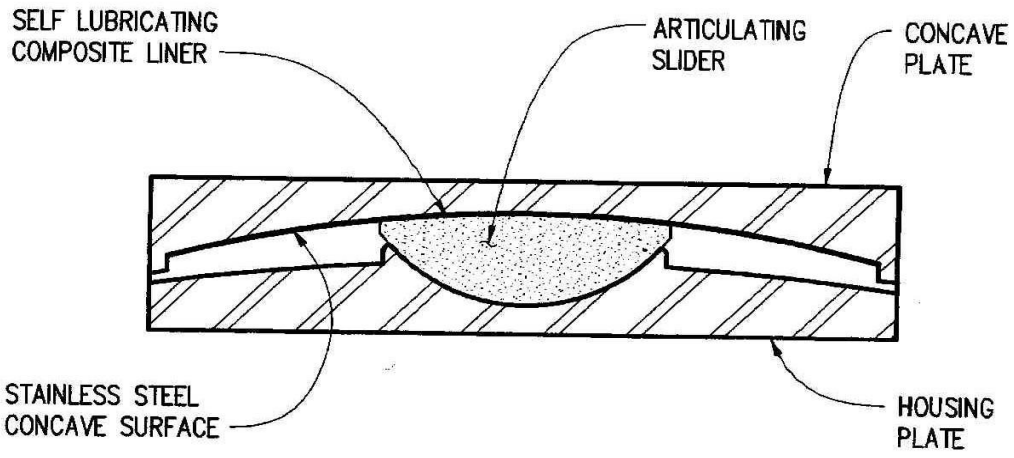

Figure 1.5 Friction pendulum system (FPS) and typical mechanism of the isolator
(Primer on Seismic Isolation 2004, courtesy of Earthquake Protection Systems, Inc.)

1.6 Technical Concept and Fundamentals of the Seismic Isolation System

Seismic isolation systems will increase the horizontal, fundamental period of the structure. This increase is very important, since the fundamental period of an isolated structure will be in a range dissimilar to the predominant period of the earthquake-induced ground motion. As a result, the energy transmitted to the isolated structure will decrease considerably. This phenomenon is demonstrated in Figures 1.6 (a) and (b). With close attention to the following seismic response spectra, the philosophy behind the installation of base isolators can be stated as follows: to lengthen the period of vibration of the protected structure, so as to reduce the base shear induced by the earthquake, while providing additional damping to reduce the relative displacements across the isolators themselves. This is why most seismic design codes suggest the use of base isolation systems that have the dual function of period elongation and energy dissipation. Structures are not normally isolated from vertical earthquake ground motion. In general, the vertical earthquake ground motion is of a smaller magnitude than horizontal ground motion, and since structures are designed to withstand static gravity loads, they are inherently stiff enough in the vertical direction, making the vertical isolation component of secondary importance. The fundamental frequencies of low-rise buildings most often fall within the horizontal ground motion of most earthquakes' predominant frequency range and consequently make the buildings

more vulnerable. Thus, application of seismic isolation systems to low-rise buildings could play an important role in seismic design and protection.

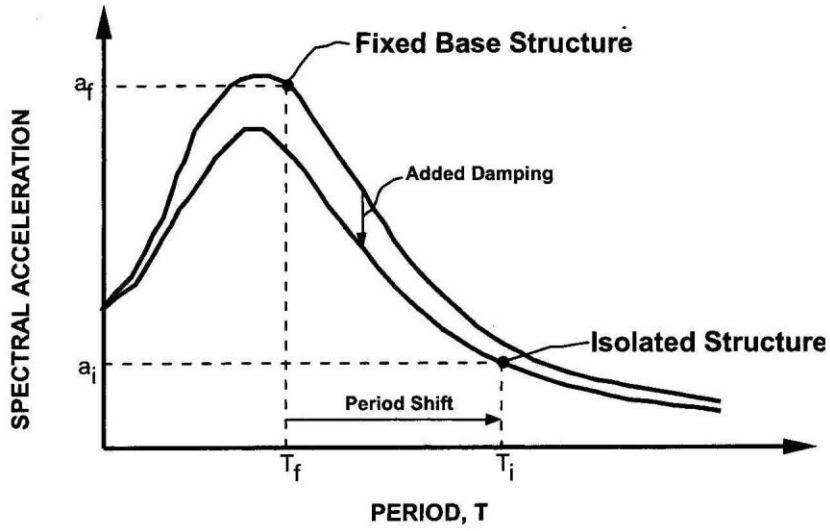

(a)

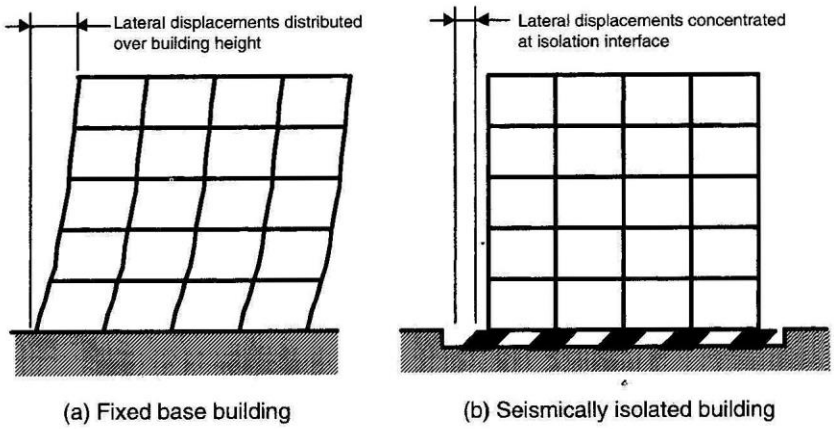

(b)

Figure 1.6 (a) Effect of period shift in reducing the base shear of isolated structure and (b) lateral displacement distribution in fixed base and isolated building structures (Primer on Seismic Isolation 2004)

Seismic isolation can have two positive effects on the seismic response of structures: reduction of earthquake lateral forces to the superstructure, and concentration of lateral displacement in the isolation interface to minimize the story drifts. In design of a proper seismic isolator for a structure, some important parameters, other than its general characteristic of shifting the structures damping and fundamental period, must be considered. The parameters include (Mayes and Naeim, 2001):

1) deformability under static loads (initial stiffness)
2) yielding force and displacement
3) capability of self-re-centering after deformation
4) the potential for torsional response of isolated structure
5) influence of wear, aging, and temperature on behaviour of the isolation system

1.7 Seismic Isolation Effectiveness and Performance in Past Earthquakes

The response and performance of the base-isolated West Japan Postal Savings Computer Center building in Kobe, Japan, during the 1995 earthquake, is an encouraging example of the effectiveness of base isolation technology in reducing the seismic demand and increasing protection. Although this building experienced ground motion with peak site acceleration of 0.40g, the computer center exhibited no damage and the maximum recorded acceleration in the building was only 0.12g (Mayes and Hinman, Base Isolation and Blast loading, 1996). The force and acceleration reductions are considerable when the response of this base-isolated structure is compared with that of a conventional structure. A reduction of up to70% of seismic forces in isolated structure is remarkable (Figure1.7).

Another significant case of an isolated structure undergoing strong ground shaking is the USC Hospital in Los Angeles, which was subjected to the Northridge earthquake on January 17, 1994. The analytical model of the structure had accurately estimated the structure response (Asher et al., 1997); the measured free field peak ground acceleration was 0.49g, while the maximum acceleration throughout most of the structure was less than 0.13g and at the roof was 0.21g due to structural amplification in the upper two stories. By modeling the structure, Asher et al. concluded that for the fixed base structure this floor acceleration would have a range of 0.37-1.03g and that damage to the structure and its contents would have been almost certain.

After the 2011 Great East Japan Earthquake, the Japan Society of Seismic Isolation (JSSI) conducted a questionnaire survey for 327 seismically isolated buildings, including 19 detached houses. It is reported that superstructures of all seismically isolated buildings suffered almost no damage even under strong ground motion with JMA intensity 6 plus. It proved the “excellent performance of seismically isolated buildings”. Some damage was observed in seismic isolation devices (Saito, 2013; Saito, 2015).

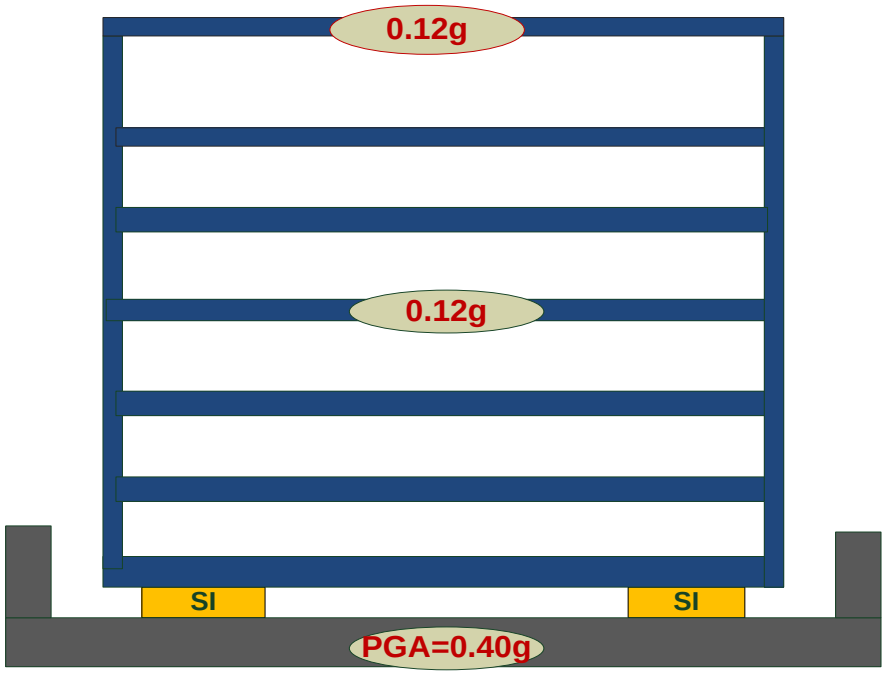

(a)

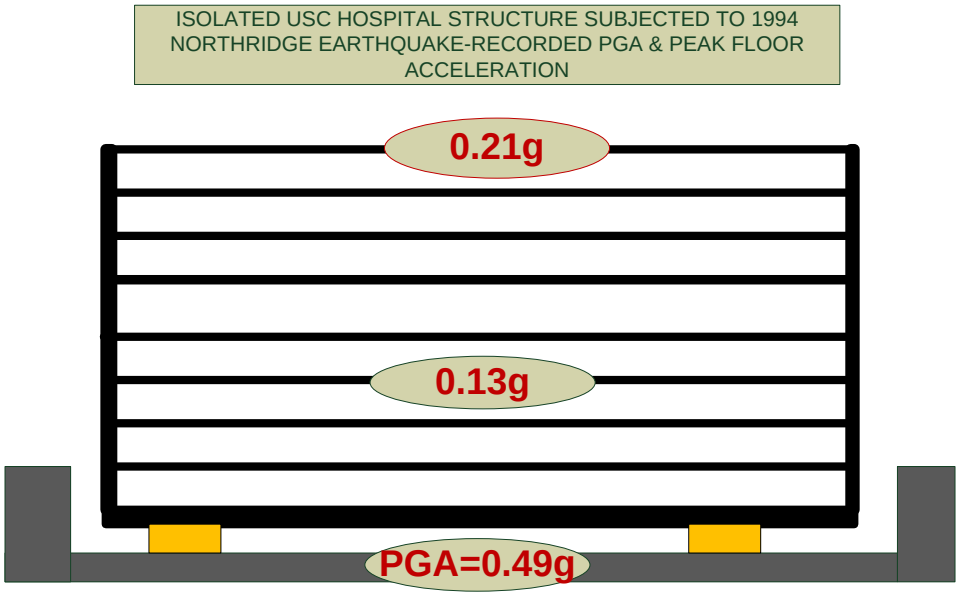

(b)

Figure 1.7 Response of Isolated building during past earthquakes (a) Postal Computer Center Building during 1995 Kobe, Japan earthquake and (b) USC Hospital building response to 1994 Northridge Earthquake

1.8 Need for This Research

The problem with adapting the isolation to developing countries is that conventional isolators are large, expensive, and heavy. An individual isolator can weight one ton or more. To extend this valuable earthquake-resistant strategy to housing and other public buildings, it is necessary to reduce the cost and weight of the isolators. The cost and weight can be reduced by replacing the steel plates in the isolators with height strength fiber material as the reinforcements (Kelly 1999). Despite recent research advances in the field of conventional base isolation, the widespread application of this technology is still faced with difficulties (May, 2002). These obstacles will make it difficult to implement base-isolation projects unless the seismic bearing design and provisions become a catalogue commodity with certified characteristics and allied simple design procedures that promote the high benefits of base-isolation systems. With the existing problems, this technology will remain difficult to implement (Bozorgnia and Bertero, 2004).

Unfortunately, the high seismic zones of the developing world suffer the most. The buildings most vulnerable to earthquake ground motion are the typical buildings in developing regions: low-rise, low-importance residential and commercial buildings. For example, following the earthquakes in Turkey, Greece, Taiwan, etc. in 1999, more than 90% of low-rise residential buildings suffered damage (Kang et al., 2008).

This unfavorable situation is due to numerous deficiencies, primarily the high production and implementation costs of seismic isolation. This prevents developing countries from benefitting from seismic isolation technology (Kelly 1999).

To justify and demonstrate the cost effectiveness of the proposed component and compound SB-CFREIs, a preliminary production cost analysis is conducted and is summarized and compared with conventional SREI of the same capability in section 3.7.2.

The production cost estimate of conventional steel reinforced isolator for supporting a compression load of 500-3500kN with design lateral displacement of 150-460mm is approximately $4000-$12000 (purchase price quote from DIS). Tax, transportation, handling, and implementation costs are not included. The large size and weight of these isolators considerably increases the isolator's handling and implementation cost. With these high production and implementation costs, widespread application of the existing conventional seismic isolators for low-rise common housing in developing countries does not seem possible.

Therefore, the existing deficiencies must be remedied to make application of base isolation, which is an effective seismic protection technology, affordable and practical worldwide. A viable and cost-effective seismic isolation system is necessary to protect human lives and properties from earthquake induced ground motions.

In the last 15 years, application of fiber reinforced elastomeric isolator FREI technology has attracted much research attention. Considerable progress has been made in design, manufacturing, and testing of proposed FRE isolators in bonded and un-bonded applications, but seismic isolation technology still faces challenges and deficiencies in achieving wide spread application.

By conducting a literature review on the subject, gaps in knowledge were defined; the need for further scientific contribution through experimental and analytical research studies, along with the proposed approach, are documented in section 2.2, "Deficiencies and Knowledge Gaps in Existing Seismic Isolation Technology and Proposed Approach."

1.9 Research Goals

The prime goal of this research is to contribute to the knowledge of seismic isolation technology to achieve a viable, efficient, and cost-effective seismic protection system to prevent loss of lives and properties due to earthquake induced ground motion. In this scientific attempt, the prime intention is to effectively protect low-rise buildings in the high seismic zone of developing countries.

1.10 Research Objectives

The main objective in this research is to investigate deficiencies in the existing seismic protection technology, and address those deficiencies toward achieving a viable and cost effective seismic isolation system. This research intends to achieve this objective by considering application of efficient, low cost seismic isolation systems as a possible alternative. The systems must be able to de-tune and shift the natural frequency of these low-rise buildings away from the earthquake predominant ground motion frequency, to significantly reduce the seismic demand. To achieve the aforementioned objectives, innovative Component and Compound Semi-Bonded Carbon Fiber-Reinforced Elastomeric Isolators (SB-CFREI and CSB-CFREI) are designed and proposed for further investigation and experimental testing.

1.10.2 Proposed research tasks to achieve the objectives

1. To perform experimental studies on component and compound isolators to investigate the dynamic characteristics, performance, and isolation efficiency of SB-CFREI and CSB-CFREI as cost effective seismic protection systems.

2. To investigate the effect of bonding variation on the isolator's effective lateral shear and axial compression stiffness and damping, also to study the influence of bonding level on the isolator's performance and isolation efficiency.

3. To investigate the effects of combination configuration on the dynamic characteristics of the compound isolator.

4. To conduct analytical studies on proposes isolators and to compare the outcomes with those of the experimental to evaluate the validity of implementing analytical methods like finite element analysis in design of SB-CFREIs.

1.11 Thesis Structure and Organization

The thesis is organized in 6 chapters along with two appendices, A and B, containing the related research work, computations, and drawings. The content summary of each chapter is as follows:

Chapter 1 starts off with an introduction to seismic isolation technology followed by a short summary of the history, background, and fundamental philosophy behind seismic isolation technology. In this chapter, general information on mechanical features, dynamic characteristics, and capabilities of different types of conventional seismic isolation systems are discussed. The chapter concludes by summarizing the research goals and objectives.

Chapter 2 summarizes the study on the state-of-the-art literature review conducted on Fiber Reinforced Elastomeric Isolators (FREIs) in general, and Carbon Fiber Reinforced Elastomeric Isolator (CFREIs) specifically. The chapter ends by discussing the lack of knowledge in the technology, and a proposed approach.

Chapter 3 concentrates on introducing the design features, capabilities, and the unique deformation mechanism of the proposed component and compound isolator SB-CFREI and

CSB-CFREI. This chapter also describes the design advantages of the proposed isolator in comparison to existing conventional and unbonded CFREIs. Difficulties and challenges in manufacturing and fabrication procedures of the innovative isolators are discussed in this chapter as well.

Chapter 4 describes the experimental program, equipment set-up, instrumentation and test specifications, and sequences. In this chapter, lateral shear and axial compression cyclic testing along with related input load signals are presented. The test outcomes, like effective lateral shear and axial compression stiffness and damping, along with the related load-displacement hysteresis diagram, are discussed. Component material testing and long duration loading experimental tests along with the tests results are presented as well.

Chapter 5 Presents the analytical studies done on SB-CFREI by finite element analysis (FEA) of the isolators, conducted with application of hyper-elastic material models under different types of loading. In this chapter the FE analysis outcomes have been discussed and compared with experimental outcomes to study the validity of FE modeling in the preliminary design of the new SB-CFRE isolators. Analysis and related outcomes are discussed and presented.

Chapter 6 of the thesis summarizes the thesis outcomes and conclusions along with related discussions and recommendations. In this chapter the prime contribution of the research is summarized. Recommendations for future research in the field of fiber reinforce elastomeric isolator ends the last section of this chapter.

Appendix A consists of computations of effective lateral and compression stiffness and damping of the isolators with different bonding levels tested under defined load cases, along with the related load-displacement hysteresis diagrams for "Component Isolators."

Appendix B contains computations for defining the effective lateral and compression stiffness and lateral damping of the "Compound Isolators" with different component combinations, and average bonding level tested under defined input loading along with the related load-displacement hysteresis diagrams.

CHAPTER 2: RECENT DEVELOPMENTS AND REVIEW OF STATE OF THE ART LITERATURE ON FIBER-REINFORCED ELASTOMERIC ISOLATORS (FREI)

2.1 Summary

A literature review of recent developments in Fiber Reinforced Elastomeric Isolator (FREI) has been conducted and the outcome of this study has been summarized in this chapter. The implementation of high strength fibers as reinforcement in elastomeric isolators was proposed by Kelly in 1999 for the first time. As the technology is relatively new, limited research has been conducted on fiber reinforced elastomeric isolators in the last 15 years. Experimental and analytical research studies on FREIs have been reviewed, and deficiencies and gaps in knowledge of the existing technology and its application have been identified.

Kelly (1999) stated that the problem with adapting base isolation to developing countries is that conventional isolators are large, expensive, and heavy. A single seismic isolator can weight one ton or more. To extend this valuable earthquake protection strategy to housing and other public buildings, the cost and weight of the isolators must reduce. The production cost and weight can be reduced by replacing the steel plates in the isolators with height strength fiber material as the reinforcements. In this study, Kevlar fiber was selected as the reinforcement for elastomeric bearing specimens, and different experimental tests were conducted on the unbounded bearing strips. The research concluded that these lightweight FRE isolators can provide vertical and lateral stiffness in the same range as steel reinforced elastomeric isolators with the same diameter and rubber thickness. The lateral shear stiffness and equivalent viscous damping of the fiber-reinforced isolator specimen were proximately 80% and 180%, respectively, of those of similar steel reinforced elastomeric isolators. The fiber cord reinforcements that are made of many single fibers are more flexible in tension compared to the individual fibers, and they are completely flexible in bending, while the steel reinforcement sheets in the isolator elastomer are rigid in tension and bending.

Tasi and Kelly (2002) took a theoretical approach in analyzing the bending stiffness of the fiber-reinforced elastomeric circular shaped isolator. The elastomers were assumed incompressible and the pressures dominant. Theoretical solutions indicated that the bending stiffness of the reinforced elastomer is influenced by the shape factor of the elastomer and the flexibility of the

reinforcements. The stiffness of the elastomer bonded to flexible reinforcement increases as the shape factor increases. The stiffness of the reinforced elastomer varies with the Poisson's ratio of the reinforcements. They also showed that under pure bending movement, the flexibility of the reinforcements shifts the location of the maximum pressure closer to the edge and decreases the maximum value. Also the flexibility of the reinforcements makes the distribution of the bonding shear stresses more concentrated on the edges and increases to its peak values in this zone.

Moon et al. (2002) performed experimental tests on different fiber type specimens; they manufactured some fiber-reinforced, multi-layered elastomeric isolator specimens using carbon, nylon, glass, and polyester fiber. They conducted experimental studies to determine their mechanical characteristics and performance under different dynamic loadings. In these experiments the carbon fiber reinforced elastomeric bearing's mechanical characteristics were compared with those of the same sized multi-layer, steel reinforced elastomeric isolators. Experimental results indicated that the performance of the carbon fiber-reinforced elastomeric isolators was superior to similar steel-reinforced isolators, especially in compression stiffness and in damping. The experiment result also indicated that the compression stiffness, shear stiffness, and equivalent viscous damping of the carbon fiber reinforced elastomeric isolators were 299%, 94%, and 256% of those of similar steel reinforced isolators, respectively. They concluded that the fiber reinforced elastomeric isolators can replace the steel reinforced elastomeric isolators.

Kang et al. (2003) conducted vertical compression and lateral shear experimental tests on CFR elastomeric isolator specimens, with and without holes and lead plugs, in order to study the effects of holes and lead plugs on the effective lateral shear and axial compression stiffness and damping. The test results indicated that the holes and lead plugs had little effect on effective stiffness and damping of the carbon fiber reinforced elastomeric isolators.

Tsai (2004) derived a closed form solution for axial compression stiffness of infinitely long strip shape, flexible reinforced elastomeric isolators, considering the effect of bulk compressibility in the elastomer layer and the effect of boundary condition at the bearing ends. The behaviour of elastomer layers and the reinforcement were also considered as linear elastic. He compared the outcomes from theoretical solution with those of the finite element analysis and stated that "the

theoretical solutions to the compression stiffness of the bearings are extremely close to the results obtained by the finite element method."

Summers et al. (2004) conducted an experimental study on prototype of carbon FREIs with rectangular cross section. The isolator elastomer material was high damped rubber compound with11% effective lateral damping and 0.4 MPa nominal shear modulus. The isolators were subjected to a 100% maximum shear strain deformation, and with average displacement rate of 100 mm/s, under constant axial compression pre-load of 1.79 MPa. The outcome hysteresis diagrams demonstrated stable behaviour.

Ashkezari et al. (2008) designed and manufactured a fully steel-bonded, carbon fiber-reinforced elastomeric isolator. For the sake of comparison they also fabricated similar steel (thin sheet layer) reinforced isolators and conducted an experimental test to study and compare the dynamic characteristics and capability of the two different isolators. The experimental results showed that the steel-reinforced elastomeric isolator can be replaced by a carbon fiber elastomeric seismic isolator. They concluded that the bonded carbon fiber-reinforced elastomeric isolators not only have a better energy dissipation capability but also are lighter in weight and more efficient in production. Due to similarities to steel reinforced isolators in their dynamic characteristics, they called them "Steel-Like Fiber Reinforced Elastomeric Isolator SL-FREI."

Kang et al. (2008) conducted dynamic analysis of an isolated structure being isolated with fiber-reinforced elastomeric isolators. They presented the advantages of performing nonlinear dynamic analysis in this type of application and compared the dynamic characteristics of a nylon and carbon FRE isolator with a multi-layer steel-reinforced elastomeric isolator. The experimental test results indicated that the carbon fiber-reinforced isolator has a lateral equivalent viscous damping of 15.85%, compared with that of steel REI of 6.20%. In another horizontal test they compared the lateral effective damping of Nylon-REI with that of Steel-REI, and the result showed 11.6% and 6.19%, respectively. The vertical compression test results indicated that the axial compression stiffness of steel REI is much higher than nylon FREI by a factor of 270%. In the same compression test, carbon FREI had much higher vertical compression stiffness (3200 N/mm) as compared to steel REI (1070 N/mm). The test outcome showed that carbon fiber is

more efficient with higher dynamic capabilities as reinforcement in elastomeric seismic isolation technology.

Mordini and Strauss (2008) performed an extensive Finite Element Analysis (FEA) on Bonded Glass Fiber Reinforced Elastomeric Isolators (B-GFREI). The dynamic characteristics of the fiber-reinforced elastomeric bearing with interposed glass fiber layers were studied in a parametric numerical study by means of Finite Element Analyses. Different GFRE bearings were investigated in both static and dynamic loading conditions to obtain a better understating of their behaviour. Many analyses were performed with different axial compression pre-loads, number of layers, geometries, boundary conditions, and material constitutive models. Dynamic analysis to compare the results from a two-dimensional and a three-dimensional model was conducted. Some of the results obtained from the finite element simulations were compared with well-known and established simplified formulations presented by Kelly's Pressure Solution Method (PSM) to define FREI's axial compression and lateral shear stiffness. Since the main intension in this study was to investigate the performance of proposed GFREI and their effectiveness in reducing seismic demand on the structures, a full dynamic analysis of the liquid storage tank isolated by the proposed GFREI was performed. non-linear simple connector elements replaced the bearings in conducting the analyses. They concluded that the expected acceleration reduction and period shift were documented.

Tait et al. (2008) performed experimental studies and investigated the influence of different end face geometry and configuration on the response behaviour of the unbounded FREI bearing. The comparison of lateral force-displacement hysteresis diagrams indicated that the end geometry can significantly affect and change the lateral force displacement response behaviour of the bearing. The lateral stiffness of the bearing was found to decrease when material (fiber-reinforced elastomer) was removed from the end face, and to increase when material was added to the bearing end faces. Also, the shape of the end face was found to influence the response behaviour of the bearing.

Modifying the end geometry of a SU-FREI bearing also affects the equivalent viscous damping. These preliminary findings indicate that the end geometry of a SU-FREI bearing is a parameter that can be modified to obtain the desired lateral force-displacement response behaviour.

Toopchi-Nezhad et al. (2009) conducted a shake table study on an ordinary low-rise building seismically isolated with SU-FREI to investigate the mechanical and dynamic behaviour and performance of the fiber-reinforced elastomeric isolators. Due to the stable lateral load-displacement response of the unbonded FREI bearings, these isolators were denoted as "Stable Unbonded" Fiber Reinforced Elastomeric Isolator (SU)-FREI.

The shake table study was performed using a two storey steel test-structure with 1/4 scale (with defined elastic response characteristics), and scaled versions of three different major earthquakes' ground motions (Tabas, El Centro, Saguenay) were used as input loads. Carbon fiber fabric was used as reinforcement and unfilled neoprene rubber was selected as the elastomer in bearings fabrication. The dynamic response of isolated structures under different input earthquake induced load cases was recorded and compared with the corresponding fixed base (FB) structure. The test outcomes indicated that by application of the SU-CFREI bearings, a significantly improved response can be achieved and concluded that:

1) SU-FREIs can be considered as an effective seismic isolation system.
2) Significant savings in the design of base-isolated structures that employ FREI bearings can be achieved.
3) Unbonded versus fully bonded (with thick steel cover plates) applications were studied, improved lateral load-displacement characteristics due to occurrence of "Rollover deformation" phenomenon, (as the result of the flexibility of the fiber reinforcements sheets and the isolator's unbonded application) and better energy dissipating mechanism (due to interaction between the elastomer and fiber fabric reinforcements in addition to the inherent elastomer damping) were stated as the advantage of unbonded to bonded CFREIs.

Kelly and Konstantinidis (2009) studied the influence of friction on unbonded steel reinforced elastomeric bearings. This research was conducted to investigate the possibility of implementing typical thermal bridge expansion bearing as a lightweight, low-cost elastomeric seismic isolator for application in housing, schools, and other ordinary public buildings in the high seismic zone of the developing world. The effect of friction resistance of the supports on this type of unbonded bearing was well investigated since they are held in place by friction only. The analysis demonstrates that friction has a very pronounced influence on both the isolator's shear

and the compression modulus. In this study the effect of slip due to either intentional or unintentional lubrication action has also been analyzed in order to have a better understanding of the resulting consequences.

Raaf et al. (2011) investigated the stability of fiber-reinforced elastomeric bearings in an unbonded application through experimental studies. They stated that: SU-FREIs remain stable at axial loads significantly greater than the design load under a wide range of cyclic lateral displacement amplitudes. They also concluded that: an increase in axial compression load results in lower lateral effective stiffness and higher effective damping in SU-FREIs.

Onorii et al. (2011) conducted experimental research to investigate the possibility of application of a new elastomeric seismic isolator, manufactured by superimposing recycled rubber layers and carbon/glass fiber sheets as reinforcements, in order to lower the cost and the weight of the isolator in an unbonded application. Both compression and shear test was conducted on square shape bearing prototypes, using different types and numbers of reinforcement layers. The innovative prototype recycled rubber bearing is made of recycled rubber and polyurethane (as the binder). The research concluded that use of FRP instead of steel sheet as elastomer reinforcement not only eliminates the need for vulcanization but also makes the fiber-reinforced elastomeric isolator more effective for specific application. Experimental test on the rubber material revealed that “it is characterized by good values of G-modulus and preserves good damping properties”. Tests on prototype bearing samples highlight the importance of the density of the rubber material to obtain desired mechanical properties.

Toopchi-Nehzad et al. (2011) conducted an extensive Finite Element Analysis investigating the dynamic characteristics of the bonded and unbonded strip fiber-reinforced elastomeric isolators. In this research carbon fiber was the fiber type used as reinforcements for both the bonded and unbonded elastomeric isolators. The term strip was selected, as the analysis was carried out for the unit out of plain length of the isolators. To make a proper comparison, material specifications and bearings dimensions were chosen to be the same for both applications of bonded and unbonded CFREIs and were analyzed under the same loading cases. The primary goal of the FE analysis was to define and evaluate the lateral stiffness of isolators at different lateral deformation amplitudes. The state of the stress in the isolator components was also determined

and demonstrated. An extensive comparative study on the lateral response of the bonded and SU-CFREI was presented. The CFRE bearing specifications implemented in this study as bonded and unbonded application had been used in the experimental studies conducted by Topchi-Nehzad et al. (2009), so some of the FE analysis results were compared with those from the experimental. Results of the FE analysis documented the following advantages in the lateral response of unbonded FREI in comparison to the bonded FREI:

1) Considerably lower horizontal stiffness, and as the consequent significantly higher isolation efficiency.
2) Significantly lower stress demand on rubber or elastomeric material
3) Minor peeling stress demand on rubber and fiber reinforcement layers.
4) Reduced tensile stress demand on the fiber reinforcements, and consequently lower shear stress demand on the bond between the fiber reinforcement and rubber layers.
5) They stated that to achieve a certain level of seismic protection, an unbonded FREI required a significant lower operating height than B-FREI; in other words, there is considerable material savings in this type of isolator and concluded that; significant potential exists for unbonded FREI to be used as a cost-effective device for seismic protection of ordinary buildings.

Gerhaher et al. (2011) conducted research on numerical modeling of elastomeric isolators, the study provided an overview on modeling and influence of the elastomer complex material behaviour and its implementation in the numerical model. Various material models were investigated in respect to the calibration, the computational effort, and the possible range of studies that can be conducted with the bearing models. They used the ABAQUS computer software and calibrated the FEA results with the experimental outcomes.

Kelly et al. (2012) conducted an extensive Finite Element Analysis study on 12 FREIs with different shape factor and fiber specifications to investigate the mechanical behaviour of the Unbonded Fiber Reinforced Elastomeric Isolators (UB-FREI). The computer software MSC MARC (2005) finite element program, was used to carry out the FE analysis. The research compared the bearing's horizontal shear and vertical compression stiffness obtained from FE analysis with that of the well-known pressure solution analytical method. They concluded that

the result from both analyses were in agreement, and consequently confirmed the reliability and performance of the unbonded FREI for low rise buildings.

For all the considered values of shape factor, the pressure solution resulted in higher values of vertical stiffness than the FE analysis. The results showed that the pressure solution method presented in the same research work loses accuracy as the shape factor increases. This result is in agreement with that from Kelly and Takhirov (2002). The authors suggested that the loss of accuracy is mainly due to the assumption of incompressibility of the rubber material, and the results can be considered valid only for low values of a shape factors less than five.

This report denoted that FREIs have high potential to meet the provisions of a low-cost, lightweight rubber isolation system. The authors also stated that FREIs have been extensively tested in laboratory test programs before, and the mechanical behaviour of this type of isolator has also been verified by finite element studies. These isolators have less severe bonding requirements than conventional isolators and have the potential of lending themselves to mass production manufacturing.

Hedayati Dezfuli and Alam (2012) conducted research on multi-criteria optimization and seismic performance assessment of CFRP-based elastomeric isolators. This study was conducted using FEA, and the Mooney-Rivlin-Prony material model was selected for the high damping rubber in the elastomeric bearing. They investigated the effect of different isolators' component parameter on the efficiency of the CFRP-based elastomeric bearing. The performance of the bearing was optimized through a multi-criteria decision-making (MCDM) process. The hysteretic behaviour of the bearing was investigated by conducting FE analysis and the outcomes were validated by comparing FE force-displacement hysteresis diagram with those of the experimental on the two-layer HDR bearing by Dall'Asta and Ragni (2006). They concluded that the hyper-viscoelastic material model used in FE software (ANSYS) could accurately capture the highly nonlinear (hyper elastic and strain-rate-dependent) behaviour of high damping rubber materials subjected to axial compression and lateral cyclic shear loads. They also concluded that by performing regression analyses, "the most significant factors for predicting the vertical compression stiffness, the effective horizontal stiffness, and the equivalent viscous damping are number of rubber layers, shear modulus of elastomer, and thickness of FRP composite plates, respectively".

Mishra et al. (2013) performed an experimental and analytical study of scrap tire rubber pad (STRP) for seismic isolation. The finite element program MSC Marc was used to study the mechanical and dynamic behaviour of the STRP isolator. The research's main intention was to evaluate the performance of the STRP isolator application in low-rise residential buildings. FEA of the STRP isolator was conducted on bonded samples. The research concluded that; "these types of isolators provided positive incremental force resisting capacity up to shear strain of 155%".

Toopchi-Nezahd et al. (2012) investigated the influence of thickness of individual elastomer layers (first shape factor) on the response of unbonded fiber-reinforced elastomeric bearings. Results of a comprehensive 2D-finite element study using MSC Marc software on a large group of bearings with different shape factors of 10, 15, 20, 30, and 40 concluded that the shape factor S1 is a critical parameter in controlling both the vertical compression modulus of the bearing and the level of stress in the fiber reinforcing layers. The bearing compression modulus was found to increase significantly with increasing shape factor S1. Overall, the shape factor S1 was not found to be a critical parameter in controlling the lateral shear stiffness of the strip bearings considered in this research study.

Karimzadeh Naghshineh et al. (2014) conducted a comprehensive experimental study on fundamental properties of new types of bonded, fiber-mesh-reinforced elastomeric seismic isolators and compared the outcome with those of conventional isolators with the same size. They also concluded that the tested fiber-mesh-reinforced elastomeric bearings have significant reduction in the isolator's lateral stiffness when compared with that of the conventional isolators at high shear strain loading. Damping values in both fiber-reinforced and steel-reinforced elastomeric bearings are pretty much comparable, and damping is mainly provided by the elastomer material. The authors believe that "the vulcanization of fiber mesh is more effective than vulcanization of steel plate to rubber".

Bakhshi et al. (2014) conducted an experimental study to investigate the dynamic and mechanical characteristics of CFREIs. They manufactured a total of 18 bonded specimens of carbon-, Polyamide-, and steel-reinforced elastomeric isolators. They concluded that in the absence of constant vertical compression load, use of flexible reinforcement results in a damping

increase of up to 20% and 30% for carbon fiber and polyamide fiber-reinforced elastomeric isolators, respectively. They also stated that the application of fiber instead of steel-reinforcement results in a decrease in the weight of the isolator by up to 20%.

Van Engelen et al. (2015) conducted experimental and finite element analysis on partially bonded carbon fiber-reinforced elastomeric isolator. In fabrication of this isolator they glued part of the unbonded isolator's elastomeric bearing pad to the top and bottom steel cover plates. The research intention was to address the concern over transmitting the shear force from the bearing to the structural support, and the tension resulting from overturning moment. The experimental data and results from finite element analysis demonstrate that portions of a FREI can be bonded without substantially influencing the rollover characteristics of the stable unbonded isolator within the considered range of average vertical compressive and tensile stresses. They concluded that "the horizontal force–displacement diagram exhibits negligible deviation from a conventional unbonded SU-FREI under a compressive vertical stress". They also postulated that "partially bonded FREIs can retain the beneficial characteristics of unbonded FREIs while addressing concerns over the tensile forces and the slip action" that may result in residual displacements.

Hedayati, Dezfuli, and Alam (2016) conducted an experiment-based sensitivity analysis of scaled CFREIs in bonded applications. They fabricated the ¼ scale CFREIs using a fast cold-vulcanization process to investigate the effects of the vertical pressure, the lateral cyclic loading rate, the number of rubber layers, and the thickness of CF reinforcement layers on the cyclic behaviour of isolator's bearings. The authors concluded that the effect of vertical pressure on the lateral response of the isolators is minor, but decreasing the rate of cyclic loading increases the lateral flexibility and damping. They concluded that for the bonded application of CFREI the equivalent viscous damping "increased from 9.1% to 13.2% when the total thickness of rubber increased from 12mm to 24 mm"; they also stated that in "this range of damping ratio the commercial high-quality neoprene has a higher effective damping capability in comparison to low-damping natural rubber".

2.2 Deficiencies and Knowledge Gaps in Existing Seismic Isolation Technology and Proposed Approach

After conducting a literature review on FREIs, the deficiencies in the technology are outlined and a proposed approach to improving the technology is discussed below.

Application of fiber type material as the reinforcement for the elastomeric seismic isolator is a fairly new technology; in 1999, Kelly proposed the first implementation of fiber material as reinforcement to replace the steel shims in order to reduce the high weight and production cost of conventional steel reinforced elastomeric isolators (SREIs), and the first comprehensive finite element analysis (FEA) study on the mechanical behaviour of FREI was in 2008 by Mordini and Strauss. Limited research has been done and consequently limited data are available on the experimental and finite element analysis of bonded and unbonded FREI. In the field of partially bonded application of fiber reinforced elastomeric isolators, and as of the author's best knowledge, only one study has been conducted on partially bonded CFREI. This was conducted by Van Engelen et al. (2014) and no research study is available in the literature on elevated semi-bonded carbon fiber reinforced elastomeric isolators (ESB-CFREI). The outcomes of the previous analytical and experimental studies that have been conducted on bonded and unbonded fiber-reinforced elastomeric isolators show "that the FREIs have suitable mechanical properties to be used as seismic isolators". These research studies are reported in the literature review section, 2.1, of the thesis.

Despite the beneficial characteristics of bonded and unbonded carbon FREIs (CFREIs), concerns still exist about their efficiency and implementation. During an earthquake, the lateral shear loads at the contact surfaces of an unbonded isolator are to be transferred through friction only, which makes unbonded FREIs susceptible to slip under certain loading conditions, which results in permanent displacements. If during an earthquake the compressive force on an unbonded isolator approaches zero, then the probability that the shear force exceeds the friction resistance increases (Van Engelen et. al., 2014). This can negatively influence the isolator's stability.

During installation of fully bonded CFREIs, the top and bottom mounting plates are bolted to the super- and substructure, respectively. These plates, on one hand, make the isolator capable of transferring the lateral shear force at the contact surfaces, and on the other hand they prevent the stable rollover deformation, which results in high tensile stress demand between the fiber and

elastomeric layers in the CFRE bearing's ends regions, which increases the lateral stiffness of the isolator. As the consequence, the presence of bonded plates not only lowers the isolator's damping and isolation efficiency but also increases the production cost.

To address the aforementioned concerns and deficiencies related to bonded and unbonded CFREIs, in this research innovative component and compound Elevated Semi-Bonded Carbon Fiber-Reinforced Elastomeric Isolator (ESB-CFREI) were designed and proposed for further investigations. The unique design features of the proposed seismic isolation systems are presented in chapter 3 of this research. Comprehensive experimental study to investigate the mechanical and dynamic behavior of the SB-CFREI and CSB-CFREI under monotonic and dynamic loadings is proposed.

Analytical studies by application of FE analysis to evaluate the validity of the FE analysis in the preliminary design of SB- CFREIs also are proposed.

The effect and influence of the bonding variation on the dynamic characteristics of carbon fiber-reinforced elastomeric isolator (CFREI) needs comprehensive investigation.

The effect of component combination on the dynamic characteristics of the compound semi-bonded, carbon fiber-reinforced elastomeric isolators (CSB-CFREI) needs experimental and analytical investigation in this research.

Based on a preliminary cost analysis conducted on fabrication cost of the proposed SB-CFREI and CSB-CFREI, the production cost of the proposed isolator is estimated to be around1/4 of that of steel reinforced elastomeric isolators having the same capability. The preliminary production cost estimate of CSB-CFREI and comparison with that of existing conventional SREI is presented in section 3.7.2 of this research document.

CHAPTER 3: SEMI-BONDED CARBON FIBER-REINFORCED ELASTOMERIC ISOLATOR (SB-CFREI) – COMPONENT AND COMPOUND ISOLATOR

3.1 Design features, Fabrications and Application of SB-CFREI and CSB-CFREI

Semi-Bonded Carbon Fiber Reinforced Elastomeric Isolator (SB-CFREI) has been designed and proposed to serve as a cost effective seismic isolation system with sufficient isolation and implementation efficiency. Innovative SB-CFREI undergoes lateral cyclic excitation with a new deformation mechanism that differs from that of the unbonded or fully-bonded carbon fiber reinforced elastomeric isolators. In designing the new seismic isolator, high-strength, low weight and flexible carbon fiber is selected as the elastomer reinforcement of the isolator. The SB-CFREI can be used in isolation, as a "Component Isolator," or combined with other component isolators to form a CSB-CFREI or "Compound Isolator." Each component isolator has a different bonding value and is expected to have different effective lateral shear, axial compression stiffness, damping, and overall dynamic characteristics. In this chapter the design features and characteristic of the proposed Component and Compound SB-CFREIs are presented and compared with those of conventional Steel Reinforced Elastomeric Isolators (SREIs). Expected capabilities of the proposed partially bonded isolators are discussed and compared with those of bonded and unbonded CFREIs.

3.2 Design Features of Proposed SB-CFREI

The Proposed SB-CFREI is partially bonded with top and bottom steel cover plates (Figure 3.3 & 3.4). Each SB-CFREI pair has a different bonding level (BL). The BL is a measure of steel-cover plate area divided by the elastomeric bearing pad top or bottom surface area, which varies from 37.87% to 100%. A fully bonded isolator, with top and bottom cover plates having the same size as the bearing top or bottom surface area, is denoted as isolator specimen with BL = 100% and is denoted as B260. An isolator with a cover plate size of 160x160mm is presented with BL = 37.87% and is denoted as B160. B260 and B160 have the highest and lowest bonding level respectively.

The partially bonding design feature is expected to provide higher lateral flexibility and lower shear stiffness, which is expected to result in higher isolation efficiency (IE) in comparison with the fully bonded application. The cover plates are designed to be variable in size in order to provide the isolators with the desired bonding level (BL). The top and bottom steel plates are

8mm thick and are glued to the CFRE bearing pad with a high strength chemical compound. The size of steel cover plates varies from 160×160 mm to 260×260 mm to provide the desired BL range. Due to the presence of this specific bonding feature, the innovative seismic isolator is named “Semi-Bonded” CFREI or “SB-CFREI” by the author.

The semi-bonded, carbon fiber-reinforced elastomeric isolator is designed with 24 layers of carbon fiber fabric of 3k carbon fiber strand. The bi-directional plain weave of 12x12 (count of warp and fill fibers) has thickness of 0.22mm and weights 0.196 kg/m^2, with a tensile modulus of 230 GPa as the high strength and flexible reinforcement for the isolator’s elastomer component (3kx3k means warp and fill both are from type 3k carbon fiber). The isolator’s elastomer is 25 layers of 4.6 mm thick natural rubber layers with hardness of 55 durometer (ASTM Shore-A) shown in figures 3.1 and 3.2.

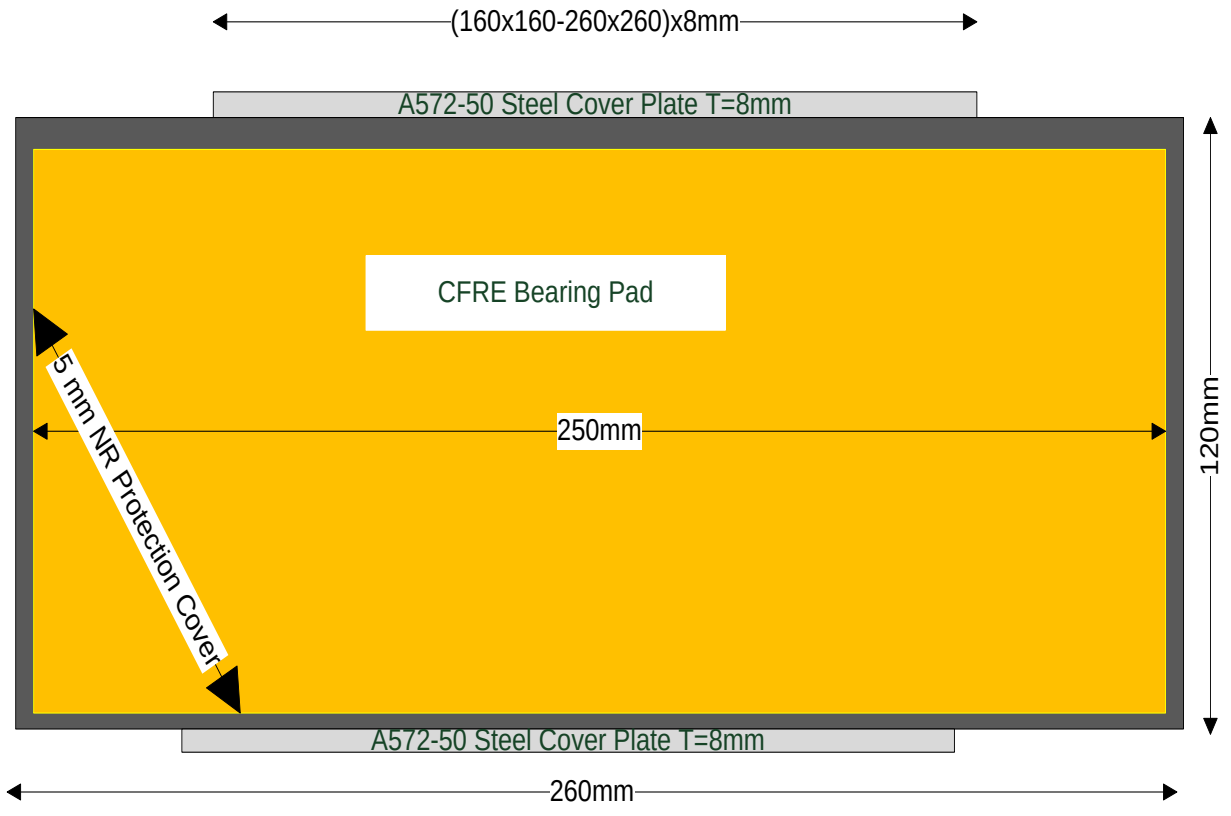

Figure 0.1 The SB-CFREI cross section view showing dimesions and NR protection cover

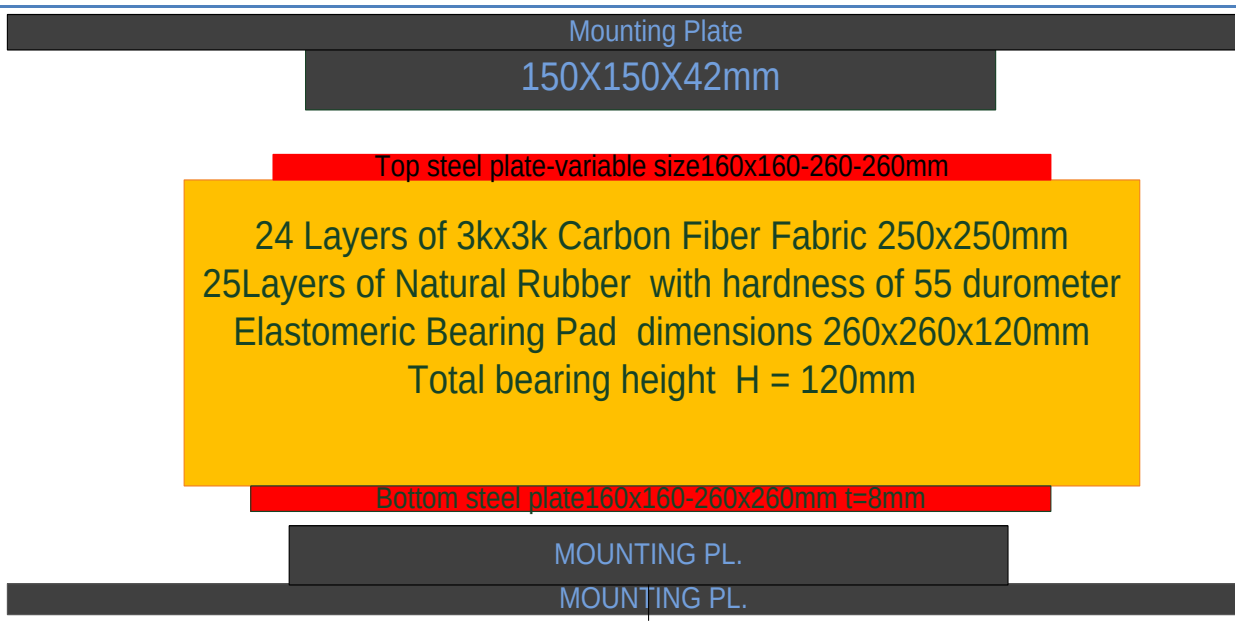

Figure 0.2 Seismic isolator test specimens (SB-CRFEI) cross-section view and material property

The 8 mm steel cover plates are not designed to fully cover the top and bottom surface of the bearing like the conventional seismic isolators. They are designed to partially cover and bond to the top and bottom surface of the bearing. This design feature is intended to make the SB-CFREI capable of sustaining higher equivalent viscus damping under higher lateral shear strain amplitude of loading. The isolator's expected damping feature and supporting discussions are presented in section 3.2.2 of this chapter. Another function of the partial cover plate is to transmit the vertical and horizontal shear load from the foundation to the CFRE bearing pads and the structural supports. In order to securely transfer the shear and compression induced forces to the isolator's bearings pad, the top and bottom plates are designed with five mounting holes of 19 mm diameter. For higher efficiency in production and implementation, the same hole spacing configuration was designed for all isolator's top and bottom steel plates with variable sizes, as shown in Figures 3.1 & 3.2. Five high strength steel insert plug (pins) with 18 mm diameter and total length of 20 mm (7mm to fit in the 8mm steel cover plate and 13mm to fit in and connect to the structural supports) were used as shown in Figure 3.12.

Variable steel cover plate dimensions of the SB-CFREIs provides the isolators with sufficient variation in bonding level in order to investigate the effects of bonding level on the isolator's

dynamic characteristics. The SB-CFREIs are also designed to be able to combine with other component isolators in order to study the effects of component configuration on the dynamic characteristic of the compound isolator as well. In conclusion, the four main objectives in design of the proposed isolator's test specimen are as follows:

1) Effective reduction of the base isolators size, weight, and production cost.
2) Sufficient implementation and isolation efficiency.
3) Combination capabilities for future development of simplified catalogue-based design method for low-cost isolators having certified characteristics.
4) Variation in bonding level (BL) in order to study the effects of bonding level on isolator's dynamic characteristic.

To reduce the innovative isolator's weight, the heavy steel sheet layers in the conventional seismic isolators are replaced by low weight, carbon fiber fabrics. "Carbon fibers exhibit excellent mechanical characteristics such as high elastic modulus (200–800 GPa), high tensile strength (2,500–6,000 MPa), and suitable fatigue life without creep or relaxation, so they are desirable candidates as reinforcement for FRP composite plates used in rubber bearings" (Moon et al., 2002).

3.2.1 SB-CFREI Deformation Mechanism

To allow the unbonded regions of the isolator's pad to move up and down freely as the isolator undergoes high lateral deformation, the CFREI's pad is elevated a distance "D" from the support base as shown in Figure 3.3a. The isolator with this specification and deformation mechanism is denoted (Elevated) SB-CFREI as shown in Figure 3.2 and 3.9-3.11. The unbonded region of the SB-CFREI's bearing pad will not be in contact with the upper and lower structural supports, therefore this new isolator bearing pad boundary condition is expected to provide the isolator with lower lateral stiffness and consequently higher isolation efficiency. The free regions of the SB-CFRI bearing pad contacts the structure's supporting plates at extreme lateral shear strain loading. At this level of lateral deformation, the isolator lateral stiffness is expected to increase due to the change in deformation pattern. This phenomenon allows the seismic isolator to achieve higher lateral stiffness at extreme lateral deformation. The nature and magnitude of the lateral stiffness increase is to be investigated in future research studies.

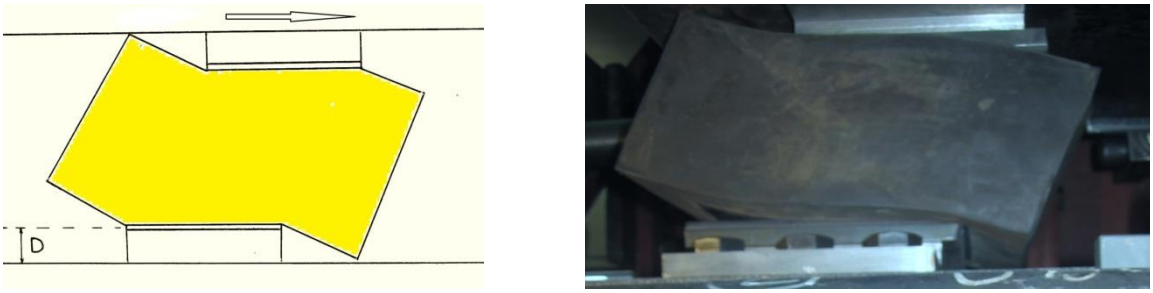

(a) (b)

Figure 0.3 Schematic (a) and experimental (b) deformation mechanism of ESB-CFREI under lateral shear load (D =50mm distance Isolator's bearing is elevation from supports)

Figure 3.3 (a) & (b) demonstrates the schematic and experimental deformation mechanism of a typical ESB-CFREI isolator, and Figure 3.4 shows the finite element deformation pattern of typical ESB-CFREI, UB-CFREI and bonded CFREI under lateral shear load.

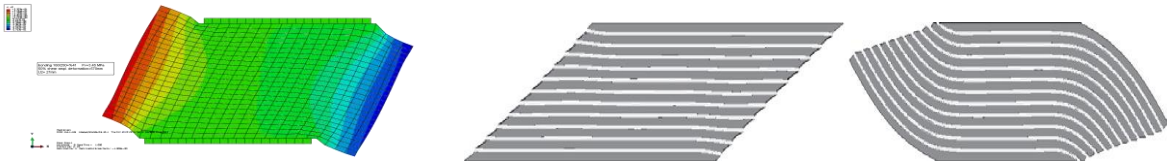

(B160) SU-CFREI (Toopchi-Nehzad et al 2010)

(a) ESB-CFREI (b) Bonded-CFREI (c) UN-BONDED-CFREI

Figure 0.4 Laterally deformed pattern of elevated semi-bonded, fully bonded and unbonded CFREI (Preliminary FE model)

3.2.2 SB-CFREI Damping and Energy Dissipation

The damping and energy dissipation advantages of FREIs in comparison with the SREIs, and the phenomenon causing high damping in the CFREI, are postulated by Kelly (1999), who states that; In contrast to SREIs, the bending flexibility of reinforcement fibers causes the plane cross section not to remain planar. On the basis of this hypothesis, interfacial slip of single fibers against each other in the threads due to vertical compression load and the curvature in the reinforcement sheets due to the bearing lateral deformation produces a significant amount of

frictional damping in reinforcement fibers, which results in considerable energy dissipation and is added to that of the inherent elastomer in the bearing.

Due to the unique deformation mechanism of the SB-CFREIs (Figure 3.3 & 3.4) under high lateral strain load, the fiber reinforcement layers experience higher curvature at high shear strain amplitude, as the unbonded regions of the CFRE bearing pad move up and down causing the fiber threads not only to rub against each other in the strands but also to slip against the surrounding rubber in higher extend, leading to greater values of friction damping that results in more considerable energy dissipation. Higher compression load on the CFRE pad is expected to increase the friction damping further. The test outcome is expected to support this postulate and show greater isolator damping values when compared with that of the bonded CFREIs (BL= 100%). Nevertheless, the unbonded regions of the SB-CFREI's bearing with lower level of bonding undergo higher vertical deformation, causing higher curvature in the fiber strands and consequently result in higher magnitude of damping.

3.3 Compound Isolator CSB-CFREI

The compound semi-bonded carbon fiber elastomeric isolator (CSB-CFREI) is a seismic isolator made by combining two or more SB-CFREI component isolators. The combination configuration depends on the seismic demand. The combination configuration and the numbers of component isolators required to create a compound isolator (CSB-CFREI) depend on the expected axial compression and the lateral earthquake induced loads. The combination of the component isolators can be in vertical and horizontal directions, as shown in Figure 3.5. The configuration depends on the desirable target isolation frequency or stiffness. Stacking isolators in a vertical direction will effectively reduce the effective lateral stiffness of the compound isolator. Kelly (2002) also supported this idea and stated that in fiber-reinforced bearings, "it is possible to effectively employ two bearings in a stacked pattern of application in which one simply sits on the top of the other".

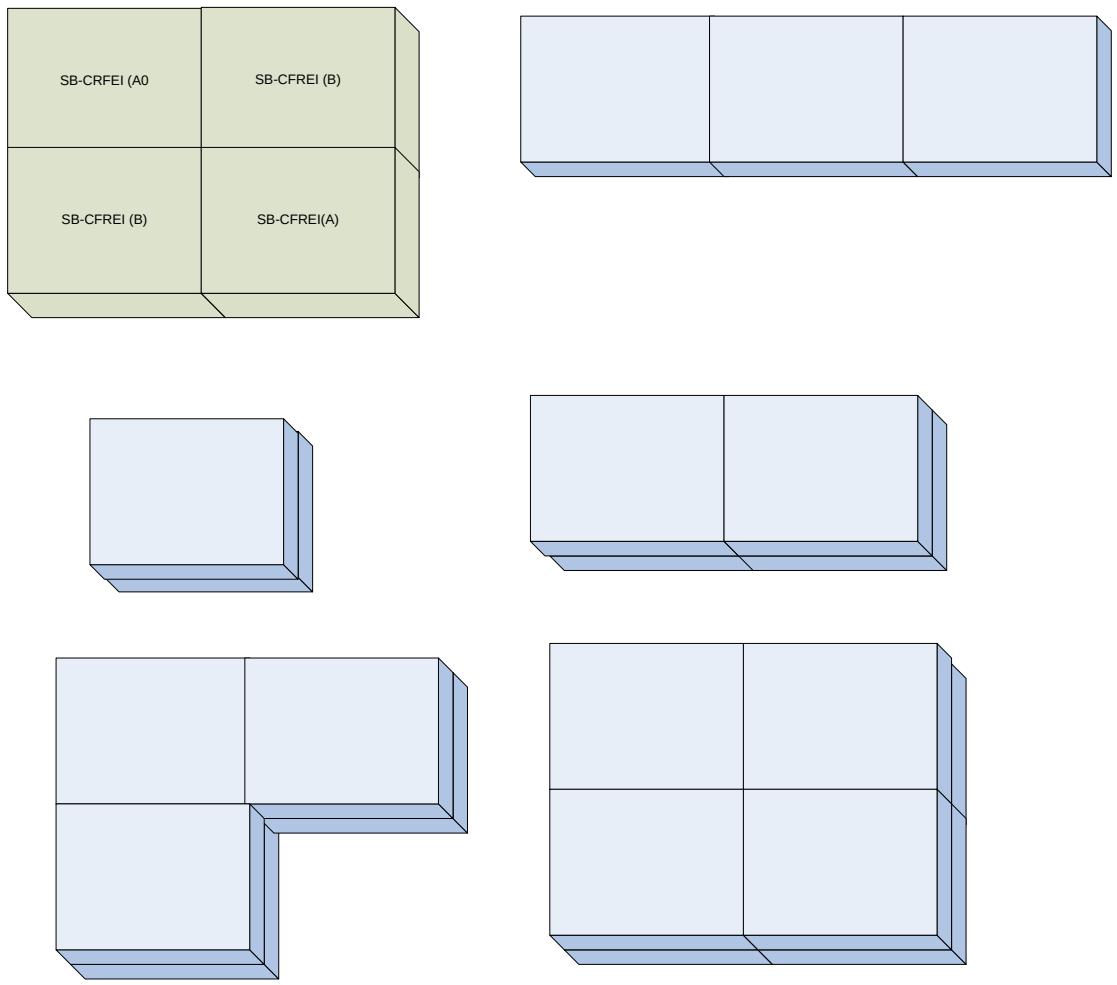

Figure 0.5 Sample combination configuration of compound isolator (CSB-CFREI)

3.4 Design Advantages of SB-CFREI and CSB-CFREI in Comparison with Typical Conventional SREIs

Unlike the fully bonded feature in conventional seismic isolators, the innovative isolator with semi or partially bonded plates on top and bottom of the SB-CFREI enables the isolators to deform laterally with a new deformation mechanism and is expected to introduce a higher energy absorption capability.

The semi-bonded CFRI is expected to provide a higher lateral deformation than the bonded conventional isolator. This considerable increase in lateral deformation is due to a lack of

flexural rigidity of the reinforcement sheets, and also to the lateral deformation mechanism and unique design characteristics of the SB-CFREI described in section 3.1.1 and 3.1.2 of this chapter.

The conventional base isolators are not capable of demonstrating such a unique and extended lateral deformation. This deformation is expected to reduce the lateral stiffness of the semi-bonded CFRE isolator considerably, and increase the isolation efficiency (IE).

In addition to the inherent damping of the elastomer, the interaction between the elastomer, and the fiber fabric reinforcement, the CFR isolator introduces an extra energy dissipation mechanism to the isolator (Kelly, Toopchi). For instance, the test result indicates that this damping increase could be as high as 8-14% when the CFRE isolator is constructed with unfilled, soft neoprene (low-damped elastomer). The conventional seismic isolators with steel reinforcement sheets are not capable of providing such a significant increase in damping mechanism. The schematic state of stress under lateral deformation for SB-CFREI and the fully bonded conventional isolator is shown in Figures 3.6 and 3.7. The tensile stress on both ends (unbonded regions) of the SB-CFREI is expected to be much lower than that of the bonded conventional isolators as a result of lower tensile stress demand between the rubber and fiber layers; considerable cost saving in fabrication of the innovative isolator is expected.

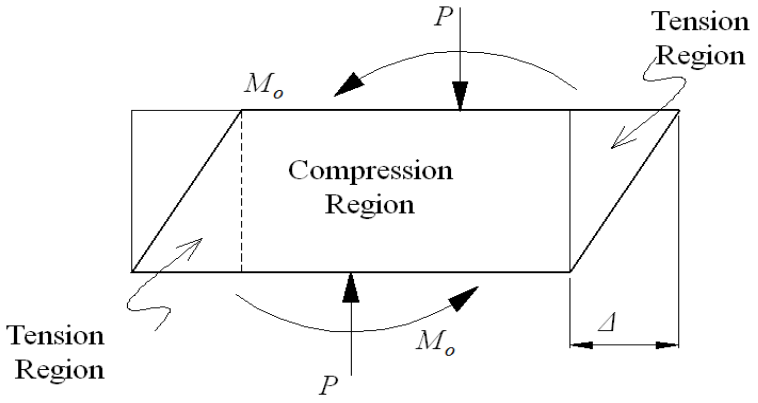

Figure 0.6 State of stress of laterally deformed, fully bonded isolator (Kelly et al., 2012)

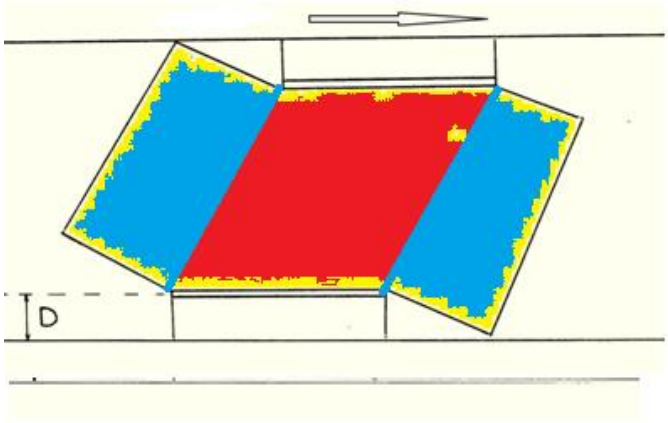

Figure 0.7 State of stress of laterally deformed SB-CFREI, Blue regions represent low tension or compression and red is the compression zone.

3.5 Design Advantages of the Innovative SB-CFREI over Unbonded Carbon Fiber-Reinforced Elastomeric Isolators (UB-CFREI)

The expected capabilities and advantages of the component and compound Semi-Bonded CFREI in comparison with the unbonded CFRE isolator are summarized as follows:

1) Due to the presence of top and bottom steel cover plates (partially bonded), SB-CFRE isolator will provide a better and more reliable construction mounting due to the presence of secure shear pin connections.
2) SB-CFRE isolator bearings can be used independently or in combination with one or more SB-CFREI to form the CSB-CFREI, which is expected to provide the desirable target horizontal and vertical stiffness and damping with higher levels of efficiency in construction. Higher efficiency is mainly due to light weight and small size of the component isolator along with easy handling and transportation.
3) SB-CFREI is capable of resisting low-level tension, resulting from a possible over-turning movement in low rise steel structures.
4) SB-CFRE and CSB-CFRE isolators have a special combination capability design feature that is expected to support future establishment of simplified, catalogue-based design provisions for application in ordinary low-rise public and residential buildings.

5) SB-CFRE isolators provide better and higher isolation stability, since unlike UB-CFRE isolators they do not rely fully on friction to transfer the earthquake induced shear loads to the structural supports.

3.6 Fabrication Procedure of the Innovative SB-CFRE Isolators

Fabrication of the SB-CFREI was carried out under the supervision of Professor Carlos Ventura, managing director of the Earthquake Engineering Research Facility (EERF) of the University of British Columbia. The first fabrication attempt started at the Scougal Rubber Corporation, which is a facility experienced in the fabrication of conventional steel reinforced elastomeric isolators in Nevada, USA. The mold was designed and manufactured and the carbon fiber fabric was cut to size, impregnated to the selected bonding compound, and placed in the mold with the rubber layers. The mold's dimensions were designed to provide large pads of 560×560×120 mm. Each bearing pad was to provide four CFRE bearings with dimensions of 260×260×120 mm. A total of three large molds for fabrication of 12 CFRE pads were placed under high pressure and temperature for over 8 hours to achieve a well-vulcanized bonding between elastomer and carbon fiber layers. The bearings were cut to size and were closely examined for fabrication quality, and the after precise inspection some porosity and de-lamination (de-bonding) were noticed. The fabrication process was repeated three times and unfortunately all the fabrication attempts were unsuccessful and rejected due to the presence of voids and de-lamination in the center regions of the large bearings. Figure 3.8 (a) and (b) shows these voids and delaminating in the rejected fabricated bearings.

(a) (b)

Figure 0.8 Porosity (a) and de-lamination (b) in the bearings detected in the first fabrication phase

The fabrication of 12 bearings was resumed in BC Rubber-Epic Polymer Corporation in British Columbia, Canada with some modification to the adhesive bonding compound and the fabrication technique; as a result the fabrication was completed successfully. The top and bottom steel cover plates were glued to the CFRE bearing pads with high-strength adhesive compound. Figures 3.9, 3.10, 3.11, and 3.12 shows the fabricated SB-CFREI, mounting plates and shear pin connections.

Figure 0.9 Fabricated SB-CFREI with experimental top and bottom mounting plates

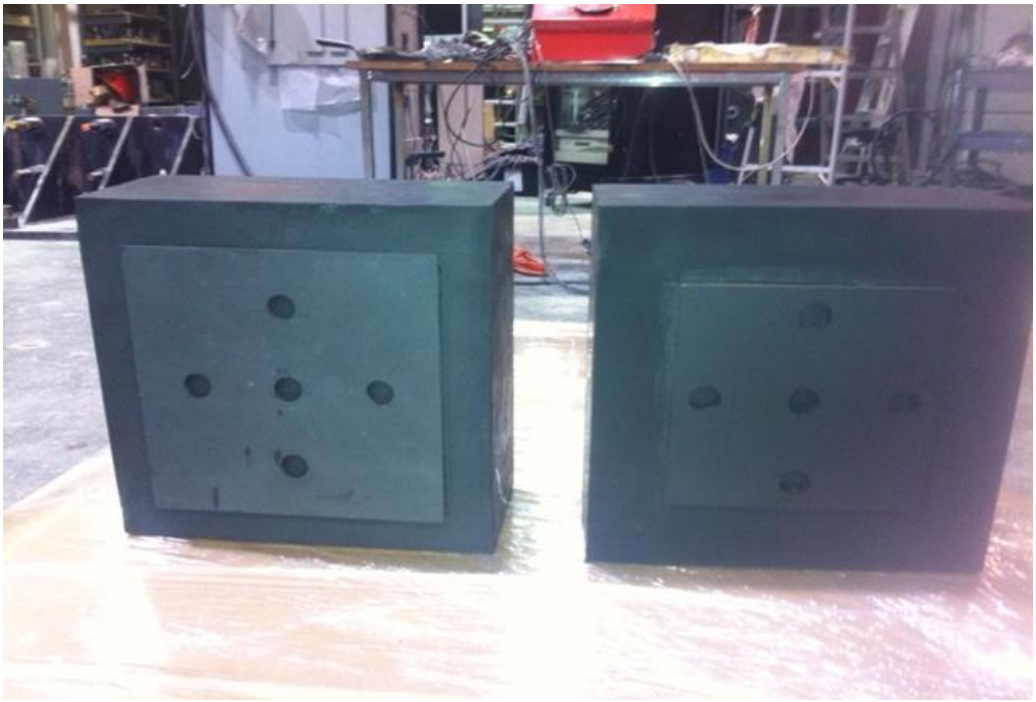

Figure 0.10 Fabricated SB-CFREI with top and bottom Steel cover plates

Figure 3.11 Fabricated SB-CFRE isolators meet all design specifications

Figure 0.12 Shear pin designed to transfer the shear force from structural support to the isolators

3.7 Application of Carbon Fiber as Elastomeric Reinforcements and Manufacturing Cost Estimate

3.7.1 Application of Carbon Fiber to lower Production Cost

To improve deficiencies in base isolation technology, adaption of other alternatives is necessary. Implementation of carbon fiber material in elastomeric isolators to replace the heavy steel shim in conventional seismic isolators has provided satisfactory performance in recent studies. This material not only has the advantage of having high strength but also has considerably lower weight in comparison to steel reinforcements. It has been shown that the lateral response characteristics of FREI bearings are an indicator of the performance of the isolator and "are equal, if not superior, to conventional SREI bearings" (Kelly, 1999; Moon et al., 2002). Additionally, a significant saving in production cost may be achievable as a result of less labour-intensive fabrication process requirements (Kelly and Takhirov, 2002). Carbon fiber-reinforced bearing "pads designed for the same natural frequency are thinner and lighter than those of steel-reinforced, because of both reduced thickness of the reinforcing material and the inherently lighter weight of carbon" (Campbell, 2004).

FREI bearings can be used as an alternative to conventional SREIs (Kelly 1999b). Similar to SREIs, FREIs are also elastomeric bearings in which elastomer layers are bonded to the fiber fabric reinforcement layers instead of steel-reinforcement plates. This change of the reinforcement layers may lead to significant cost savings as FREIs become much lighter in weight compared to SREIs. Additionally, labour expenses can be reduced if FREIs are produced in long rectangular strips through a mass production manufacturing technique and then cut to the required size (Kelly 2002).

3.7.2 Production cost estimates and comparison

Low production cost is the prime feature of the proposed SB-CFREI. In this section an estimate of production cost of the innovative seismic isolator is presented. The production cost is compared with that of the conventional SREIs on the basis of design compression load. The manufacturing cost is based on the documented retail custom order of a limited quantity of 12 isolators, fabricated by the Epic Polymer-BC Rubber Company (Figures 3.9-3.12).
Production cost includes:

1- Fabrication
2- Material
3- Sample testing for selection of proper high strength adhesive bonding compound
4- Connection mounting pins (10 per isolator)
5- Delivery cost to EERF
6- Tax and other governmental cost

Total cost of 12 isolators = CAD $10,000.00 (each isolator costs CAD $833.33)
SB-CFREI (component isolator) is capable of supporting axial compression load of 250kN. It is important to mention that although the isolators have been tested for this axial compression load, the ultimate loading capability is higher. Production cost of a conventional SREl from DIS (Dynamic Isolation System) Company on the basis of a design compression load of 700kN is (US $4000.00) equal to CAD $5400.00 (reference DIS price quote).
To meet the above SERI design capability, a triple compound isolator with 3 component isolators is required with a retail production cost of 3 x $833.33 = $2500. This compound isolator has an axial load capacity of 750 kN. Comparing the production cost of CSB-CFREI/SREI = 2500 /5400 = 46%. It means CSB-CFREI production cost is estimated to be around 46% of that of SERI on the basis of a retail costume order of a few isolators.
Mass production of the proposed isolator's CFRE pad is possible and will provides considerable extra savings. The mass production technique is anticipated to considerably lower the production cost of SB-CFREI to around1/3- 1/2 of the custom made manufacture cost of the12 fabricated isolators by Epic Polymer Company. Therefore, by mass production the manufacturing cost of this specific compound SB-CFREI can be estimated to reduce by a factor of 1/3-1/2 (of $2500), around CAD $850-$1250.00, which means with the proper mass production technique, CSB-CFREI estimated production cost having the same design compression load capability is anticipated to be as low as1/4 of that of the conventional SREIs.

CHAPTER 4: EXPERIMENTAL PROGRAM

4.1 Summary

A program of testing isolators is normally part of every seismic isolation project. The nature and extent of the testing varies, depending on the isolation system and the project's goal and objectives. For an established isolation system, testing usually includes preliminary tests of the prototype to verify the assumed design properties, and a quality control test of materials of the completed isolators prior to installation in the structures. If the isolation system is new and unproven, then more extensive testing is necessary to determine the basic properties of the systems (Taylor and Igusa, 2004).

To investigate the performance and dynamic characteristics of the proposed isolator, a series of cyclic lateral shear and axial compression tests was conducted on the innovative specimens of Semi-Bonded Carbon Fiber Reinforced Elastomeric Isolators (SB-CFREI). The experimental tests were not only conducted on a single isolator as a "component isolator" but also on "double and triple compound isolators" as well. In total over 200 different experimental tests were conducted on the 12 fabricated isolators. Cyclic monotonic and dynamic lateral shear and axial compression loading with different combinations and test configurations was conducted to investigate the dynamic characteristics and performance of the component and compound isolators. To have a better insight into the isolator's performance under earthquake excitation, long duration cyclic tests were conducted on the isolator test specimens. Component material tests were also conducted in UBC's civil engineering material laboratory to study the hyper-elastic behaviour of the rubber as the isolator's main material component. In the following section of this report, the equipment set-up, test sequences, input loading signals, and related outcome and achievements are presented.

4.2 Test Specimen's Design Specifications and Mounting Features

Specimens of SB-CFREI have been fabricated in British Columbia by Epic Polymer-BC Rubber Company in accordance with the given design specifications. All the test specimens are made of natural rubber with a hardness of 55 durometer (ASTM shore A). These isolator's specimens are partially bonded with a certain bonding level. The bonding level (BL) is defined as the ratio of bonded steel cover plate area divided by the surface area of top or bottom CFRE bearing pad. In

this research project all CFRE pads have the same top and bottom surface dimension of 260×260 mm. In total 12 test isolators in six pairs with different bonding levels have been fabricated. These plates and five sets of steel shear insert plugs (pins) securely transfer the shear and compression forces from the structure's supports to the isolator's CFRE bearing. The schematic and fabricated SB-CFREIs are shown in Figures 3.1, 3.2, 3.9 to 3.12 and 4.1 to 4.3.

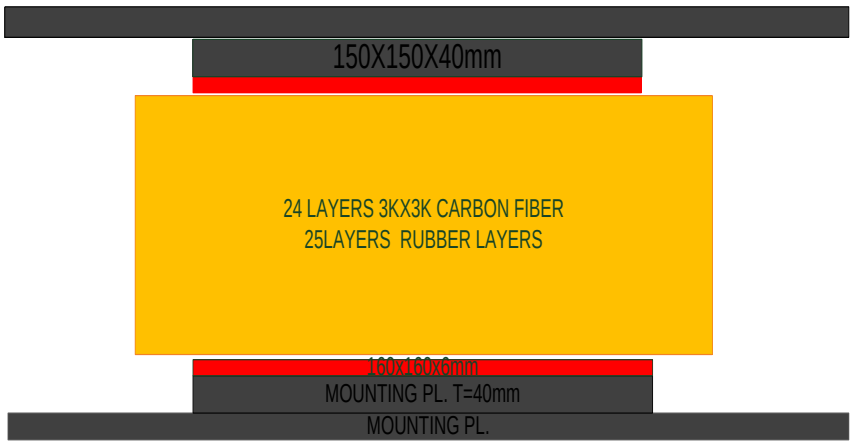

Figure 0.1 SB-CFREI with top and bottom experimental mounting plates

The CFREI bearings have dimensions of 260×260×120 mm, with 24 layers of plain weave tape 3k×3k carbon fiber fabric with dimensions of 250×250 mm, and 25 layers of rubbers of 260×260 mm. The schematic and fabricated SB-CFREI and the experimental mounting plates along with connection pins are shown in Figures 4.1 to 4.3. The bearings have been designed in 6 identical pairs; this feature not only meets the requirements of ASCE 7-05 provisions that require experimental testing of two isolator prototypes of each type when manufacturing new seismic isolators, but also provides the capability of testing them with dual shear configuration to achieve more precise test results with standard test configuration. To prevent premature de-lamination damage of the carbon fiber reinforcement layers at the bearings' edges under cyclic loadings, a 5 mm rubber cover is designed to provide adequate protection to the isolator bearings as shown in Figure 3.1. Further information related to the test specimen design features is presented in section 3.2 of the thesis.

Figure 0.2 Fabricated SB-CFREI with top and bottom experimental mounting plates and shear pin connection

Figure 0.3 Fabricated SB-CFREI with top and bottom experimental mounting plates (left) and typical SB-CFRE isolator (right)

4.3 Experimental Testing Program

The lateral shear and axial compression cyclic tests were conducted at the Earthquake Engineering Research Facility of the University of British Columbia (UBC-EERF) on 12 isolators to investigate the dynamic characteristics and performance of the proposed component and compound isolator (SB-CFREI and CSB-CFREI) under the defined cyclic input loads. Long

duration cyclic loading tests and component material tests were conducted as well, as part of the testing program.

4.3.1 Axial Compression Tests and Objectives

The prime objectives in conducting the axial compression test are to study the isolator's performance under defined axial compression cyclic loads. In this task the isolator's effective compression stiffness and modulus were defined by the compression test outcomes. By conducting these tests, the isolator's isolation efficiency (IE) defined by the ratio of the axial compression stiffness to that of the lateral ($K_{eff\text{-}v}$ / $K_{eff\text{-}h}$) were determined as well. Isolation efficiency demonstrates the isolator's efficiency and performance. The effect of bonding variation on the effective compression stiffness and modulus of the component and compound isolators was investigated through this part of the experimental testing. Axial compression input load signals are presented in Figure 4.8 and 4.9 of this chapter.

4.3.2 Lateral Shear Tests and Objectives

The horizontal shear test objectives are to investigate the following important mechanical and dynamic properties of the isolator:

1) To determine the effective horizontal stiffness of each isolator type under all levels of shear strain amplitude $K_{heff(\gamma)}$.
2) To determine the shear modulus of each isolator type $G_{Heff(\gamma)}$.
3) To investigate the damping and energy dissipation capability of the isolator type by plotting the force-deformation hysteresis loops and to determine the effective lateral equivalent viscous damping ratio ζ_{eff} for each loading cycle.
4) To investigate and to determine the effect of bonding variation on the isolators effective lateral stiffness and damping.
5) To experimentally study the effect of component combination configuration on the effective lateral stiffness and damping of the resulting compound isolator.
6) To determine the isolator's isolation efficiency (IE).
7) To study the scragging behaviour of the rubber as the main isolator material component. The shear stiffness of the isolators that is loaded for the first time in shear is known as "unscragged stiffness" and it is always higher in first cycle than subsequent load cycles,

known as “scragged stiffness.” After a period of time, the isolator recovers some or all of its unscragged stiffness. This process is referred to as “recovery.” The effect and importance of the scragging and recovery should be evaluated on a project-specific basis (Taylor and Igusa, 2004).

4.4 Test Setup and Instrumentation

The test equipment setup is capable of applying controlled lateral displacement and axial compression load to the test specimen simultaneously. Based on isolator specimen specification, experimental program requirements, efficiency, and precision, dual shear test configuration is selected in conducting the experimental program. The vertical actuator was assembled to apply axial compression load on the top center of the thick steel plate, and the horizontal actuator was set to apply strain loading on the middle pull-push plate shown in Figures 4.4 and 4.5. The vertical actuator puts compression load under load control and the horizontal actuator imposes lateral shear load under displacement control. In order to measure vertical displacements, four Novotechnik model TR linear potentiometers were installed along the perimeter of the upper and lower plates to monitor the vertical displacement, and two Celesco PT101 string potentiometers were installed on the push-pull plate to monitor the horizontal displacements along with load cell of the actuators, as shown in Figure 4.6.

Figure 0.4 Equipment set-up showing both vertical and horizontal actuators hooked-up to test machine

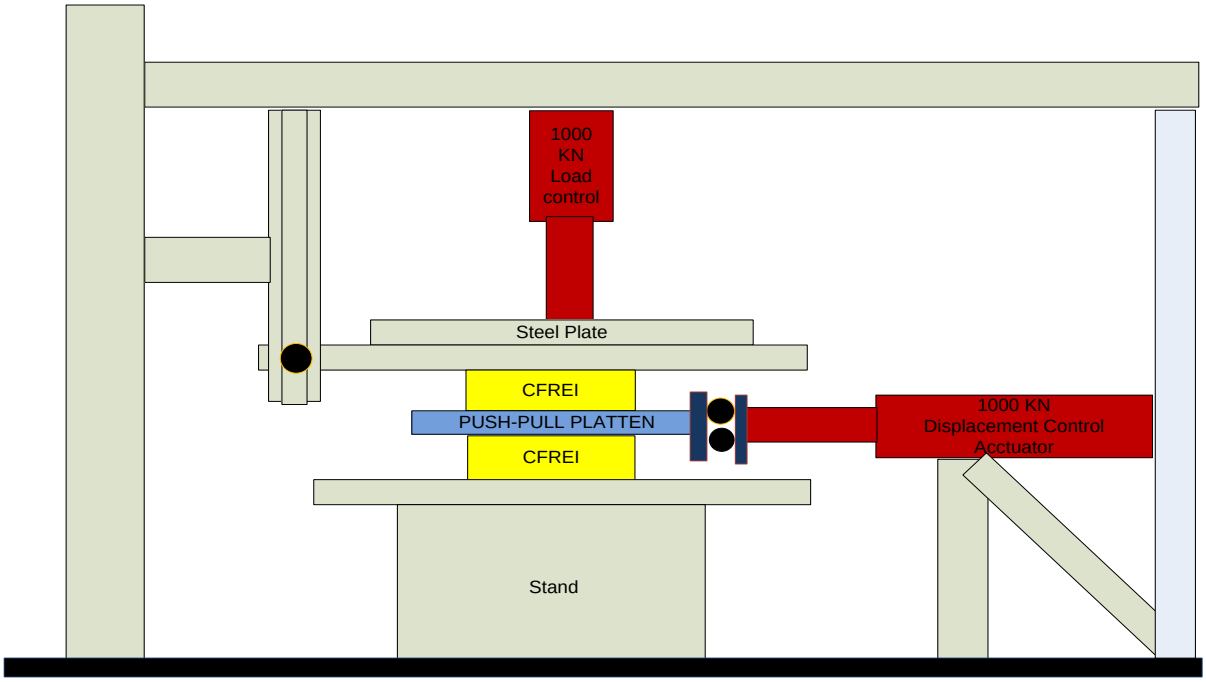

(a)

(b)

Figure 0.5 Equipment set-up (a) Schematic and (b) Experimental

Figure 0.6 Testing apparatus with dual shear configuration was fabricated in UBC- EERF for lateral cyclic loading of single component, double and triple compound isolators

The limit detector was set in accordance with the defined load and displacement limits to lock up and stop the testing process in case of accidental loading exceedance.

To be able to perform the cyclic test on the compound isolators CSB-CFREI, the push-pull plate and top and bottom steel plates with the dimensions of 1000×500×80 mm were designed and fabricated as shown in Figure 4.12. The two horizontal and vertical actuators with high loading capabilities (max compression load of 1200 kN) have been selected. The details of the equipment set up, software, and related instrumentation configuration is presented in the following section.

4.4.1 Instrumentation and Control System

The instrumentation and control setup used in the UBC Civil Engineering structures lab is comprised of a four-channel MTS Flextest GT control system and a computer-based data acquisition system. The MTS Flextest GT control system is run by Structural Test System (STS) software, version UBC 1.0, and controls a 70 gpm hydraulic power supply (MTS model 506.62)

and MTS model 293.22 hydraulic service manifold (dual station) that feeds the hydraulic actuators. The horizontal actuator is an MTS 244.51 200 Kip dynamic actuator with a stroke of 20 inches, and the vertical is a MTS 202.02 200 Kip with a 6-inch stroke simulating the lateral and compression load signals.

4.4.2 Data Acquisition

The data acquisition is comprised of a National Instruments SCXI signal conditioning system (using SCXI-1520 modules), a PCI-6035E data acquisition board (with 16 bit analog input and 16 bit analog out resolution spread over a range of +/- 10Volts), and Dasylab (ver. 11) software running on a windows XP based computer. The signals from displacement transducers (Celesco PT101 string potentiometers and Novotechnik model TR linear potentiometers) assembled on the test apparatus, along with the analog load and displacement signals from the two hydraulic actuators (hooked up to the MTS Flextest system) are acquired, displayed, and stored on the Dasylab computer system. All linear variable differential transformers (LVDTs) were calibrated with the measuring gauges as shown in Figure 4.7 before conducting each testing series. Figure 4.8 shows the gauges installed to monitor the uplift displacement of the testing frame (girder and its bolted connections) as the result of vertical actuator's reaction when conducting axial compression tests. The reading from these gauges was used to correct the final recorded load displacement data. Celesco PT101 string potentiometers and Novotechnik model TR linear potentiometers and their locations on the test apparatus are shown in Figure 4.9.

Figure 0.7 Gauges installed to monitor the frame girder and bolted connection uplift as the result of vertical actuator's reaction force when conducting axial compression tests

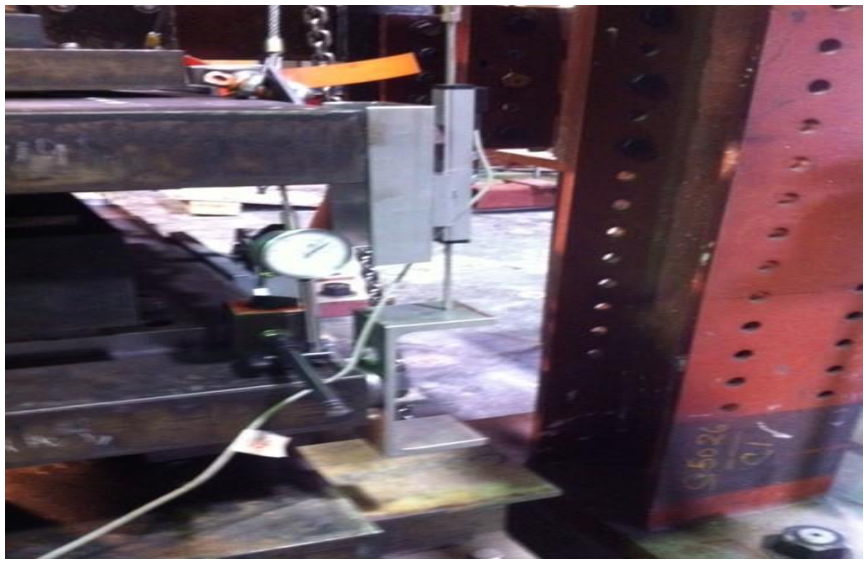

Figure 0.8 Calibrations of the LVDTs (Novotechnik model TR linear potentiometers) by measuring gauges

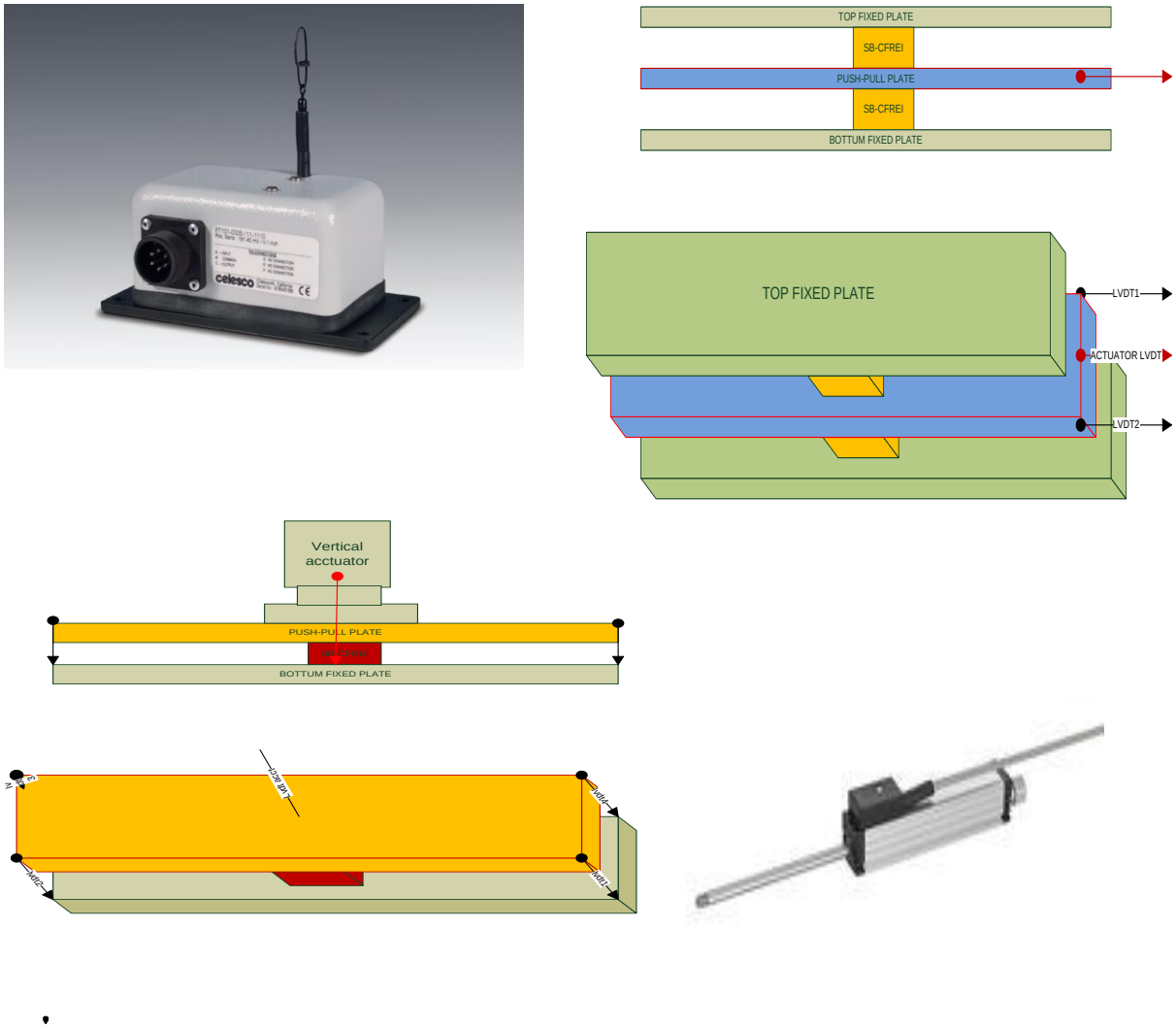

Figure 0.9 Celsco PT101 string Potentiometer (upper left), locations of the linear displacement and two analog load and displacement transducers from the 2 hydraulic actuators (Celesco PT101 string and Novotechnik TR linear potentiometers) on the test apparatus (up right & lower left), Novotechnik TR linear potentiometer (lower right)

4.5 Testing Configurations

The test apparatus was designed and fabricated consistent with "Dual Shear" test configuration. Testing of the seismic isolators requires a free lateral translation and fixity against rotation of the isolator's top. To achieve such a frictionless rolling or sliding interface in practice is difficult. The dual shear configuration not only does not need the sliding or rolling interface but also provides more accurate and reliable test outcomes since the test results reflect the average properties and performance of two identical isolators. Figures 4.10 and 4.11 show the schematic

and experimental dual shear test configuration for single, double, and triple isolator combinations.

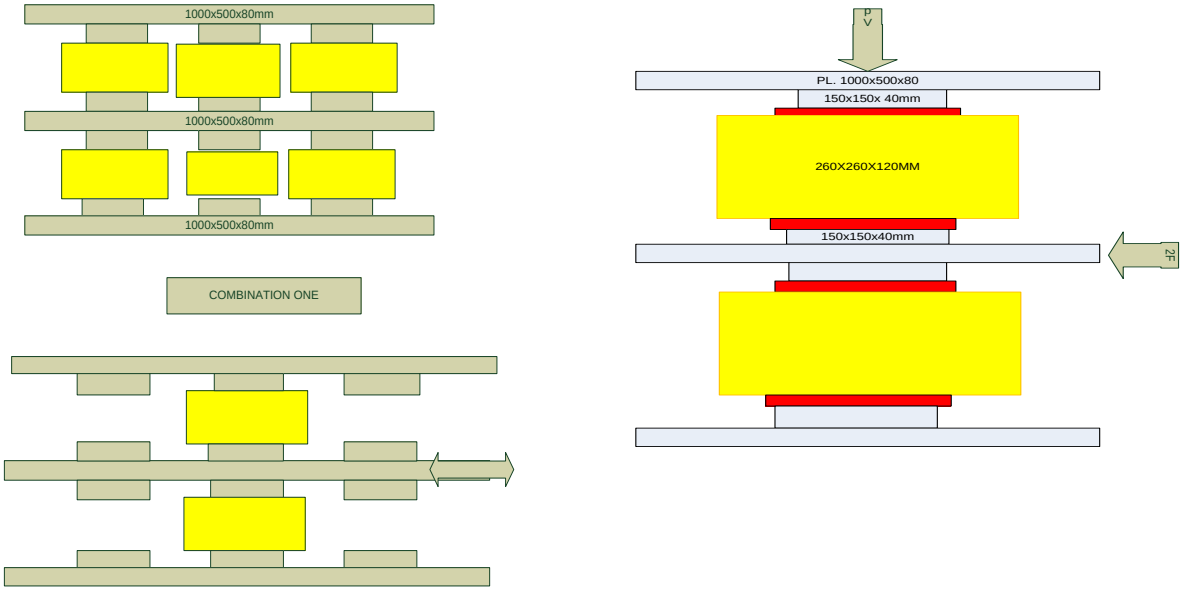

Figure 0.10 Schematic dual shear test configuration for single and triple isolator combinations

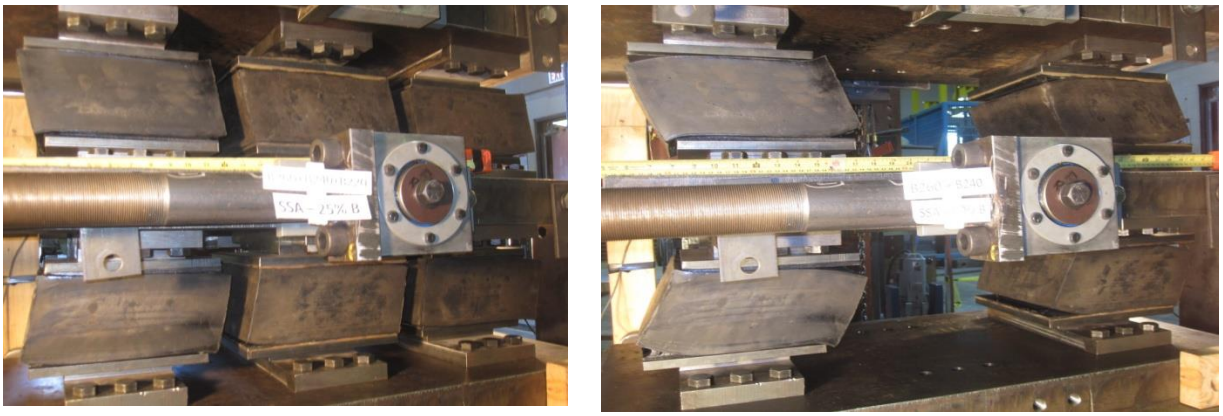

Figure 0.11 Experimental testing with dual shear configuration set-up double (right) and triple (Left) compound isolators assembled in the test apparatus under lateral shear load

4.6 Lateral Shear Input Loading Signals

The horizontal cyclic tests were conducted on component and compound double and triple isolators under constant vertical compression pre-load of 250, 500, and 750 kN respectively. The lateral shear strain amplitudes (SSA) were set to 25%, 50%, 75%, and 100%t_r. where t_r is the

total thickness of the rubber layers in the isolator. In the first phase of the experimental program each isolator specimen was subjected to two levels of shear strain loading in two complete loading and unloading cycles. The lateral shear cyclic loadings were applied while isolators were supporting the compression pre-load simultaneously. Input monotonic and dynamic horizontal cyclic load signals for all isolators are shown in Figures 4.12 and 4.13.

4.6.1 Low Frequency Monotonic Lateral Cyclic Tests

This part of the horizontal testing contains a monotonic lateral loading on all isolator types under constant vertical compression load of 250 kN, with displacement control to achieve shear deformation of SSA equal to 25%, 50%, and 100%t_r (28.75, 57.5 & 115 mm). These displacements were imposed on the isolators in accordance with dual shear configuration. By conducting this task, the force-displacement hysteresis diagrams for defining the effective damping for the isolators were plotted. Lateral cyclic tests were repeated and the force-displacement diagram for second complete cycles was achieved to study the isolator's rubber component performance. In subsequence sections, the effective lateral stiffness and the force-displacement diagrams obtained will be compared with those obtained from the finite element analysis.

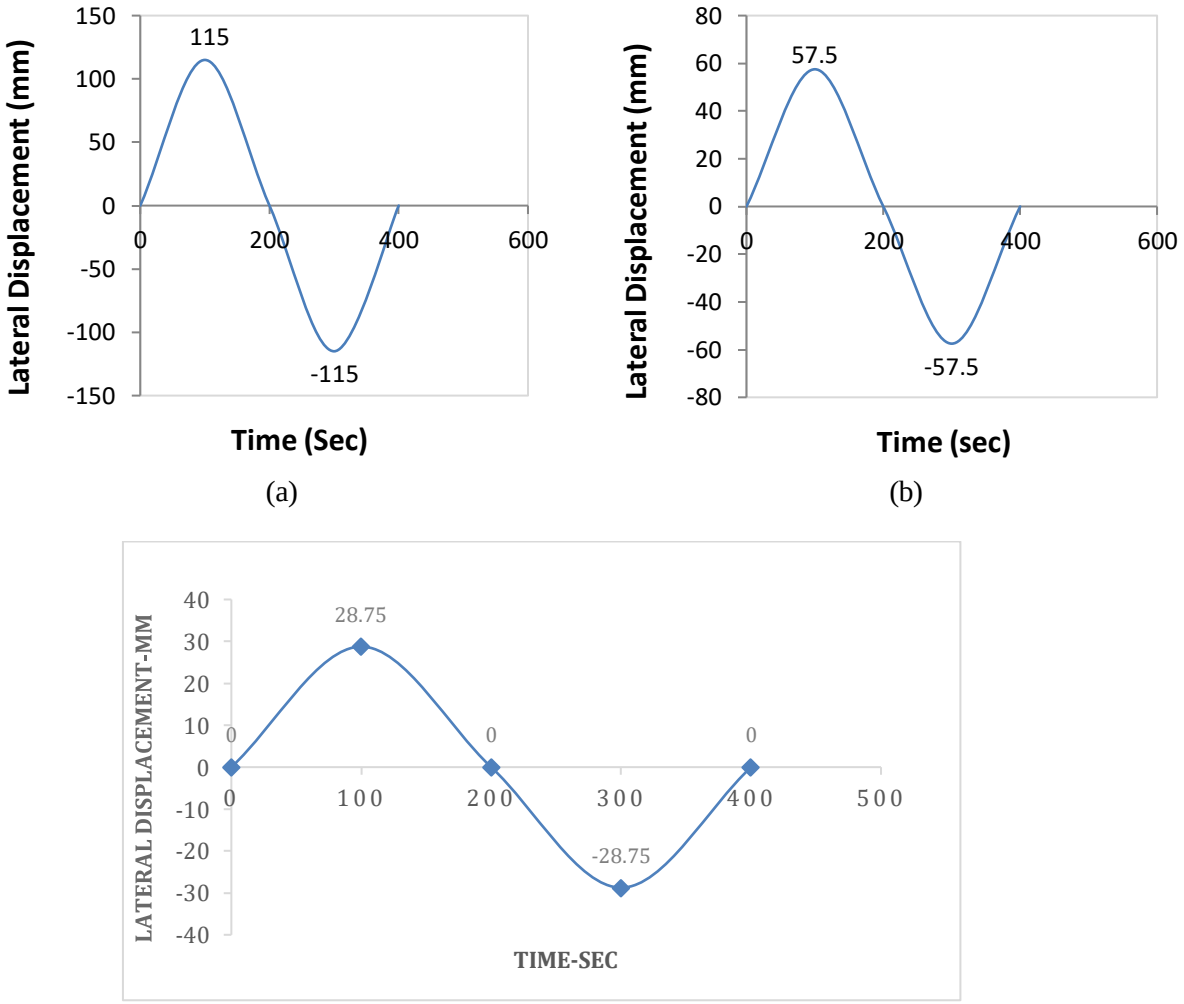

Figure 0.12 Low frequency monotonic input lateral load signal; (a) SSA=100%t_r, (b) SSA=50%t_r and (c) SSA=25%t_r

4.6.2 Lateral Shear Dynamic Load Input Signal

In conducting the experimental task an average displacement rate of 57.5 mm/sec at shear strain amplitude of 50%t_r was selected for the lateral cyclic strain loading. This displacement rate is consistent with the lateral input strain loading used by Kelly (2002), and Moon et al. (2003).

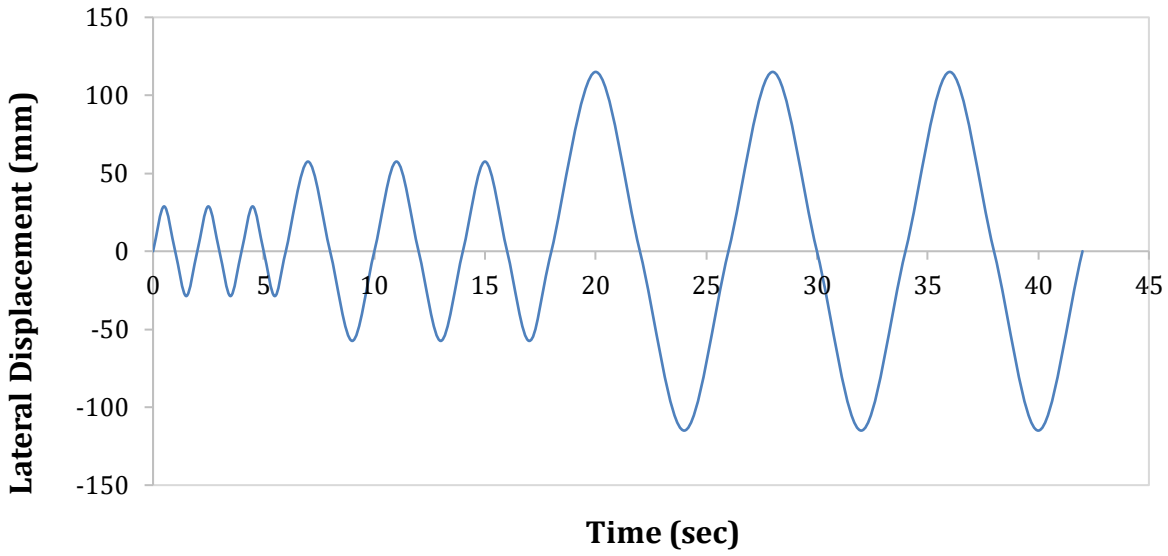

Figure 0.13 Dynamic lateral load signal (SSA=25%, 50%, & 100%tr)
(28.75, 57.5 & 115 mm amplitude under constant compression pre-load of PL 250, 500 750 kN)

4.7 Compound Isolators Lateral Shear and Axial Compression Cyclic Testing

To investigate the mechanical and dynamic properties of compound isolators, different vertical compression and lateral shear cyclic tests were conducted on:

1) The compound isolator created by two SB-CFREIs (compound double isolator).
2) The compound isolator created by three isolators (compound triple isolator).
3) The compound isolator created by combining one fully bonded isolator and other partially bonded isolator types with different bonding level, combined in a horizontal stacked configuration.
4) The compound isolators created by combining different isolator types, each with different bonding level, combined in horizontally stacked configuration.

4.8 Input Axial Compression Load Signal

The isolators were tested under vertical load control. The axial compression input load signal monotonically increased load on the test specimens to different levels of constant pre-loads of PL =116, 233, 466, and 600 kN, and then continued with three fully reversed cycles of loading with amplitude of $\Delta P = \pm 25\%PL$. In the final stage the specimens were monotonically unloaded. The

input compression load signals for component and compound isolators are presented in Figures 4.14 and 4.15. The blue dotted lines represent lower level of pre-load levels of PL= 116, 233, and 348kN, and the red line represents the higher pre-load level of PL= 233,466, and 600kN.

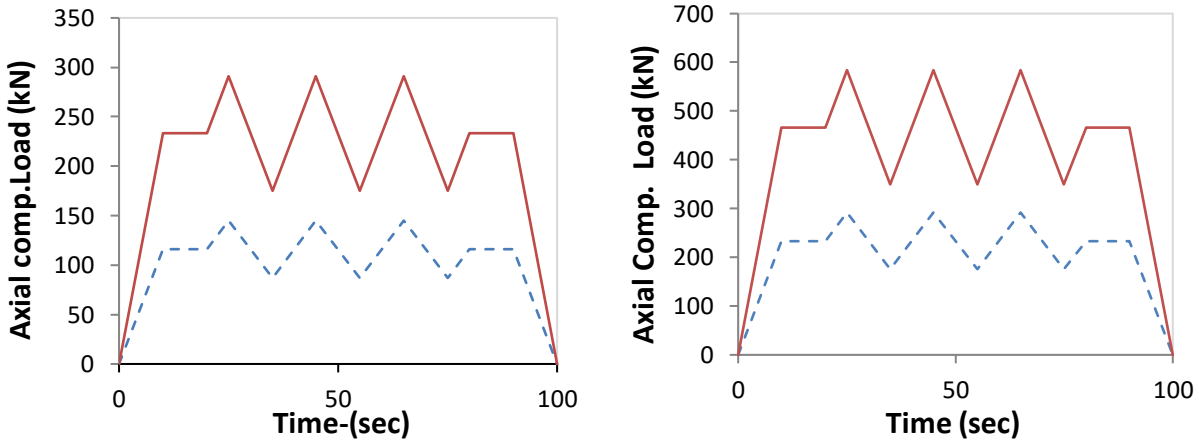

(a) (b)

Figure 0.14 (a) Two levels of Axial Compression Input Load Signals for component isolators PL=116 & 233 kN, (Dotted line) and (b) Two levels of compression load signals for Compound Double Isolators PL=233 & 466 kN(Red)

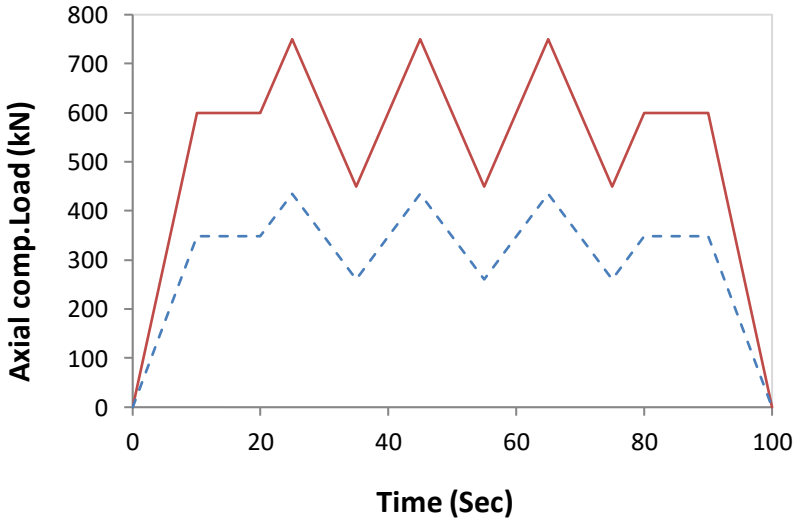

Figure 0.15 Two levels of vertical compression loading signal for triple compound isolator (stacked horizontally, PL= 348kN in doted line and 600 kN in red)

4.8.1 Remarks

1) Lateral cyclic tests were conducted with the input lateral loading signals containing three complete cycles of loading with 25, 50, and100% of t_r shear strain amplitude (based on rubber thickness of t_r = 115mm) under constant vertical compression pre-load (PL) of 250 for single, and 500 and 750 kN for double and triple compound isolators, respectively.
2) Safety precautions were considered by setting a limit detector on the test control system for lateral displacement and compression loads to prevent any unexpected extreme loads or lateral displacements that could cause sudden failure of the specimen and the test apparatus. In some cases, this type of failure could also harm the testing staff.
3) All lateral cyclic load amplitudes were in ascending (increasing with time) pattern.
4) All tests were conducted at room temperature and the data was sampled at 50 sample per second for vertical compression and lateral cyclic tests.

4.9 Effective Lateral Stiffness and Damping of Component Isolator and discussions

The average effective lateral stiffness $K_{eff\text{-}h(\gamma)}$ and effective equivalent viscous damping $\zeta_{eq(\gamma)}$ of the component isolator at shear strain amplitude of (γ) for each cycle are defined using the equations [1] – [5] by Naeim and Kelly (1999), Chopra (1995) "Theory and Applications to Earthquake Engineering (2nd edn)" and recommended by ASCE and FEMA. The effective lateral stiffness $K_{eff(\gamma)}$ and equivalent viscus damping $\zeta_{eq(\gamma)}$ are determined and shown in Table 4-1 for shear strain amplitudes of 25, 50, and 100% of t_r for all component isolators.

It is important to mention that low-damping natural rubber with equivalent viscous damping of 2-3% is selected as the isolator's elastomer material. The higher damping values presented in Table 4-1 are attributed to:

1- Frictional damping of the carbon fiber
2- The contribution of the isolator's unique deformation mechanism

The supporting discussion on the above two phenomena, especially their contribution to increased damping in higher shear strain amplitude of loading, is provided in section 3.1.4 of the thesis. The value of the effective lateral damping in table 4-1 for isolators with a lower bonding

level (BL), such as the B160 isolator, is much higher than those isolators with higher BL, such as B240 and B260. This increase in effective damping can be due to higher curvature and deformation of the unbonded region of the CFRE bearing pad, causing the carbon fiber to contribute higher frictional damping to the isolating system.

A hysteresis diagram represents the plot of force against displacement, therefore, the area within such a loop represents the dissipated energy by the bearing in a complete cycle of loading. The equivalent viscous damping ratio exhibited by the bearing is evaluated according to the following equations (Chopra, 1995).

$$K_{\text{eff-h}} = \frac{|Fmax|+|Fmin|}{|Dmax|+|Dmin|} \quad [1]$$

$$\zeta_{\text{eq}} = \frac{W_D}{4\mu\, Ws} \quad [2]$$

Where: W_D represents a dissipated energy in one load cycle and equals to the hysteresis loop area (N-mm), and Ws corresponds to the stored or elastic energy (N-mm) defined by the following formula:

$$\zeta_{\text{eq}} = \frac{W_D}{2\mu D^2 K_{\text{eff}-h(\gamma)}} \quad [3]$$

$$W_S = (D^2/2)\, K_{\text{eff-h}(\gamma)} \quad [4]$$

$$D = \frac{|Dmax|+|Dmin|}{2} \quad [5]$$

Where: *Fmax* and *Fmin* are the maximum and minimum lateral shear force, respectively, related to the maximum and minimum displacement *Dmax* and *Dmin* on the force-displacement

hysteresis diagram. The shear strain amplitude is defined by % of t_r (total thickness of rubber layers). $K_{eff\text{-}h(\gamma)}$ represents effective lateral stiffness of the isolators at shear strain of γ.

Table 4-1 SB-CFREI Effective Lateral Stiffness $K_{eff\text{-}h}$ and Equivalent Viscous Damping (ζ_{eq}) (Load Cycles 1 and 2)

Test name and number	Isolator name	Bonding Level, BL (%)	Axial comp. load, P_v (kN)	Axial stress, σ (MPa)	Shear strain amplitude % (t_r)	Effective lateral stiffness, $K_{eff\text{-}h}$ (N/mm) 1st cycle	Effective lateral stiffness $K_{eff\text{-}h}$ N/mm 2nd cycle	Effective Equivalent viscous Damping 1st cycle %	Equivalent Viscous Damping 2nd cycle %
Lateral -1	B160	37.87	250	9.77	50	88.06	61.54	14.70	24.97
Lateral -2	B160	37.87	250	9.77	25	165.62	157.53	7.75	7.18
Lateral -3	B180	47.93	250	7.72	50	200.91	182.25	5.37	6.27
Lateral -4	B180	47.93	250	7.72	25	289.20	282.05	3.85	3.30
Lateral -5	B200	59.17	250	6.25	50	268.24	256.78	4.89	6.23
Lateral -6	B200	59.17	250	6.25	25	--------	372.87	-------	3.25
Lateral -7	B220	71.60	250	5.17	50	341.40	329.06	3.96	4.02
Lateral -8	B220	71.60	250	5.17	25	433.91	432.0	3.64	3.64
Lateral -9	B220	71.60	250	5.17	75	195.57	180.02	11.53	13.00
Lateral -10	B220	71.60	250	5.17	100	101.38	--------	27.61	------
Lateral -11	B 240	85.21	250	4.34	50	393.28	391.55	4.76	5.21
Lateral -12	B240	85.21	250	4.34	25	524.42	521.88	4.69	2.72
Lateral -13	B240	85.21	250	4.34	75	309.99	301.50	4.75	4.56
Lateral -14	B240	85.21	250	4.34	100	216.92	196.45	8.83	10.49
Lateral -15	B260	100	250	3.69	50	432.59	427.08	3.36	3.42
Lateral -16	B260	100	250	3.69	25	532.43	530.69	2.26	2.85

4.9.1 SB-CFREI Lateral Load-displacement Hysteresis Diagrams

Typical SB-CFREI's force-displacement hysteresis is shown in Figure 4.16. All component isolator's hysteresis diagrams and the computations to determine the related effective lateral stiffness and damping are presented in Appendix A. The computed effective lateral stiffness and damping are summarized in Table 4-1. Effects of bonding variation on the isolator's dynamic characteristics are discussed in the following subsections. Future studies on the dynamic characteristics of component and compound seismic isolation system are under investigation by the author.

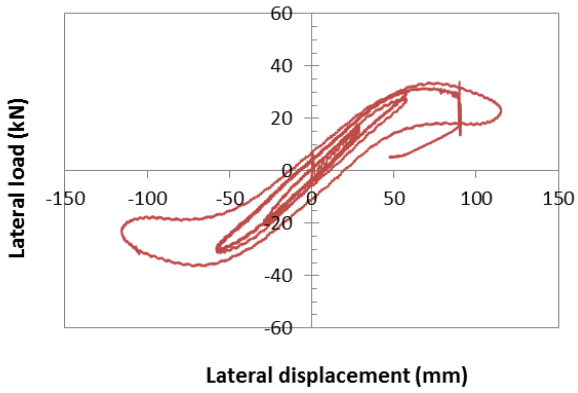

(a) B220 Dynamic Load profile Ϭ= 5.17 MPa and SSA = 25-50-100%t_r A

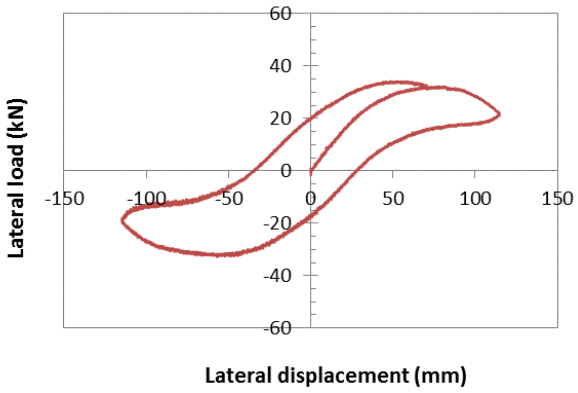

(b) B220-SSA = 100%t_r A Monotonic load Profile Ϭ = 5.17MPa

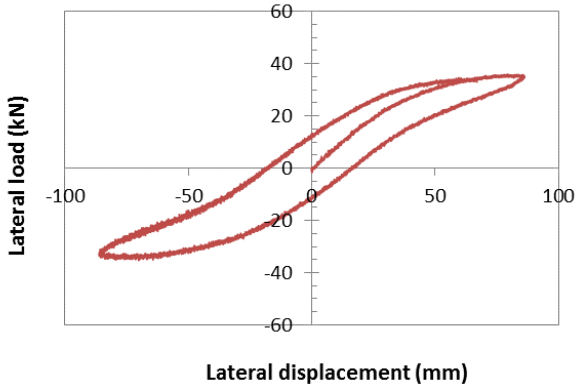

(c) B220-SSA = 75%t_r A and Ϭ = 5.17 MPa

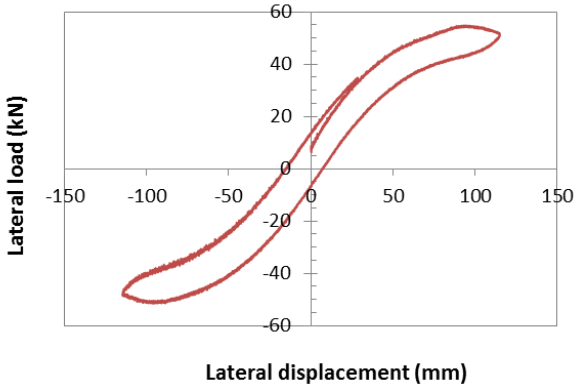

(d) B240 SSA = 100%t_r A and Ϭ=4.34MPa

Figure 0.16 Force-displacement hysteresis diagrams of B220 (a, b, c) and B240 (d) isolators under constant pre-load of 250 kN (SSA= 50-75-100%t_r)

4.10 Effect of Bonding Variation on Dynamic Characteristics of SB-CFREI

In this section, the experimental lateral shear test outcomes are analyzed to demonstrate the effects of bonding variation on the isolator's energy dissipation and damping, effective lateral shear stiffness, and isolation efficiencies.

4.10.1 Effect of Bonding Variation on the Isolator's Effective Lateral Stiffness

To demonstrate the effect of bonding variation on the isolator's effective lateral stiffness $K_{eff\text{-}h}$, a lateral shear test was conducted on six identical pairs of ESB-CFREIs in dual shear configuration

and under a constant axial compression load of 250 kN. The experimental outcome values of K_{eff-h} (kN) related to each isolator's type are summarized in Table 4-1. The effective lateral shear stiffness of the isolators with different bonding levels is plotted versus BL. These tests were performed at two different levels of shear strain amplitudes. Figure 4.17 presents the effect of bonding variation on the isolator's effective lateral stiffness at the shear strain amplitudes of 25%t_r and 50%t_r, under a constant vertical compression load of 250 kN. The plotted results in Figure 4.17 also show that bonding variation has a considerable effect on the isolator's effective lateral stiffness, and solidly supports the idea that as the bonding increases, the isolator's effective lateral stiffness increases as well.

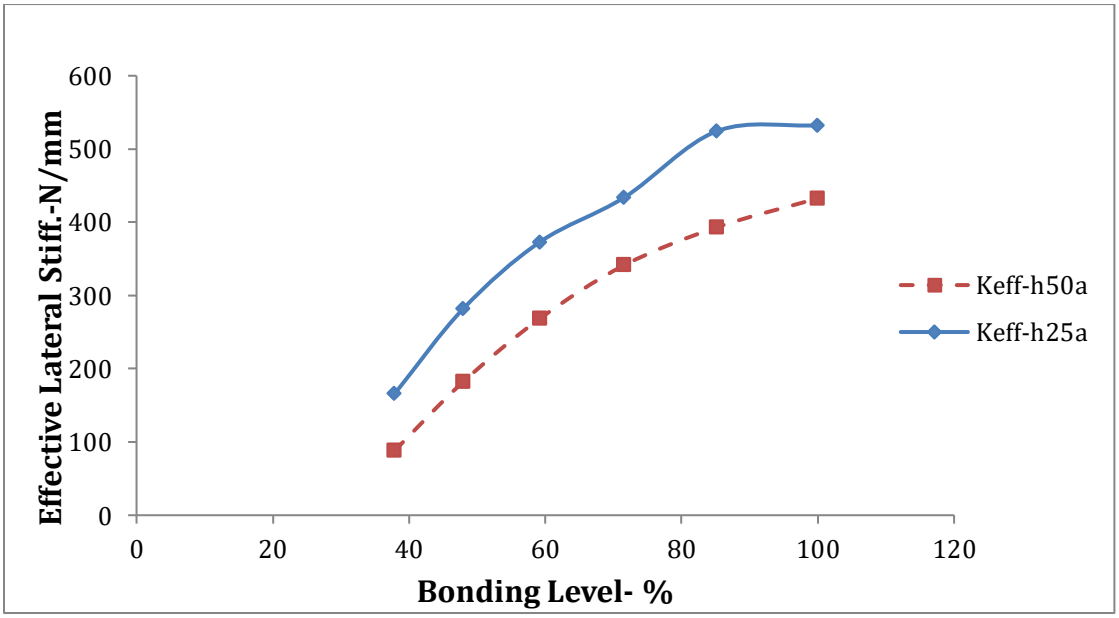

Figure 0.17 Effect of BL on the isolator effective lateral stiffness For SSA= 25 and 50%t_r PL = 250 kN

4.10.2 Effect of Bonding Variation on SB-CFREI's Effective Lateral Damping

To investigate the effect of bonding variation on the isolator's effective damping, a lateral cyclic shear test was conducted on each isolator's type under a constant axial compression pre-load of 250 kN. Depending on the isolator bonding, the compression pre-load imposes a pressure of 3.69 to 9.77 MPa on the isolators. For this part of the study, the shear strain amplitude SSA was 25% and 50% tr for all tests. As demonstrated in Figure 4.18 and Table 4-1, isolators with lower level bonding, like B160, have much higher effective damping in comparison with isolators having

higher bonding, like B240 and B260, with BL of 85.21% and 100%, respectively. The graphs show a sharp drop of damping as the bonding varies from 37.87% to around 48%. The graph also shows that damping decreases as bonding increases to the maximum of 100%. In other words, the test results indicate that for an isolator to perform with a higher level of effective equivalent viscous damping, the bonding should be reduced. In general, after plotting the lateral force-displacement hysteresis diagrams and defining the related equivalent viscous damping for all tests, the outcome shows that all SB-CFREIs at shear strain amplitude of 25-100%t_r exhibit a higher level of damping in comparison with the bonded CFREIs (BL=100%). Combining low and high bonding isolators leads to compound isolator CSB-CFREIs, which are expected to have higher damping.

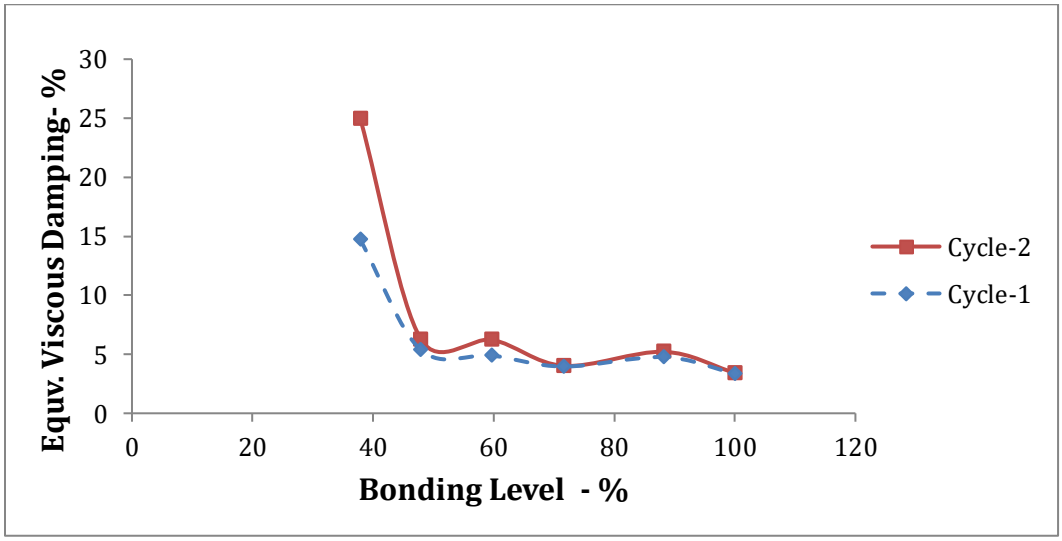

Figure 0.18 Effect of isolators BL on the lateral effective equivalent viscous damping SSA=50%t_r load cycle 1 & 2 PL = 250 kN

4.10.3 Effect of Shear Strain Level on SB-CFREI Effective Lateral Stiffness

To investigate the effect of shear strain amplitude on effective lateral stiffness (K_{eff-h}) of the SB-CFREIs, a lateral shear test was conducted on isolators B220 and B240 under a constant compression load of 250 kN. Cyclic shear loading was imposed on each isolator with shear strain amplitude of 25, 50, 75, and 100%t_r. The lateral load-displacement hysteresis diagram of both isolators was defined and plotted for all input lateral shear strain loadings. At each shear strain amplitude the linear effective lateral stiffness keff-$h_{(\gamma)}$ was defined. Therefore, all the values of

Keff-h related to each isolator under four levels of shear strain loading were defined. The effect of shear strain amplitude on isolator's effective lateral stiffness is plotted and shown in Figure 4.19

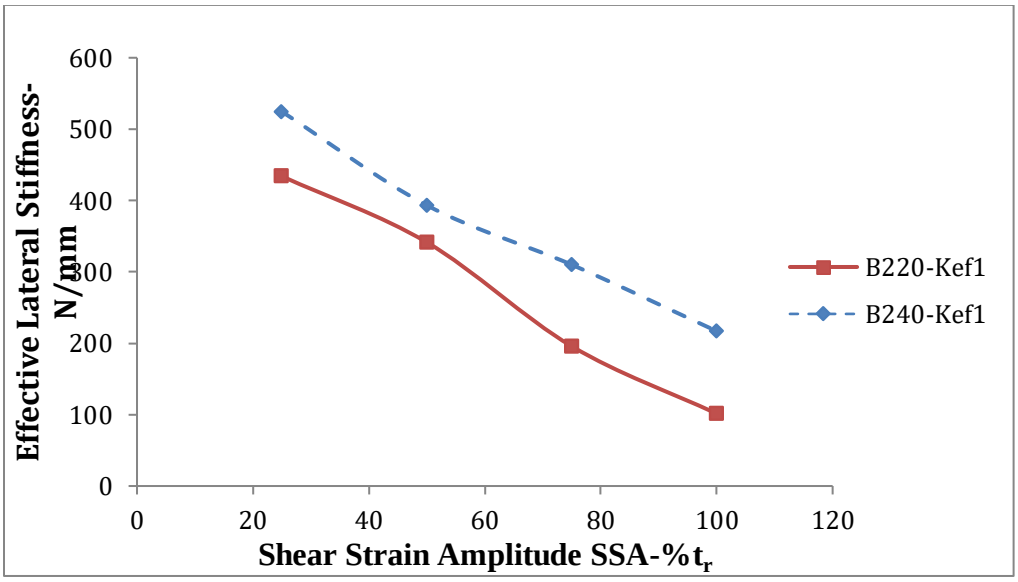

Figure 0.19 Effect of shear strain amplitude variation on the effective lateral stiffness of the SB-CFREIs under constant compression load of 250 kN (B220 & B240 Isolators)

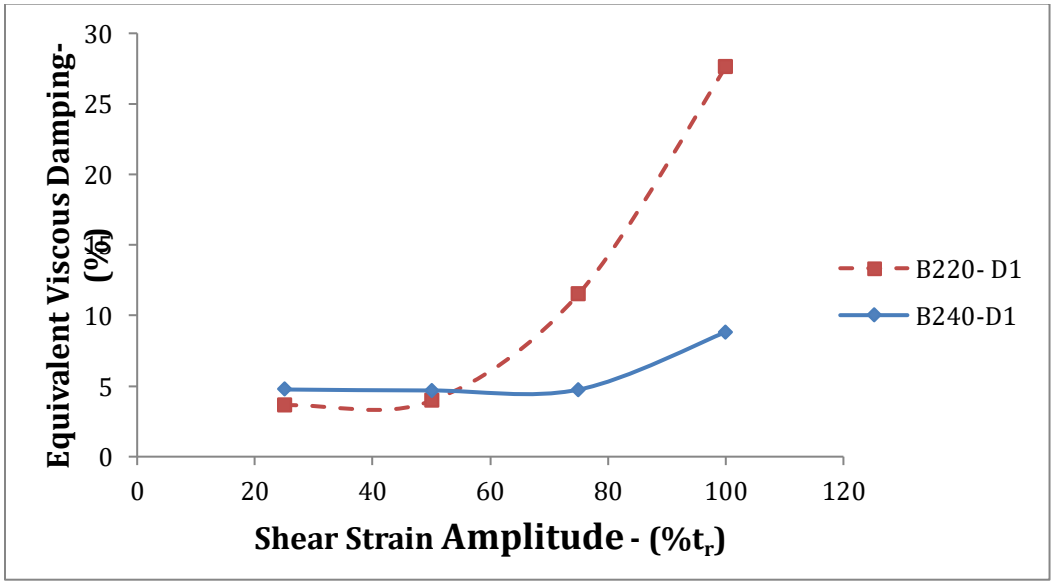

Figure 0.20 Effect of shear strain amplitude variation on the SB-CFREI effective equivalent viscous damping Pv = 250 kN (B220 & B240)

4.10.4 Effect of Shear Strain Amplitude Variation on the SB-CFREI Effective Equivalent Viscous Damping

The effective lateral equivalent viscous damping of the isolators with respect to shear strain amplitude is investigated and is demonstrated in Table 4-1. For component isolators B220 and B240 the load-displacement hysteresis diagrams for shear strain amplitudes of 25, 50, 75, and 100%t_r under constant axial compression load of 250 kN are defined and the experimental results are plotted. The force-displacement hysteresis diagram for isolator B220 and B240 are plotted in Figure 4.16. Variations of the effective equivalent viscous damping with change in shear strain amplitude for typical SB-CFREIs are defined and plotted in Figure 4.20. The test outcomes indicate that the isolator's effective damping will increase as the shear strain amplitude of loading increases.

4.10.5 SB-CFREI Equivalent Viscus Damping Values and Comparison

Force-displacement hysteresis diagrams are plotted as the result of two cycles of lateral shear loading on all isolators, with different bonding levels shown in Figure 4.19 and Appendix A of this thesis. Equations (1) and (2) of section 4.1.7 were implemented in calculating the effective equivalent viscous damping for each loading cycle, and the outcome is summarized in Table 4-1. The displayed isolator's damping values show higher damping values for isolators with lower bonding level. This isolator's unique damping characteristic is also demonstrated in Figure 4.20.

To demonstrate the superior damping and energy dissipation capability of the SB-CFREIs, the experimental outcome of a few recent research studies conducted by others on bonded and un-bonded CFREIs are shown in Table 4-2. All isolators have been tested under almost the same axial compression stress of 6.9 MPa and the same input load signals (suggested by Kelly). Some of the research outcomes listed in Table 4-2 have been taken from graphs and are approximate values.

Table 0-2 Recent Research Studies Damping Outcomes Conducted on Bonded, Unbonded, and Semi-Bonded CFREI

Isolator Type	Reference	Isolator Size (mm)	SSA $\%t_r$	Approximate Effective Lateral damping %
UB-CFREI (Unbonded) NR 37+/-5 hardness ASTM Shore A	de Raaf (2009)	280×280×96	50 100	11.90-13-40 10.30-11.40
Bonded CFREI NR	Ashkezari et al. (2008)	150×150×56	50 100	6.4-6.5 4.9-5.2
Bonded CFREI with Thermoplastic mesh NR-60 hardness	Karimzadeh Naghshineh et al. (2014)	D=150, H=79 Circular cross section	50 100	9.60-11.40 7.7-10.40
SB-CFREI NR-55 hardness	Adibnatanzi et al. (2015)	260×260×120	50 100	14.70 24.97

4.11 SB-CFRE Isolator Effective Compression Stiffness Keff-v

Axial Compression cyclic tests were conducted on all SB-CFREI's with different bonding levels under load control at two different pre-load magnitudes of 116 and 233 kN. In the first phase of the tests, specimens were slowly loaded up to PL_1= 116 kN vertical compression pre-load, and then continued with three fully reversed cycles of amplitude ±25%PL_1. At the final stage the specimens were monotonically unloaded in a similar way. The loading and unloading process was repeated for the higher pre-load of PL_2 = 233 kN. To evaluate the compression performance and the isolator's effective axial compression stiffness and modulus, effective axial compression stiffness $K_{eff\text{-}v}$ at lower and higher values of axial load is defined using the experimental compression force-displacement diagrams. Vertical stiffness is computed using the results of the compression test and is defined as the slope of a linear line through the outcome hysteresis force-displacement plots of the cyclic part of the input compression load signal. The defined vertical stiffness is referred to as the average compression stiffness of the specimen or $K_{eff\text{-}V(avg)}$.

These test sequences were repeated for all isolators with different bonding levels. Due to difference in bonding level, the isolator experienced a local pressure of 1.72 MPa to a maximum of 11.38 MPa due to the lower and higher compression loading levels, respectively. The imposed pressure on SB-CFREI in some cases is even higher than the allowable pressure range on common elastomeric bearings. For elastomeric bearings used in bridges and buildings, the allowable pressure under permanent load is 4.5 MPa for the serviceability limit state (SLS) and

7.0 MPa for the ultimate limit state (ULS) (GoodCo Z-Tech, 2010). The "isolation bearings are generally used at axial pressure levels ranging from 5 to 7MPa" (Kelly, 1997). In early years of base isolation application in Japan, the compressive stress on isolators used to be between 3.0 and 8.0MPa (Pan et al., 2005). "For low-rise residential buildings, the elastomeric bearings are subjected to a vertical pressure of around 3.0 MPa" (Hedayati Dezfuli and Alam, 2016).

The input load signals are shown in Figures 4.14 and 4.15 and the resultant average effective compression stiffness and modulus are defined and presented in Table 4-3. Figure 4.21 displays a typical force-displacement diagram under compression loading. The figure shows the slope and equation of a linear line passing through the cyclic portion of compression force-displacement diagram. Slope of this line or the coefficient of the parameter "x" represents the value of compression stiffness.

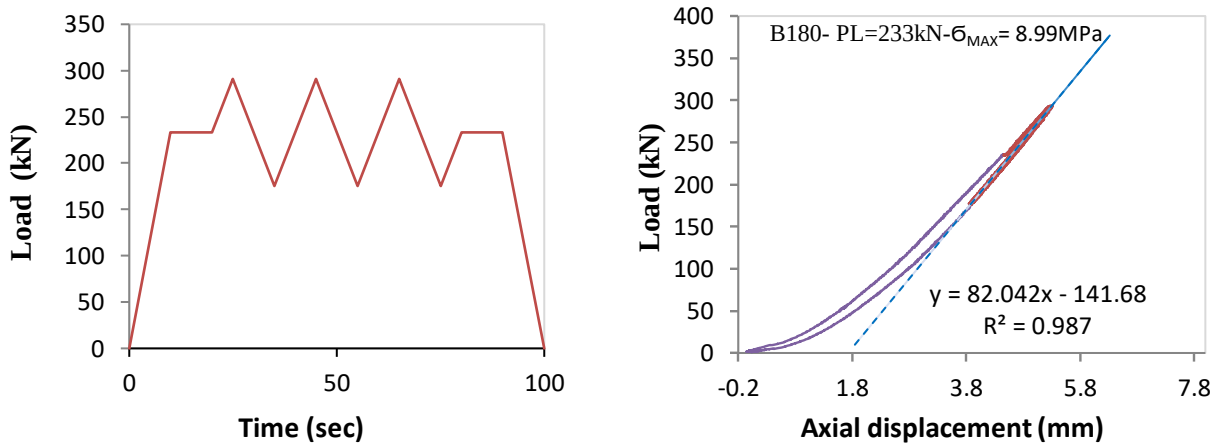

Figure 0.21 SB-CFREI axial compression input load signals pre-load PL= 233 kN (left). Typical isolator axial compression load-displacement diagram (showing Keff-v as the slope of the straight line described by displayed linear function or coefficient of parameter X) (right)

The effective compression stiffness obtained from the vertical actuator recorded data was noticed to be lower than that of the average values of the four LVDT's recorded data placed on the four corners of the upper plates. These LVDTs monitored the vertical displacement of the isolator specimens under axial compression load. To define the true values of compression deformation, three gauges were installed to measure and account for the effects of spring type displacement of the lower supporting steel beams and upward displacement of the upper steel girder, and also the frame and columns of the test set-up as shown in Figure 4.7 and 4.8. These displacements are the

result of the vertical actuator's end reaction force on the top steel girder, the steel frame, and on the supporting base steel beams. The outcome's axial compression stiffness was corrected for the above mentioned displacements and the final corrected outcome is shown in Table 4-3 along with SB-CFRE isolator effective compression modulus E_c.

Effective compression modulus of bearings is calculated in accordance with equation [6] that describes the relationship between the bearing's compressive stiffness K_v and modulus E_c.

$$K_v = \frac{E_c A}{h} \qquad [6]$$

Where: K_v is vertical compression stiffness of bearing (kN/mm), E_c is compression modulus of the bearing under specified level of vertical load (MPa), A is area in which the load is applied (mm^2), and h is total thickness of the rubber (mm). Vertical stiffness of each SB-CFREI bearing is obtained from the experimental testing and is related to the compression modulus Ec. by the standard formulation that can be found in mechanics of materials (Naeim and Kelly, 1999). In the present study, equation [6] is used to obtain the isolator's compression modulus E_c.

Table 0-3 SB-CFREI Component Isolator Effective Compression Stiffness and Modulus

Test #	Test name	Isolator Type	Bonding Level, BL (%)	Axial Compression Pre-Load Pv (kN)	Max. Axial Compression Stress (MPa)	AVARAGE K_{eff-v} (kN/mm) LVDTs & ACT.	Effective Compression Modulus, E_C (MPa)
1	Vertical	B-160	37.87	116	5.66	98.45	172.12
2	Vertical	B160	37.87	233	11.38	104.95	193.11
3	Vertical	B180	47.93	116	4.48	109.43	201.35
4	Vertical	B180	47.93	233	9.00	120.10	220.80
5	Vertical	B200	59.17	116	3.63	131.58	242.11
6	Vertical	B200	59.17	233	7.28	137.10	252.26
7	Vertical	B220	71.60	116	3.00	138.10	254.10
8	Vertical	B220	71.60	233	6.02	142.07	261.41
9	Vertical	B240	85.21	116	2.52	152.63	280.84
10	Vertical	B240	85.21	233	5.06	157.43	289.74
11	Vertical	B260	100	116	2.15	145.18	217.78
12	Vertical	B260	100	233	4.31	144.00	264.96

4.11.1 Effects of bonding variation on the effective compression stiffness of SB-CFREIs

The axial compression test was conducted on isolators with different bonding level (BL). The input compression load signals with two pre-load levels of 116 and 233 kN, shown in Figure 4.14 and 4.15, were selected. The test outcomes demonstrated that as the bonding increases, the effective axial compression stiffness $K_{eff\text{-}v}$ of the isolators increases as well. Figure 4.22 demonstrates the effects of bonding variation on the isolator's effective axial compression stiffness.

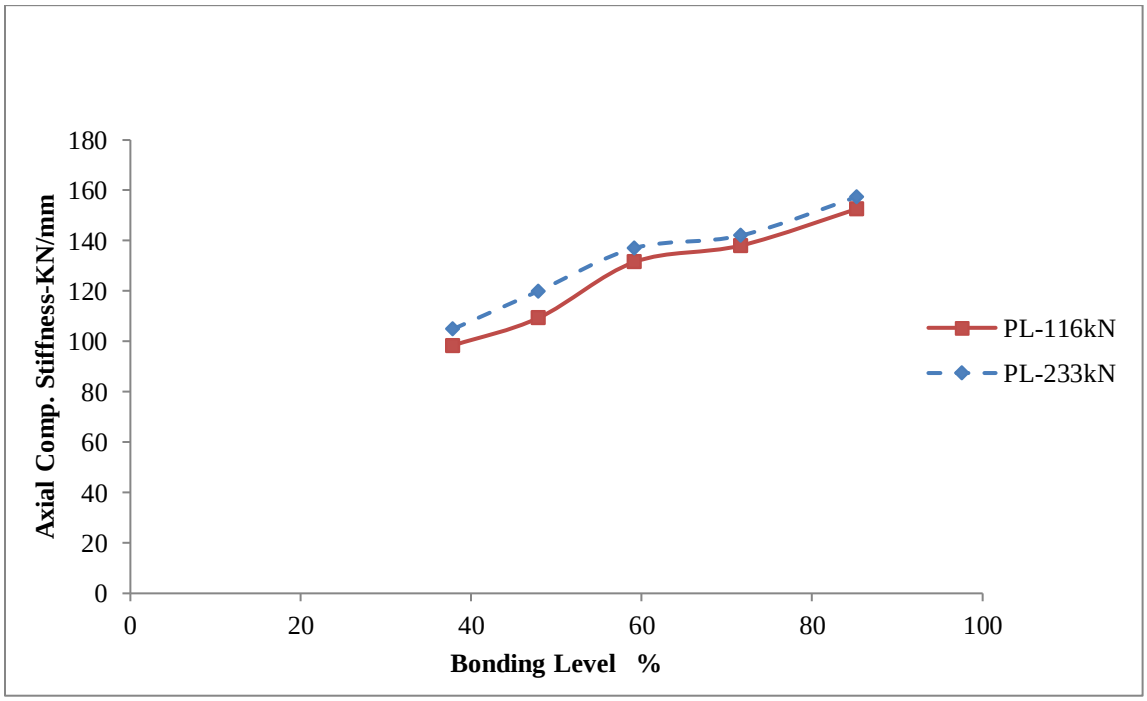

Figure 0.22 Effects of Bonding Level (BL) on the Component Isolator's Effective Compression Stiffness ($K_{eff\text{-}v}$) PL=116 & 233 kN

4.12 Isolation Efficiency (IE) of the SB-CFREIs

The force-displacement hysteresis diagrams of SB-CFRIs are nonlinear as shown in Figure 4.16. This form of deformation decreases the effective horizontal stiffness with increased lateral displacement. When stiffness decreases, the period of isolation consequently increases, which could be considered an increase in isolation efficiency. The ratio of average axial compression stiffness of an isolator to its average lateral stiffness represents the isolation efficiency (IE). The ratio of $K_{v(avg)}$ / $K_{h\ (avg)}$ is recommended by the Euro code to be higher than 150 (Eurocode8.

Design of structures for earthquake resistance, 2004). As shown in Table 4-4, this ratio for all SB-CFREI types is much higher than 150; in another words, isolation efficiency of the innovative SB-CFREIs as an important isolator performance is highly satisfactory. Figure 4.23 demonstrates the effect bonding level (BL) on the isolator's isolation efficiency (IE). The IE is plotted vs. BL and the plotted test outcome values in Table 4-4 indicate that isolation efficiency will increase as the bonding level decreases.

Table 0-4 Component Isolator Average Effective Compression Stiffness anf Isolation Efficiency (IE)

Test #	Test Name	Isolator type	Bonding Level, BL (%)	Axial Comp. Pre-Load, Pv (kN)	Max. Axial Comp. Stress (MPa)	Average $K_{eff\text{-}v}$ (kN/mm) LVDTs & ACT.	Average Lateral Stiffness of (1st & 2nd load cycle SSA=25, 50%t_r $K_{h(avg)}$ (N/mm)	Isolation Efficiency (IE) = $K_{v\,avg}/K_{h\,avg}$
1	Vertical	B160	37.87	233	11.38	104.95	118.19	888
2	Vertical	B180	47.93	233	9.00	120.10	238.60	503
3	Vertical	B200	59.17	233	7.28	137.10	299.30	458
4	Vertical	B220	71.60	233	6.02	142.07	384.09	370
5	Vertical	B240	85.21	233	5.06	157.43	457.78	344
16	Vertical	B260	100	233	4.31	144.00	480.70	300

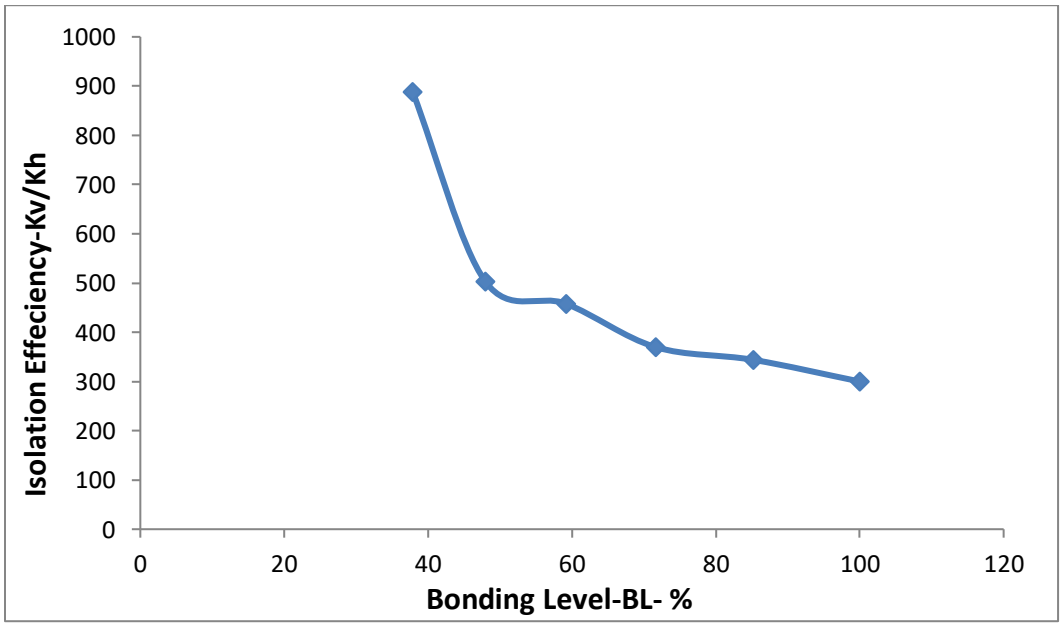

Figure 0.23 Effects of bonding level (BL) on Isolation Efficiency (IE=Kv/Kh) Pv = 250 kN

4.13 Compound Isolators (CSB-CFREI)

A combination of two or more component isolators undergoing lateral shear and axial compression excitations as an integrated isolator unit is defined as a compound isolator or Compound Semi-Bonded Carbon Fiber Reinforced Elastomeric Isolator CSB-CFREI (named by the author). In an attempt to lower the size, weight, and production cost and to ease the fabrication, handling, transportation, and implementation of seismic isolators, compound isolators with some number of component isolators could be designed and combined so as to meet the isolator's desired dynamic characteristics and capabilities. The compound isolator can meet the required target isolator dynamic characteristics, such as effective axial compression and lateral shear stiffness and damping, for low-rise, low-importance buildings in order to push the isolated building natural period away from that of the predominant earthquakes. This period shift of the low-rise stiff structure as a typical building in developing countries would reduce the seismic demand effectively and increase seismic safety and protection considerably. In design of seismic isolation systems, implementation of the compound isolators is recommended when the axial compression load of the building is high. In this part of the research study, the effects of bonding variation and component combination on dynamic characteristics of the compound isolators is investigated through a series of pre-defined experimental tests.

4.13.1 Double Compound Isolators

4.13.1.1 Test Configuration for Double Compound Isolators

Dual shear configuration is selected as the test configuration for testing the double compound isolator, by using three thick steel plates with dimensions of 1000×500×80 mm, as shown in Figure 4.24. These plates were drilled with holes at pre-defined locations capable of creating a strong adjustable bolted connection to the 5 mm elevated mounting plates. Adjustable shear pins were designed and fabricated to transfer the shear and compression forces to the reinforced bearing pad. The 12 mm diameter pins will fit tightly into the thick mounting plates by one end and to the five drilled holes of the 8 mm partially bonded plates at the other end. The middle push-pull plate is capable of transferring the horizontal actuator lateral shear load to the compound isolators and is allowed to move back and forth in the horizontal direction as well as in the vertical direction. The upper plate is only allowed to move in the vertical direction to transfer the axial compression load induced by the vertical actuator to the isolators. The testing

machine capable of testing component isolators with different configuration combinations was designed, fabricated, and assembled with extensive and precise machinery work in the UBC Earthquake Engineering Research Facility.

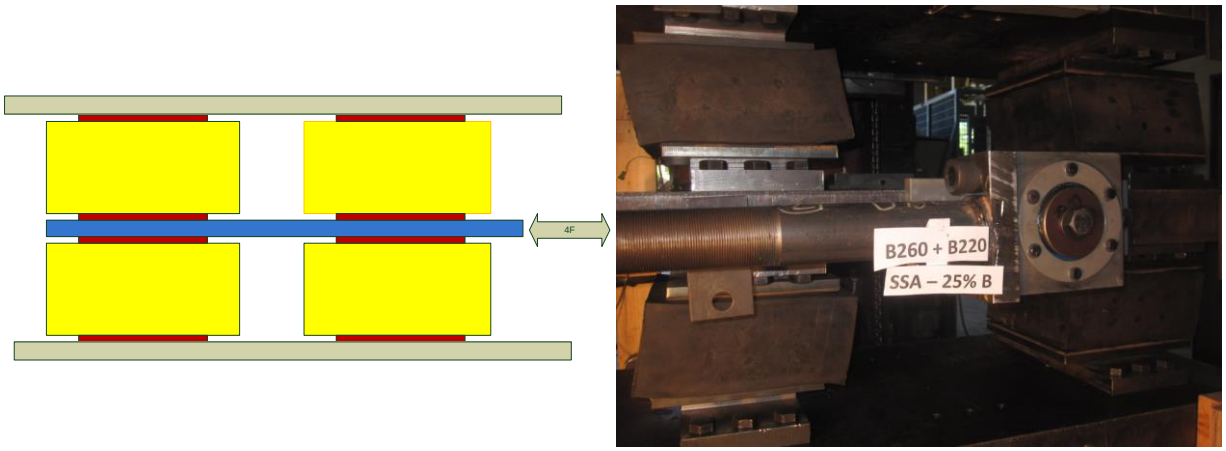

Figure 0.24 Schematic (left) and experimental (right) of compound double isolators dual shear test configuration

4.13.2 Effect of Repeated Loading on Compound Double Isolator's Effective Lateral Stiffness and Damping

Dynamic characteristics of compound isolators with a combination of two component isolators having a range of bonding from 48.50% to 100% are investigated by conducting a series of compression and lateral shear tests on all compound isolators with pre-defined combination configurations. Each component isolator was tested twice under lateral shear load at shear strain amplitudes of SSA=25% and 50%t_r and a constant axial compression load of 500 kN. The related force-displacement hysteresis diagrams were plotted. All compound isolators demonstrated satisfactory performance with no damage or failure. The effective lateral stiffness $K_{eff\text{-}H}$, effective equivalent viscous damping and force displacement hysteresis diagrams related to the first lateral loading are defined and compared with those of the second loading. The test outcomes are demonstrated in Table 4-5.

The outcome comparison shows lower values of effective lateral stiffness for the second loading cycle. Part of this decrease in effective lateral stiffness of the isolator is related to the phenomenon called rubber "Mullins effect. This phenomenon probably reflects a breakdown of weak bonds between rubber molecules and filler particles, and at very small strains, between

filler particles themselves incurred during previous loading" (Dehghani-Ashkevarzi, 2007). On the other hand, when comparing the isolators damping related to the first and second loading cycle (Table 4-5), as anticipated the compound isolators demonstrate higher effective lateral viscous damping in the second round of loading in comparison to the first loading cycle.

4.13.3 Effective Lateral Stiffness and Damping of the Double Compound Isolator

The average effective lateral stiffness $K_{eff\text{-}h}$ and equivalent viscous damping ζeq of the double compound isolators are defined with the same computation method as that of the component isolators by using the equations [1] to [5] suggested, that have been discussed in section 4.8.2 of the component isolator. The effective lateral stiffness and damping are presented in Table 4-5 for the first and second consecutive tests (1st and 2nd test).

Table 0-5 Compound Double Isolator CSB-CFREI Lateral Effective Stiffness and Damping 1st and 2nd Loading Cycle

Test #	Test specification	Compound Isolator	Bonding Level, BL (%)	Axial Load (kN)	Axial Stress (MPa)	Shear Strain Amplitude SSA $\%t_r$	Average Effective Lateral Stiffness (N/mm)		Equivalent Viscous Damping, ζ (%)	
							1ST Test	2nd Test	1ST Test	2ND Test
1	Lateral	B200+B160	48.52	500	7.62	50	220.53	201.81	19.22	19.87
1A	Lateral	B200+B160	48.52	500	7.62	25	368.27	367.53	8.80	11.03
2	Lateral	B200+B180	53.55	500	6.91	50	246.70	214.90	6.91	8.0
3	Lateral	B220+B160	57.28	500	6.76	50	368.80	357.54	8.32	9.24
3A	Lateral	B220+B160	57.28	500		25	--------	513.88	5.91	6.51
4	Lateral	B220+B180	59.97	500	6.76	25	598.33	594.86	4.25	5.24
4A	Lateral	B220+B180	59,97	500	6.19	50	432.85	429.78	7.47	7.97
5	Lateral	B260+B180	73.96	500	5.00	50	568.28	555.51	5.15	5.52
5A	Lateral	B260+B180	73.96	500	5.00	50(spt2)	567.70	----------	5.12	----
5B	Lateral	B260+B180	73.96	500	5.00	25	732.500	730.32	2.57	3.77
6	Lateral	B260+B200	79.59	500	4.65	50	638.95	634.33	5.16	6.34
6A	Lateral	B260+B200	79.59	500	4.65	25	------	-------	3.55	----
6A	Lateral	B260+B220	85.80	500	4.32	50	713.50	706.06	3.89	4.51
6B	Lateral	B260+B220	85.80	500	4.32	25	905.51	904.65	3.15	3.16
7A	Lateral	B260+B240	92.60	500	3.99	50	794.96	791.30	3.58	3.89
7B	Lateral	B260+B240	92.60	500	3.99	25	1011.5	1010.77	2.88	2.51
8A	Lateral	B260+B260	100	500	3.70	50	865.18	854.16	3.36	3.42
9B	Lateral	B260+B260	100	500	3.70	25	1064.85	1061.38	2.26	2.85

4.13.3.1 Typical Hysteretic Behaviour of Double Compound Isolators with Low and High Bonding Level

In order to demonstrate the hysteretic behaviour of compound double isolators, a series of lateral shear tests was conducted on a number of compound isolators with low and high levels of bonding. Figure 4.25 and Figure 4.26 show plots of load-displacement hysteresis diagrams related to different compound double isolators with low and high BL respectively. The plots indicate that isolators with a low level of bonding have lower effective lateral stiffness and higher hysteresis loop area, which represents a higher level of energy dissipation and damping. The hysteresis plots of compound isolators with higher levels of bonding show higher effective lateral stiffness but lower damping. All tests were conducted for shear strain amplitudes of 25 and 50%t_r under constant axial compression load of 500 kN.

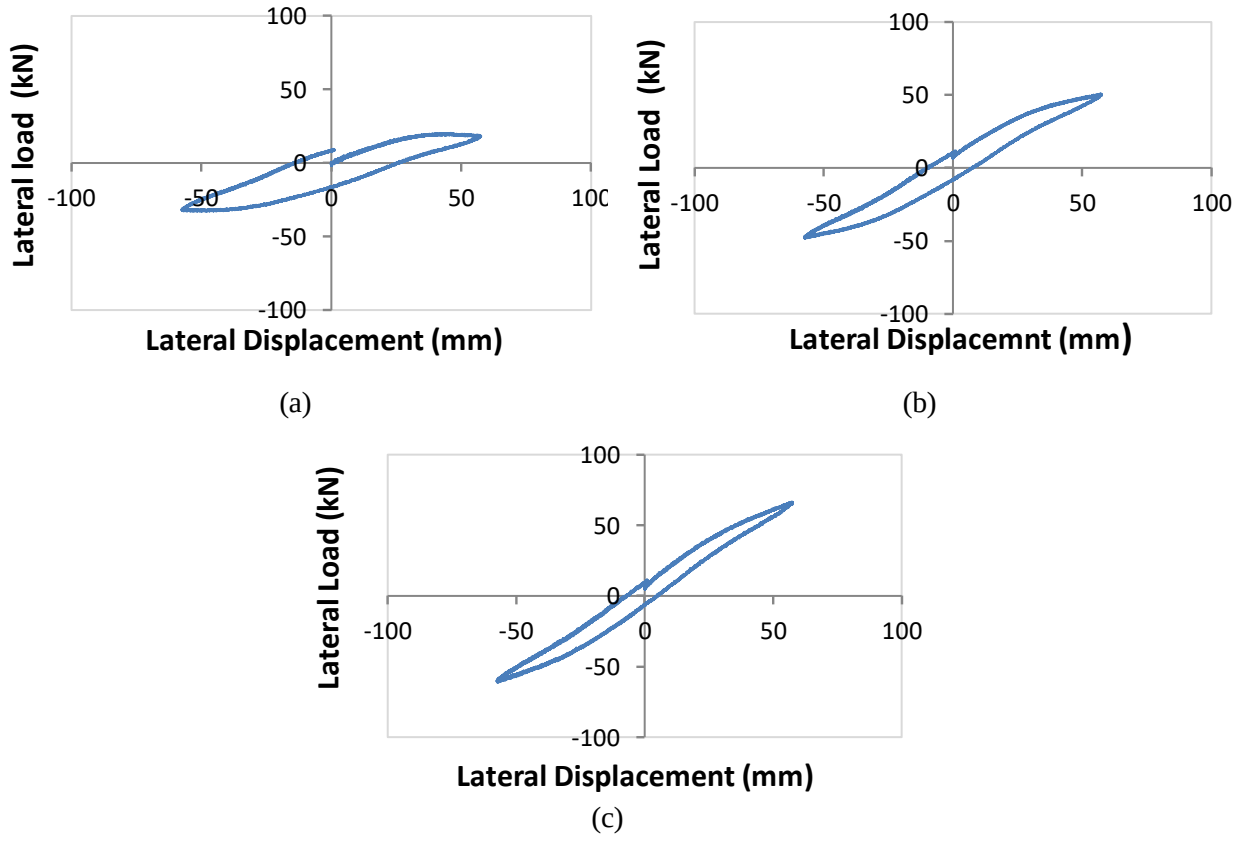

Figure 0.25 Compound double Isolators lateral load-displacement hysteresis diagram SSA=50%t_r A & B (Low BL Isolators) a) B200+B160 SSA= 50%t_rB, Ϭ=7.62 MPa, b) B200+B180 SSA= 50%t_r B, Ϭ=6.91MPa, c) B260+B180 SSA=50%t_r B, Ϭ=5.0 MPa

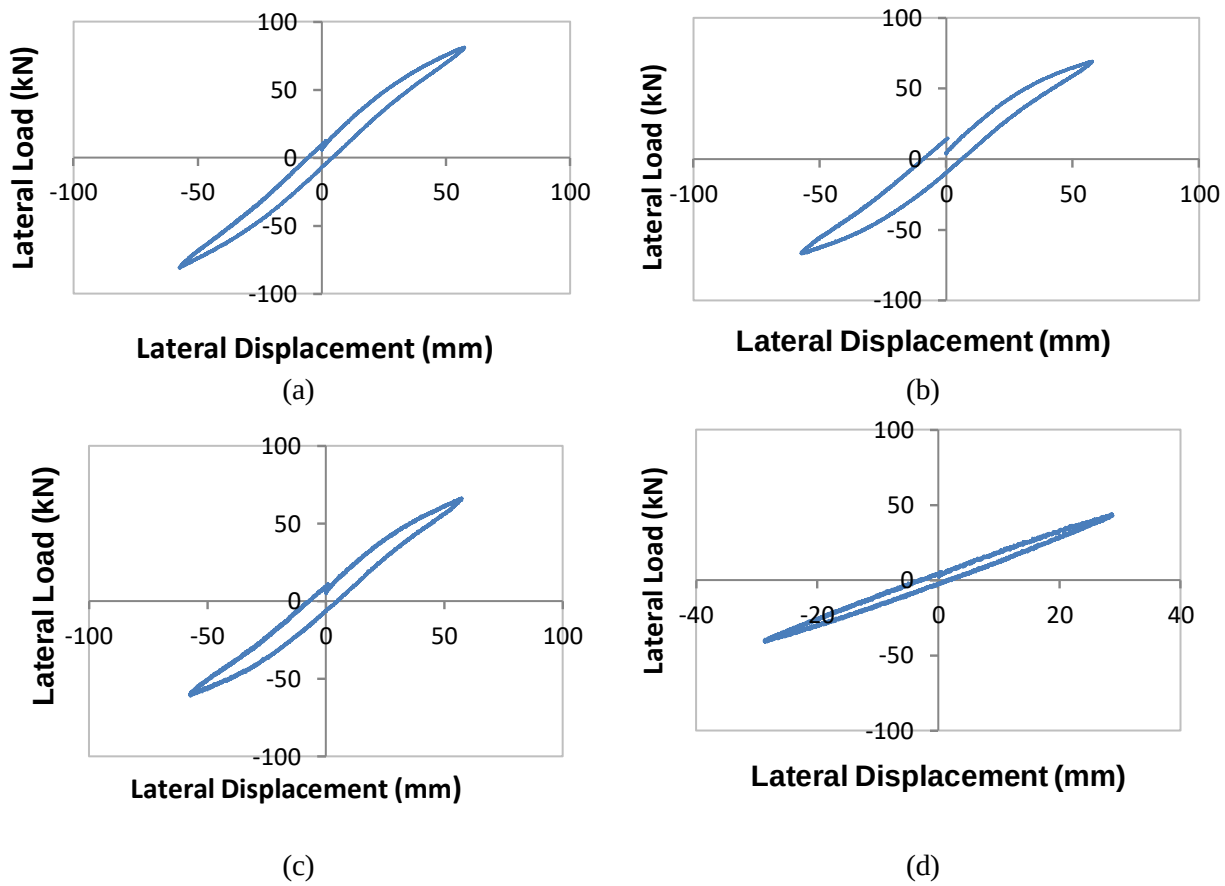

Figure 0.26 Force-displacement hysteresis diagram with bonding of 0.79.59%, 85.80%, and 73.96% respectively (high BL isolators), a) B260+B220 SSA=50%t_r B, Ϭ=4.30 MPa, b) B260+B200 SSA=50%t_r B, Ϭ=4.65MPa, c) B260+B180 SSA=50%t_r B, Ϭ=5.0 MPa, and d) B260+B180 SSA=25%t_r B, Ϭ=5.0 MPa

4.13.3.2 Effect of Bonding Variation on Compound Double Isolator Effective Lateral Stiffness

The dynamic characteristics of compound double isolators are very much dependent on their average bonding level. Figure 4.27 demonstrates the effect of total bonding level (BL) on the compound isolator's effective lateral stiffness Keff-h for two levels of lateral shear strain amplitudes: 25 and 50%t_r. These plots are based on a series of experimental outcomes on CSB-CFREIs with different bonding levels under a constant axial load of 500 kN. The graphs of Figure 4.32 indicate that the compound isolator's lateral stiffness will increases as the average bonding level increases to maximum of 100%, which is the BL of a fully bonded isolator.

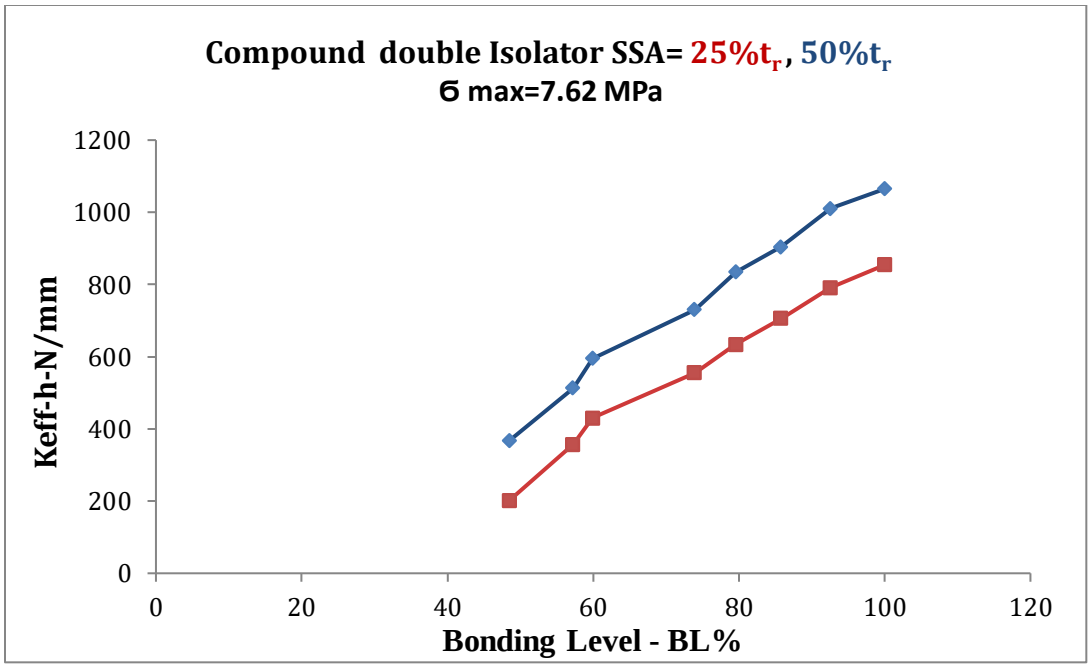

Figure 0.27 **Double Compound Isolator Effective Lateral Stiffness Vs Bonding level**

Pv= 500kN SSA= 25%t_r (red lower graph) & 50%t_r (blue above groph)

4.13.4 Effect of Bonding Level on the Compound Double Isolator's Equivalent Viscous Damping

To investigate the effect of bonding level on a compound double isolator's damping, hysteresis load-displacement diagrams of all conducted experimental lateral shear tests are plotted and the isolator's effective damping related to specific loading was defined according to equations [2] and [5]. The damping values for the 1st and 2nd loading are defined and shown in Table 4-5. The effect of average BL on equivalent viscous damping for compound double isolators is shown in Figures 4.28 and 4.29, and these graphs indicate that as the BL decreases, the damping increases. All lateral shear tests were conducted for shear strain amplitudes of 25 and 50%t_r with a constant compression load of 500kN. All related force-displacement hysteresis diagrams are plotted for each loading cycle and are shown in Figures 4.25 and 4.26, and Appendix B of the thesis.

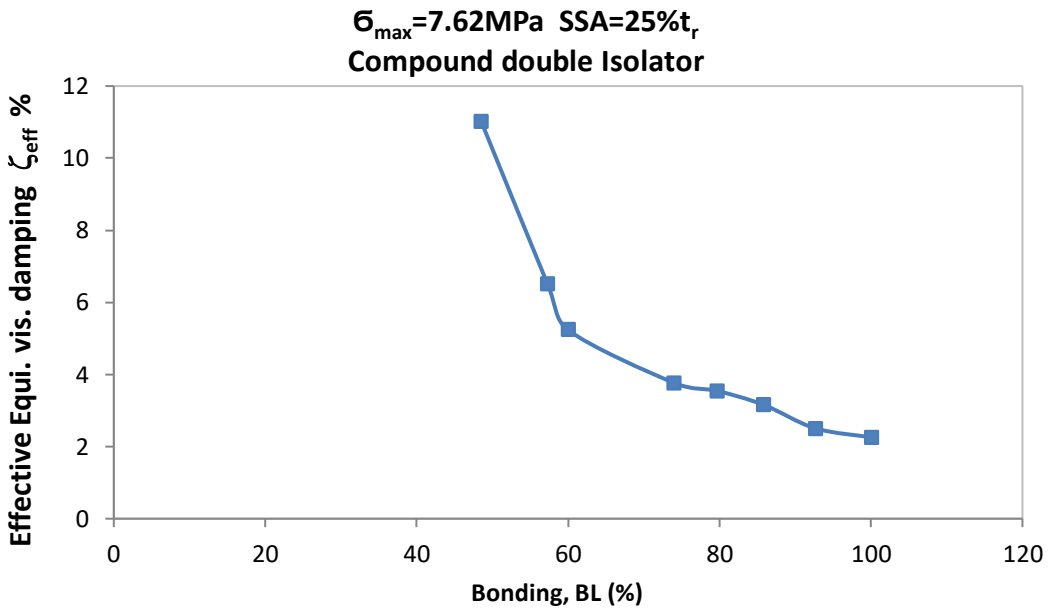

Figure 0.28 Lateral effective equivalent viscous damping vs. bonding level 2nd Test cycle SSA=25%t_r

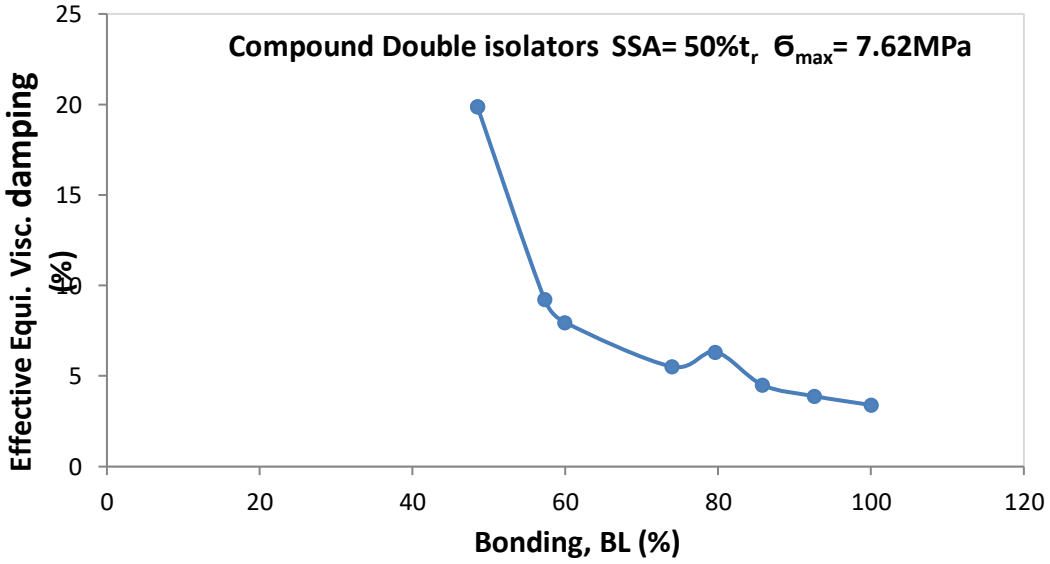

Figure 0.29 Lateral effective equivalent viscous damping vs. bonding level 2nd Test cycle-SSA=50%t_r

4.14 Compound Triple Isolators CSB-CFREI

4.14.1 Compound Triple Isolator's Test Configuration

The compound triple isolator test set-up is dual shear configuration, therefore three identical pairs of isolators are assembled on the test machine. The test machine is designed to set each component isolator in place or replace them easily. The test configuration is shown in Figure 4.30.

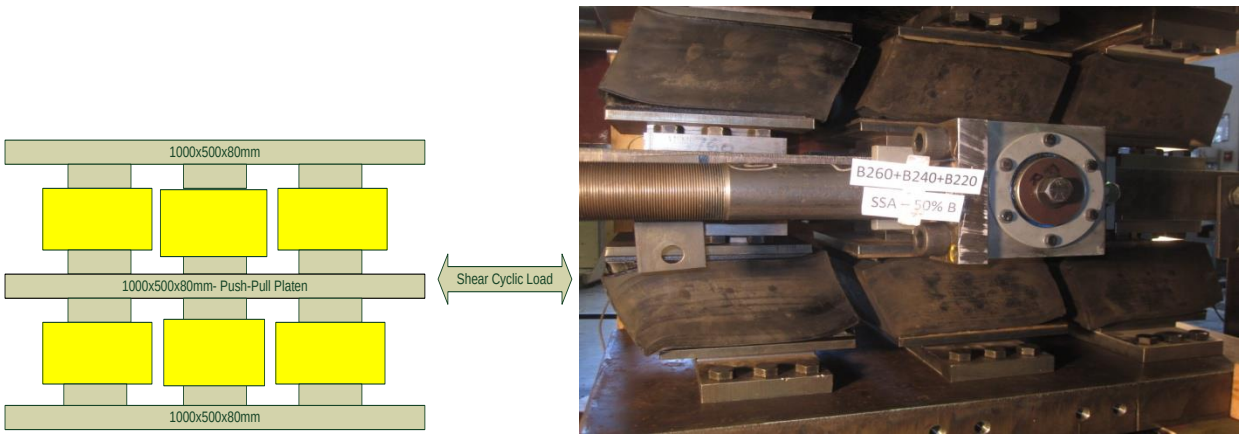

Figure 0.30 Schematic (left) and experimental (right) compound triple dual shear test configuration

4.15 Dynamic Characteristic of Compound Triple Isolators CSB-CFREI

4.15.1 Hysteretic Behaviour of Compound Triple Isolators

Compound triple isolators are capable of higher compression axial loads. In design of an isolated structure when the column axial compression load is high, a triple compound isolator will be most applicable. The test compression and lateral shear are conducted according to the pre-defined input load signals of the experimental program. Figure 4.31 (a-f) shows typical hysteresis force-displacement diagrams for low and high bonding level compound triple isolators. The monotonic low frequency and dynamic input lateral load signals are shown in Figure 4.12 and 4.13 with shear strain amplitude of 25, 50, and 100%t_r. The constant compression pre-load for triple isolators is equal to PL= 750 kN.

Typical triple compound isolator's hysteresis force-displacement diagrams (a, b, c, d, e f)

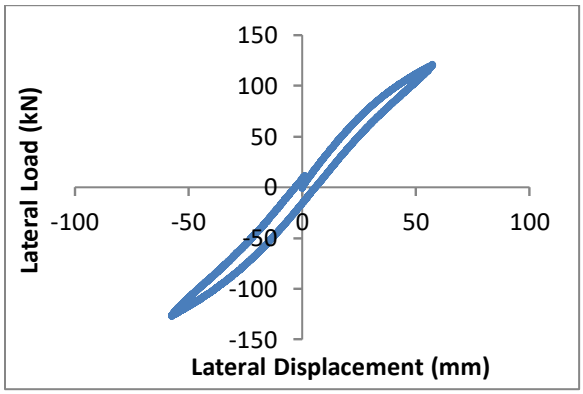

(a) B260+B240+B220 SSA=50%t_r A Ϭ=4.32MPa

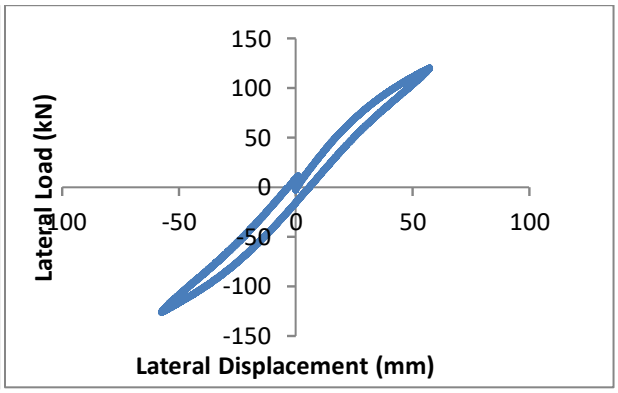

(b) B260+B240+B220 SSA=50%t_r B Ϭ=4.32MPa

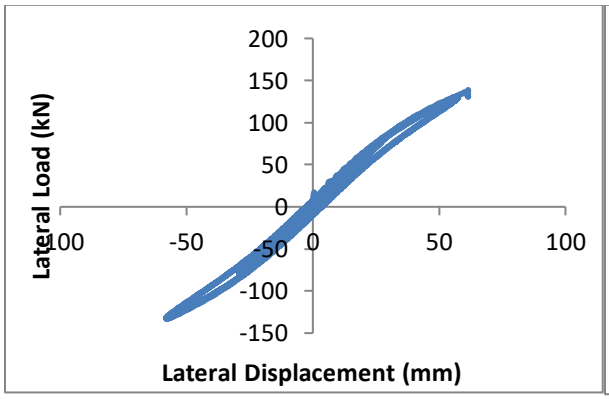

c) B260+B240+B220 SSA=25-50%t_r Ϭ=4.32MPa

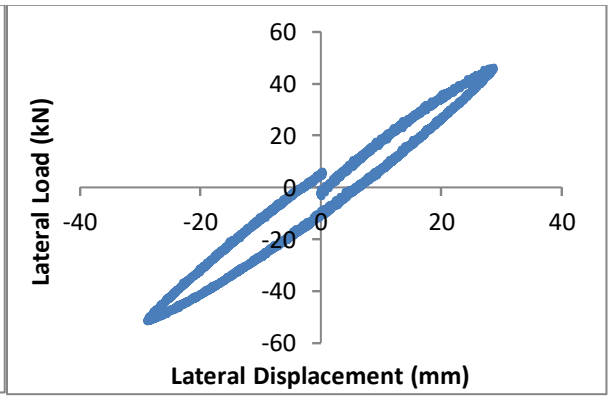

(d) B220+B200+B180 SSA=25%t_r Ϭ=6.21MPa

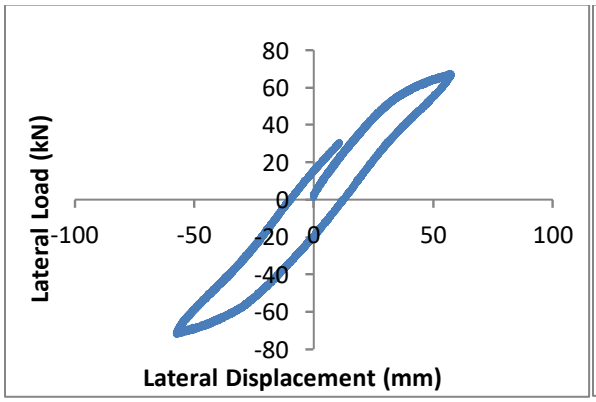

(e) B220+B200+B180 SSA=50%t_r A Ϭ=6.21MPa

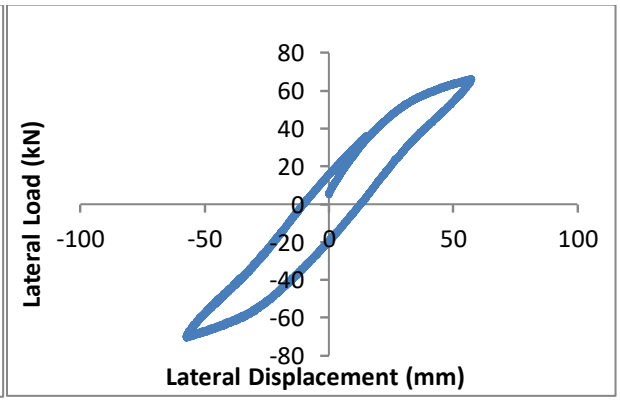

(f) B220+B200+B180 SSA=50%t_r B Ϭ=6.21MPa

Figure 0.31 Typical triple compound isolator's hysteresis force-displacement diagrams (a, b, c, d, e f) under constant axial compression load of PL = 750 kN

4.15.2 Effective Damping and Energy Dissipation of the Triple Compound Isolators

Lateral shear tests were conducted on triple isolators with different average bonding levels. The test outcomes are shown in Table 4-6. Similar to component and compound double isolators, the results indicate that as the isolator's bonding level decreases, the damping will increase.

Table 0-6 Compound Triple Isolator CSB-CFREI Lateral Effective Stiffness and Damping 1st and 2nd Loading Cycle

Test #	Test Name	Compound Triple Isolator	Bonding, BL (%)	Axial Load (kN)	Axial Stress (MPa)	Shear Strain SAA (%)t_r	Effective Lateral Stiffness K_{eff-h} (N/mm)		Effective Equivalent Viscous Damping, ζ (%)	
							1st cycle	2nd cycle	1st cycle	2nd cycle
1	Lateral	B260+B240+B220	85.6	750	4.32	25	1259.81	1257.65	2.98	3.67
2	Lateral	B260+B240+B220	85.6	750	4.30	50	1075.66	1074.94	4.09	4.80
3	Lateral	B220+B200+B180	59.57	750	6.21	25	851.20	854.50	6.57	6.30
4	Lateral	B220+B200+B180	59.57	750	6.21	50	605.10	594.85	10.65	12.08

4.15.3 Effects of Bonding Variation on Effective Lateral Stiffness of the Triple Compound Isolators

Table 4-6 shows the results of experimental tests for two levels of 25 and 50%t_r shear strain loading. The outcome indicates that as the compound isolator's average bonding increases, the effective lateral stiffness increases as well. Reducing the average bonding, on the other hand, will reduce the effective lateral stiffness of the compound triple isolator and consequently increases the isolator's isolation efficiency (IE).

4.15.4 Effect of Shear Strain Amplitude of Loading on Compound Isolator's Effective Stiffness and Damping

The experimental outcome indicates that increasing the shear strain amplitude from 25 to 50%t_r will decrease the effective lateral stiffness of the compound triple isolator and increase the effective damping. All lateral shear tests were conducted under constant axial compression load of 750kN and the results are shown in Table 4-6.

4.16 Compound Triple Isolator's Effective Compression Stiffness

To calculate and define the effective lateral stiffness of the compound triple isolators, the same procedure has been applied as was used for the component and compound double isolators discussed in previous sections of this chapter. Figures 4.14 and 4.15 show the input compression load signals and Figure 4.32 shows the resulting compression force-displacement diagrams. More test outcomes of compound triple isolators are available in Appendix B of the thesis.

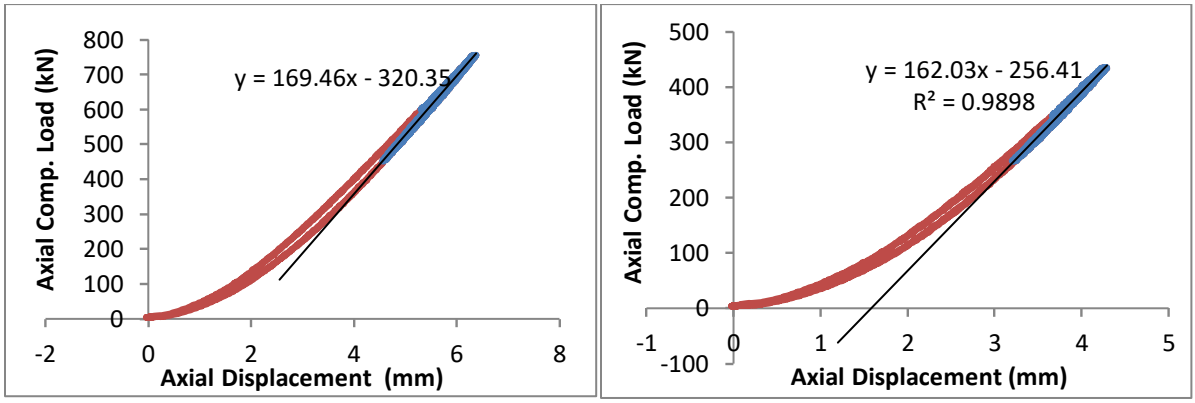

(a) 2B260+1B240 PL= 600KN σmax=3.89MPa (b) 2B260+1B240 PL=348kN σmax=2.26MPa

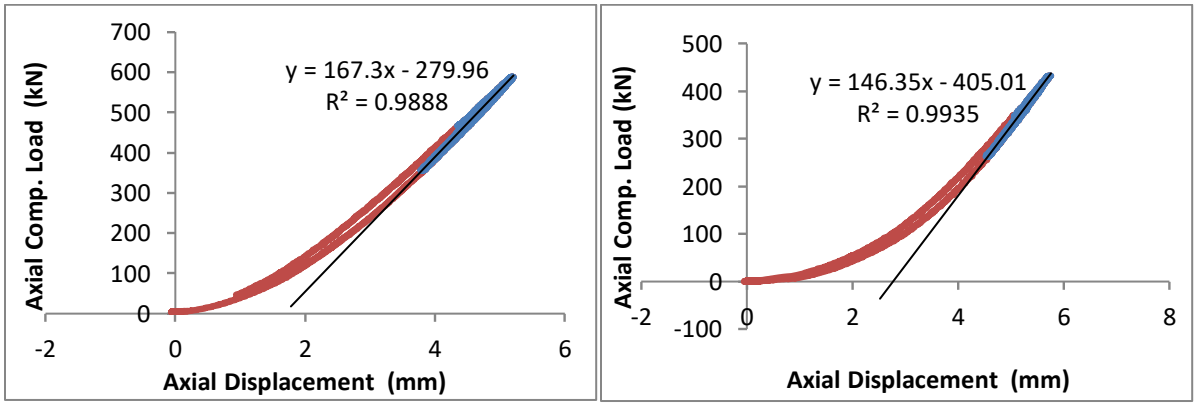

(c) 2B260+1B240 PL=466 kN σmax=3.31MPa (d) 2B260+1B180 PL=348 kN σmax=3.29MPa

Figure 0.32 Compound Triple Isolators 2B260+1B240 (a, b, c) & 2B260+B180 (d) Compression Load-Displacement Hysteresis diagram (pre-load of 348, 466, & 600 (kN)

4.16.1 Compound Triple Isolators Average Effective Compression Stiffness and Effects of Axial Load Level on the Isolator's Compression Stiffness

The load-displacement hysteresis diagrams are plotted in Figures 4.32. Equation Y= aX+b on the compression force-displacement plots defines the average effective compression stiffness ($K_{eff\text{-}v}$ avg). In this equation Y and X represents the force and displacement respectively, the average vertical stiffness is presented by (a) the coefficient of X. The related value of R shown in the plots of figure 4.32 is a measure of the degree of linear relationship between two variables force and displacement and is referred to as correlation coefficient, and shows the degree to which a linear model may describe the relationship between two variables (Karimzadeh Naghshineh et al.). In defining the effect of load level on triple isolators, the compression load-displacement hysteresis diagram obtained from the vertical actuators has been used and the correction for the effects of frame uplift and steel girder deflection has not been considered. Comparison of average effective stiffness present in Figure 4.32 a, b, c and d indicates that as the pre-load level (PL) increases from 348 kN to466 and 600 kN, the compound triple isolator's effective compression stiffness will increase as well. ASCE 7-05 requires that the change in effective lateral stiffness of the isolators related to first and second loading must not differ more than 15%. According to the lateral shear test outcome, the effective lateral stiffness's variation (shown in Table 4-6) of the 1st and 2nd cycle of loading meets the ASCE 7-05 provision.

4.17 Component Material Tests

The component material tests were conducted in two experimental tasks:

1) Isolator components durability and performance under long duration cyclic loading.
2) Experimental tests to study isolator's rubber component hyper elastic behaviour.

4.17.1 Isolator Components Durability and Performance under Long Duration Cyclic Load

The objective of this experimental task is to study the durability and performance of the isolator component under a long duration cyclic loading, like an earthquake. Temperature increase of the isolator's rubber component was the main concern in this study. To conduct this experimental study, B220 as one of the SB-CFREI was randomly selected and tested under a constant axial

compression pre-load of 250 kN and a long duration lateral cyclic loading shown in Figure 4.33. The long duration, 120-second input load signal contains different shear stain amplitude and frequency. This two-minute cyclic loading was conducted twice with no delay time in order to study the isolator components' durability and performance under the 4-minute long duration loading. Figure 4.34 shows the input load signal.

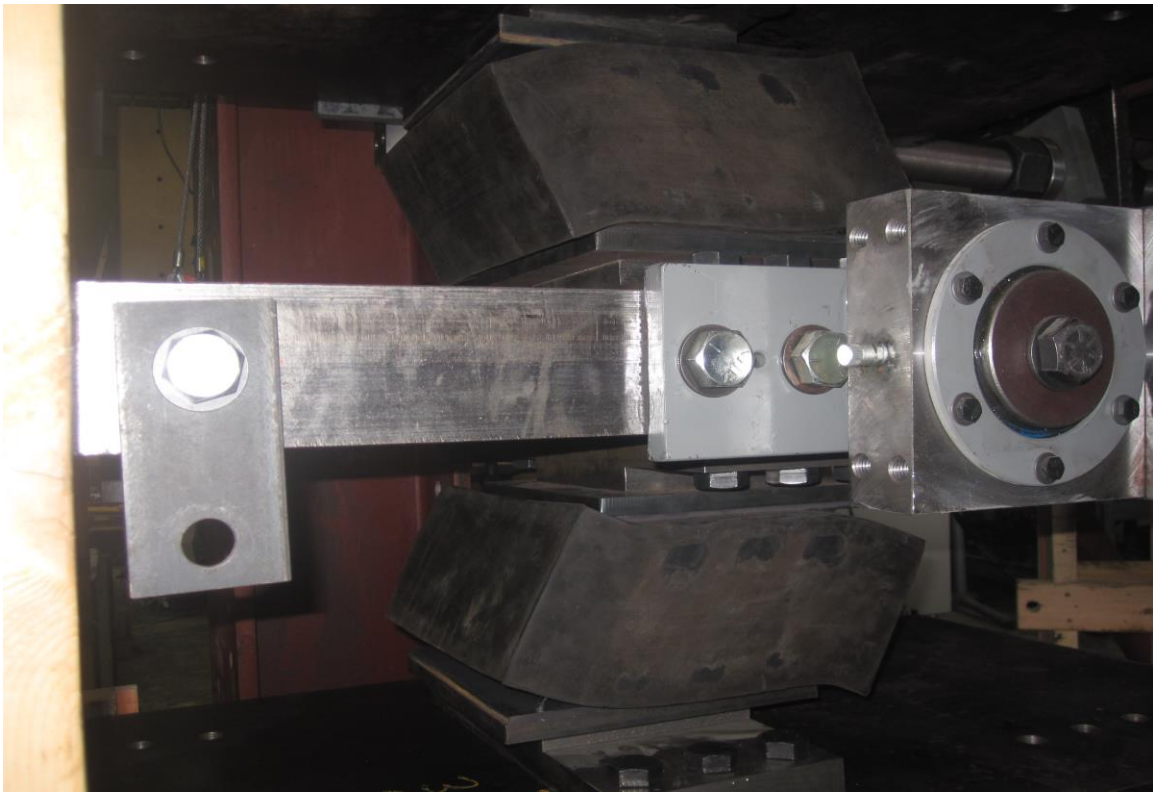

Figure 0.33 B220 isolators under long duration cyclic loading test

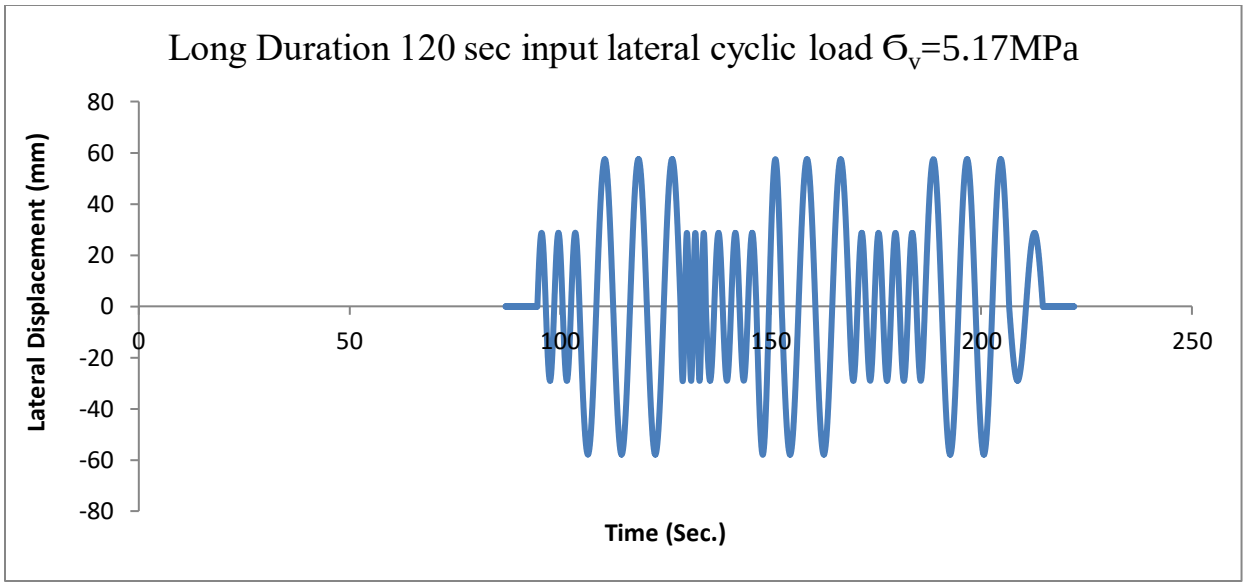

Figure 0.34 Long duration 120-second lateral excitation input load signal

During the 4-minute cyclic test all the isolator components were closely monitored. Temperature increase of the isolator bearing component was the main concern, since occurrence of considerable temperature and heat-up in the isolator's rubber component could effectively influence the isolator design properties and lead to delamination of the rubber layers and failure. Temperature variation was measured every 10 seconds as shown in Table 4-7 and 4-8, indicating no considerable temperature variation in rubber component during the 4-minute excitation. The isolator was closely inspected and no de-bonding or other damage was detected. Figure 4.35 shows the B220 isolator after the test.

Note: Temperature was monitored using the "Amprobe IR608A" Infrared Thermometer. This thermometer is capable of measuring the temperature of a 3x3 inch spot size on the isolator bearing from a distance of about 24 inches.

Table 0-7 Temperature variation of B220 isolator bearing pads under first 120 sec long duration lateral cyclic input load

Test A1 Top Block B220 Isolator			Test B1 Lower Block B220 Isolator	
Time Sec.	Temperature (C)	Temperature Change (C)	Temperature (C)	Temperature change (c)
0.0	21.40	0.00	20.60	0.00
10	21.60	+0.20	20.60	0.00
20	21.40	0.00	20.80	+0.20
30	21.40	0.00	20.80	+0.20
40	21.60	+0.20	20.80	+0.20
50	21.60	+0.20	21.00	+0.40
60	21.60	+0.20	20.80	+0.20
70	21.60	+0.20	20.80	+0.20
80	21.70	+0.30	20.80	+0.20
90	21.60	+0.20	20.80	+0.20
100	21.60	+0.20	20.80	+0.20
110	21.40	0.00	20.80	+0.20
120	21.40	0.00	21.00	+0.40

Table 0-8 Temperature Variation in B220 Isolator CFRE bearing Pad under second lateral cyclic excitation with 120 sec. duration

Test A2 Top Block B220 Isolator			Test B2 Lower Block B220 Isolator	
Time Sec	Temperature (C)	Temp Change (C)	Temperature (C)	Temperature Change
0.0	22.3	0.00	22.80	0.00
10	22.80	+0.50	23.00	+0.20
20	22.80	+0.50	23.20	+0.40
30	22.80	+0.50	23.20	+0.40
40	22.80	+0.50	23.20	+0.40
50	23.00	+0.70	23.20	+0.40
60	23.00	+0.70	23.20	+0.40
70	23.00	+0.70	23.20	+0.40
80	23.00	+0.70	23.40	+0.60
90	23.00	+0.70	23.40	+0.60
100	23.00	+0.70	23.40	+0.60
110	22.80	+0.50	23.30	+0.50
120	22.80	+0.50	23.40	+0.60

Figure 0.35 B220 Isolators after long duration cyclic loading test, no damage was detected

4.17.2 Material Testing to Define the Isolator's Rubber Hyper-elastic Behaviour

4.17.2.1 Introduction

The powerful nonlinear finite element (FE) software, ABAQUS, allows input of different test data to define the proper elastomer material model. Testing of elastomers for the purpose of defining material models is often misunderstood. Several standards are available for the testing of elastomers in tension. "The appropriate experiments are not yet clearly defined by national or international standards organizations. This difficulty derives from the complex mathematical models that are required to define the nonlinear and the nearly incompressible attributes of elastomers" (MSC. Software: Whitepaper - Nonlinear Finite Element Analysis of Elastomers). The objective in conducting the component material tests is to define the isolator's rubber hyper-elastic material model by implementation of the experimental outcome test data as the input required in FE software. Uniaxial tension tests with the following experimental procedures were conducted. Simple tension tests are very popular to study the elastomer material hyper-elastic behaviour. The most significant requirement is that in order to achieve a state of pure tensile strain, the specimen must be much longer in the stretching direction than in the width and

thickness dimensions. The experimental test set-up should assure no lateral constraint to specimen thinning. By conducting finite element analysis on the specimen geometry the specimen length-to-width ratio can be defined. The FE result recommends that the ratio of the length to width or length to thickness of the specimen not to exceed10. Since the experiment is not intended to fail the specimen, it is not required to use dumbbell shape specimens and also there is not an absolute specimen size requirement. The initial length of the specimen (L_0) is the length between the instrument clamps and the stretched length during the test is (L). Therefore, the specimen straining, L/L_0 must be measured on the specimen and away from the clamp, where a pure state of tension strain is occurring. The load, P, is measured by a load cell during the tension test and calipers can be used to measure the instantaneous area, A, normal to the load. The elastomer material is assumed to be incompressible, if the instantaneous area is not measured. This means assuming no change occurs in the specimen's initial and instantaneous volumes V_0 and V respectively (MSC- Software White paper).

4.17.2.2 Rubber Material Test Specimen

The rubber test specimens are cut in shape from the same rubber material used in the isolators as the isolator's elastomeric component. These dog-bone shaped specimens have the thickness of T= 7mm and dimensions of 100×10 mm (gage length L=100 mm, width W=10 mm), and rectangular shaped specimens have dimensions of 100×18×7 mm with 50 mm gage length and 200×10×7 mm with the gage length of 100 mm as shown in Figure 4.36 SP2a and SP2b. The two dog-bone shaped specimen demonstrated a more consistent outcome.

Figure 0.36 Rubber sample specimens used in uniaxial tension tests

4.17.2.3 Uniaxial Tension Material Testing, Analysis and Outcomes

Component material tests were conducted in the UBC material lab in order to investigate the mechanical and dynamic properties of the elastomer component. Natural rubber is the main and important elastomeric component of the SB-CFREI and its hyper-elastic characteristics have a crucial effect on the isolator's performance. A uniaxial tension test was conducted on four rubber test specimens of the isolator's rubber material. The test was conducted with three cycles of loading and unloading with a constant strain rate of 100 mm/min., up to a maximum stretched length of 250 mm. Figure 4.37 shows the uniaxial test apparatus and the rubber specimen under cyclic tension loading and the resulting load-displacement curves related to rubber test specimen loading and unloading.

The solid line shown in Figure 4.38 represents the material average or mean engineering stress-strain relationship as the result of the uniaxial tension tests on the isolator's rubber component.

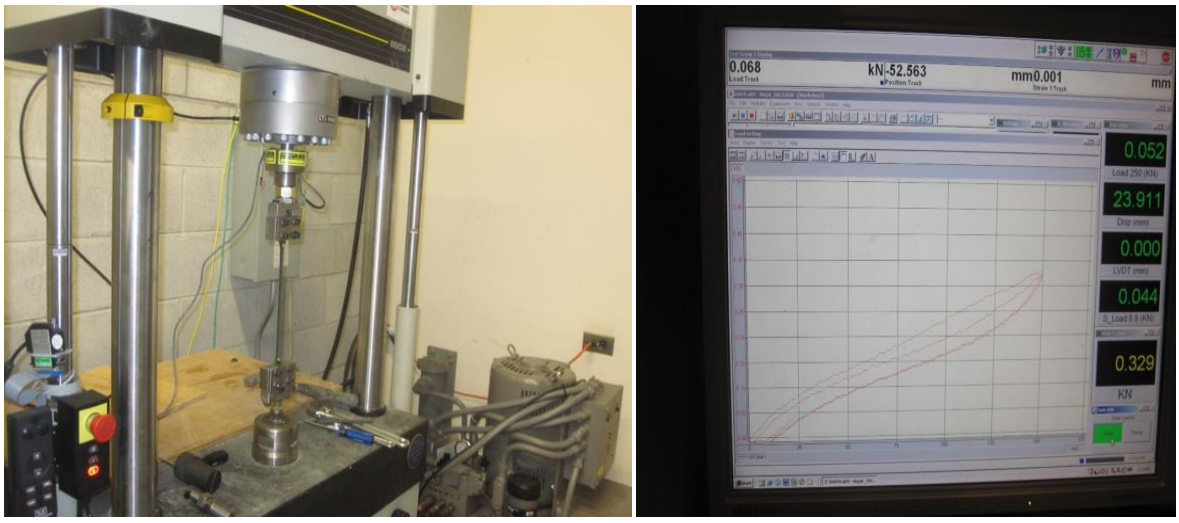

Figure 0.37 The Uniaxial test apparatus in the material lab of the University of British Columbia UBC

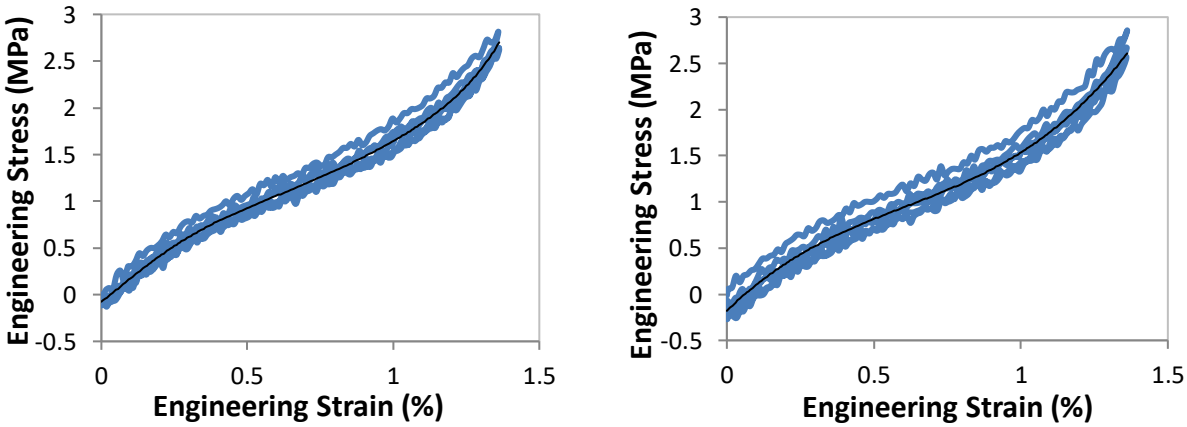

(a) (b)

Figure 0.38 Stress-strain relationships: 2 cycle uniaxial tension test loading and unloading on 100×10×7mm rubber specimen a) SP2a, and b) SP2b

To define and obtain the material model that properly represents the isolator's rubber component hyper-elastic behaviour, two cycles of uniaxial loading and unloading are shown in Figure 4.38. These mean curves (solid line) were shifted to show zero stress for zero. The mean curve was implemented in the ABAQUS finite element software as the input test data. The software defines the material constants and recommends the model that represents the elastomer material model for finite element analysis and modeling of the SB-CFREIs.

Another objective of the tests was to experimentally obtain the nominal tensile modulus of rubber at 100% elongation. This isolator's rubber nominal tensile modulus was defined equal to E = 2.209 MPa after the mean stress-strain curve was shifted higher to correct location (to show zero stress for zero strain). The nominal tensile modulus implies a nominal shear modulus of G = 0.75 MPa for an incompressible elastomer having a Poisson's ratio of μ= 0.5 according to the equation [7].

$$G = \frac{E}{2(1+\mu)} \qquad [7]$$

Nominal shear modulus of the rubber G is one important parameter to define the rubber hyper-elastic material model. Another method to estimate the value of the rubber shear modulus is using the graph in Figure 4.39 proposed by GoodCo Z-Tech (2010). Using these plots for rubber with hardness of 55 durometer at room temperature of around 20 degrees centigrade indicates the rubber component shear modulus of G = 0.765MPa, which is relatively close to the value achieved from component tests.

As described earlier, the Neo-Hookean material model is the simplest material model describing the rubber component's hyper-elastic behaviour. In this material model, the rubber is assumed as an elastic isotropic material with a strain energy function that is characterized by the shear (G) and bulk (k) moduli of the rubber. If the rubber component of the isolator that has a shear modulus of o.75 MPa (achieved from the experimental), performs as a nearly incompressible material with a Poisson's ratio of approximately 0.5, then the bulk modulus (K) can be estimated by using the well-known elasticity equation [7] :

$$\frac{\boldsymbol{K}}{\boldsymbol{G}} = \frac{\mathbf{2(1+\mu)}}{\mathbf{3(1-2\mu)}} \qquad [8]$$

Taking the rubber bulk modulus **k =** 2400 MPa with G = 0.75 Mpa results in Poisson's ratio of 0.4998, which is sufficiently close enough to 0.50 to simulate the incompressible behaviour of the rubber in the finite element analysis.

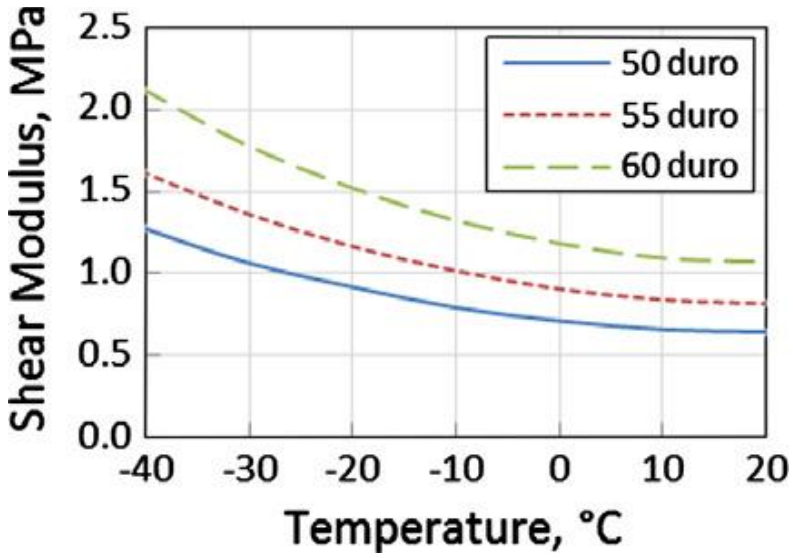

Figure 0.39 Shear modulus of rubber as a function of temperature from GoodCo Z-Tech. Elastomeric bearings catalog. Montreal (Canada 2010)

4.17.2.4 Conclusion on Isolator's Component Material Tests

The first series of component material tests was conducted on two B220 isolators to investigate the performance and durability of the isolator's rubber component under long duration cyclic loading. The main concern was the temperature increase in the rubber component during the two 120-second loading durations, as heat-up or temperature increase would affect the rubber properties and consequently change and shift the isolation frequency to a range that has not been accounted for in the design. During the excitation period the rubber component temperature was monitored at 10-second intervals. Tables 4-7 and 4-8 demonstrate the temperature variation of the rubber and the results do not show considerable temperature increase during the cyclic loading. The final outcome for both B220 isolators indicates that the temperature variation was less than 1 degree centigrade. Figure 4.35 shows both B220 isolators after the long duration tests. Both isolators demonstrated a satisfactory performance, as no heat-up and no delamination cracks or any other damage was detected.

The second series of component material tests was conducted to investigate the hyper elastic behaviour of the isolator's rubber component. The test results on different dog-bone shaped rubber specimens were analyzed and plotted. These outcome test data are implemented in FEA of the SB-CFREIs in Chapter 5 of the thesis. The solid curves shown in Figures 4.38 represent

the mean average stress-strain behavior of the rubber component and are used as the input test data in conducting analytical tasks to investigate the SB-CFREIs by application of the ABAQUS finite element software.

4.18 Conclusion and Outcome Related to Experimental Studies

4.18.1 Conclusion Related to Experimental Test on Component and Compound Isolators

The experimental findings and achievements to date are as follows:

1) Increase in bonding level (BL) will increase the SB-CFREI's effective axial compression stiffness and modulus.
2) All isolators with different levels of bonding have undergone axial compression stress of 1.72 to 11.38 MPa induced from constant compression pre-load and maximum cyclic loading respectively. All isolators under constant axial compression load have simultaneously undergone lateral deformations and demonstrated satisfactory performance. After completion of tests, no delaminating damage was detected.
3) Isolators with a lower bonding level demonstrate higher equivalent viscous damping.
4) Test outcomes indicate that as the isolator's bonding level increases, the effective lateral stiffness will increase as well.
5) SB-CFREIs have higher effective lateral stiffness at a lower level of shear strain amplitude (SSA), and it decreases as SSA increases.
6) Isolator's equivalent viscous damping will increase at higher SSA, and the increasing pattern differs for isolators with different bonding levels.
7) Plots of damping vs. bonding levels of the SB-CFREIs indicate that isolators with a low bonding level have higher damping and energy dissipation capabilities.
8) Compound isolator's effective lateral stiffness increases as the average bonding level increases and the increase pattern depends on the combination configuration of the compound isolator.
9) Test outcomes on compound isolators indicates that the axial compression load controls the required number of component isolators and the bonding level and combination configuration controls the damping and isolation efficiency of the desired compound isolator.

10) Component material test outcome indicates that the isolator's rubber component has a shear modulus of around G = 0.75MPa and bulk modulus K of 2400 MPa. Neo-Hookean rubber material model with energy function that is characterized by the two defined moduli, is most justified to describe the hyper-elasticity of the isolator rubber component. ABUQUS material evaluation proposes Ogden (N=3) and polynomial (N=2) strain energy function as other alternatives.

CHAPTER 5: ANALYTICAL STUDY OF SB-CFREI

5.1 Summary

Finite element analysis (FEA) is a powerful design tool that can be employed in the preliminary design of FREIs, as the design will be finalized (ready for production) after experimental testing of the isolator's prototype and meeting the objectives. Seismic codes require that, for all isolator's type the final mechanical design properties and specifications of isolators to be evaluated through experimental testing. Accordingly, the prime objective of the isolator's preliminary design is to provide the required information for the fabrication of the seismic isolator's prototypes, and parameters like the vertical compression and lateral shear stiffness. Also the equivalent viscous damping ratio of an isolator should be reasonably estimated (Toopchi-Nehzad et al., 2012).

Robust FE model that is capable of addressing large deformations and accounts for the nearly incompressible behaviour of the elastomer is required for analysis of the isolator's elastomeric components (Toopchi-Nehzad et al., 2012). In conducting the finite element task, the commercial finite element program ABAQUS with high capabilities in simulation of the elastomeric material behaviour was implemented in the analytical task of this research. The finite element modeling of fully bonded conventional steel-reinforced elastomeric isolators is relatively straightforward, but it is more challenging to simulate the SB-CFREI's behaviours under seismic excitation as the isolator's bonding varies. The finite element model should also be capable of simulating the hyper-elastic properties of the rubber as the most critical component of the fiber-reinforced elastomeric isolators. As the deformation characteristic and mechanism of the fiber reinforcement is not the same as that of the steel reinforcing plates, "available closed-form equations for the stiffness solution of conventional steel reinforce elastomeric isolators, are not generally applicable to FREIs to define the vertical compression and bending stiffness of strip, rectangular, and circular FREIs" (Toopchi-Nehzad et al., 2012) therefore, in conducting the preliminary design of FREIs in general and SB-CFREI specifically, the application of FE modeling and analysis becomes more significant.

5.2 Objectives

The prime objective of the analytical task is to study the dynamic characteristics of SB-CFREI under lateral cyclic loading by implementing finite element analysis (FEA) and to investigate the validity and reliability of the FEA in presenting the dynamic behaviour of the innovative SB-CFREI seismic isolators.

Another important objective in conducting the analytical task was to define the effective lateral stiffness Keff-$H_{(\gamma)}$ and the force-displacement relationship of SB-CFREI under different constant axial compression pre-load at varying shear strain amplitude (γ), and to compare this important isolator's dynamic parameter defined by FEA with that of the experimental outcomes. The comparison of the experimental and the finite element load-displacement diagrams of isolators with different bonding level (BL) demonstrates the validity of finite element application in preliminary design of SB-CFREIs.

5.3 Finite Elements Modeling of SB-CFREI

5.3.1 Material Modeling

In this section the FE modeling will be described in more detail, especially the hyper-elastic material model and the computer program and software implemented in this study. ABAQUS (Hibbitt, Karlsson & Sorensen Inc., 2002), the commercial finite element program capable of analyzing elastomeric material behaviour, was implemented. In this research task two material models are used to present the rubber component hyper-elastic characteristics: first, the Neo-Hookean material model was implemented as the simplest hyper-elastic material model, often used to present the rubber material in the FE modeling of the isolator. The Neo-Hookean material model requires only two material parameters: 1-Bulk modulus K and 2- Shear modulus G. The second method to describe the rubber hyper-elastic behaviour with more accuracy was the test input of the rubber material sample. This is done by conducting experimental uniaxial tension tests on the rubber specimens of the same elastomeric material used in the isolators. The mean stress-strain curves are implemented as the input test data into the ABAQUS finite element software in order to achieve the most suitable rubber hyper-elastic material model.

5.3.2 SB-CFREIs 2D and 3D Finite Element Modeling

The mathematical model of SB-CFREIs can be presented by 2D and 3D finite element models. Mordini and Strauss (2008) stated that;

under axial compression load, the 2D and 3D models provide results considerably different. This is because the 2D finite element model includes plane strain elements with constrained out-of-plane deformation and this leads to a strong vertical displacement reduction and a fictitious vertical stiffness increment. In conducting lateral shear cyclic loading, on the contrary, the 2D model provides results almost identical to the 3D model because the out-of-plane constraint has low influence on the CFREI's lateral deformation mechanism. Therefore, "it can be concluded that the 3D model is necessary to study the vertical stiffness, while the 2D model is enough to evaluate the behavior implying shear displacements" Mordini and Strauss (2008). Therefore, in this research to investigate the lateral force-displacement relationship, the 2D finite element models of the isolators are implemented.

5.3.3 Large Deformation and Element Distortion

Under high and extensive lateral shear loads elastomeric seismic isolators may undergo very large deformations. Therefore, in conducting the finite element analysis of these type of isolators, the application of updated lagrangian instead of the conventional total Lagrangian formulation is recommended and in this current research studies an updated Lagrangian approach has been implemented. In this approach, during the analysis the orientation of the local coordinate system is updated, based on the element's deformed configuration (Toopchi-Nehzad et al., 2013; Strauss and Mordini, 2008). The lower order finite elements are recommend as the performance of these elements are superior to higher-order elements in simulating large distortions. (Toopchi-Nehzad et al. 2013)

5.3.4 FE Modeling of Carbon Fiber Reinforcement

In order to model the reinforcements in a rubber metrix, two main concepts can be adopted: 1-the discrete approach and 2-the smeared approach. The first approach, treats each group of fibers as a truss embedded in the rubber matrix and is suitable for both 2D and 3D finite element modeling (Mordini and strauss 2008). "Using the smeared concept, on the other hand, means

describing the carbon fiber fabric as a continuous sheet with an equivalent cross-sectional area. Membrane elements are used in 3D models and truss elements are used in 2D" (Mordini and Strauss 2008).

In this research task the CF reinforcement is modeled using the equivalent thickness of t_{fs} = 0.22mm with elastic modulus of E = 230 GPa (ACP Composite inc.20120) and poison ratio of 0.2. In 2D modeling of the carbon fiber reinforcement, a two-node linear truss element T2D2 from the ABAQUS element library is selected.

5.4 Rubber Material Incompressibility in FEA

Implementation of rubber properties in the finite element analysis needs special attention due to the rubber's incompressibility that can result in serious numerical errors if standard isoparametric elements are used. As in the finite element analysis the state of stress is determined from the state of strain. Since in the rubber as a nearly incompressible material the volumetric strain in finite elements is almost zero, therefore, defining the mean stress or pressure based on the volumetric part of the strain is challenging" (Zienkiewicz and Taylor, 1989). In an incompressible material, standard isoparametric elements can show a pathological behaviour, called volumetric mesh-locking, which is related to the inaccurate performance of an element due to the over-constrained condition and inadequate active degrees of freedom (MSC Software Corporation). To avoid these problems, modern finite element techniques implements "mixed-methods" for incompressible materials (Zienkiewicz and Taylor, 1989). Both the strains and stresses are assumed as the unknowns in the mixed-methods. In conducting the FE analysis on SB-CFREIs in this research, a commonly used mixed method developed by Hermann has been used.

Incompressible material is modeled in ABAQUS using solid elements with the "Hybrid" formulation. "In this formulation, Hybrid elements introduce more variables into the problem to alleviate the volumetric locking problem" (ABAQUS element selection criteria).

5.5 Rubber Hyper-elastic Material Model

Hyper-elastic materials are generally described in terms of strain energy potential, which defines the amount of strain energy stored per unit volume of material as a function of the strain in the material and is described by Eq. [9]. ABAQUS offers several forms of strain energy potentials.

The material model, like the Neo-Hookean, is recommended when only limited experimental test data are available. The Neo-Hookean material model, applied first in the current research, was used to describe the isolator's rubber hyper-elastic behaviours based on the rubber properties. The Neo-Hookean material model is the simplest form of the strain energy potential and often serves as a prototype for elastomeric materials in the absence of accurate material data. It provides a reasonable approximation to the behaviour of rubber-like materials and can give an adequate first approximation to the material behaviour (Cadge and Prior, 1999).

$$U = C_{10}(I_1-3) + \frac{1}{D1}(J_{el}-1)^2 \qquad [9]$$

Where:
U is the strain energy potential; $\mathbf{J_{el}}$ is the elastic volume ratio; $\mathbf{I_1}$ is the first invariant of the deviatoric strain; and C_{10} and D_1 are material constants. C_{10} describes the shear behaviour of the material, and *D*1 introduces compressibility. The initial shear modulus and bulk modulus are related to D1 and C_{10} as defined in Eq.[9] of this chapter.

The second method used in this study to define the rubber material hyper elastic model was by inputting the experimental test data. ABAQUS has high capability in using different test data as the input to define the proper elastomer material model.

5.5.1 Neo-Hookean Material Model Coefficients

The elastomer material in the seismic isolators is often modeled using Neo-Hookean hyper-elastic material model, which assumes the elastomer as an elastic isotropic material with a strain energy function that is characterized by the elastomer's shear and bulk moduli, G and k, respectively. The Neo-Hookean model is a basic hyper-elastic material model that relies on a minimum set of material data properties mainly described by two important material coefficients C_{10} and D_1.

In general, the two Neo-Hookean material model coefficients C_{10} and D_1 are defined by equations [10].

$$C_{10} = \frac{G}{2} \qquad D_1 = \frac{2}{K} \qquad [10]$$

In conducting finite element analysis of SB-CFREIs, these coefficients are determined using equation [10]. $C_{10} = 0.75/2 = 0.38$ MPa and $D_1 = 2/2400 = 0.0008$MPa are implemented in the FE modeling of the rubber component. Table 5-1,5-2 and 5-3 shows the geometrical and material properties of the isolator's rubber and carbon fiber components.

5.6 SB-CFREI -Material and Geometric Properties and FE Model

The finite element model of the SB-CFREIs was prepared with special attention to the isolator's geometric properties, boundary conditions, and axial compression and lateral shear load cases. The top and bottom steel plates were modeled as rigid and rubber layers and carbon fiber layers were assumed fully connected by application of the "Tie" option available in ABAQUS. Other boundary conditions and bonding specifications were set to account for the true deformation mechanism and dynamic behaviours of the isolators under lateral shear and axial compression loadings. Carbon fiber and rubber layers were modeled with the method mentioned in previous sections. The preliminary FE model of a typical isolator (B260) is shown in Figure 5.1.

To evaluate the validity of finite element modeling in the preliminary design of the SB-CFREIs, FE analysis was conducted for typical isolators with different bonding levels (low and medium range BL) and under the same loading conditions, the force-displacement diagrams were plotted and compared with those of the experimental.

5.6.1 Material and geometrical properties of SB- CFREI

The material and geometric properties of the isolators are summarized in table 5-1 ad 5-2 showing the Isolator's Material and Geometric Properties respectively and table 5-3 shows the rubber material property (Neo-Hookean material model coefficients).

Table 0-1 Rubber and CF Material Properties

G_e Shear modulus of the elastomer (rubber)	0.75Mpa
γ_f Poisson's Ratio of the fiber reinforcement	0.2
E_f Yong Modulus of the fiber reinforcement	230 GPa
K Rubber Bulk Modulus	2400 MPa

Table 0-2 Geometrical Properties

B width of the Isolator's bearing	260mm
L Length of the Isolator's bearing	260mm
t_e Thickness of a single elastomer	4.60mm
t_r Total thickness of the elastomer layers	115mm
t_f Thickness of carbon fiber reinforcement	0.22mm
H Height of the isolator	120mm
S Shape Factor for fully bonded	14.13

Table 0-3 Rubber Material Properties

Neo-Hookean Material Model Coefficients	
C_{10} = G/2	0.38MPa
D_1= 2/K	0.0008MPa

5.6.2 Boundary Condition and Load Cases

Boundary Condition: The top steel cover plate is assumed fully connected to the CFRE pad; this connection is modeled using the "Tie" option available in ABAQUS. The top steel cover plate is assumed rigid but free to displace in X-X and Y-Y directions. The bottom steel cover plate is also assumed rigid. The boundary condition set for this plate was assumed fixed at the reference point located at the plate center. The CFRE pad is restricted to move in the X-Y plane only. Vertical pre-loads of 116 and 250 kN were assumed as distributed over the length of the top steel cover plate. This load imposes local pressure ranging from 1.72 MPa to 9.77 MPa depending on the size of the top steel cover plate. The distributed compression pre-load was modeled to act

only in the X-Y plane as shown in Figure 5.1 and 5.2. Lateral shear load cases were imposed on the isolator at the center point of the top steel cover plate in the form of shear straining with amplitude of 25, 35, 50, 75, and 100%t_r. The lateral load cases were imposed on the isolator in the X-X direction while the axial compression pre-load was imposed in the Y-Y direction. Figure 5.2 shows the un-deformed shape of the B260, and 5.3 shows FE deformed shape of the isolators under shear strain loading. Table 5-4 shows the element type selected from the ABAQUS library in FE modeling.

Table 0-4 2D FE Model (Element Type)

Material	Element Type from ABAQUS Library	Element Name from ABAQUS Library
Carbon Fiber	2 node Linear Trust Element	T2D2
Rubber	4 node 2D Plane Strain quadrilateral, hybrid, reduced integration, hour glass control	CPE4RH

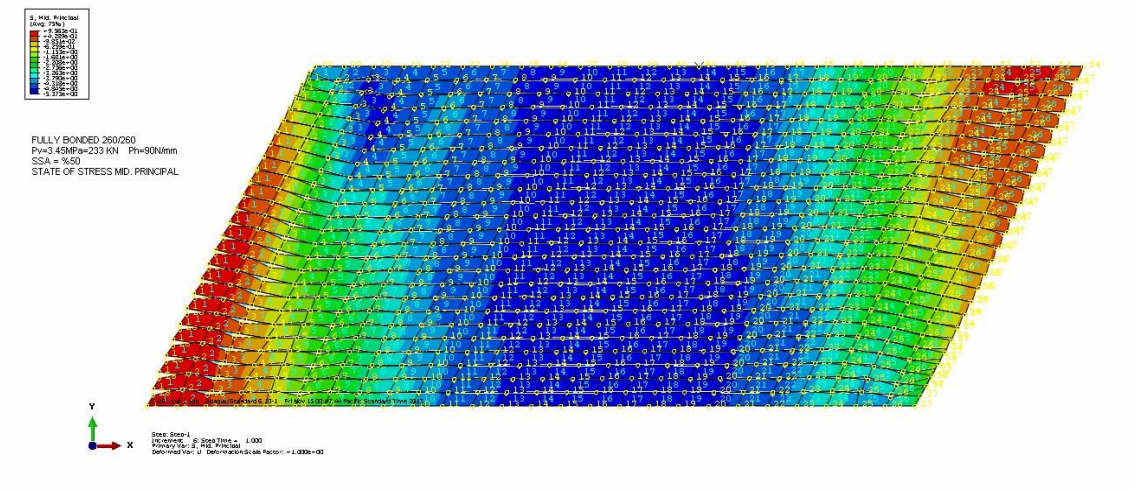

(a)

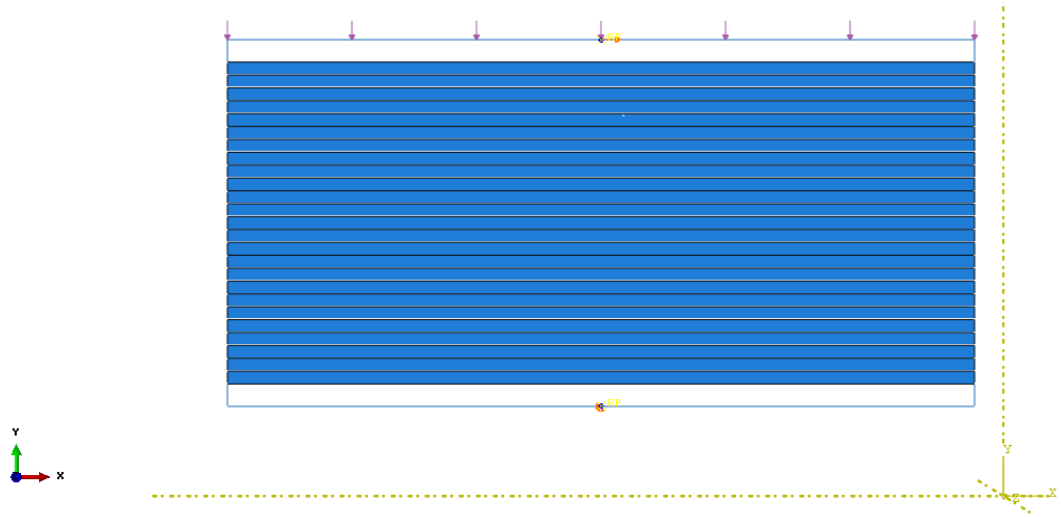

(b)

Figure 0.1 FE model of B260 isolator showing FE (a) deformed and (b) un-deformed shape rubber & fiber reinforcement layers, top and bottom discreet rigid plates with axial compression distributed load on top

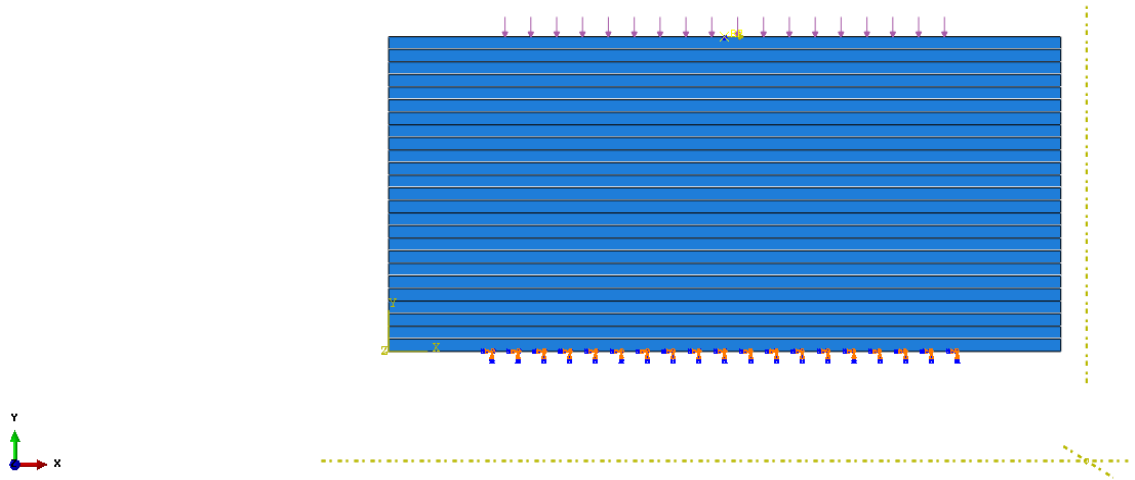

Figure 0.2 Typical FE boundary condition and loading

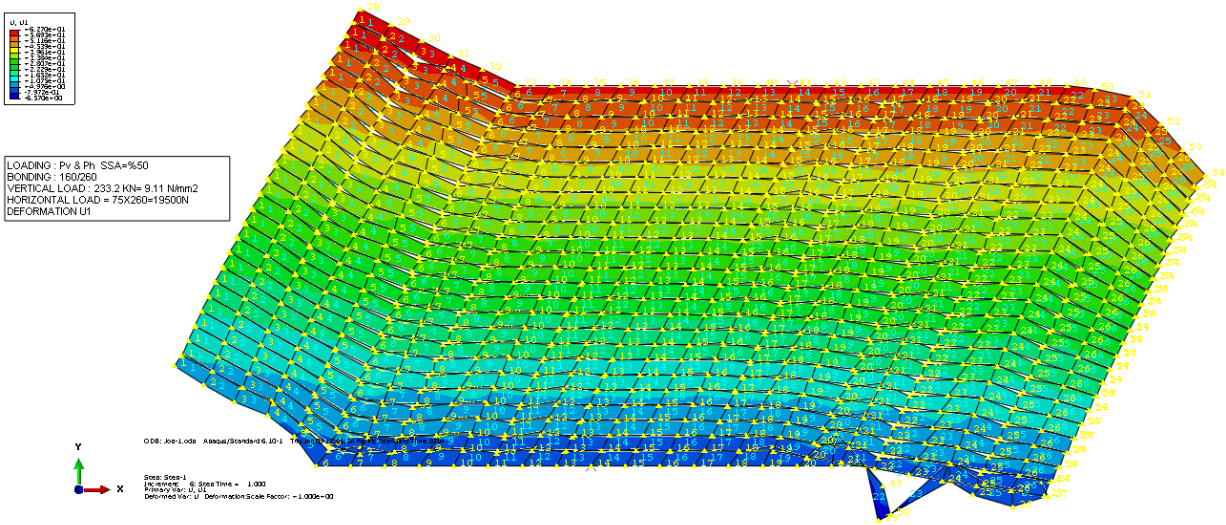

Figure 0.3 FE model of B160 isolator showing FE deformed and un-deformed shape, rubber & fiber reinforcement layers, top and bottom discreet rigid plates with axial compression distributed load on top

5.6.3 Finite Element Analysis Results and Discussion

5.6.3.1 FE Force-Displacement Relationship and Comparison with Experimental (Medium Bonding Level Isolator)

B220 isolator with BL of 71.60% is considered as typical semi-bonded isolator with medium level of bonding. The force-displacement diagrams of this isolator were plotted using the FEA and experimental outcomes. The shear strain loading of 15-50%t_r and constant axial compression load of 250kN were the selected pre-defined load cases. The hyper-elastic material model of the elastomer was presented by the test input data, which were obtained by conducting the component material tests. Table 5-5 and Figure 5.4 demonstrate the FE and experimental outcome values and related force-displacement relationship graphs for B220 isolator. The plots of force-displacement diagrams for the experimental and FE are fairly close at lower shear strain loadings of SSA of 35%t_r and lower. As the shear strain increases to SSA=50%t_r, the FE curves begins to move apart and shift to a higher position as shown in Figure 5.4. This difference is mainly due to occurrence of the peel-off phenomenon in the experimental testing, which reduces the lateral stiffness of the isolators. The occurrence of peel-off becomes less intensive as the bonding level decreases and as the consequence the differences between the force and displacement values decreases and the force-displacement diagrams become closer to match when comparing the FE and experimental outcomes for the lower BL (B180) isolator. These results are demonstrated in plots of Figures 5.4

Table 0-5 Force-displacement relationship of B220 Isolator by Finite Element and Experimental

Shear Strain Load Cases		FE and Experimental Reaction Forces			Comparison
SSA % t_r	Displacement (mm)	FE Model Force (kN)	Exp. 1st cycle Force (kN)	Exp. 2nd cycle Force (kN)	Difference in FE & Exp. 2 (%)
0.0	0.0	0.0	0.0	0.0	0.0
15	17.25	4.89	6.79	4.88	0.2
25	28.75	7.48	10.28	8.21	8.9
35	40.25	11.05	13.34	11.96	7.61
50	57.50	19.43	15.96	14.65	32.63*

*(The difference is higher because the influence of the peel-off phenomenon, which reduces the isolator's effective lateral stiffness, was not accounted for in FEA. At higher shear strain loading this influence is higher, especially for an isolator with higher BL.)

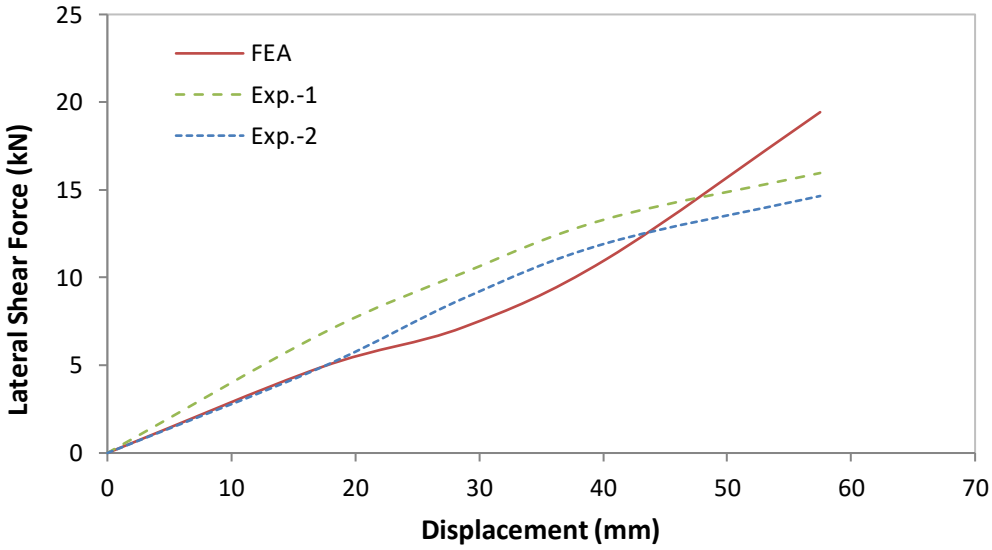

Figure 0.4 Finite Element and Experimental Force-displacement Relationship
(Isolator B220 Exp. 1 and 2)

As shown in Figure 5.4 the difference in values of the force-displacement plots are higher at shear strain amplitude of 50%t_r. This is due to not accounting for the peel-off phenomenon in FE modeling. This difference is higher at higher lateral loading like SSA=50%t_r and higher. In low shear amplitude the FE and Exp. force-displacement relationship are fairly close and the effect of the peel-off is not considerable. In order to use a more stable force-displacement relationship in the experimental outcome, the results of the second loading cycle were considered. In conducting the finite element modeling, the rubber bulk and shear modulus K = 2400 MPa and G = 0.75 MPa were considered. The isolator's rubber properties were defined by the component material test discussed earlier. Figure 5.5 demonstrates the deformed shape of the B220 isolator FE model under axial compression and lateral shear loads.

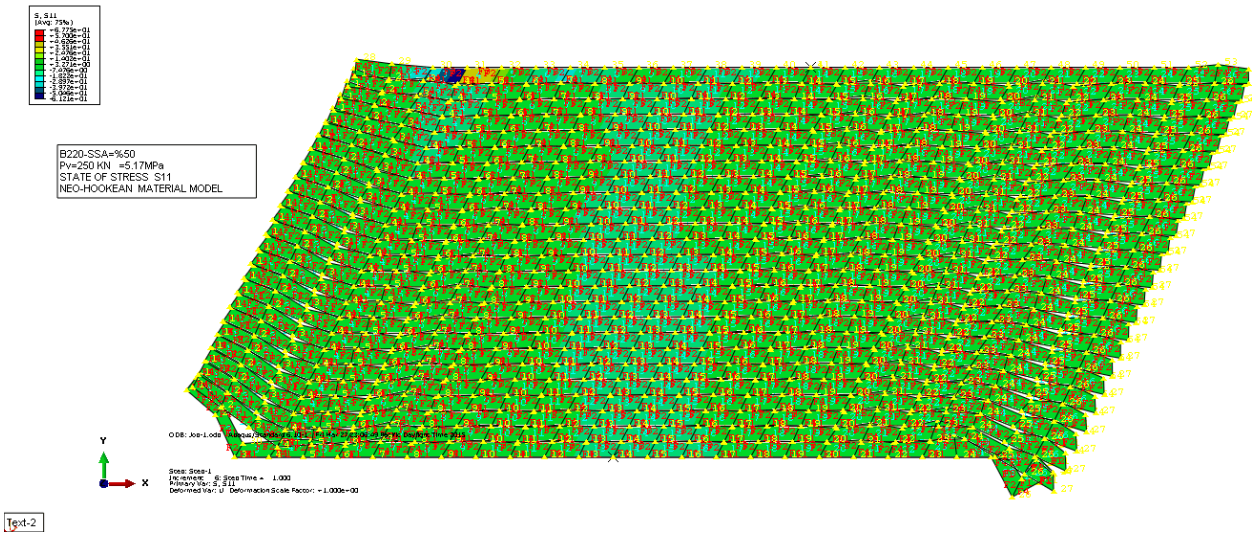

Figure 0.5 B220 isolator FE modeling–deformed shape under lateral shear and axial compression load (Pv = 250 kN, SSA=50%tr)

5.6.4 FE and Experimental Force-Displacement Relationship (for low bonding level isolator B180)

The lateral shear force-displacement values from FEA and the experimental program are shown in Table 5-6 for shear strain amplitudes of 15, 25, 35 and 50%t_r, and a constant axial compression load of P_v=250 kN. The Neo-Hookean material model has been implemented to represent the rubber hyper-elastic behaviour in the finite element modeling. The isolator's force-displacement diagrams obtained from the finite element modeling and experimental results are shown in Figure 5.7 for a typical low bonding level isolator. The experimental and finite element analyses were conducted on the B180 isolator and the comparison of the outcomes shows relatively close agreement. In conducting the FE analysis for the B180 isolator with a bonding level of BL = 47.93%, the influence of the peel-off phenomenon is minor and can be ignored in the FE modeling when conducting the isolator's preliminary design. In the following sections, it is shown that with isolators with higher bonding levels, like B220 with BL= 71.60%, the effect of peel-off is considerable and definitely should be considered in the future finite element modeling of the isolators, especially in shear strain amplitude of 50%t_r and higher.

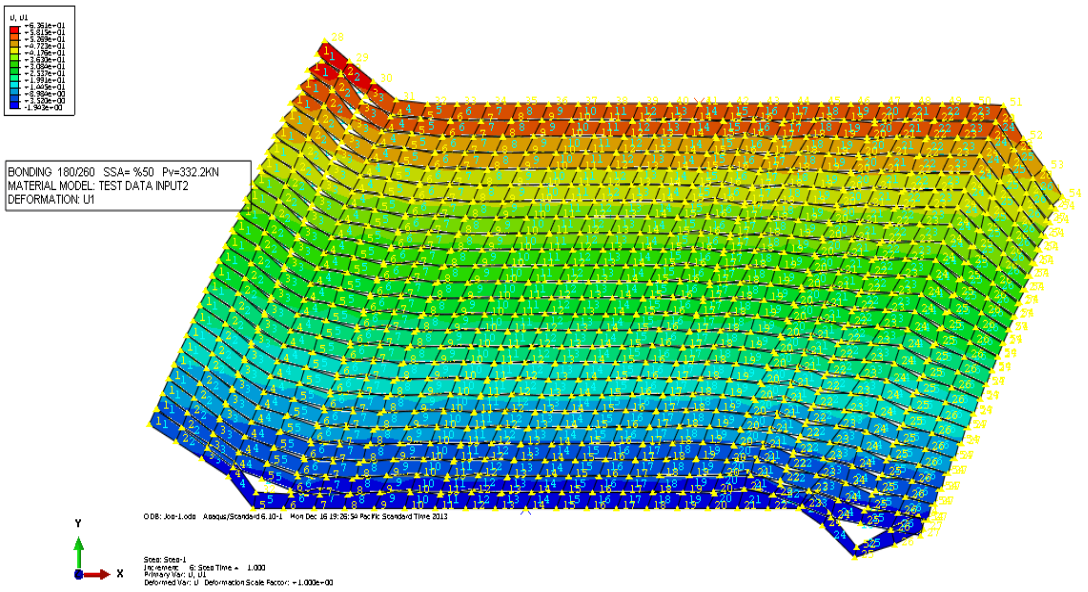

Figure 0.6 B180 Isolator state of deformation U1 under lateral shear load of SSA = 50%tr and axial compression load of 250 kN

Table 0-6 B180 Component Isolator Finite Element Modeling and Experimental Force-Displacement Outcome Values

SSA (t_r%)	Displacement (mm)	FE-Modeling Force (kN)	EXP1-1st cycle Force (kN)	EXP2-2nd cycle Force (kN)	Difference FE & Exp.(%)
0	0	0	0	0	0
15	17.25	5.82	5.27	5.2	9.45
25	28.75	8.50	8.15	7.8	4.12
35	40.25	10.08	10.27	9.60	-1.88
50	57.50	12.94	11.20	10.29	13.45

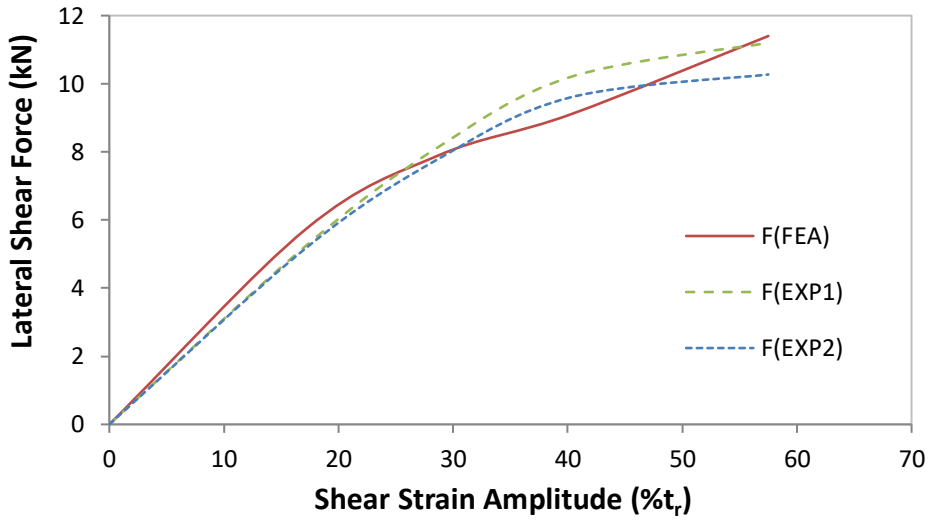

Figure 0.7 Force-Displacement Diagram: FEA and Experimental (Low BL -B180 isolator)

5.7 Peel-Off Phenomenon

One of the prime objectives in conducting the analytical task was to investigate the reliability of FE modeling in the preliminary design of SB-CFREIs. Therefore, FE modeling of the isolators needs to be well justified by considering all parameters affecting the outcomes in order to represent the isolator's real behaviour under dynamic loadings. Occurrence of the peel-off phenomenon is one of the parameters that needs special attention when conducting FE modelling of the isolators.

In fabrication of the SB-CFREIs the steel cover plates and top and bottom bearing rubber are bonded by adhesive compound (cold Vulcanized), therefore limited peel-off phenomenon was anticipated. The partial peeling-off of the CFRE pad from the steel cover plates was allowed in limited magnitude to avoid concentration of high local (peeling) tensile stresses. The magnitude of the peel-off region could depend on bonding level (BL), shear strain amplitude (SSA), and axial compression load Pv. The other isolator's mechanical properties and boundary condition may also influence the intensity of this phenomenon. To have better understanding of this phenomenon, further research studies and investigations in this area are suggested.

In conducting FE modeling, the effects of the peel-off phenomenon was not accounted for, as the nature and magnitude of this phenomenon is not yet well defined for different isolators undergoing different loadings; therefore, as expected, the FE results show higher lateral stiffness in comparison with those of the experimental.

The effective lateral stiffness of isolators with low bonding level is less affected by the peel-off phenomenon in comparison with isolators having higher BL. This finding is demonstrated by comparing the experimental and FE force-displacement diagrams of B180 (BL = 47.93%) and B220 (BL = 71.60%), shown in plots of the Figures 5.4 and 5.7.

5.8 Results and Discussion

After conducting the Finite Element Analysis on SB-CFREI and comparing the outcomes with those of the experimental, the following results are achieved.

1) Application of 2D Finite Element Modeling is justified and can be implemented to determine the force-displacement relationship and the effective lateral stiffness Keff-h for the preliminary design of the SB-CFRE isolators.

2) The Neo-Hookean material model is the simplest material model. It can be considered to present the hyper-elastic behaviour of the SB-CFREI's rubber component, especially when material testing of the isolator rubber component is not possible.

3) The force-displacement relationship achieved by FEA is not very sensitive to the size of rubber elements in the FE mesh. Selecting larger element size to save computation time and cost is justified and still provides fairly reliable estimates of the lateral load-displacement relationship.

4) Since 2D finite element modeling of the SB-CFREI assumes no out of plane deformation, it is not recommended to define the bearing effective compression stiffness and modulus.

5) In conducting the FEA, the peel-off phenomenon was not considered, since the nature and magnitude of this phenomenon is not well defined yet and needs more investigation in future. The force-displacement diagram of isolators with lower BL achieved from FE analysis matches closely with that of experimental, but this is not true for high BL isolators especially at higher SSA of loadings. Therefore, it can be concluded that in FE modelling of SB-CFREIs with higher BL, it is crucial to account for peel-off phenomenon.

CHAPTER 6: THESIS CONCLUSION, CONTRIBUTIONS AND FUTURE RESEARCH RECOMMENDATIONS

6.1 Summary

This final chapter of the thesis summarizes the thesis achievements and conclusions. It highlights how the research objectives were met and describes the scientific steps taken toward the research goals. By conducting a literature review on the subject, the lack of knowledge and needs in the seismic isolation technology, especially in the area of CFREIs, were defined and led the author to design and propose the Elevated Semi-Bonded CFREI for further investigation. Dynamic characteristics of component and compound SB-CFREIs, bonding variation, and its effect on isolator's effective lateral shear and axial compression stiffness and damping were investigated and defined. In this research, better understanding is gained of component combination configuration as an important development toward achieving the desired cost effective and efficient compound isolator. The research findings provided better insight on the proposed isolator's isolation efficiency (IE). Conducting two consecutive, long-duration (120 second) dynamic excitations on the innovative isolator with no damage or heat-up failure demonstrated the isolator's satisfactory performance. Scientific findings and achievements from conducting over 200 experimental tests and analytical study on the proposed Component and compound SB-CFREIs has greatly contributed to seismic isolation technology. In the following section these findings and conclusions are summarized.

6.2 Conclusions on Literature Review

After conducting a literature review (chapter two of the thesis) on Fiber Reinforced Elastomeric Isolator (FREI), the following was concluded:

1-All research studies conducted on FREIs support the idea that high-strength fibers can replace the steel shims as the reinforcements in elastomeric isolators.
2-The majority of research studies on FREIs implemented carbon fiber as the high-strength, low-weight fiber material serving as reinforcement in elastomeric isolators.
3-All studies since 1990 have been conducted on either bonded or unbonded reinforced elastomeric isolators, with one research study on partially bonded, carbon fiber-reinforced elastomeric isolators in 2014.

4-As of the author's best knowledge, no research work has been conducted on "Elevated Semi-Bonded Carbon Fiber Reinforced elastomeric Isolators". This lack of knowledge in the FREI area has been the center of attention in the present research work and the subject has been investigated by conducting extensive experimental and analytical studies.

5.9 Conclusions on Experimental Studies of Component and Compound Semi-Bonded Carbon Fiber Reinforced Elastomeric Isolator (SB-CFREI) & (CSB-CFREI)

The experimental findings and achievements to date can be summarized as follows:

1-Increase in the isolator's bonding level (BL) will increase the SB-CFREI's effective axial compression stiffness and modulus.

2-Isolators with lower bonding levels demonstrate higher effective equivalent viscous damping. For example, the B220 isolator under shear strain loading of SSA=100% isolates with equivalent viscous damping of 27.76%, while B240 isolator exhibits a damping of 8.83% and 10.49% for 1st and 2nd loading cycle at the same shear strain amplitude.

3-Test outcomes indicate that an increase in an isolator's bonding level increases its effective lateral stiffness K_{eff}-h.

4-SB-CFREIs have a higher effective lateral stiffness at a lower level of shear strain amplitude and it decreases as shear strain amplitude (SSA) increases.

5-The isolator's effective equivalent viscous damping increases at higher shear strain amplitude; the increasing pattern differs for isolators with different bonding levels. The experimental outcome demonstrates that the effective equivalent viscous damping increases as isolators undergo higher shear strain loading; this is a desirable characteristic for seismic isolators.

6-Plots of damping vs. bonding level of the SB-CFREIs indicate that isolators with low bonding level have higher damping and energy dissipation capability.

7-In case of high compression loading, implementation of a compound isolator with high compression loading capability has demonstrated a satisfactory performance when undergoing lateral cyclic excitations. For example, all triple compound isolators with different bonding

levels underwent lateral cyclic shear loading while under constant axial compression load of 750 kN.

8-Combination configuration of the component isolators to achieve desirable compound isolator depends on the axial compression load and damping demand.

9-All isolators with different levels of bonding have undergone axial compression stress of 1.72 to 11.38 MPa induced from constant compression pre-load and maximum cyclic compression loading respectively, while simultaneously being imposed to lateral shear strain deformation of up to $\%100t_r$ with no failure or instability. Isolators demonstrated good resistance under the above loading level and after experimental testing, all isolators were closely examined for delamination or cracks and no damage was detected.

10-Performance of the innovative isolators under long-duration cyclic loads was investigated. Isolators were tested for duration of 4 minutes (two consecutive cyclic lateral excitations of 120 second duration) and the isolator's elastomeric bearing pad's temperature was monitored in intervals of 10 seconds. The temperature increase was negligible and no heat-up-related damage was detected. This experimental task confirms the isolator's satisfactory performance under long duration cyclic loading.

5.10 Conclusion and Outcomes of Analytical Studies on SB-CFREI

2D finite element analysis outcomes of the isolator in general are fairly close with those of the experimental under the same loading conditions. This result validates the implementation of 2D-FEA in studying the isolator's effective lateral stiffness and force-displacement relationship under lateral shear loading for the preliminary design of SB-CFREIs.

1-Comparison of the FE outcomes with those of the experimental supports application of the Neo-Hookean material model as the simplest hyper-elastic model to describe the rubber components material model in the preliminary design of the SB-CFRE isolators, especially when component material testing is not possible.

2-The force-displacement diagrams from conducting FE modeling and the experimental tests were achieved. These plots indicate that up to shear strain amplitude of $SSA=50\%t_r$ the

experimental and the FE plots are fairly in close agreement, but as the shear strain loading increases the FE plot rises to a higher position and gets further apart, and consequently demonstrates higher force value for the same SSA of loading. The reason behind this difference and plot shift is that the effect of peel-off is not accounted for in the FEA as the nature of this phenomenon is not defined yet. Due to application of cold vulcanized bonding compound between steel cover plates and CFRE bearing pad, limited peel-off was anticipated and allowed to occur at higher SSA in order to prevent local excessive concentration of tensile stresses. This phenomenon makes occurrence of limited roll-over deformation possible and consequently reduces the effective lateral stiffness of the isolator as shear strain amplitude increases to a value of 50%t_r and higher.

3-The FE force-displacement relationship for SB-CFREIs undergoing lateral shear load under constant axial compression load, when compared with that of experimental, also indicates that selecting relatively larger sized elements or coarser FE mesh for rubber elements to save analysis time and cost still provides a fairly reliable estimate of the lateral load-displacement relationship in preliminary design of the isolators.

4- Since 2D finite element modeling of the SB-CFREI assumes no out of plane deformation, defining the isolator's effective compression stiffness and modulus by conducting 2D (plane strain) FEM is not recommended.

5-In conducting the finite element modeling, the results indicate that the effect of the peel-off phenomenon during lateral cyclic loading is important in evaluating the isolator's behaviour with more accuracy and to capture the real isolator's dynamic characteristics. The test outcome indicates that for isolators with a higher bonding level (BL), the influence of the peel-off phenomenon is higher than for isolators with lower bonding level. The magnitude of this phenomenon could be related to and influenced by the isolator's bonding level, shear strain amplitude, and axial compression load, and other parameters like the bonding compound specifications and rubber material. To have a better understanding of the influence of these parameters, further investigation is needed.

5.11 Thesis Contribution

The prime contribution of this thesis is attributed to the improvement of the present seismic isolation technology to achieve an affordable, efficient and effective seismic protection system with widespread application. To achieve this importance, innovative component and compound seismic isolator (SB-CFREI & CSB-CFREI) have been designed, manufactured and proposed. To investigate the viability and performance of these isolators over 200 experimental tests and intensive analytical studies have been conducted in this current research. The tests outcomes not only have served the objectives of this research, but also has resulted in a great source data for future research studies. Considerable progress and achievements have been reached on better understanding of the dynamic characteristic and performance of the component and compound elevated semi-bonded isolators after post-processing and analysis of the recorded experimental data. As a cost effective seismic isolator, each isolator types demonstrated satisfactory performance with sufficient isolation efficiency, durability, and energy dissipation capabilities, supported by the present research experiments and analytical outcomes. Better understanding of the influence of bonding variation and component combination on the dynamic characteristics and behaviour of the compound SB-CFRE isolator is another important contribution to pave the way for achieving a viable, and cost effective seismic isolation system.

5.12 Future Research Recommendations

1- It is recommended to conduct shake table testing of the proposed SB-CFREI and CSB-CFREIs to study and investigate their performance and effectiveness when exposed to different earthquake excitations while isolating typical low-rise building.
2- It is suggested that with further research and development, elevated SB-CFREI and CSB-CFREI can be implemented as a sufficient low-cost seismic isolation system for low-rise buildings worldwide, especially in the high seismic zones of developing countries, as the research experimental and analytical outcomes support the isolator's sufficient isolation efficiency (IE), energy dissipation capability, and cost-effectiveness.
3- The unbonded region of the SB-CFREI's bearing pad is elevated and will not be in contact with the upper and lower structural supports during lateral excitation. This new boundary condition and deformation mechanism provides the isolator with lower lateral stiffness and consequently higher isolation efficiency (according to test results). The free

regions of the CFRE pad may touch the top or bottom structural support only at extreme shear strain loading. At this level of lateral deformation, the isolator lateral stiffness is expected to increase due to a change in boundary conditions and deformation pattern. This phenomenon causes the seismic isolator to exhibit higher lateral stiffness at extreme lateral deformation. It is recommended that further investigation on the nature and magnitude of the lateral stiffness increase in future research studies, as this delayed increase in lateral stiffness could increase the isolation stability which is desirable in seismically isolated buildings.

4- The peel-off phenomenon and its magnitude could be influenced by the isolator's bonding level (BL), axial compression load P_v, shear strain amplitude (SSA), material and bonding compound specification, and other parameters that are not yet defined. It is suggested to conduct future research studies to investigate the peel-off phenomenon in order to have better understanding of parameters that influence this phenomenon, and their effectiveness and limitations in maintaining isolation stability.

Bibliography

(ASCE) American Society of Civil Engineers, Minimum design loads for buildings and other structures. ASCE/SEI 7-05. New York: ASCE, 2010.

(ASTM) American Society for Testing and Material. Standard test method for rubber property durometer hardness, ASTM D2240, West Conshohocken, PA: ASTM, 2005.

(FEMA) Federal Emergency Management Agency. 1997. *Instructional Material Complementing FEMA 451, Design Examples Seismic Isolation*. Washington, DC.

(FEMA) Federal Emergency Management Agency. 1998. National Hazards Reduction Program Guidance for Rehabilitation of Buildings. FEMA-273, Washington, DC.

(ISO) International Organization for Standardization. 2005. *Elastomeric Seismic-protection Isolators*. ISO 22762, Geneva.

ABAQUS Inc. ABAQUS Version 6.9, http://www.simulia.com.

Adibnatanzi, H., Ventura, C. and Tesfamariam, S. 2015. Dynamic characteristics of semi-bonded carbon fiber reinforced elastomeric isolator SB-CFREI. 11th Canadian Conference on Earthquake Engineering, July 21 – 24, 2015, Victoria, BC, Canada, paper No. 94063.

Asher, J.W., Hoskere, S.N., Ewing, R.D., Mayes, R.L., Button, M.R. and Van Volkinburg, D.R. (1997). Performance of seismically isolated structures in the1994 Northridge and 1995 Kobe earthquakes. Proceedings of Structures Congress (ASCE) vol. XV.

Ashkezari G.D., Aghakouchak, A.A. and Kokabib, M. 2008. Design, manufacturing and evaluation of the performance of steel like fiber reinforced elastomeric seismic isolators. *Journal of Materials Processing Technology*, 197(1–3), 140-150.

Bakhshi, A., Jafari, M.H. and Tabrizi, V.V. 2014. Study on dynamic and mechanical characteristics of carbon fiber- and polyamide fiber-reinforced seismic isolators, *Materials and Structures*, 47(3), 447-457.

Beskos, D.E. and Anagnostopoulos, S.A. 1997. Computer Analysis and Design of Earthquake Resistant Structures: Handbook. Southampton, UK; Boston: Computational Mechanic.

Booth, E. and Key, D. 2006. *Earthquake Design Practice for Buildings*. London: Thomas Telford.

Bozorgnia, Y. and Bertero, V.V. 2004. *Earthquake Engineering: from Engineering Seismology to Performance-based Engineering*. Boca Raton, FL: CRC.

Campbell, S.D. 2004. Carbon fiber-reinforced elastomeric pads for building isolation. In: Proceedings of the 33rd International Congress and Exposition on Noise Control Engineering; 22–25 August, 2004, Prague, Czech Republic.

Chopra, A.K. 1995. Dynamics of Structures: Theory and Applications to Earthquake Engineering (3rdnd edn). Prentice Hall: Upper Saddle River, New Jersey.

Clough, R.W. and Penzien, J. 1975. *Dynamics of Structures*. New York: McGraw-Hill.

Constantin, M.C. and Tadjbakhsh, I. 1985. Hysteretic dampers in base isolation: random approach. *Journal of Structural Engineering*, 111(4), 705-721.

Constantin, M.C., Mokha, A. and Reinhorn, A. 1990. Teflon bearings in base isolation II: Modeling. *Journal of Structural Engineering*, 116(2), 455-474.

Corporation, Whitepaper 2010 (From MSC Marc software catalogue)

Dall'Asta, A. and Ragni, L. 2006. Experimental tests and analytical model of high damping rubber dissipating devices. *Journal of Structural Engineering*, 28, 1874–84.

de Raaf, M.G. 2009. Experimental Study of Unbonded Fiber Reinforced Elastomeric Bearings. MS thesis, McMaster University, Hamilton, Ontario.

de Raaf, M.G.P., Tait, M.J. and Toopchi-Nezhad, H. 2011. Stability of fiber-reinforced elastomeric bearings in an unbonded application. *Journal of Composite Materials*, 45, 1873-1884.

Dezfuli, H. and Alam, S. 2013. Multi-criteria optimization and seismic performance assessment of carbon FRP-based elastomeric isolator. *Engineering Structures*, 49, 525–540.

Dezfuli, H. and Alam, S. 2016. Experiment-Based Sensitivity Analysis of Scaled Carbon-Fiber-Reinforced Elastomeric Isolators in Bonded Applications, Journal of Fibers 2016, 4, 4; doi:10.3390/fib4010004

Dorfmann, A. and Ogden, R.W. 2004. A constitutive model for the Mullins effect with permanent set in particle reinforced rubber. *International Journal of Solids and Structures*, 41, 1855–1878.

Fenz, D. and Constantinou, M.C. 2006. Behaviour of the double concave friction pendulum bearing. *Earthquake Engineering & Structural Dynamics*, 35, 1403–1424.

Gerhaher, U. Strauss, A. Bergmeister, K. 2011. Numerical modeling of elastomeric bearings in structural engineering. *Advances in Material Science*, 11(3), 51-63.

Gerhaher, U., Strauss, A., and Bergmeister, K. Design and development of fiber reinforced elastomeric bearings.17th Congress of IABSE, 2008. Chicago.

Goda, K. Lee, C.S. and Hong, H.P. 2009 Lifecycle cost–benefit analysis of isolated buildings. *Journal of Structural Safety*, 32, 52-63.

GoodCo Z-Tech. 2010. Elastomeric Bearings Catalog. Montreal (Canada).

Haringx, J.A. 1948. On highly compressible helical springs and rubber rods, and their application for vibration-free mountings – part III. *Philips Res Rep*, 4, 206–20.

Harris, H.G. and Sabnis, G.M. 1999. *Structural Modeling and Experimental Techniques*. Boca Raton: CRC.

Jangid, R.S. and Londhe, Y.B. 1998. Effectiveness of elliptical rolling rods for base isolation. *Journal of Structural Engineering*, 24(4), 469–472.

Kang, B.S., Kang, G.J. and Moon, B.Y. 2003. Hole and lead plug effect on fiber reinforced elastomeric isolator for seismic isolation. *Journal of Materials Processing Technology*, 140(1), 592-597.

Kang, G.J. and Kang, B.S. 2009 Dynamic analysis of fiber-reinforced elastomeric isolation structures. *Journal of Mechanical Science and Technology*, 23, 1132-1141.

Karimzadeh Naghshineh, A., Akyui, U. and Caner, A. 2014. Comparison of fundamental properties of new types of fiber-mesh reinforced seismic isolators with conventional isolators. *Earthquake Engineering & Structural Dynamics*, 43(2), 301–316.

Kelley, J.M. 1990. Base isolation: linear theory and design. *Earthquake Spectra,* 6(2), 223-244.

Kelly J.M and Takhirov, S.M. 2011. *Analytical and Experimental Study of Fiber-reinforced Elastomeric Isolators*. PEER Report 2012/101, Pacific Earthquake Engineering Research Center, University of California, Berkeley.

Kelly, J.M. 1982. Aseismic base isolation. *The Shock and Vibration Digest,* 14(5), 17-25.

Kelly, J.M. 1982. *The Influence of Base Isolation on the Seismic Response of Light Secondary Equipment*. United States Government Technical Report Number PB-82-255266; UCB/EERC-81/17 (1982).

Kelly, J.M. 1986. Aseismic base isolation: Review and bibliography. *Soil Dynamics and Earthquake Engineering*, 5, 202–216.

Kelly, J.M. 1997. *Earthquake-resistant Design with Rubber*. 2nd ed. London: Springer; 1997.

Kelly, J.M. 1998. *Base Isolation in Japan*. Berkeley: EERC, December 1988

Kelly, J.M. 1999. Analysis of fiber-reinforced elastomeric isolators. *Journal of Seismology and Earthquake Engineering*, 2(1), 19-34.

Kelly, J.M. 2002. Seismic isolation systems for developing countries, *Earthquake Spectra,* 18(3), 385–406.

Kelly, J.M. and Calabrese, A. 2012. *Mechanics of Fiber Reinforced Bearings*. PEER Report 2012/101, Pacific Earthquake Engineering Research Center, University of California, Berkeley.

Kelly, J.M. and Konstantinidis, D.A. 2011. *Mechanics of Rubber Bearings for Seismic and Vibration Isolation*. Wiley.

Koh, C.G. and Kelly, J.M. 1987. *Effects of Axial Load on Elastomeric Isolation Bearings*. EERC Report - 86/12, University California, Berkeley.

Matsagar, V. and Jangid, R. 2004. Influence of isolator characteristics on the response of base isolated Structures. *Engineering Structures*, 26(12), 1735-1749.

Milani, G. and Milani, F. 2012. Stretch–stress behavior of elastomeric seismic isolators with different rubber materials: Numerical insight. *Journal of Engineering Mechanics,* 138(5), 416–429.

Mishra, H.K. and Igarashi, A. 2012. Experimental and analytical study of unbonded and bonded scrap tire rubber pad as base isolation device. 15th World Conference on Earthquake Engineering, 24-28 September 2012, Lisbon, Portugal.

Mishra, H.K., Igarashi, A. and Matsushima, H. 2013. Finite element analysis and experimental verification of the scrap tire rubber pad isolator. *Bulletin of Earthquake Engineering*, 11(2), 687-707.

Moon, B.Y., Kang, G.-J., Kang, B.-S. and Kelly, J.M. 2002. Design and manufacturing of fiber reinforced elastomeric isolator for seismic isolation. *Journal of Materials Processing Technology*, 130–131, 145–150.

Mordini, A. and Strauss, A. 2008. An innovative earthquake isolation system using fibre reinforced rubber bearings. *Engineering Structures*, 30(10), 2739-2751.

Morman, K., Kao, B. and Nagragaal, J. 1981. Finite element analysis of viscoelastic elastomeric structures vibrating about nonlinear statically stressed configurations. In: Proceedings of the Society of Automotive Engineers International Congress and Exposition, Detroit, MI, USA. Paper No. 811309.

Naeim, F. and Kelly, J.M. 1999. *Design of Seismic Isolated Structures: from Theory to Practice*. New York: John Wiley.

Onorii, C. Spizzuoco, M. Calabrese, A. Giorgio Serino, 2011, Applicability and reliability of innovative low-cost rubber isolators. Dipartimento di Ingegneria Strutturale – Univ. degli Studi di Napoli Federico II, Via Claudio 21, 80125 Napoli.

Pan, Peng, Zamfirescu, Dan, Nakashima, Masayoshi, Nakayasu, Nariaki, Kashiwa, Hisatoshi (2005). Base-isolation design practice in Japan: Introduction to the post Kobe approach. *Journal of Earthquake Engineering* **9:1**, 147-171.

Skinner, R.I., Robinson, W.H. and McVerry, G.H. 1993. *An Introduction to Seismic Isolation*. Wiley, England.

Stanton, J.F., Scroggins, G., Taylor, A.W. and Roeder, C.W. 1990. Stability of laminated elastomeric bearings. *Journal of Engineering Mechanics*, 116, 1351–1371.

Stevenson, A. 1985. Longevity of natural rubber in structural bearings. *Plastics and Rubber Processing and Applications*, 5(3), 253-258.

Su, L., Ahmadi, G. and Tadjbakhsh, I. G. 1989. A comparative study of performances of various base isolation systems, part I: Shear beam structures. *Earthquake Engineering & Structural Dynamics*, 18(1), 11–32.

Summers, P., Jacob, P., Marti, J., Bergamo, G., Dorfmann, L., Castellano, G., Poggianti, A., Karabalis, D., Silbe, H., and Triantafillou S. 2004. Development of new base isolation devices for application at refineries and petrochemical facilities. Proceedings, 13th World Conference on Earthquake Engineering, Vancouver, BC, Canada, Paper No. 1036.

Taniwangsa, W. and Kelly, J.M., 1996. *Experimental and Analytical Studies of Base Isolation Applications for Low-Cost Housing*. Earthquake Engineering Research Center, University of California, Berkeley, CA, USA.

Taylor A.W. and Igussa T. 2004. *Primer on Seismic Isolation*. American Society of Civil Engineers, ASCE, Reston, Virginia.

Toopchi-Nezhad H., Tait, M.J. and Drysdale, R.G. 2008. Lateral response evaluation of fiber reinforced neoprene seismic isolators utilized in an unbonded application. *Journal of Structural Engineering*, 134(10), 1627–38.

Toopchi-Nezhad, H., Drysdale, R.G. and Tait, M.J. 2009. Parametric study on the response of stable unbonded-fiber reinforced elastomeric isolators (SU-FREIs). *Journal of Composite Material*, 43, 1569–1587.

Toopchi‐Nezhad, H., Tait, M.J. and Drysdale, R.G. 2008. Testing and modeling of square carbon fiber‐reinforced elastomeric seismic isolators. *Structural Control and Health Monitoring*, 15(6), 876-900.

Toopchi-Nezhad, H., Tait, M.J. and Drysdale, R.G. 2009. Shake table study on an ordinary low-rise building seismically isolated with SU-FREIs (Stable Unbonded Fiber Reinforced Elastomeric Isolators). *Earthquake Engineering & Structural Dynamics*, 38, 1335 1357.

Toopchi-Nezhad, H., Tait, M.J. and Drysdale, R.G. 2009. Simplified analysis of a low-rise building seismically isolated with stable unbonded fiber reinforced elastomeric isolators. *Canadian Journal of Civil Engineering*, 36(7), 1182-1194.

Toopchi-Nezhad, H., Tait, M.J. and Drysdale, R.G. 2011. Bonded versus unbonded strip fiber reinforced elastomeric isolators: Finite element analysis. *Composite Structures*, 93, 850-859.

Toopchi-Nezhad, H., Tait, M.J. and Drysdale, R.G. 2012. Influence of thickness of individual elastomer layers (first shape factor) on the response of unbonded fiber-reinforced elastomeric bearings. *Journal of Composite Materials*, DOI: 10.1177/0021998312466686.

Tsai, H.C. 2004. Compression stiffness of infinite-strip bearings of laminated elastic material interleaving with flexible reinforcements. *International Journal of Solids Structure*, 41, 6647–6660.

Tsai, H.C. and Hsueh, S.J. 2001. Mechanical properties of isolation bearings identified by a viscoelastic model. *International Journal of Solids Structure*, 38(1), 53–74.

Tsai, H.C. and Kelly, J.M. 2002. *Compression and Bending Stiffness of Fiber-reinforced Elastomeric Bearings*. Berkeley: Pacific Earthquake Engineering Research Center, University of California.

Tsai, H.C., and Kelly, J.M., 2005. Buckling load of seismic isolators affected by flexibility of reinforcement. *International Journal of Solids Structure*, 42, 255–269.

Turer, A. and Ozden, B. 2008. Seismic base isolation using low-cost Scrap Tire Pads (STP). *Material and Structures*, 41, 891-908.

Van Engelen, N., C. Osgooei, P.M., Tait, M.J. and Konstantinidis, D. 2015. Partially bonded fiber-reinforced elastomeric isolators (PB-FREIs). *Structural Control and Health Monitoring*, 22(3), 417–432.

Yoshioka, H., Ramallo, J., and Spencer, B., Jr. 2002. "Smart" base isolation strategies employing magnetorheological dampers. *Journal of Engineering Mechanics*, 128(5), 540–551.

Zayas, V. Low, S.S., and Mahin, S.A. 1987. *The FPS Earthquake resisting System, Experimental Report*. Report No. UCB/EERC-87/01, Earthquake Engineering Research Center, University of California, Berkeley.

Zhao, Y.H. and Weng, G.J. 1996. Influence of random bridging on elastic and elasto-plastic properties of fiber-reinforced composites. *Acta Mechanica*, 116(1), 29-44.

APPENDIX A: COMPONENT ISOLATORS HYSTERISIS DIAGRAM, EFFECTIVE LATERAL STIFFNESS, DAMPING, AND RELATED COMPUTATIONS

I-Component (single) Isolators

A1-B160 Component isolator bonding level BL = 37.87% PL=250kN

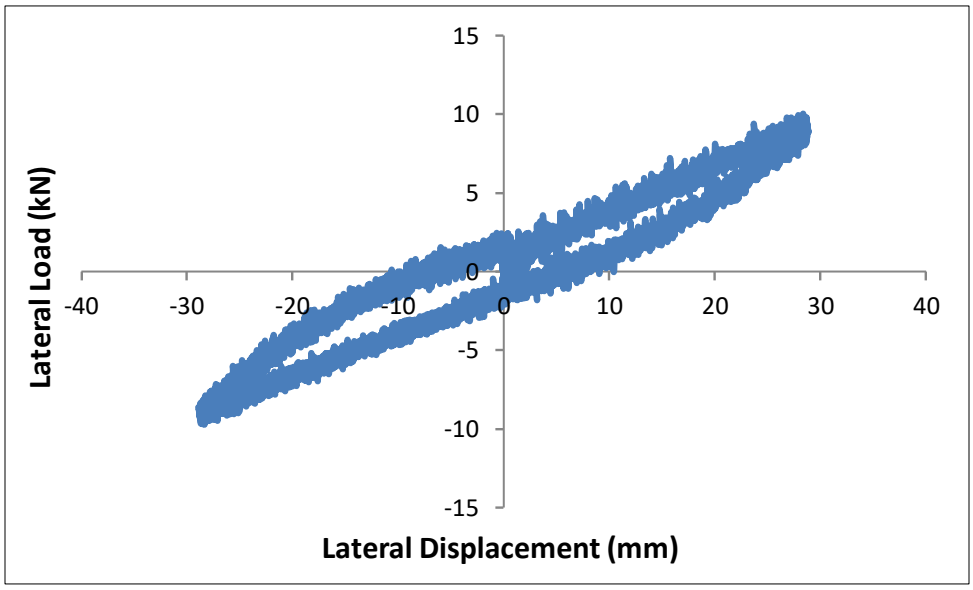

Figure-A1-1 B160 component isolator SSA=25%t_r -A Ϭ=6.77 MPa

1-Keff-H=331.24 N/mm 2-Keff-h=165.62N/mm

2-Loop area=133204 N-mm 3-ζ = 7.75%

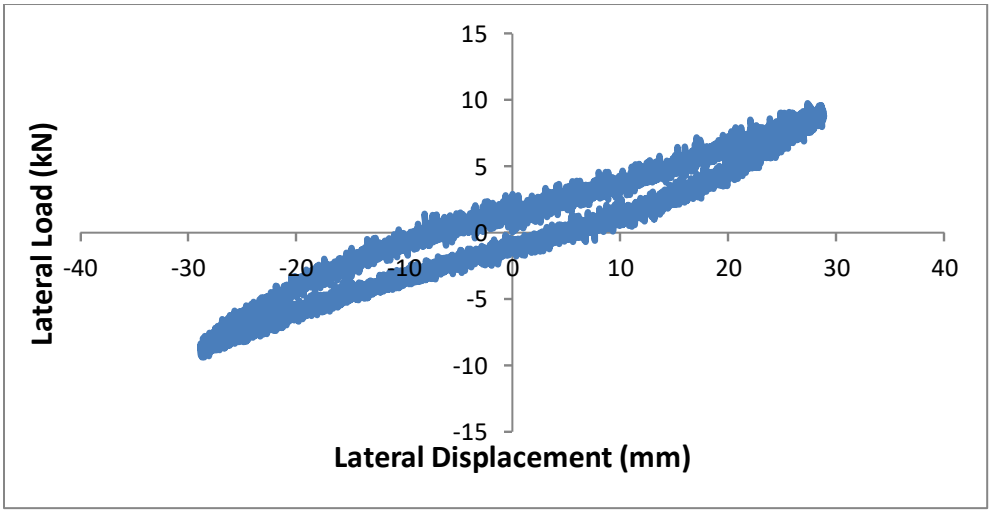

Figure-A1-2 B160 SSA= 25%t_r B Ϭ=9.77 MPa

1-Keff-H=315.05 N/mm 2-Keff-h=157.53N/mm

2- Loop area=117902.3 N-mm 4- ζ = 7.19%

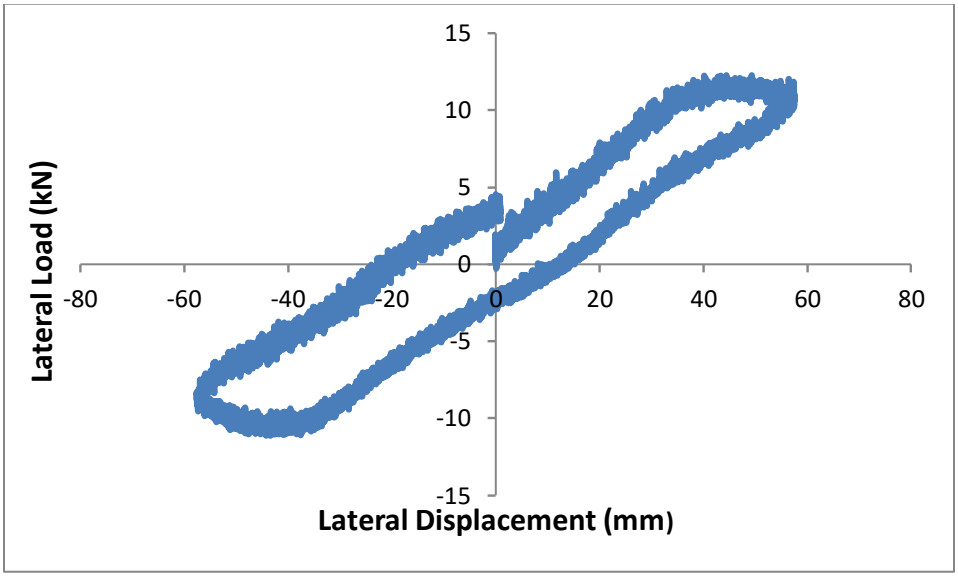

Figure A1-3 B160 –SSA=50%t_r A Ϭ=9.77 MPa

1- Keff-H = 176.11N/mm 2-Keff-h=88.06 N/mm
3-Loop area= 536823.80 N-mm 4-ζ = 14.70%

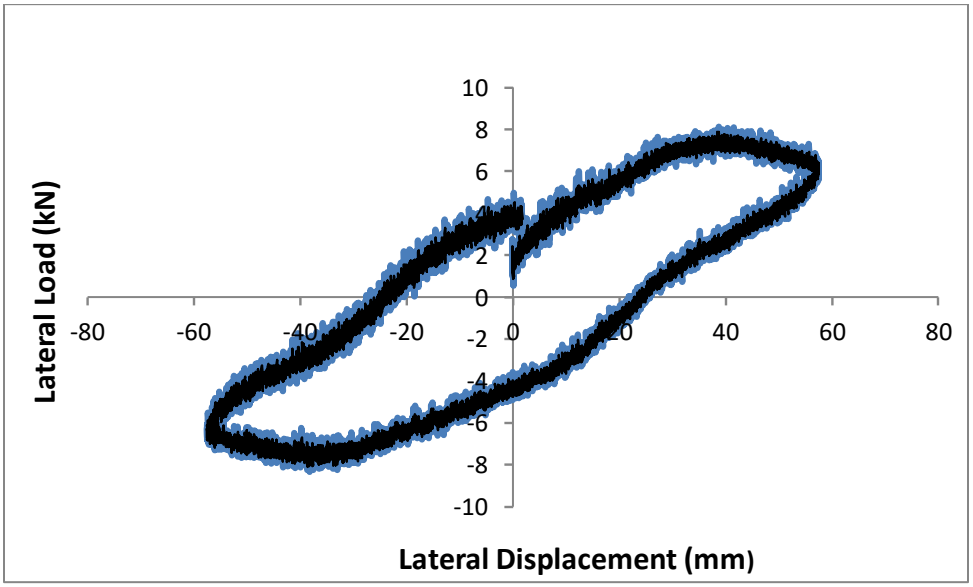

Figure A1-4 B160 Lateral load-displacement hysteresis diagram SSA=50%t_r -B

1-Keff-H syst. =123.08N/mm 2-Keff-h=61.54N/mm
3-Hysteresis loop area=638004 N-mm 3-ζ= 24.97%

B160 Dynamic Load Profile input PL = 250kN SSA= 25-50%t_r

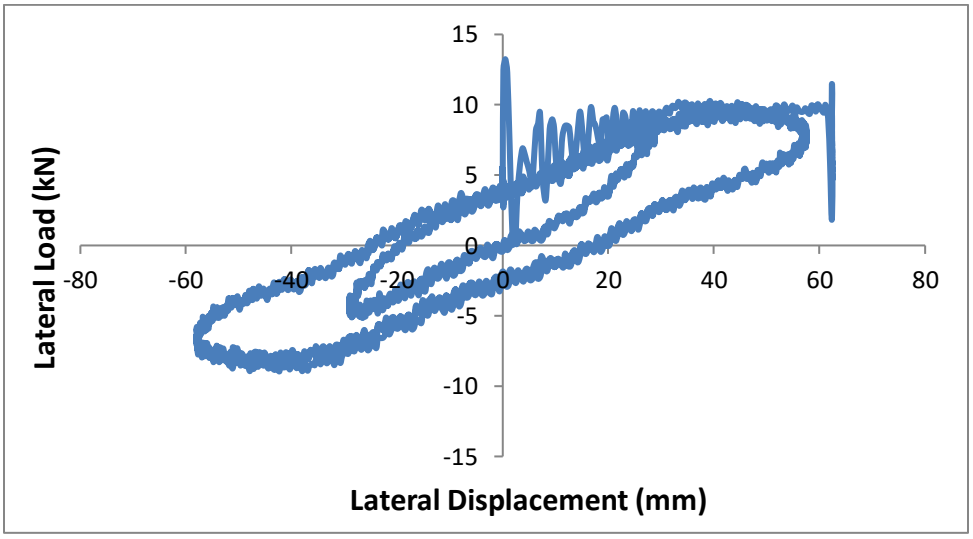

Figure A1-5 B160 Component isolator lateral load-displacement hysteresis diagram SSA=25-50%t_r Ϭ=9.77MP

NOTE:
For isolator B160 with a lowest bonding level of BL=37.87%, the difference between Keff-h at shear strain amplitude of SSA=50% t_r is more than 15% for the first and second cycles of loading A and B. According to the ASCE provision 7-05, this difference should not exceed 15%. Since for B160 isolator the difference is exceeded and consequently this isolator cannot be implemented in isolation independently, but it could be used as component isolator toward achieving a compound isolator.

A2- B180 Component Isolator

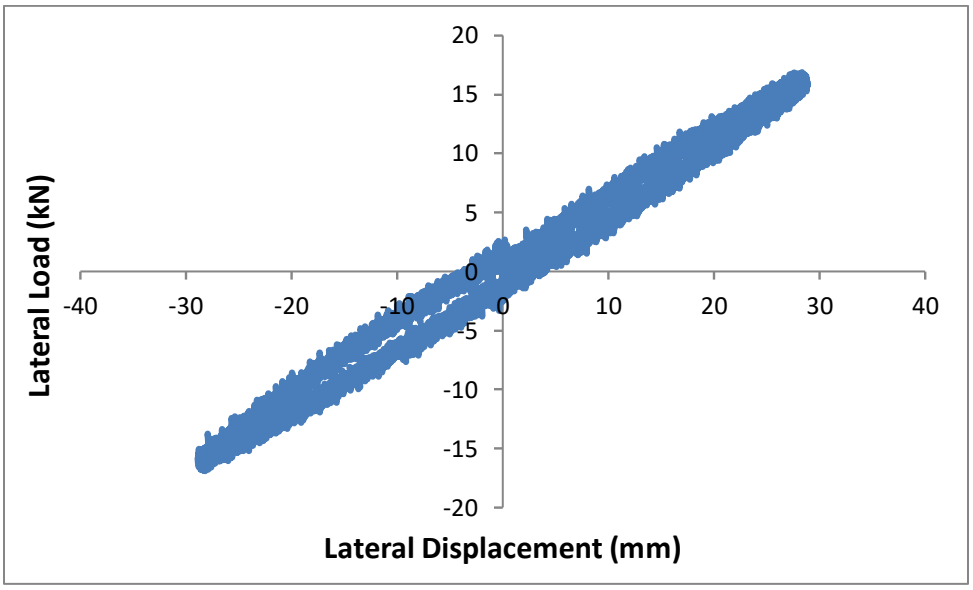

Figure A2-1 B180 SSA=25%t_r A 0 SSA=-25%t_r

1-Keff-H=579.2 N/mm 2- Keff-h = 289.60 N/mm

3-Loop area =115227.0N-mm 4-ζ= 3.85%

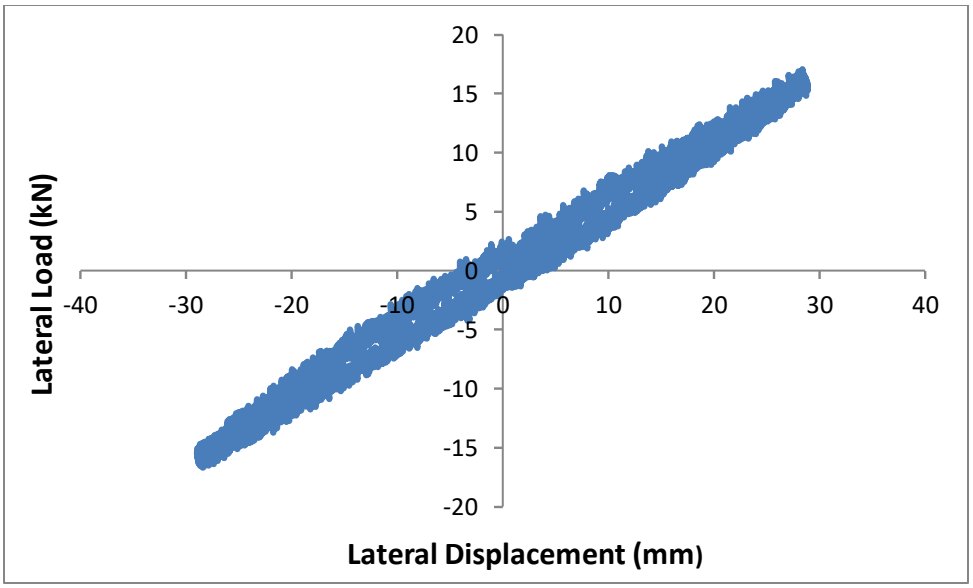

Figure A2-2 B180 SSA= 25%t_r B

Keff-H=564.10 N/mm 2-Keff-h = 282.05N/mm
3- Loop area= 96453.11 N-mm 4-ζ =3.30%

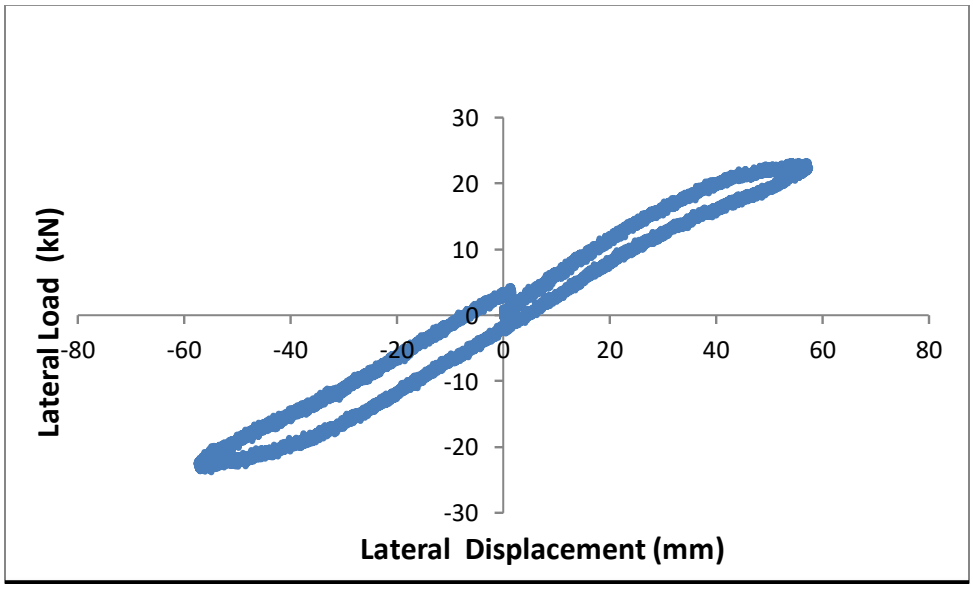

Figure A2-3 B180 Lateral Load-Displacement Hysteresis Diagram SSA=50%t_r A

1-Keff-H= 401.83N/mm 2-Keff-h= 200.91 N/mm
3-Loop area= 446601.9N-mm 4-ζ =5.37%

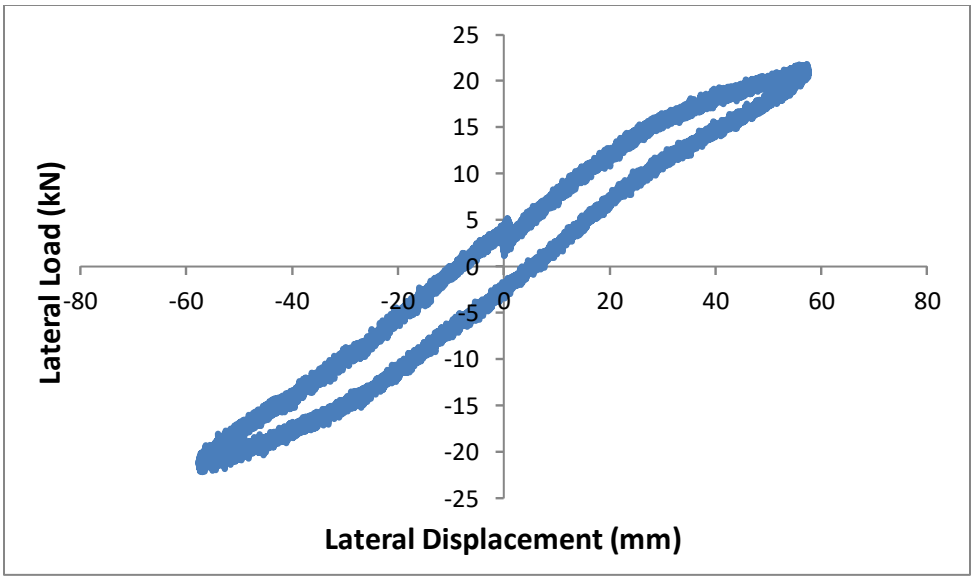

Figure A2-4 B180 Lateral Load displacement Hysteresis Diagram SSA=50%t_r B

1-Keff-H syst.= 374.50N/mm 2- Keff- h=182.25N/mm

3-Loop area=488029.3 N-mm 4-ζ = 6.27%

A3-B200 Isolator Bonding Level = 59.17% PL = 250 kN

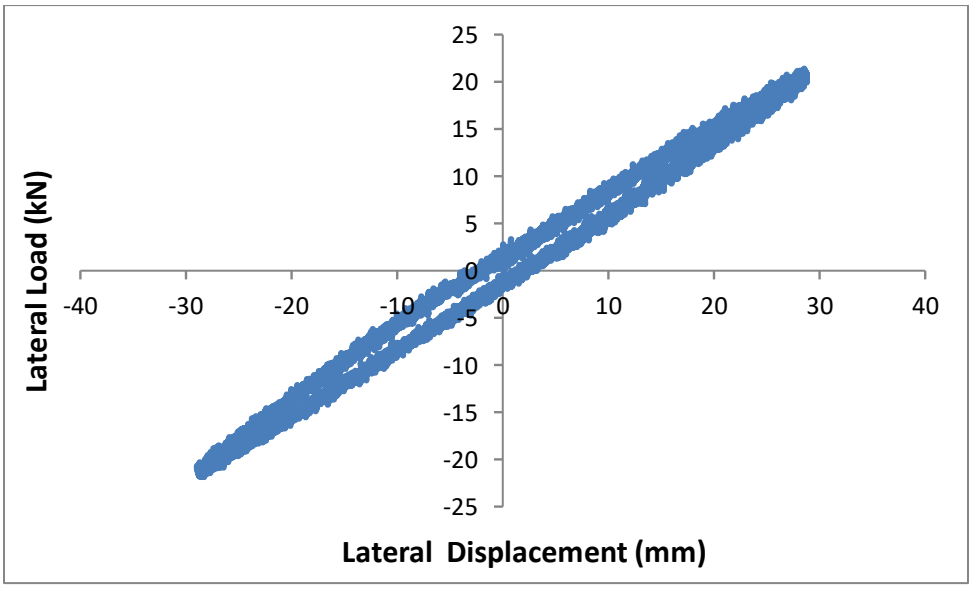

Figure-A3-1_B200 Lateral Load-Displacement Hysteresis Diagram SSA=25%t_r B PL=250kN

1-Keff-H=745.73 N/mm 2- Keff-h= 372.87 N/mm

3-Loop area = 123900.80 N-mm 4-ζ =3.25%

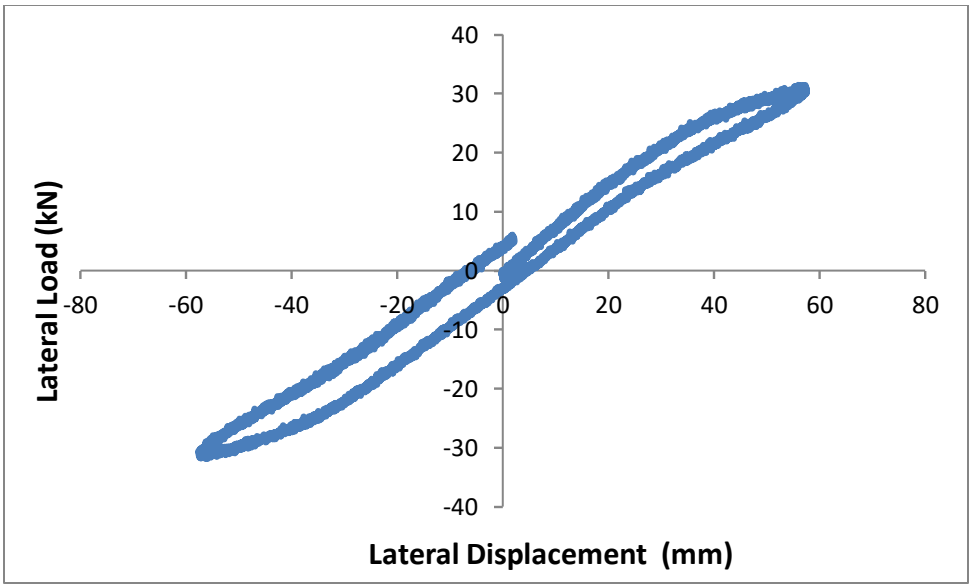

Figure A3-2 B200 Lateral Load-Displacement Hysteresis Diagram SSA=50%t_r -A

1-Keff-H=536.48 N/mm 2-Keff-h=268.24N/mm

3-Loop area =545270.40 N-mm 4-ζ = 4.89%

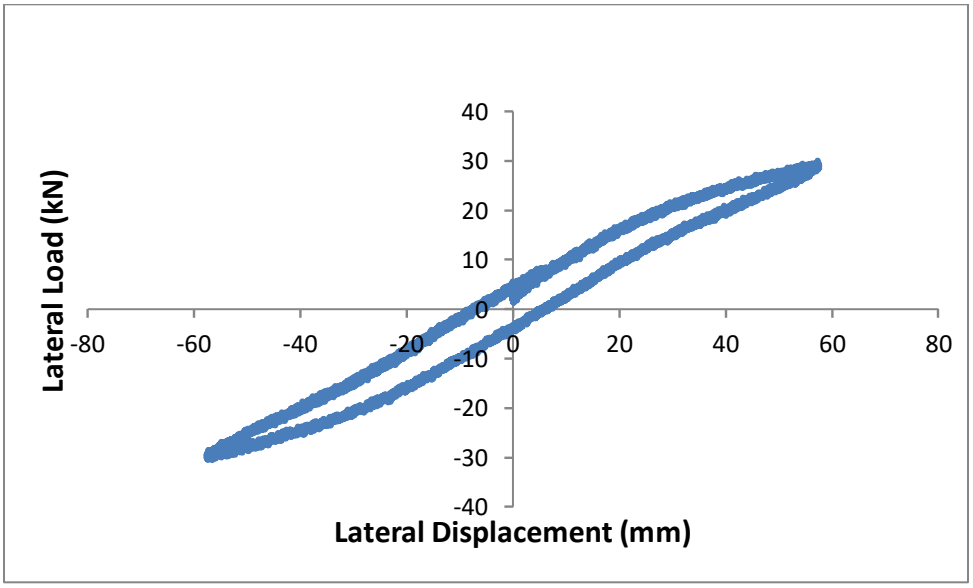

Figure A3-3 B200 Lateral Load-Displacement Hysteresis Diagram SSA=50%t_r -B

1-Keff-H=513.56 N/mm 2-Keff-h=256.78N/mm

Loop area= 664516.8-N-mm 4- ζ =6.23%

A4 - B220 PL=250kN SSA= 100%t_r

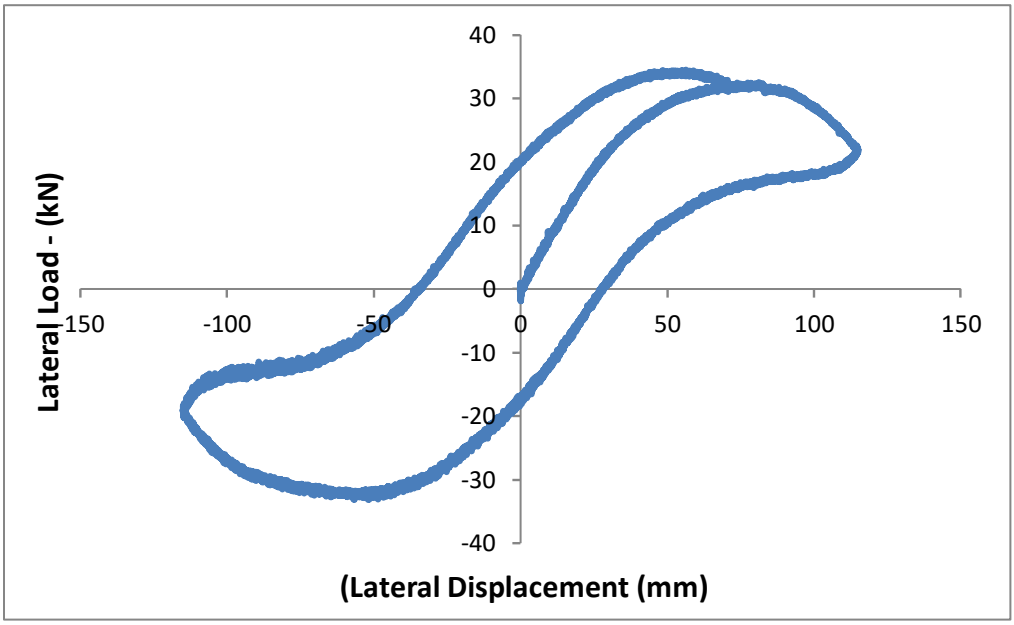

Figure A4-1 B220 Lateral load-displacement hysteresis diagram SSA=100%t_r -A Б=5.17 MPa

1-Keff-H= 180.22 N/mm
2-Keff-h= 101.38 N/mm
2-Hysteresis loop area =4604374.0N-mm
3- ζ= 27.61%

B220 SSA=75%t_r A Б = 5.17MPa

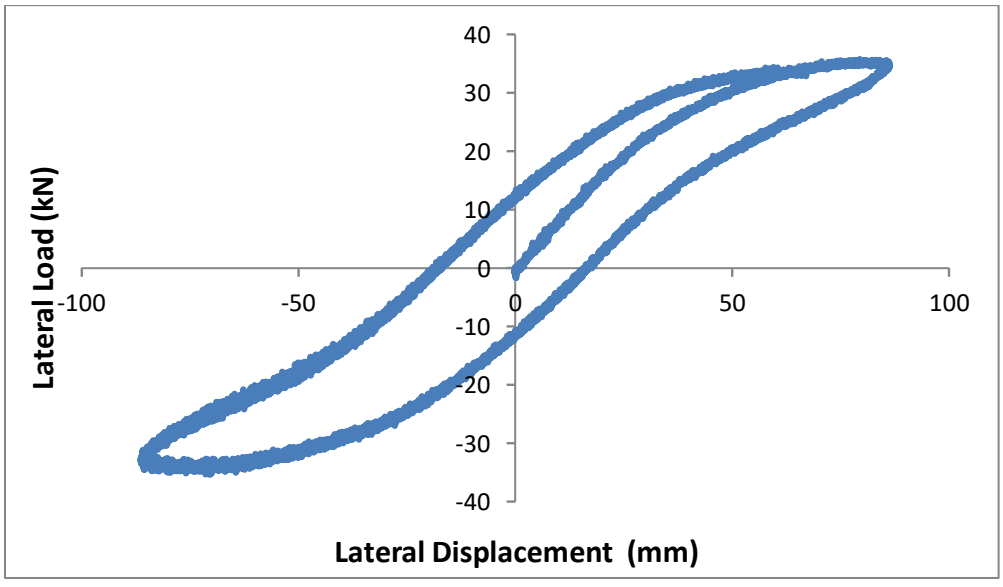

Figure A4-2 B220 lateral load-displacement hysteresis diagram PL =250kN SSA=75%t_r -A Ϭ=5.17MPa

1- Keff-H = 397.41 N/mm 2-Keff-h = 198.70 N/mm

2-Hysteresis loop area = 2135365 N-mm 3- ζ= 11.53%

B220 Component Isolator SSA=50%t_r -B PL = 250kN

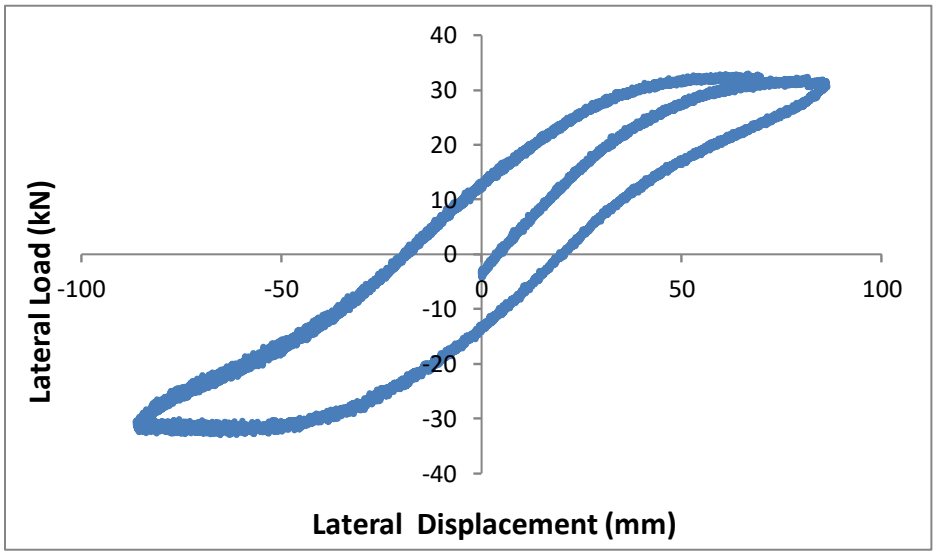

Figure A4-3 B220 Lateral load-displacement hysteresis diagram SSA=75%t_r -B

1-Keff-H= 362.55 N/mm 2-Keff-h=180.27 N/mm

3-Loop Area = 2185550 N/mm 3-ζ = 13%

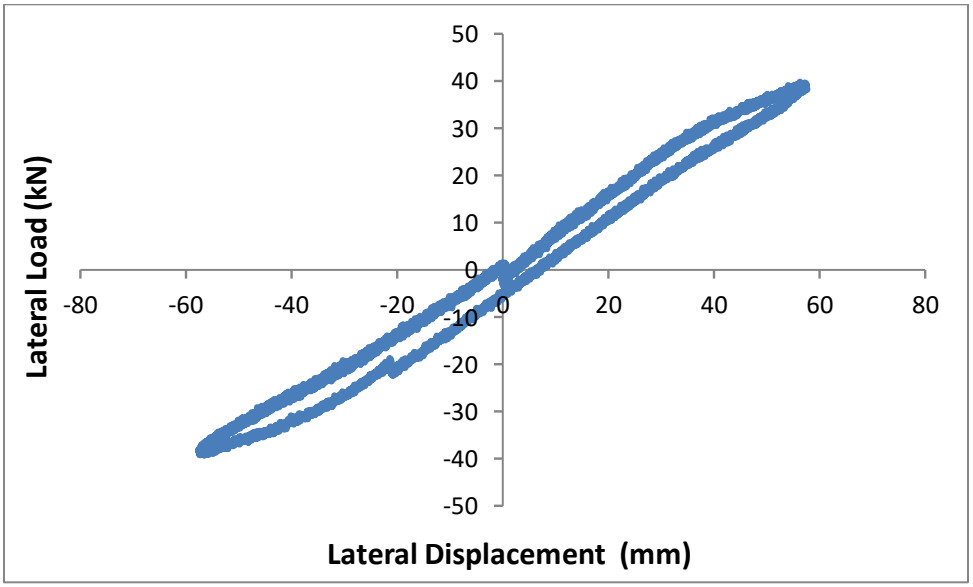

Figure A4-4 B220 Lateral load-displacement diagram SSA=50%t_r A

1-Hysteresis loop area = 561186.6 N-mm 2-Keff-H = 682.79 N/mm

3-Keff-h= 341.40N/mm 4-ζ = 3.96%

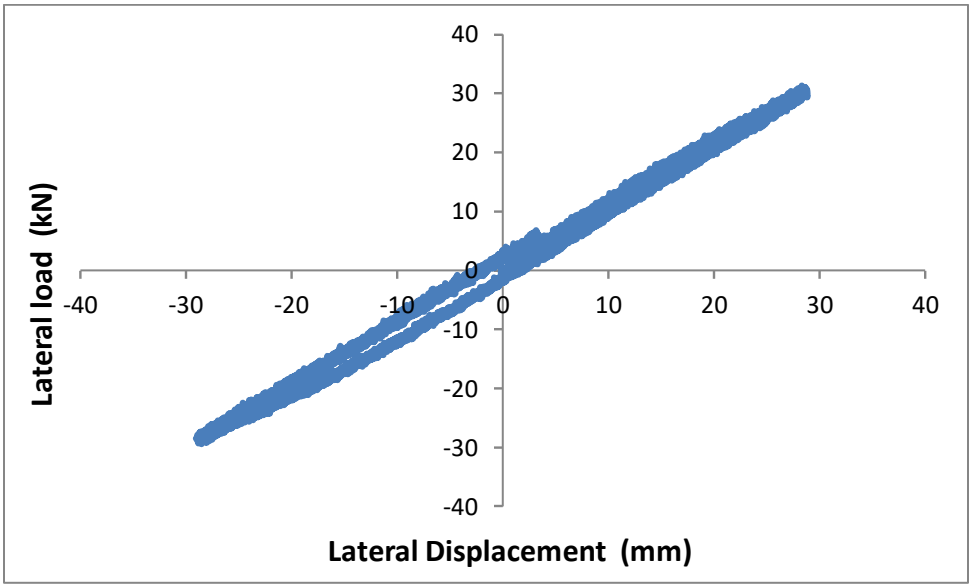

Figure-A4-5 B220 Component isolator SSA=25%t_r B

1-Keff-H=864.79N/mm 2- Keff-h 432.0 N/mm

3-Loop area= 135395.8N-mm 4-ζ = 3.01%

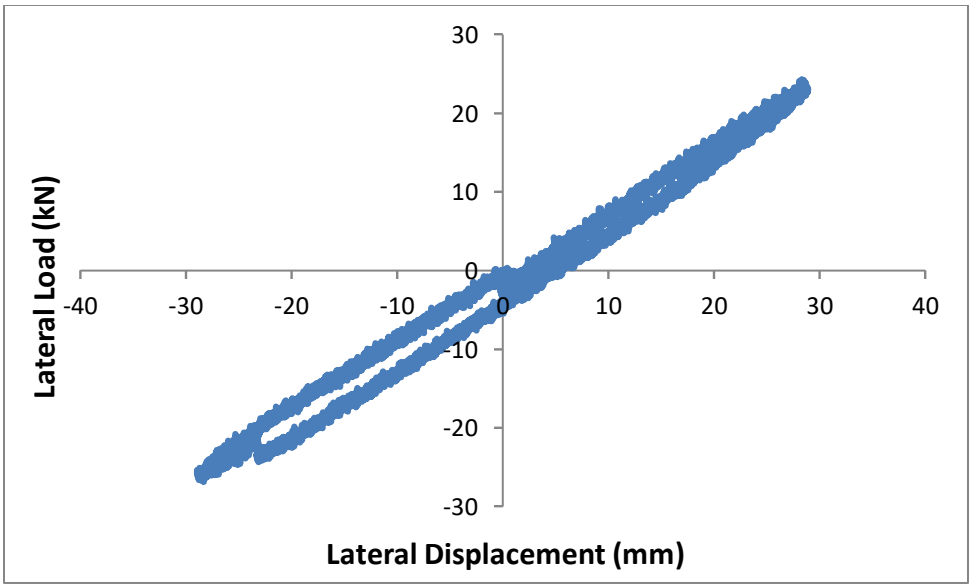

Figure A4-6 B220 SSA = 25%t_r A force-displacement hysteresis diagram

1-Keff-H=867.82 N/mm 2-Keff-h=433.91N/mm

3-Loop Area=164650.40 N-mm 3-ζ =3.64%

A4-7 B220 SSA =50%t_r -A with SP2

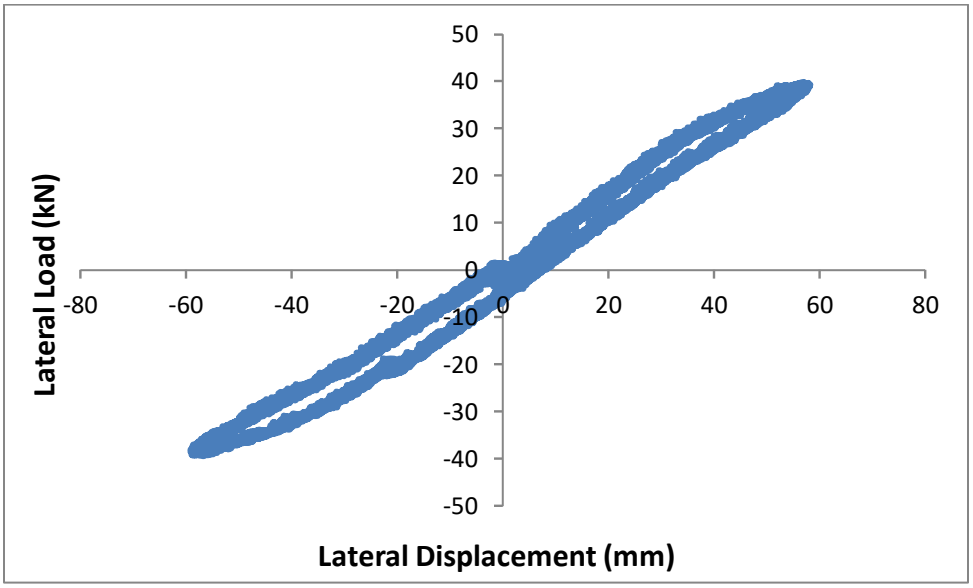

Figure A4-8 B220 Lateral load-displacement hysteresis diagram SA=50%t_r -A-SP2

1-Keff-H= 663 N/mm 2-Loop area=356126.3 N-mm 3-ζ = 2.49%

B220 SSA=%50t_r B

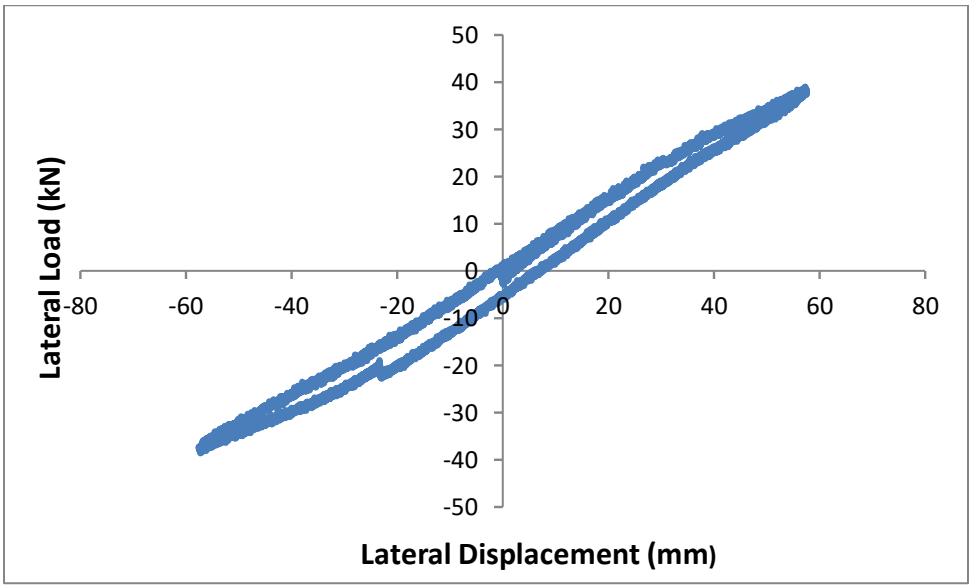

Figure-A4-9 B220 Lateral load-displacement hysteresis diagram SSA=50%t_r -B

1-Loop Area = 550311.1 N-mm 2-Keff-H= 658.12N/mm
3- Keff-h =329.06 N/mm 4- ζ = 4.02%

B220 SSA=25-100%t_r Dynamic Load profile PL=250kN

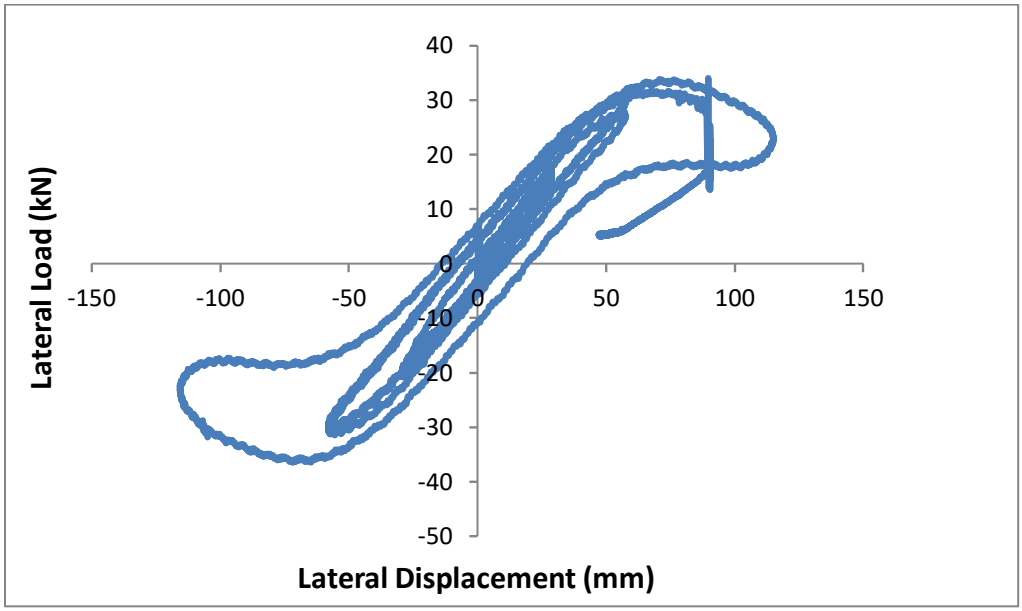

Figure A4-10 B220 Lateral load-displacement hysteresis diagram SSA=25-100%t_r Ϭ=5.17 MPa (Dynamic Load profile)

A5-B240 COMPONENT ISOLATOR (BL= 85.52%) PL=250kN

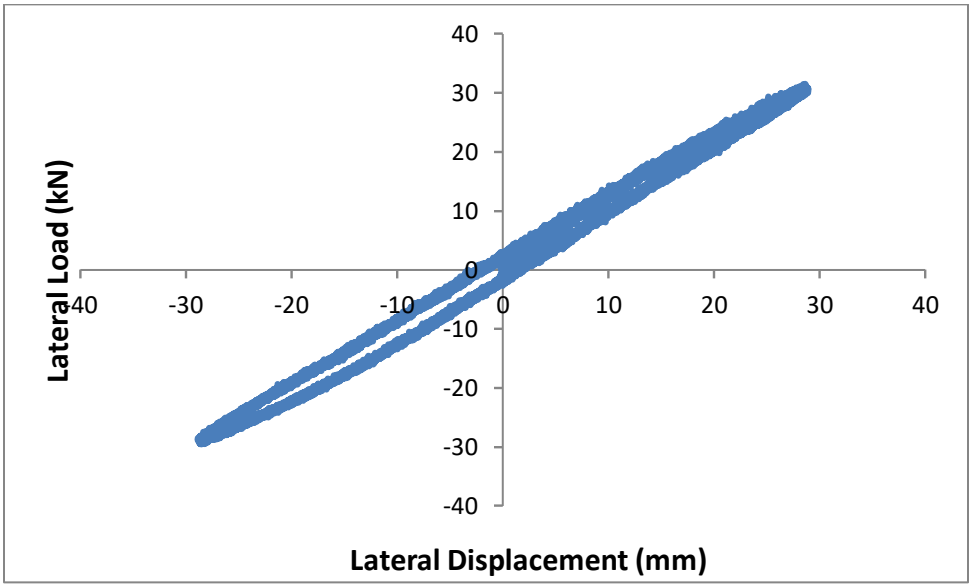

Figure A5-1 B240 component isolator SSA=25%t_r -A

1-Keff-H=1048.84N/mm 2-Keff-h=524.42N/mm

3-Loop Area = 243624.9N-mm 4-ζ = 4.47%

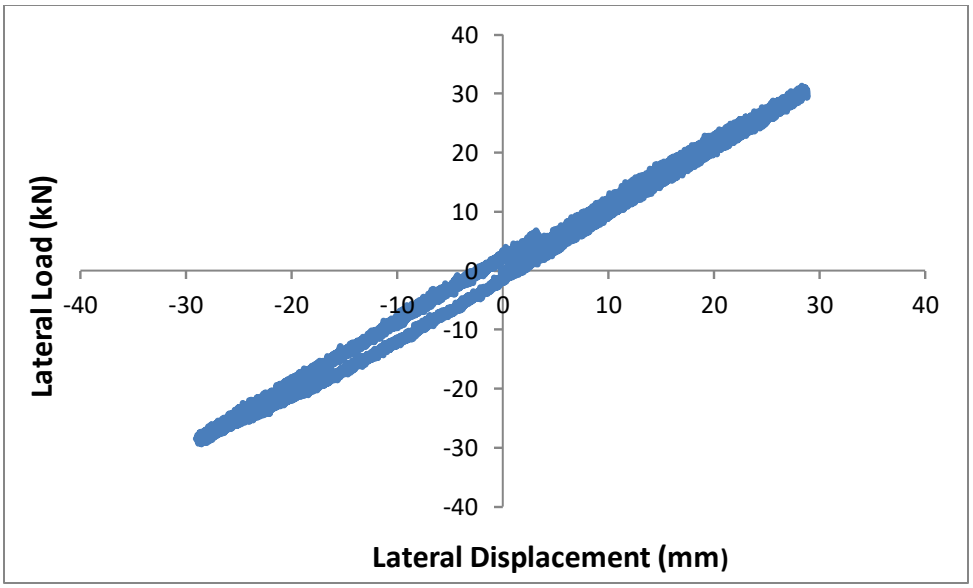

Figure-A5-2 B240 lateral load-displacement hysteresis diagram SSA= 25%t_r B

1-Keff-H=1043.75N/mm 2- Keff-h=521.88 N/mm

2-Loop area= 137411.30 N-mm 4-ζ= 2.72%

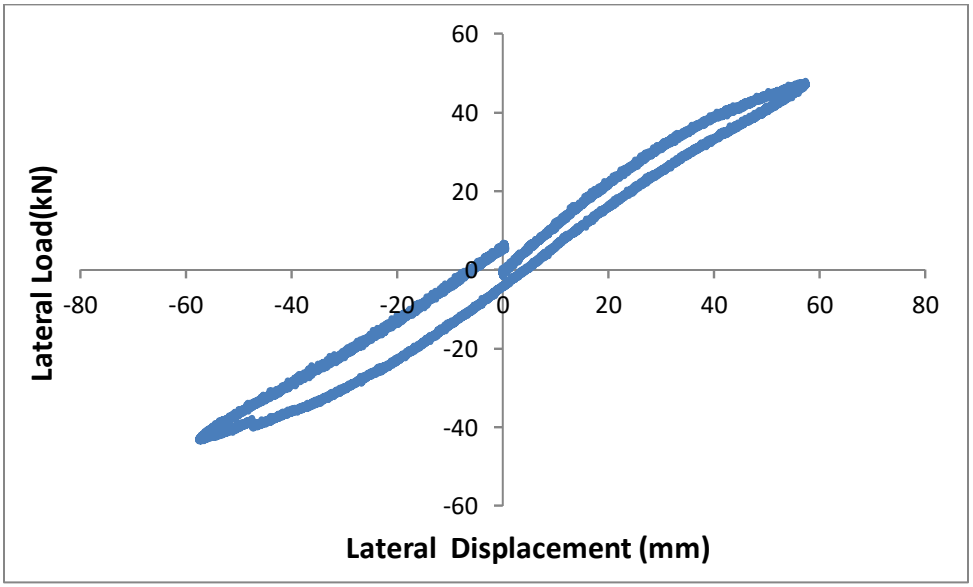

Figure-A5-3 -B240 Lateral Load-Displacement Hysteresis Diagram SSA 50%t_r A

2Keff-H = 786.55N/mm 2-Keff-H= 393.28 N/mm

3-Loop area= 740055.7 N-mm 4-ζ= 4.76%

B240 SSA=50%t_r B

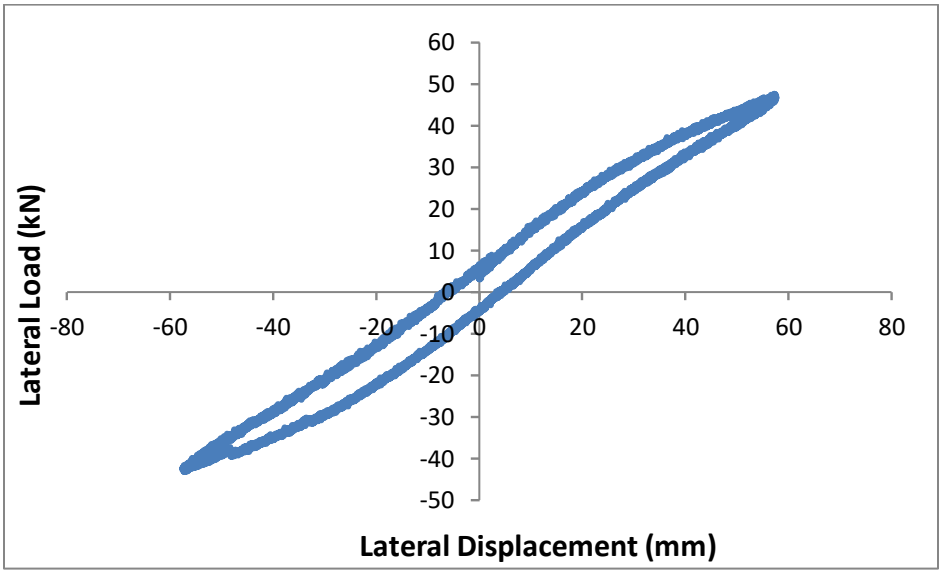

Figure A5-4 B240 Lateral load-displacement hysteresis diagram SSA=50%t_r -B Б=4.34MPa

1-Loop area = 803927.9 N-mm 2-Keff-H = 783.11 N/mm

3-Keff-h= 391.55 N/mm 4- ζ = 5.21%

B240 SSA= 75%t_r A

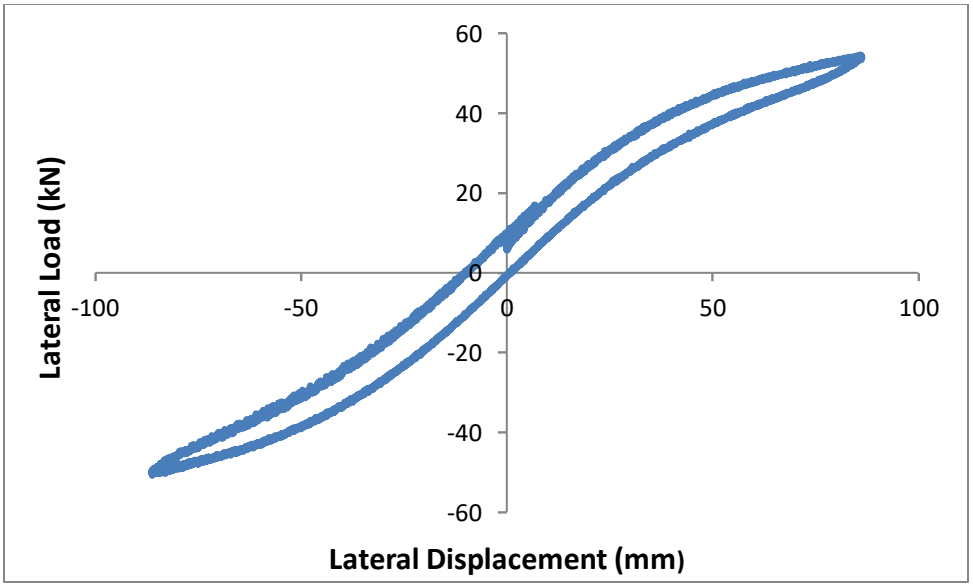

Figure A5-5 B240 Lateral load displacement hysteresis diagram SSA= 75%t_r A

1-Keff-H=619.83N/mm 2-Keff-h= 309.99 N/mm

3-Loop area=1374694N-mm 4-ζ= 4.75%

B240 SSA= 75%t_r B

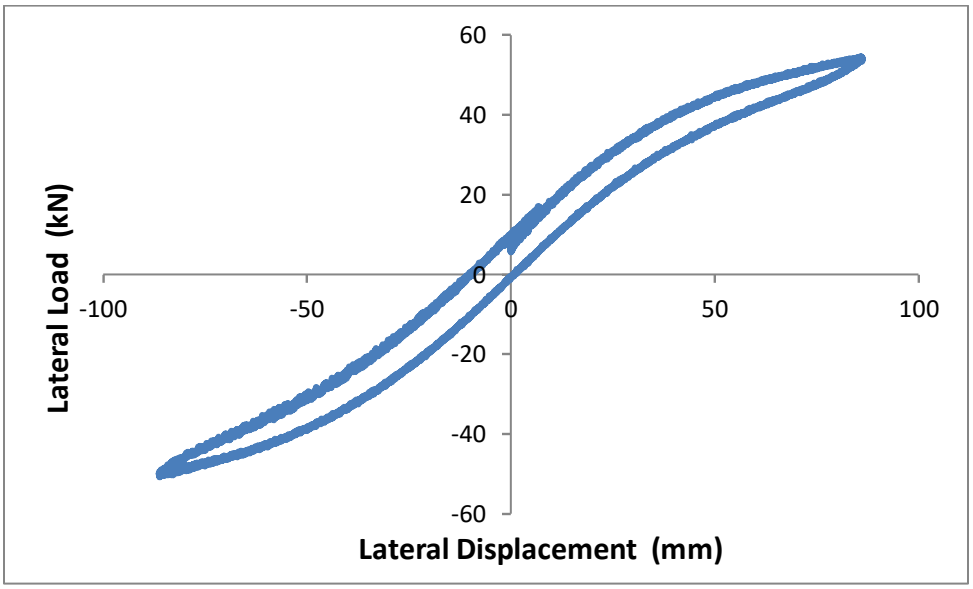

Figure A5-6 B240 Lateral load displacement hysteresis diagram SSA=75%t_r -B Ϭ=4.34MPa

1-Keff-H=603.07 N/mm 2-Keff-h= 301.50N/mm

2-Loop area=1285211.0 N-mm 4- ζ = 4.56%

B240 SSA=100%t_r –A PL = 250kN

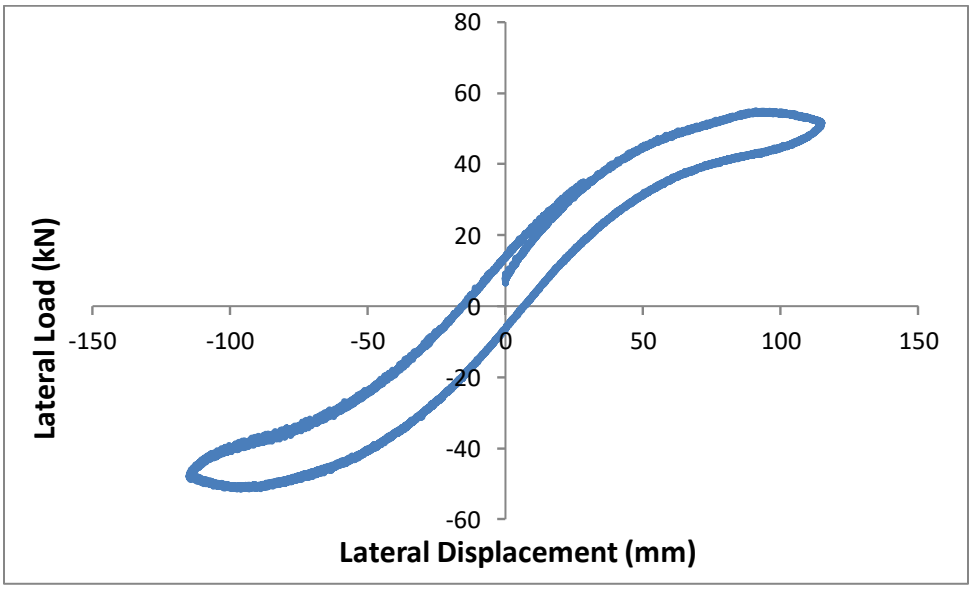

Figure A5-7 B240 Lateral load displacement hysteresis diagram Figure A5 SSA=100%t_r

1-Loop area =3158706 N-mm 2-Keff-H=433.83 N/mm

3-Keff-h=216.92N/mm 4-ζ = 8.83%

B240 SSA=100%t_r B

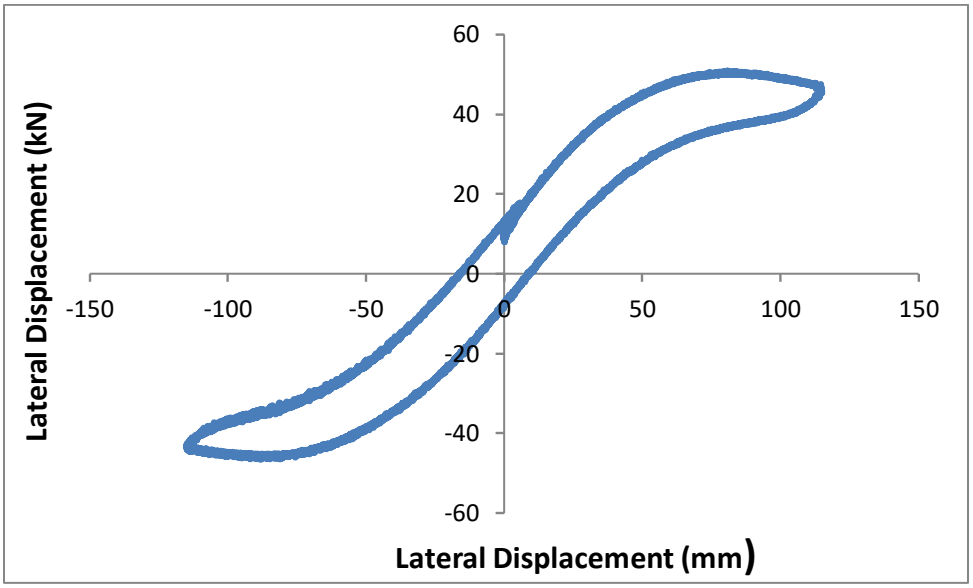

Figure A5-8 B240 lateral load-displacement hysteresis diagram SSA=100%t_r B

1-Keff-H syst. = 392.89 N/mm 2- Loop area=3412481.0 N-mm

3= Keff-h=196.45 4- ζ= 10.49%

A6-B260 SSA=%50 Bonding BL = 100% PL = 250kN

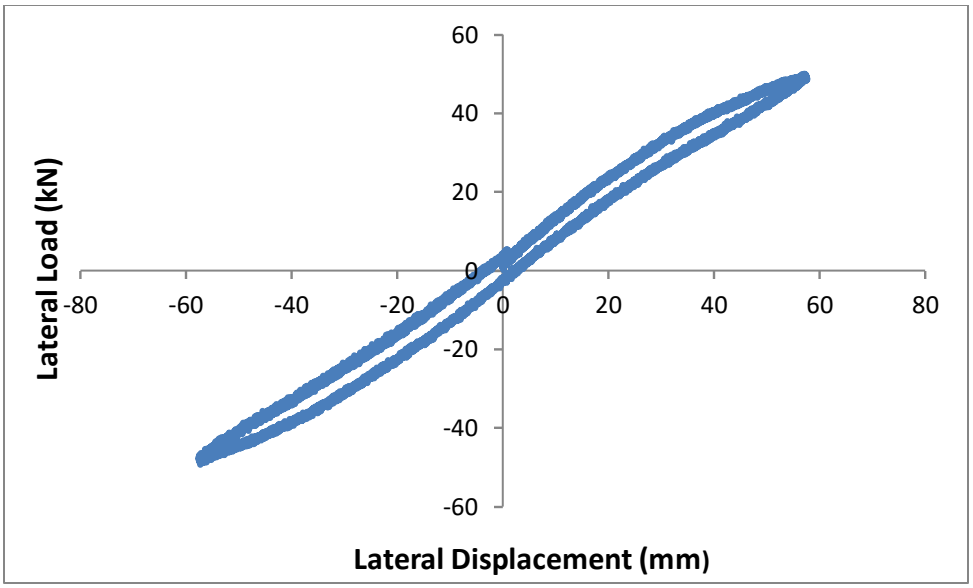

Figure A6-1-B260 SSA=50%t_r A Bonding Level = 100% б=3.69MPa

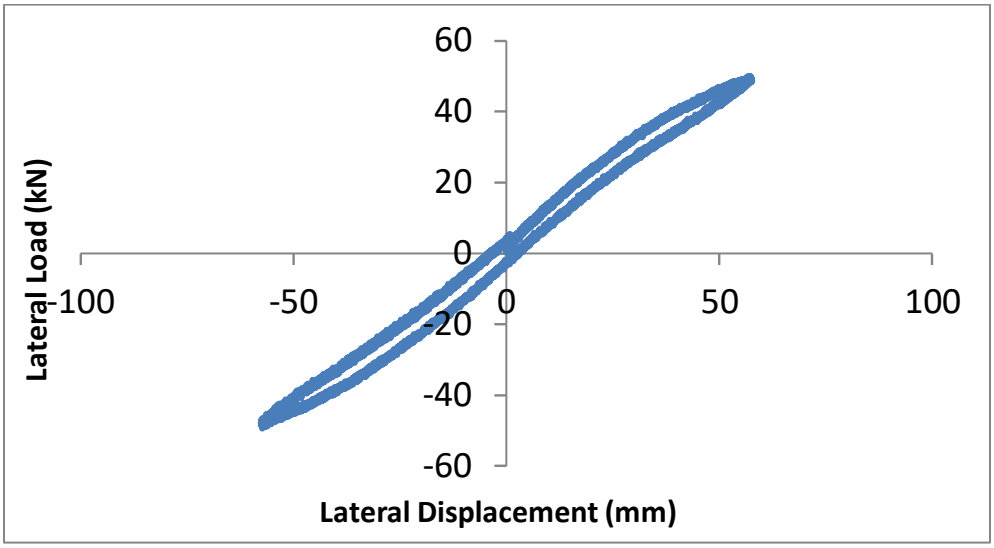

Figure A6-2 B260 Lateral load-displacement hysteresis diagram SSA= 50%t_r B PL=250 kN

1-Keff-H = 854.16 N/mm 2-Keff-h=427.08N/mm
3-Loop area=156810.90 N-mm 4-ζ = 3.42%

B260 SSA=25-50%t_r Dynamic Load profile PL = 250kN

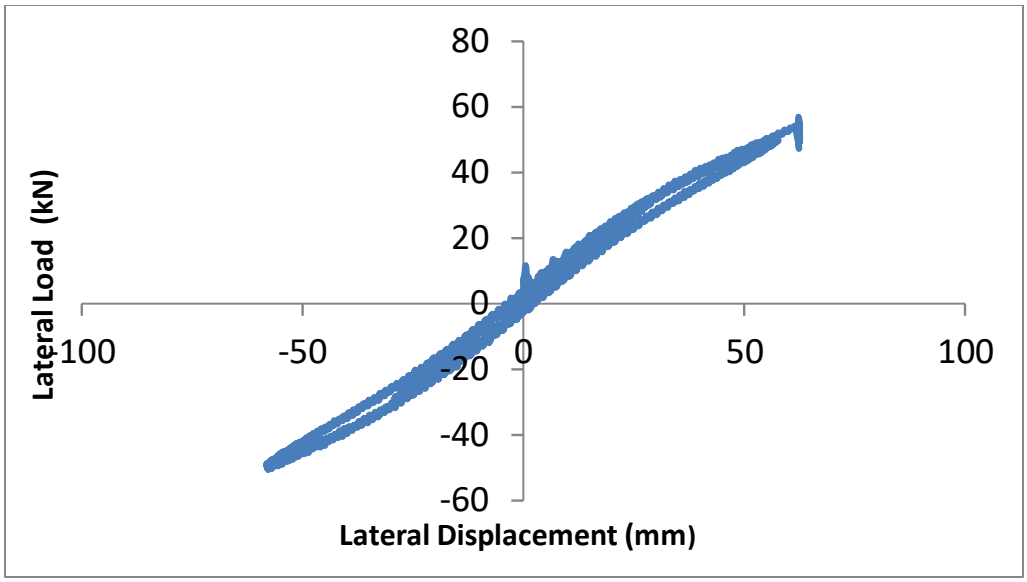

Figure-A6-3 B260 SSA=25-50%t_r A Dynamic Load profile Б =3.69MPa

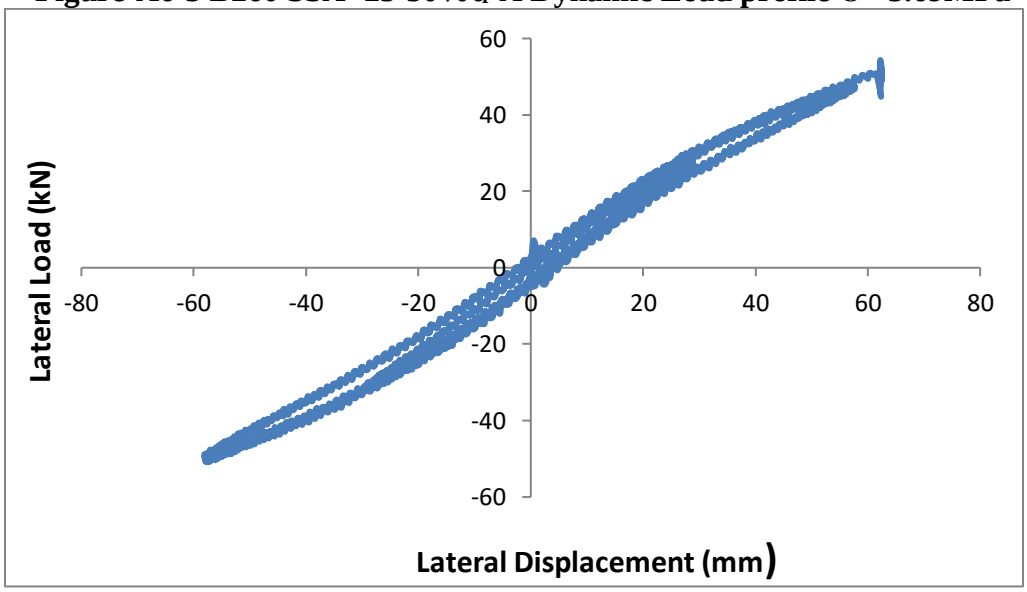

Figure A6-4- B260 Lateral Load-Displacement Hysteresis Diagram SSA= 25-50%t_r Б=3.69 MPa (Dynamic load profile B)

B260 Bonding Level BL=100%

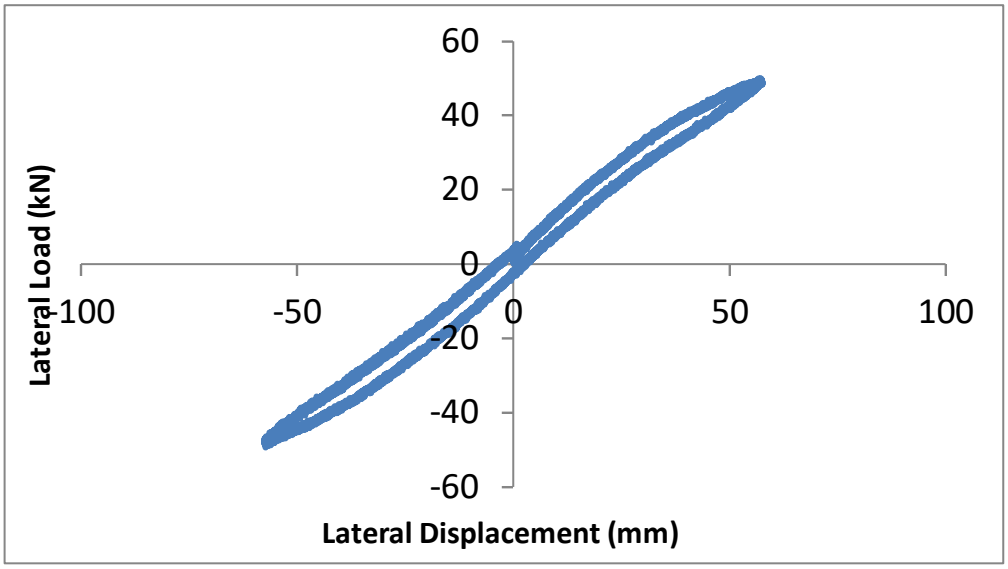

Figure A6-5 B260 lateral load-displacement hysteresis diagram SSA=50% t_r A

1-Keff-H = 865.18N/mm 2-Keff-h =432.59N/mm

3-Loop area = 604306.80N-mm 4-ζ = 3.36%

B260 SSA = 25%t_r –A

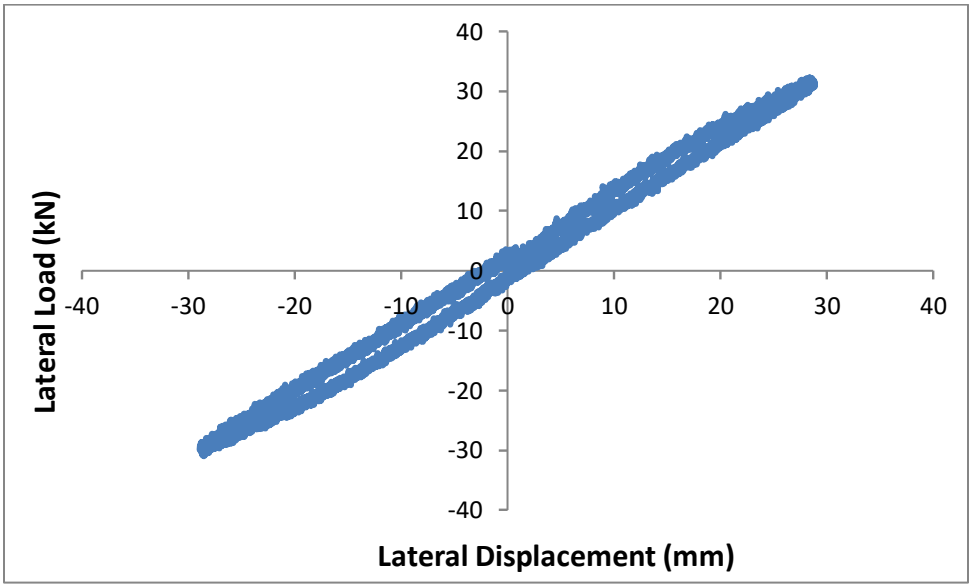

Figure A6-6 Lateral load displacement hysteresis diagram SSA=25%t_r A

1-Keff-H=1064.85 N/mm
2- Keff-h=532.43 N/mm
3-Loop Area= 1064.85N-mm
4- ζ= 2.26%

APPENDIX B: COMPOUND DOUBLE AND TRIPLE ISOLATORS, LATERAL LOAD-DISPLACEMENT HYSTERESIS DIAGRAMS, EFFECTIVE LATERAL STIFFNESS, DAMPING AND RELATED COMPUTATIONS

II-COMPOUND DOUBLE ISOLATORS

B1 Compound Isolator B200+B160 Average Bonding =48.52% PL= 500kN

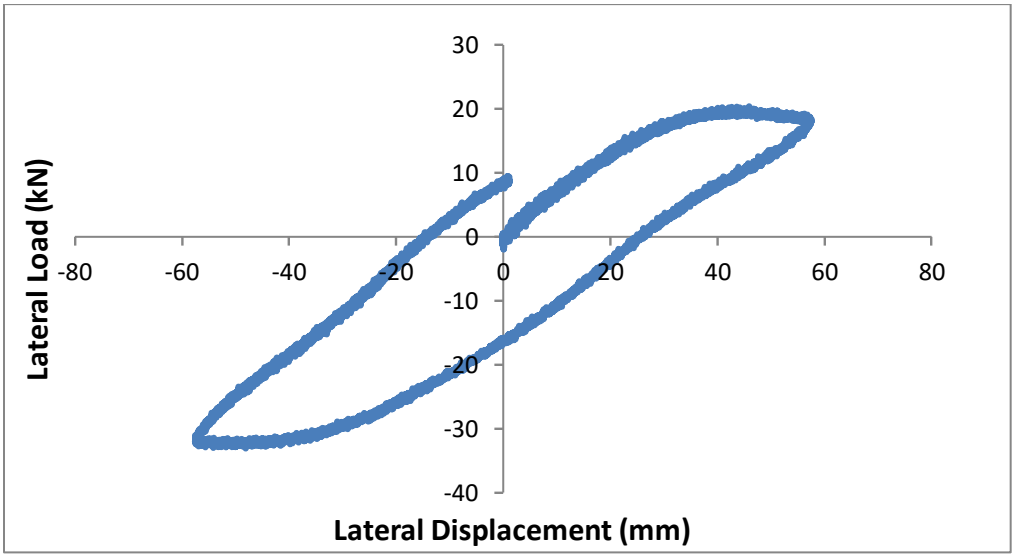

Figure B1-1 Compound isolator B200+B160 SSA= %50t_r-A Ϭ=7.62MPa

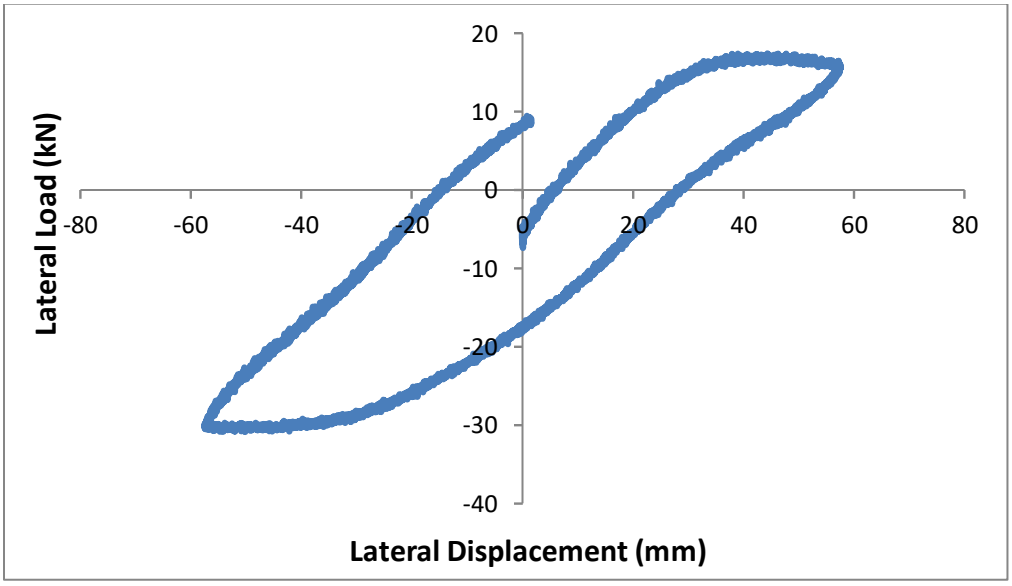

Figure B1-2 B200+B160 Lateral load-displacement hysteresis diagram SSA=50%tr-B

1-Keff-h-A =219.09 N/mm 2- Keff-H=436.90 N/mm

3-Hysteresis loop area =1737199.0N-mm 4-ζ-A= 19.22%

For Cycle B:

1-Keff-H-B= 403.62 N/mm 2-Keff-h-B= 201.81N/mm

3-Loop Area-B =1665631 N-mm 3-ζ -B= 19.87%

NOTE: This high level of damping and energy dissipation (loop area) is due to the presence of the Component Isolator B160

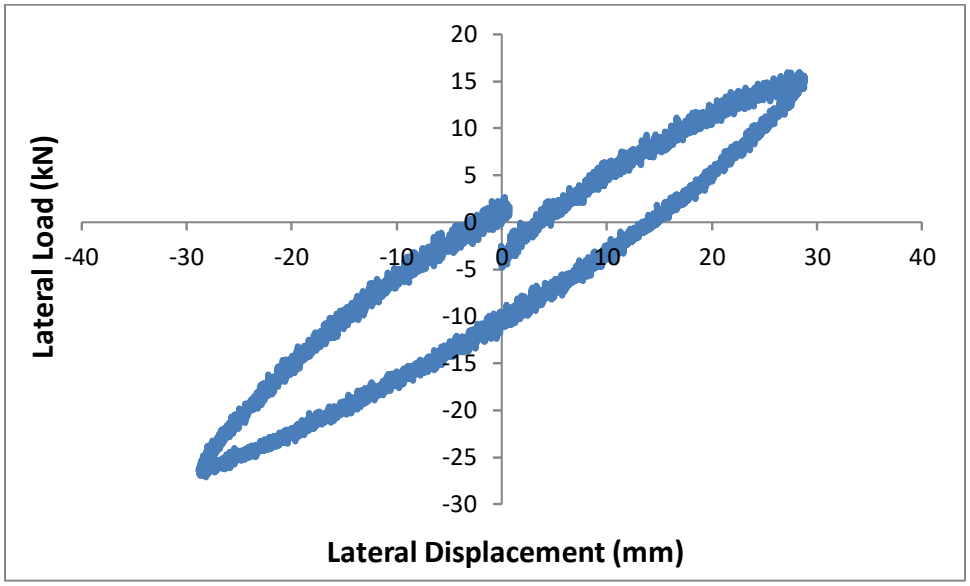

Figure B1-3 B200+B160 SSA = 25%t_r - A Pv=500kN

1-Keff-H =736.54N/m 2-Keff-h = 368.27 N/mm

3-Loop Area=327817.9 N-mm 4-ζ = 8.80%

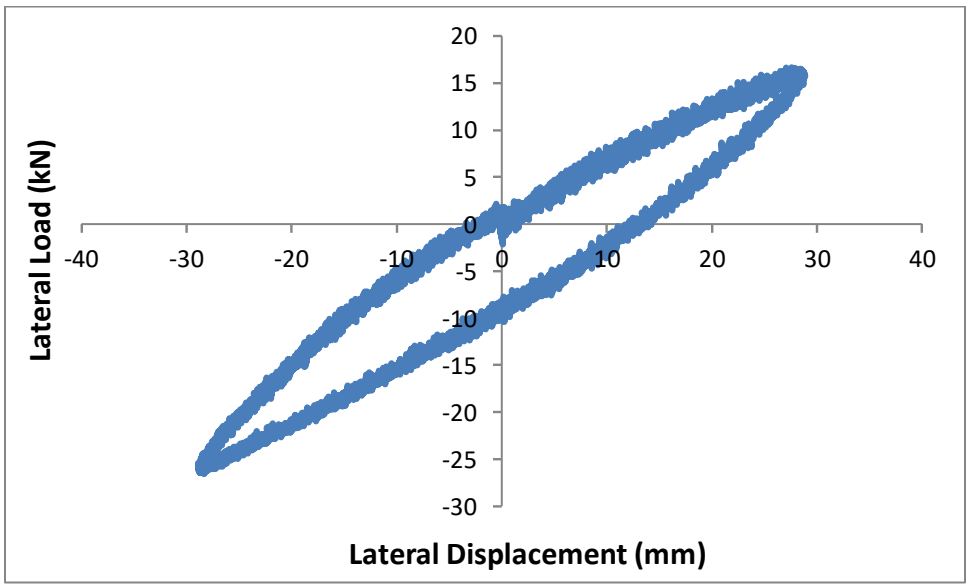

Figure B1-4 B200+B160 SSA=25%t_r- B B1-4 B200

1-Keff-H=735.07N/mm 2-Keff-h=367.53 N/mm

3-Loop area =422114.9 N-mm 4-ζ = 11.03%

B200+B160 Lateral load-displacement hysteresis diagram SSA= 25%t_r

B2 Compound Isolator B200+B180 (Average Bonding = 53.55%) PL = 500kN

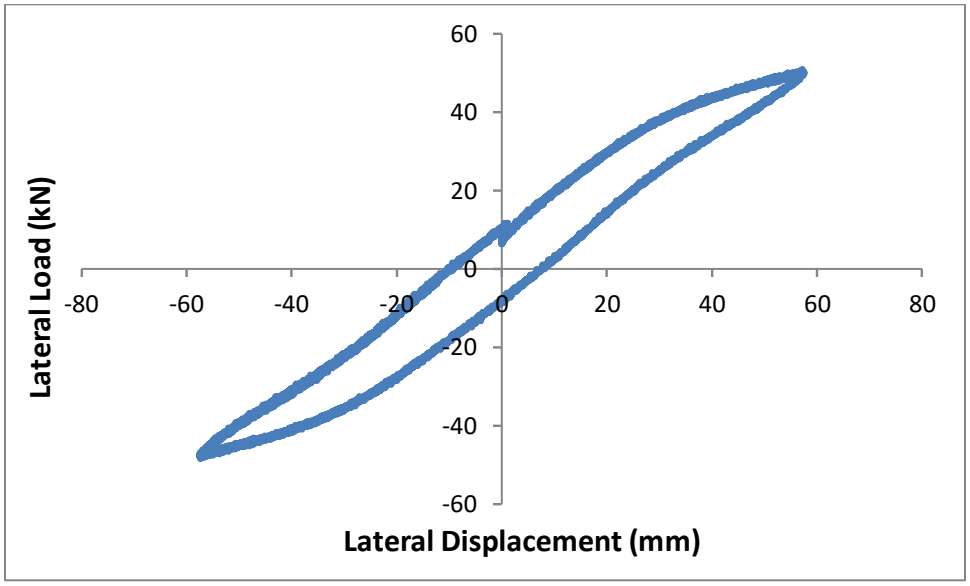

Figure B2-1 B200+B180 SSA=50%t_r-B Load-displacement Hysteresis Diagram

1-Loop Area =1349640 N-mm 2-Keff-h=431.40 N/mm

3- Keff-H = 862.80N/mm 4- ζ= 7.0%.

B3- B220+B160 Compound Isolator (Bonding Level =54.73%)

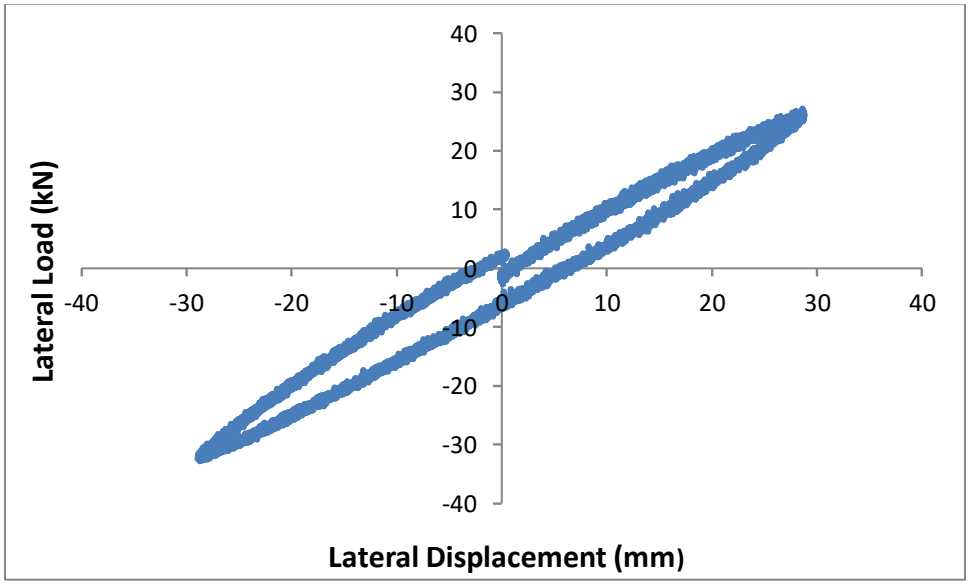

Figure B3-1 B220+B160 SSA=25%t_r-A PL = 500 kN

1-Keff-H=1027.76N/mm 2-Keff-h=513.88N/mm

3-Loop area= 316480.40N-mm 4-ζ=5.91%

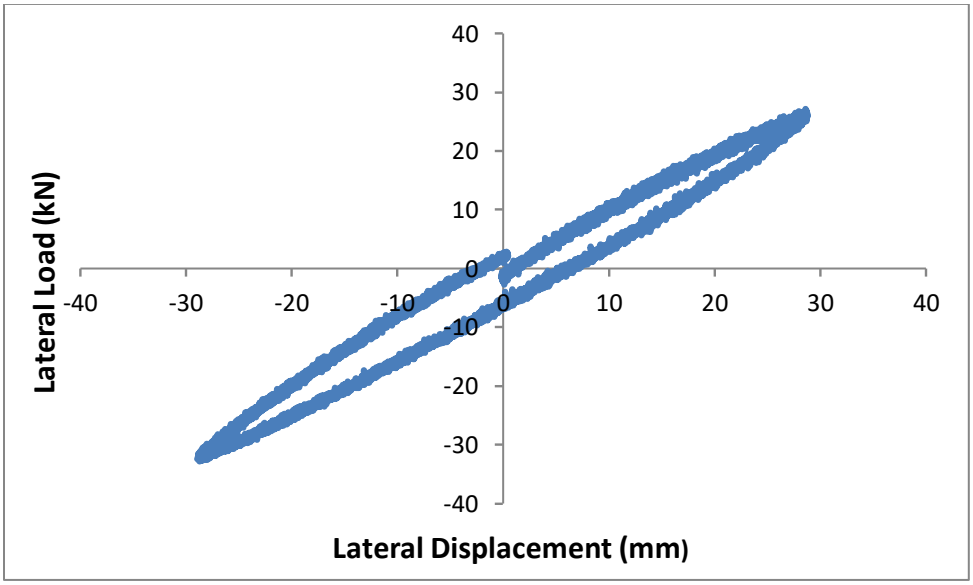

Figure B3-2 B220+B160 SSA=25%t_r A ϭ = 6.76 MPa

B220+B160 Compound Isolator SSA=%25t_r A

1-Keff-H =1036.07N/mm 2-Keff-h=518.04 N/mm

3-Loop Area=165488N-mm 4-ζ = 3.15%

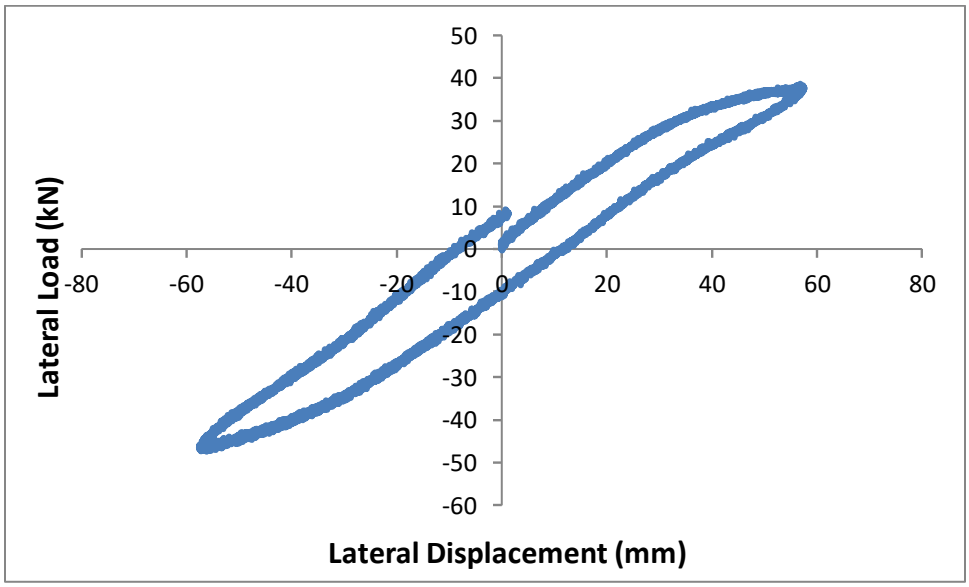

Figure B3-3 B200+B160 SSA= 50%t_r - A Pv= 500kN

1-Keff-H=737.60 N/mm 2- Keff-h=368.80 N/mm

3-Loop area=1100129 N-mm 4-ζ = 7.2%

B4-B200+B180 compound Isolator SSA=50%t_r Bonding 53.55% PL =500kN

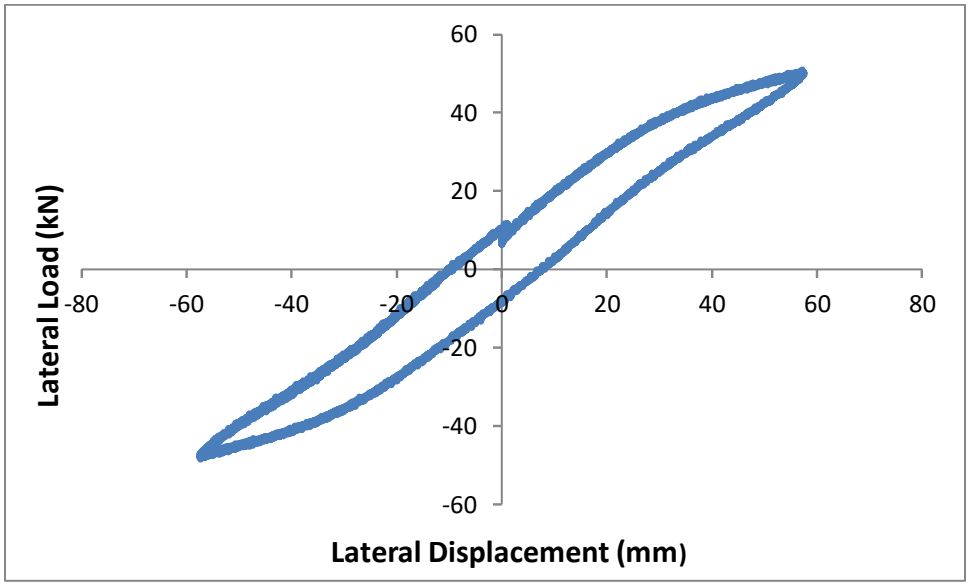

Figure B4-1B200 +B180 SSA= 50%t_r B PL = 500 kN

1-Loop Area=1349640 N-mm 3-Keff-h = 428.90 N/mm

2-Keff-H =857.79 N/mm 4-ζ= 7.92%

B5-Compound Isolator B220+B180 Bonding = 59.7% PL=500kN

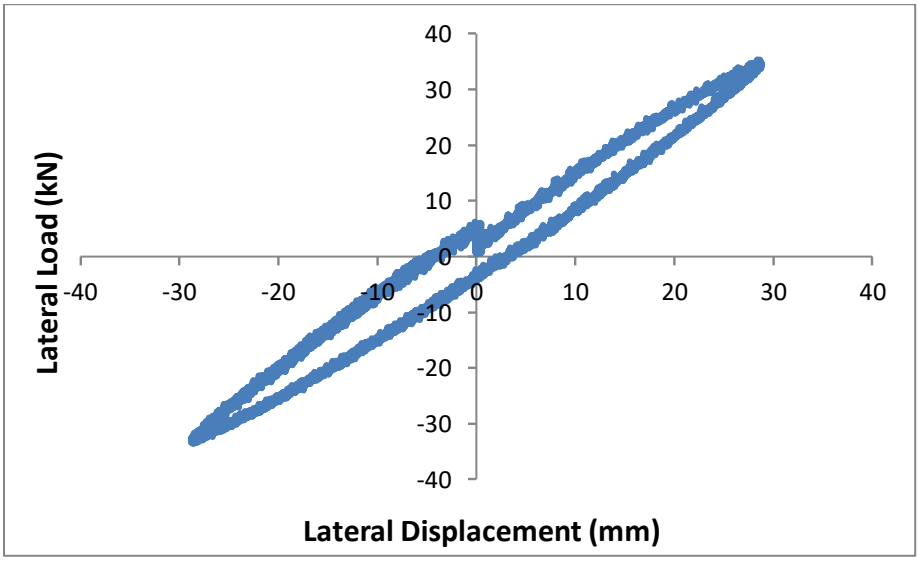

Figure B5-1 B220+B180 SSA= 25%t_r -A

1-Keff-H =1196.55 N/mm 2- Loop Area=263306.3N-mm

3-Keff-h= 598.28 N/mm 4- ζ =4.25%

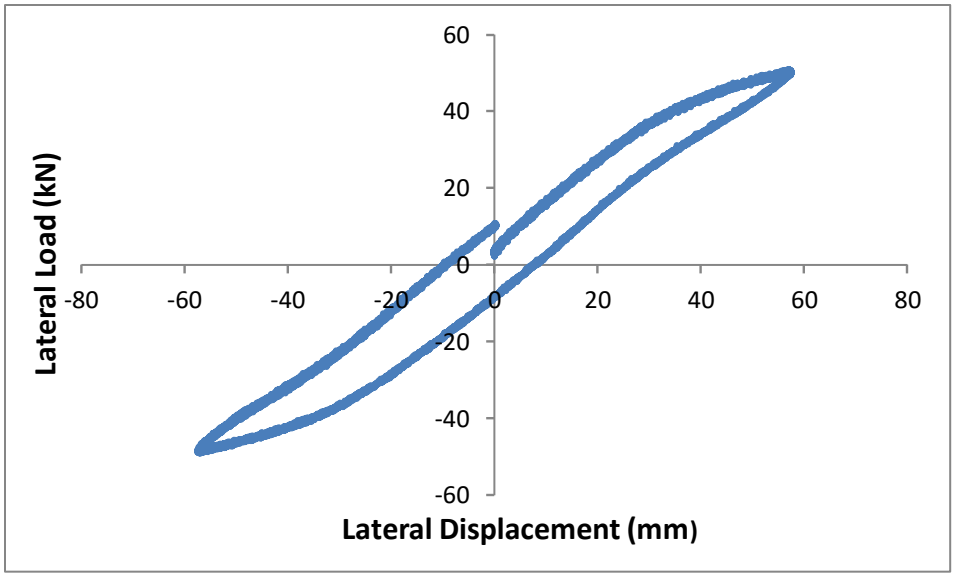

Figure B5-2 B220+B180 SSA=50%t_r –A PL= 500kN

1-Keff-H=865.70 N/mm 2-Keff-h= 432.85

3-Loop area=1432181 N-mm 4-ζ =7.47%

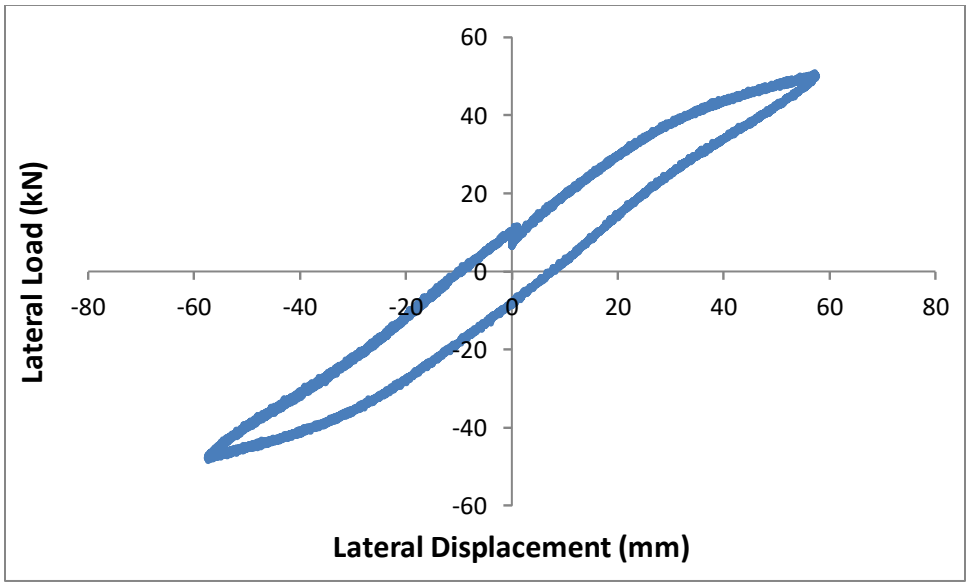

Figure B5-3 B220+B180 SSA=%50t_r – B

1-Keff-H=859.57 N/mm 2-Keff-h=429.78 N/mm

3-Loop area =1411798.0 N-mm 4- ζ =7.97%

B6 Compound Isolator B260+B180 Bonding= 73.96% PL=500kN

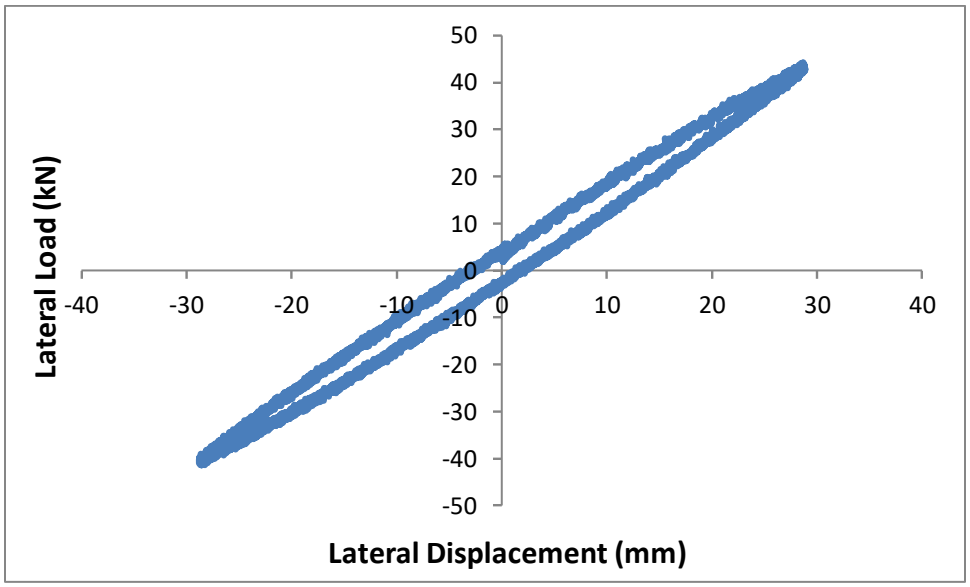

Figure B6-1 B260+B180 SSA=25%t_r- B

1-Keff-H =1460N/mm 2- Keff-h=730.32 N/mm

3-Loop Area=286580.5 N-mm 4-ζ = 3.77%

A-Results and outcome from spring pot #1 (SP1) recorded data

1-Keff-H=1478.70 N/mm 2-Loop area=259604.3 N-mm

3-Keff-h= 739.35 N/mm 3-ζ_{SP1} = 3.40%

B- The computed outcomes from SP2 recorded data

1-Keff-H=1463.4 N/mm 2-Loop area=191694.1 N-mm

3-ζ_{SP2} = 2.52% 4-Avarage ζ=2.45%

B260+B180 SSA= 50%t_r B

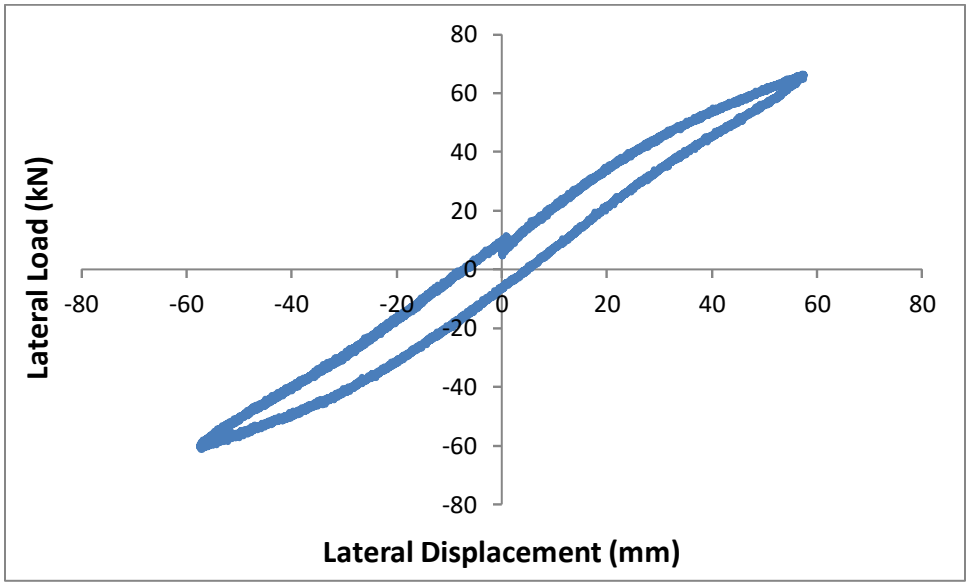

Figure B6-2 B260+B180 SSA=50%t_r – B

1-Keff-H= 111.02 N/mm 2-Keff-h= 555.510

2-Loop area=1053880 N-mm 3-ζ =9.36%

B7 B260+B200 Compound Isolator bonding = 79.59% PL=500kN

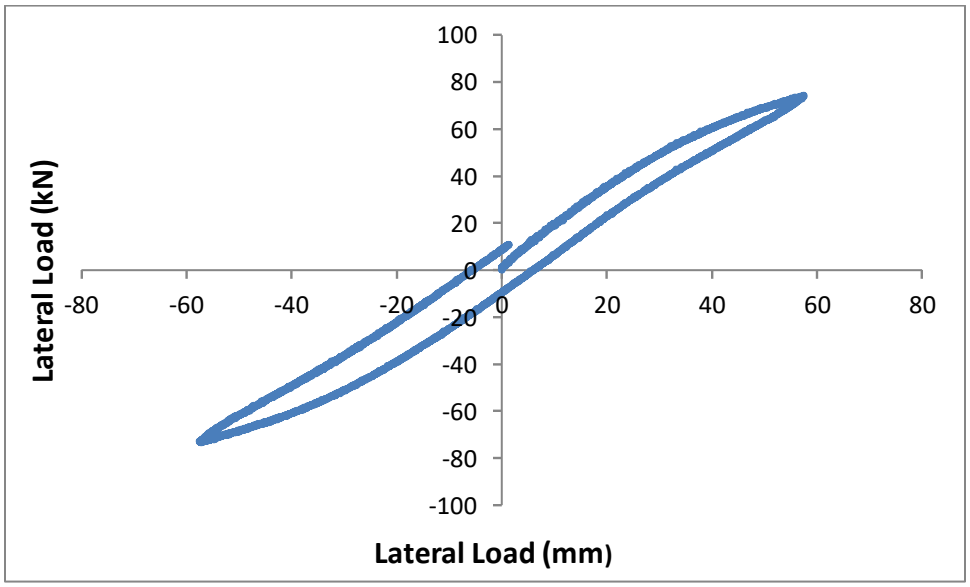

Figure B7-1 B260+B200 SSA=50%t_r –A

1-Keff-H=1277.91N/mm 2-Keff-h=638.95N/mm

3-Loop area=1374045 N-mm 4-ζ= 5.16%

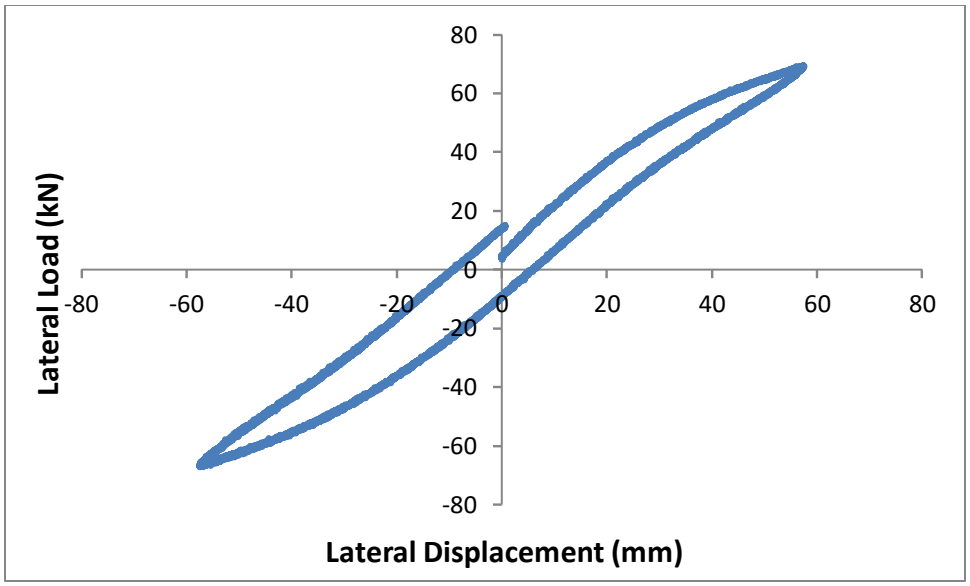

Figure B7-2 B260+B200 SSA=50% t_r -B

1-Keff-H=1180.9 N/mm 2-Keff-h=590.40N/mm

3-Loop area=1484655.0N-mm 4-ζ = 6.04%

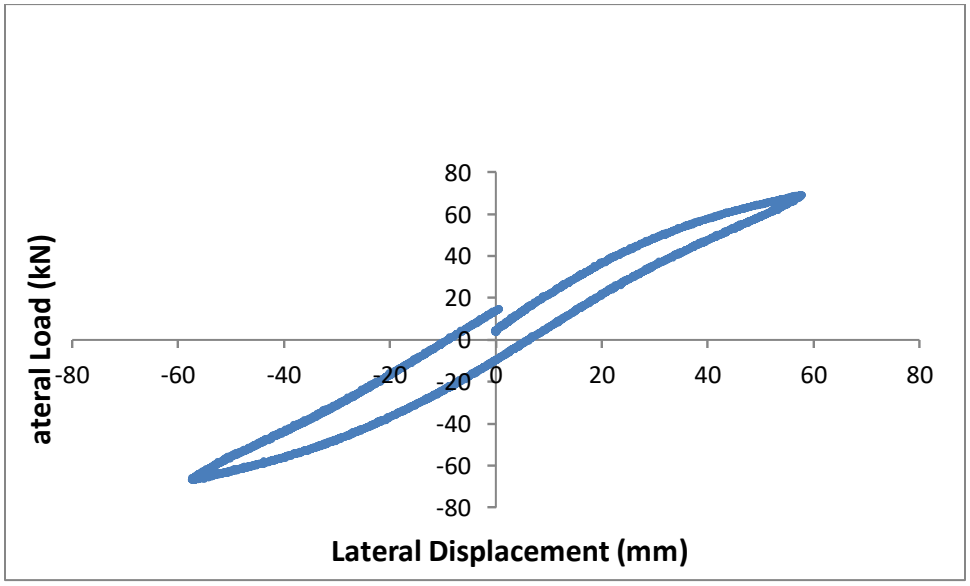

Figure B7-3 B260+B200 SSA=50% t_rB –Spot2 -3

1-Keff-H=1181.70 N/mm 2-Keff-h =590.85N/mm

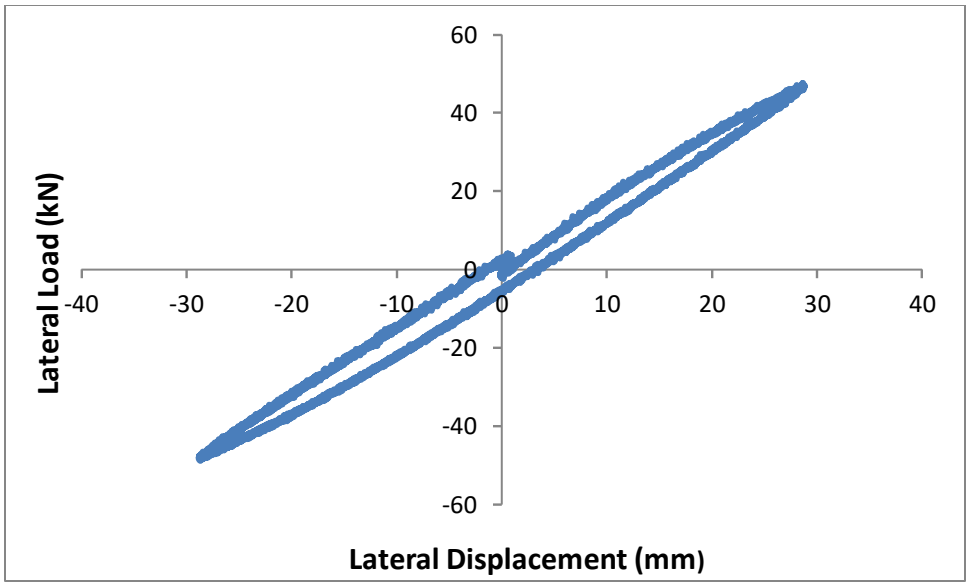

Figure B7-4 B260+B200 SSA=25%t_r A

1-Keff-H=1669.86 N/mm 2-Keff-h=834.93N/mm

2-Loop area=307467.9 N-mm 4-ζ = 3.55%

B8- Compound IsolatorB260+B220 Bonding =85.80% Pv= 500kN

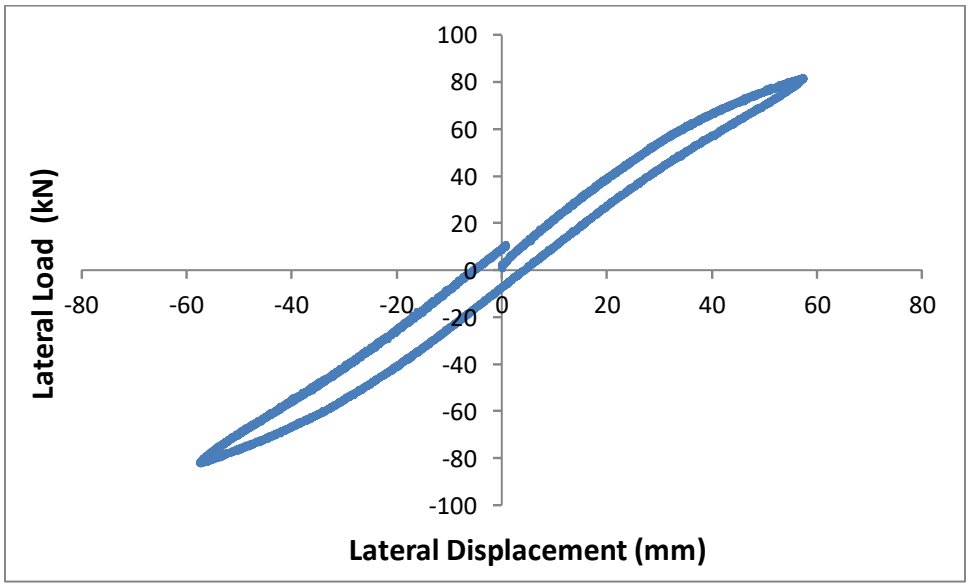

Figure B8-1 B260+ B220 SSA=50%t_r - A

1-Keff-H=1427.13 N/mm 2 - Keff-h =713.56N/mm

3-Loop area=1146063 N-mm 4-ζ = 3.88%

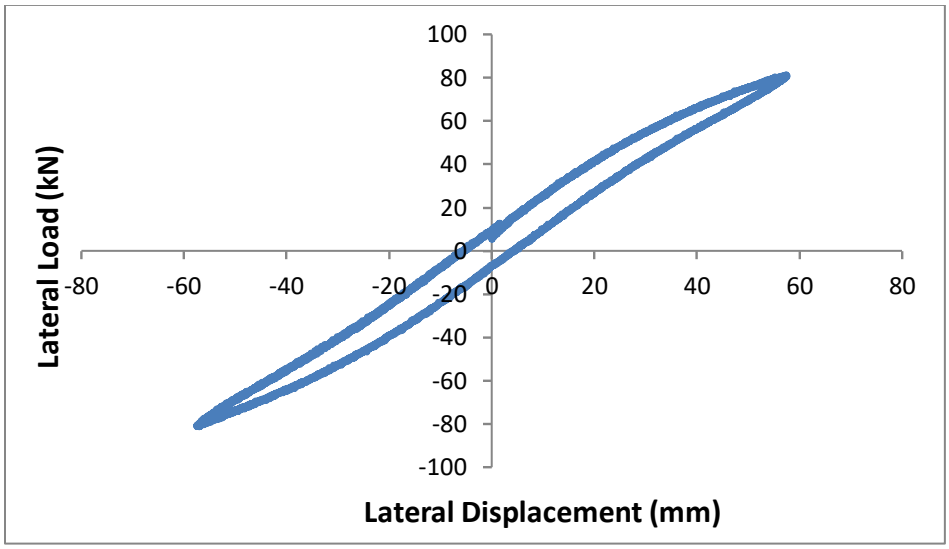

Figure B8-2 B260+B220 SSA=50%t_r B

1-Keff-H=1412.11N/mm 2-Keff-h=706.06 N/mm
2-Loop Area=1199927.0 N-mm 4-ζ = 4.09%

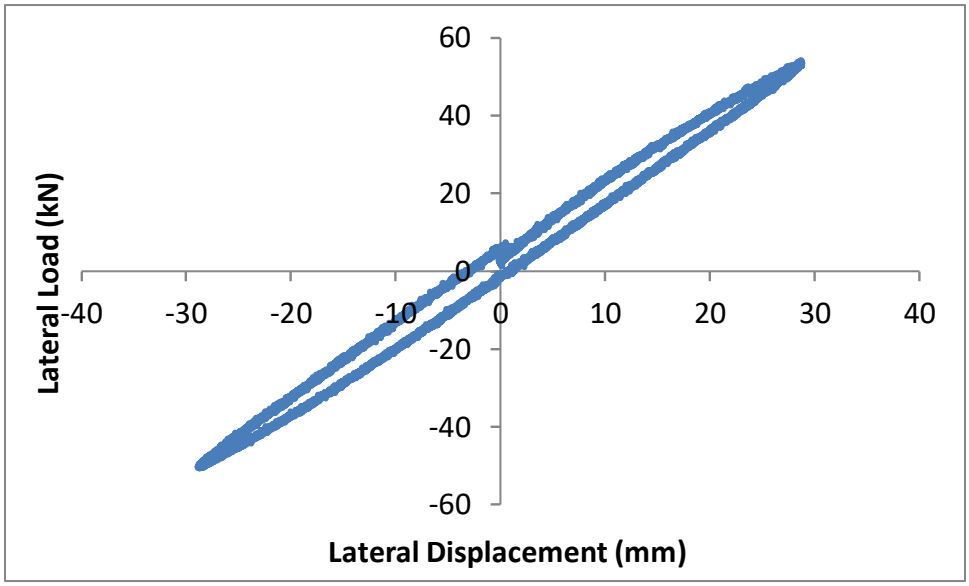

Figure B8-3 B260+B220 SSA=25%t_r A

1-Keff-H=1815.03 N-mm 2-Keff-h=907.51N/mm
3-Loop area= 297288.0 N-mm 3-ζ = 3.15%

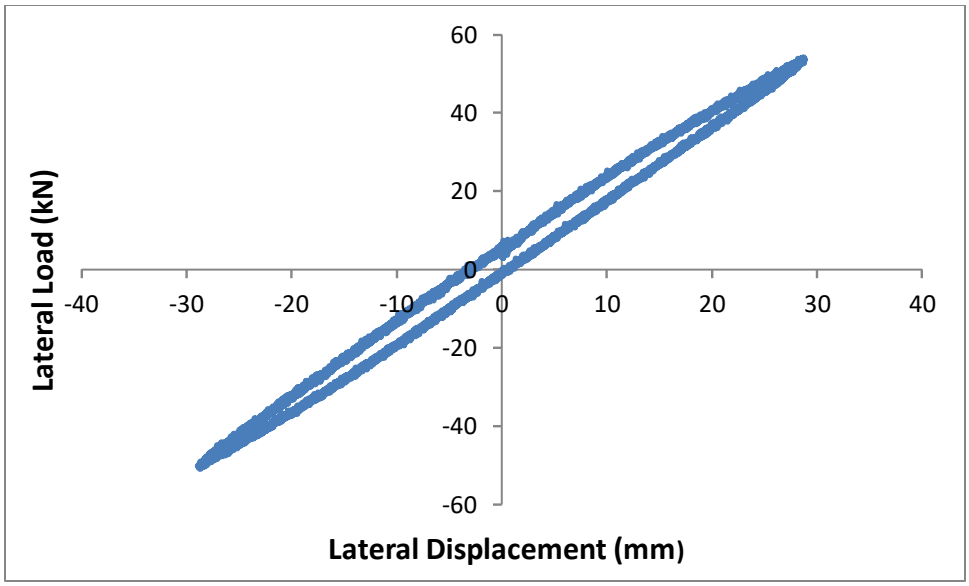

Figure B8-4 B260+B220 SSA=25%t_r -B

1-Keff-H=1809.3N/mm 2-Keff-h=904.65 N/mm

2-Loop area= 297289.4 N-mm 4-ζ = 3.16%

B-9 Compound B260+B240 Bonding =92.60% PL = 500 kN SSA= 25%t_r A & B & 50%t_r A &B

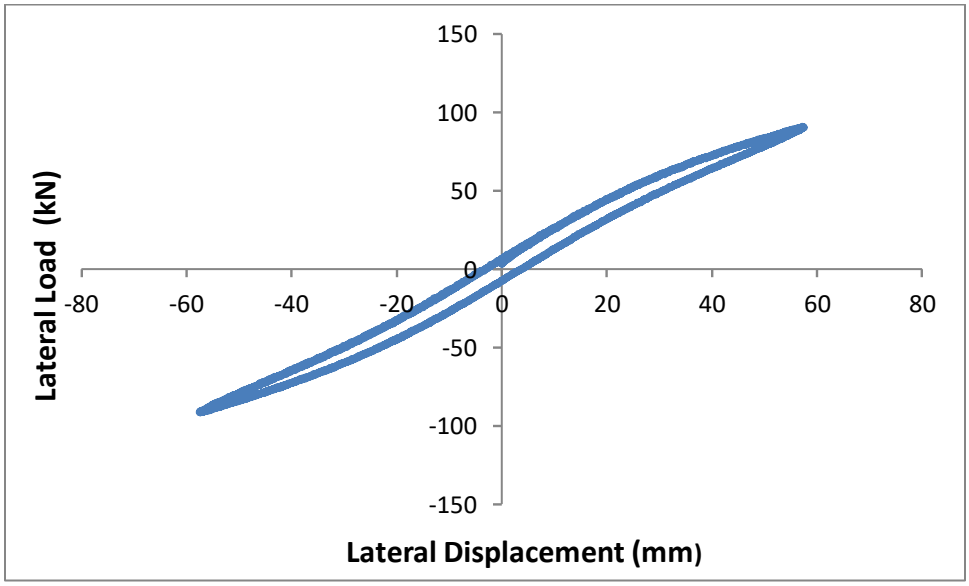

Figure B9-1 Compound Isolator B260+B240 Lateral load displacement Hysteresis Diagram SSA=50%t_r -B Compound Isolator B260+B240 BL= 92.60% Ϭ=3.99MPa

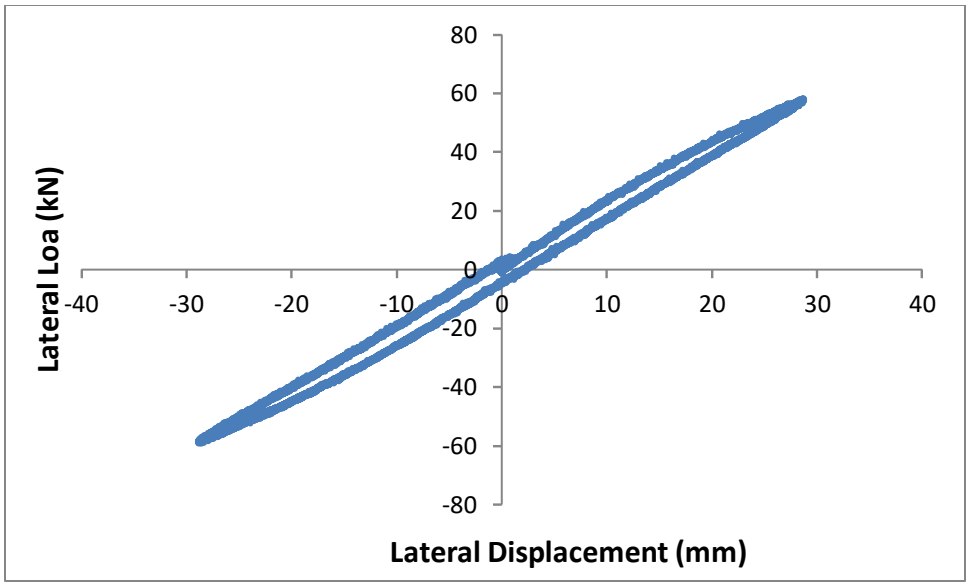

Figure B9-2 B260+B240 compound isolator SSA=25%t_r -A

1-Keff-H (syst.) = 2023.1 N/mm 2-Keff-h=1011.5 N/mm
2-Loop Area= 303837.4 N-mm 3-ζ= 2.88%

Compound Double Isolator B260+B240

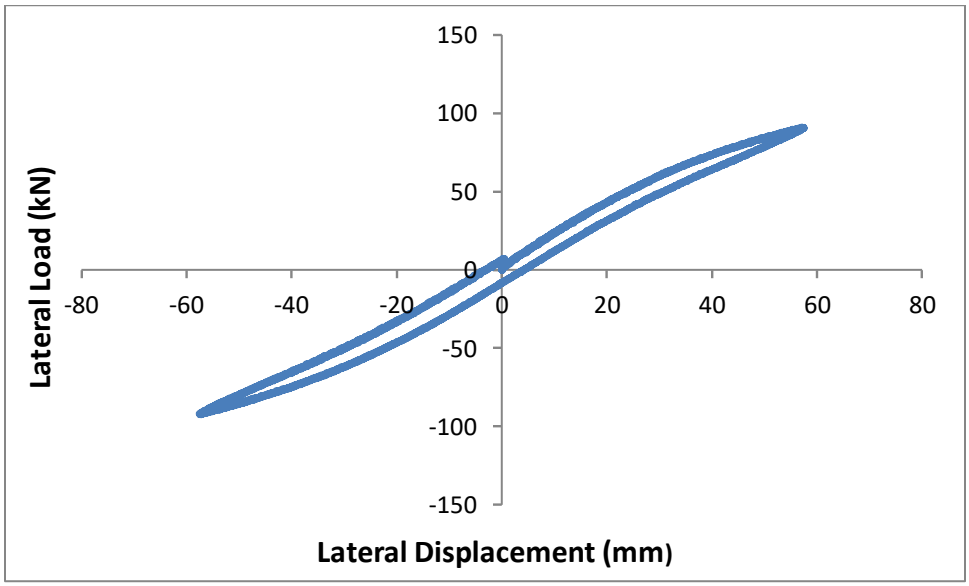

Figure B9-3 B260+B240 SSA=50%t_r –A

1- Keff-H (syst.) =1587.6N/mm 2-Keff-h=793.8N/mm
3-Loop Area=1857700N-mm 3-ζ =5.67%

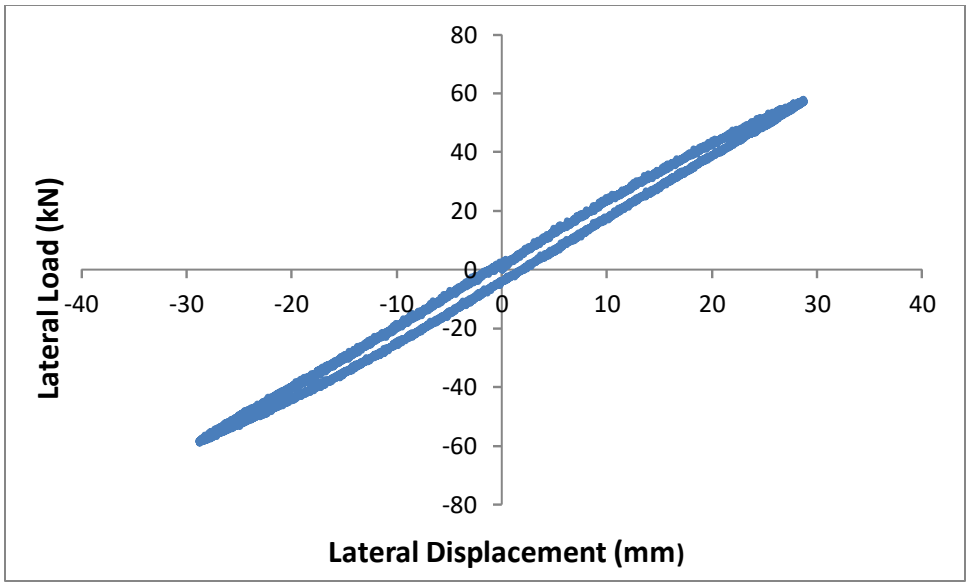

Figure B9-4 B260+B240 SSA=25%t_r -B

1-Keff-H=20215.54N/mm 2-Keff-h=1010.77N/mm
2-Loop area =264459.9 N-mm 4-ζ =2.51%

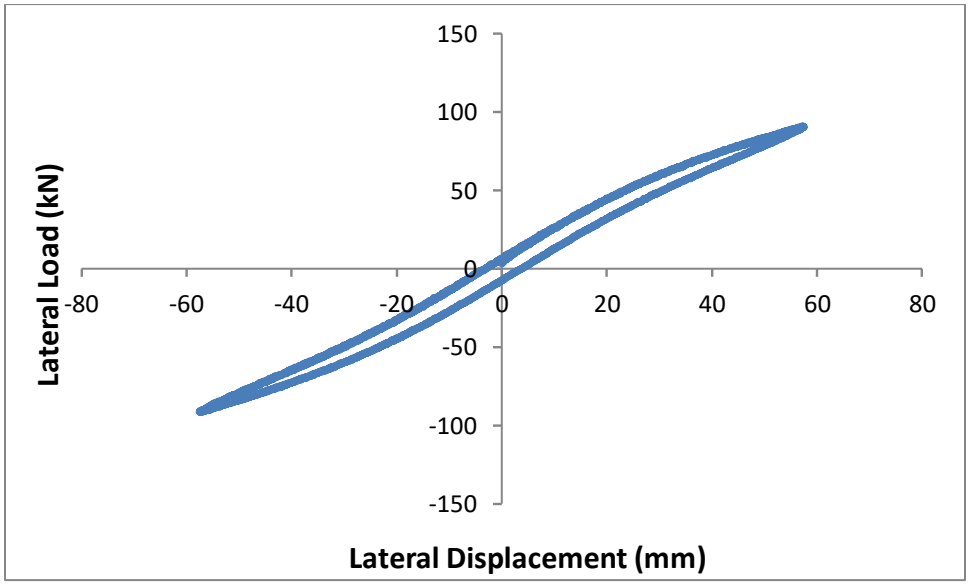

Figure-B9-5 B260+B240 SSA=50%t_r –B

1-Keff-H=1580.48N/mm 2-Keff-h=790.24 N/mm
3-Loop area+1176077 N-mm 4-ζ = 3.57%

B-10 Compound isolator B260+B260 –Bonding Level =100% PL = 500 kN

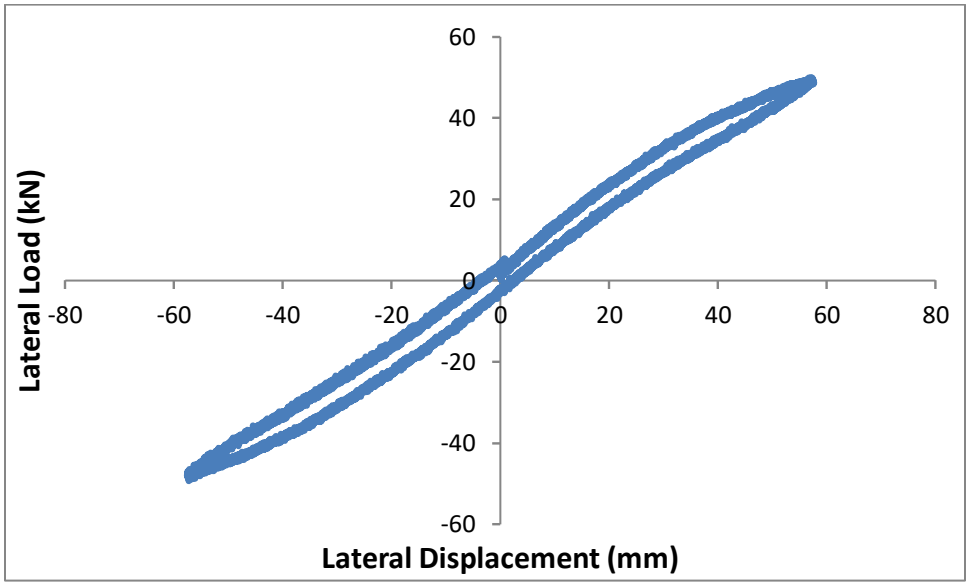

Figure B10-1 B260+B260 SSA=50%t_r A

1-Keff-H=851.00 N/mm 2-Keff-h=Keff-H
3-Loop are=601901.8N-mm 4-ζ=3.41%

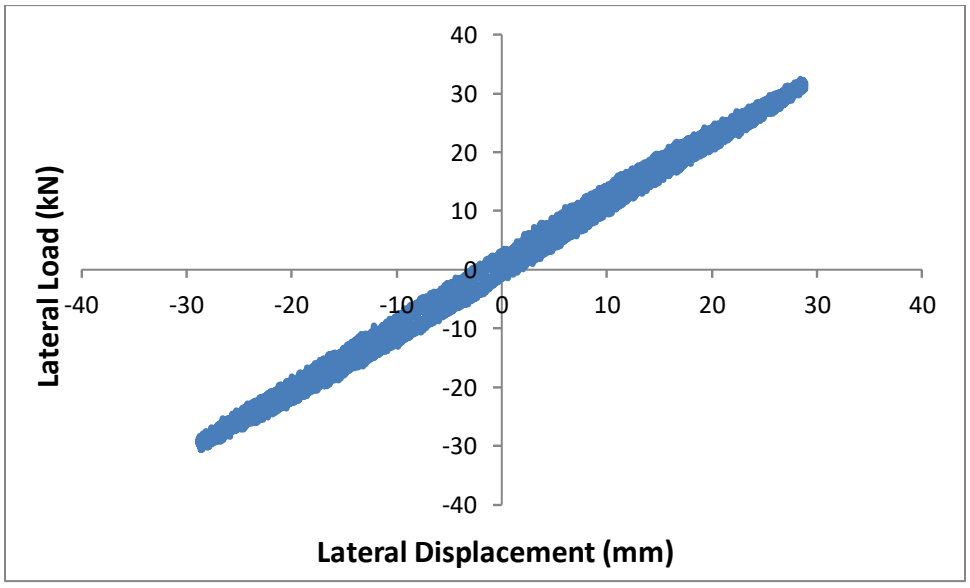

Figure B10-2 B260+ B260 SSA= 25%t_r –B

1-Keff-H=1064.85N/mm 2-Keff-h=532.43 N/mm
3-Loop area=125996.7N-mm 4-ζ= 2.26%

III- COMPOUND TRIPLE ISOLATORS

B11- CSB-CFREI with B260+B240+B220 Compound triple isolator

Bonding Level= 85.60% PL = 750kN

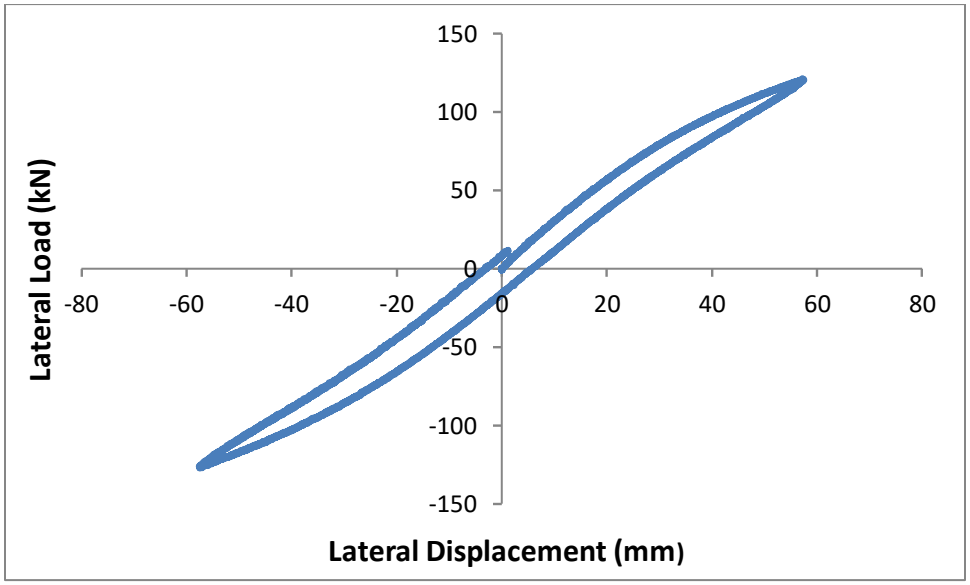

Figure B11-1 B260+B240+B220 Compound triple Isolator SSA=50%t_r -A PL= 750kN (F-d Hysteresis Diagram)

1-Keff-H=2151.32N/mm

2-Keff-h =1075.66 N/mm

2-Loop area= 1826837 N-mm

4-ζ = 4.084%

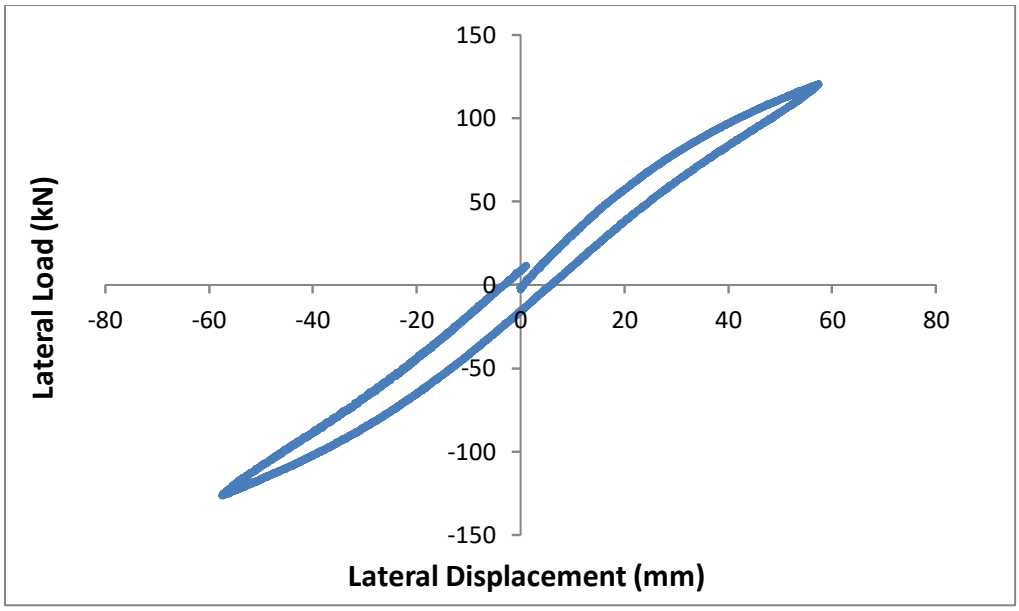

Figure B11-2 B260+B240+B220 SSA=50%t_r A

1-Keff-H=2149.87N/mm 2-Keff-h= 1074.94 N/mm

3-1820314N-mm 4- ζ =4.08%

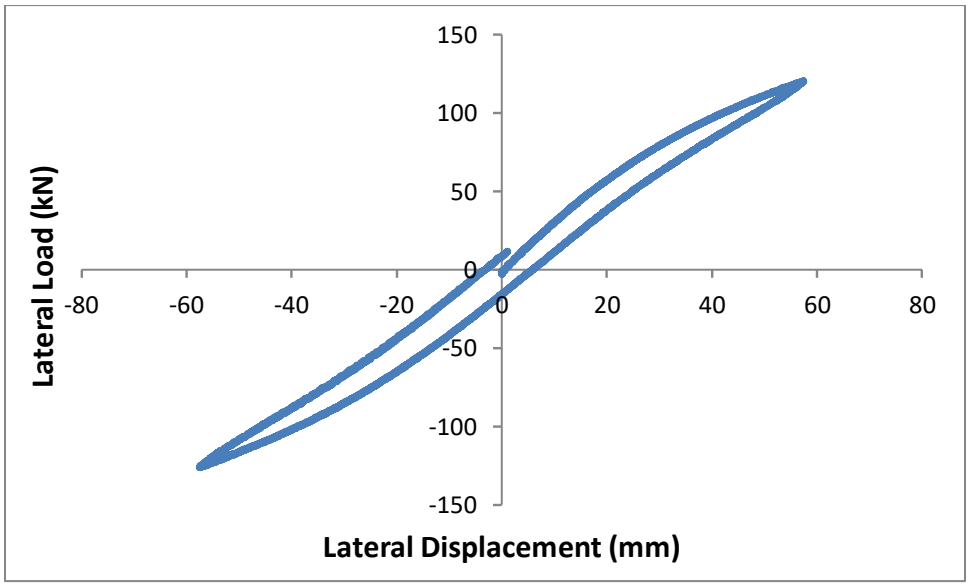

Figure B11-3 B260+B240+B220 SSA=50%t_r -B

1-Keff-H=2149.87 N/mm 2-Keff-h= 1359.81 N/mm

3-Loop are= 1820314N-mm 4-ζ= 4.08%

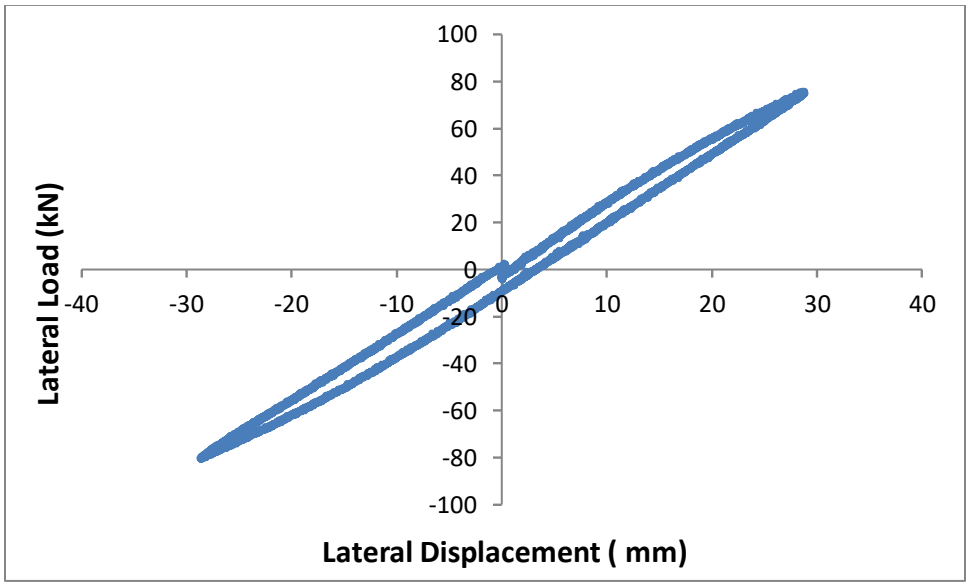

Figure B11-4 B260+B240+B220 SSA=25%t_r -A

1-Keff-H =2719.62N/mm 2-Keff-h =1359.81 N/mm

2-Loop Area = 418225.5 N-mm 4- ζ =2.98%

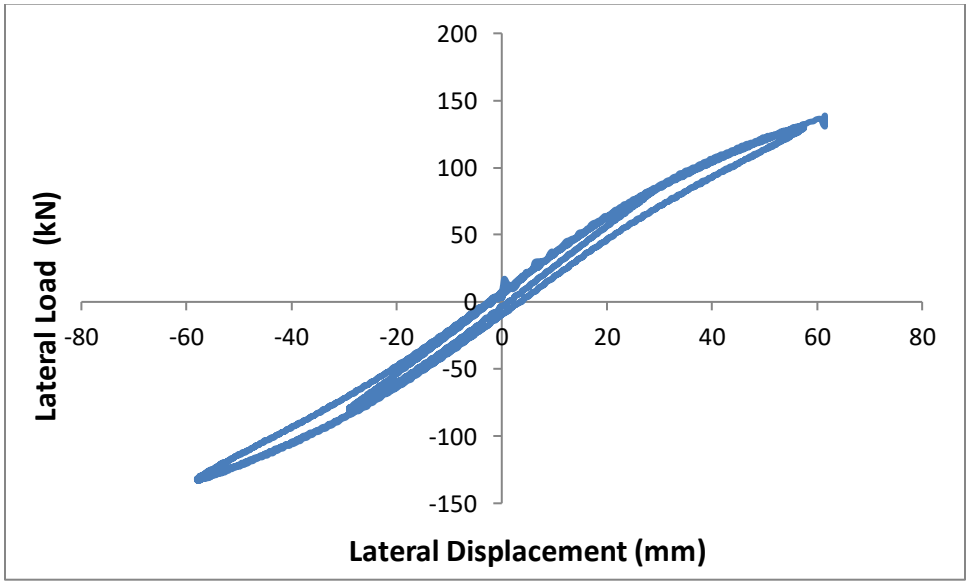

Figure B11-5 B260+B240+B220 F-D Hysteresis Diagram Ϭ=3.70 MPa SSA 25 - 50%t_r A PL =750 kN (Dynamic Load Profile)

B-12 Compound Isolator B220+B200+B180 PL = 750kN Bonding Level BL= 59.70%

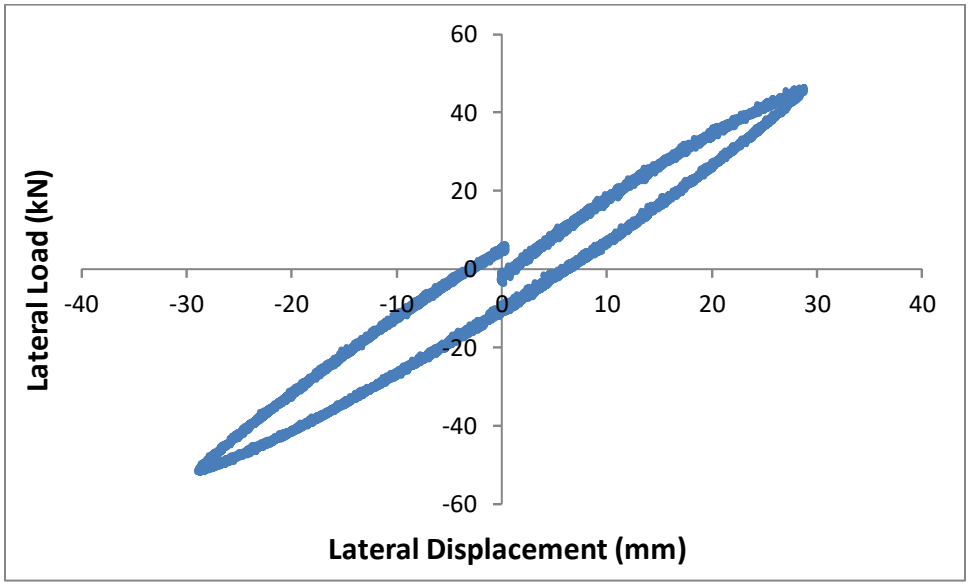

Figure B12-1 B220+B200+B180 SSA=25%t_r -A PL=750kN

1-Keff-H = 1702.41N/mm 2-Keff-h = 851.20 N/mm

2-Loop Area= 585114.7N-mm 3-ζ = 6.5%

K_{eff}-h and ζ_{eff} defined by sp1 data:

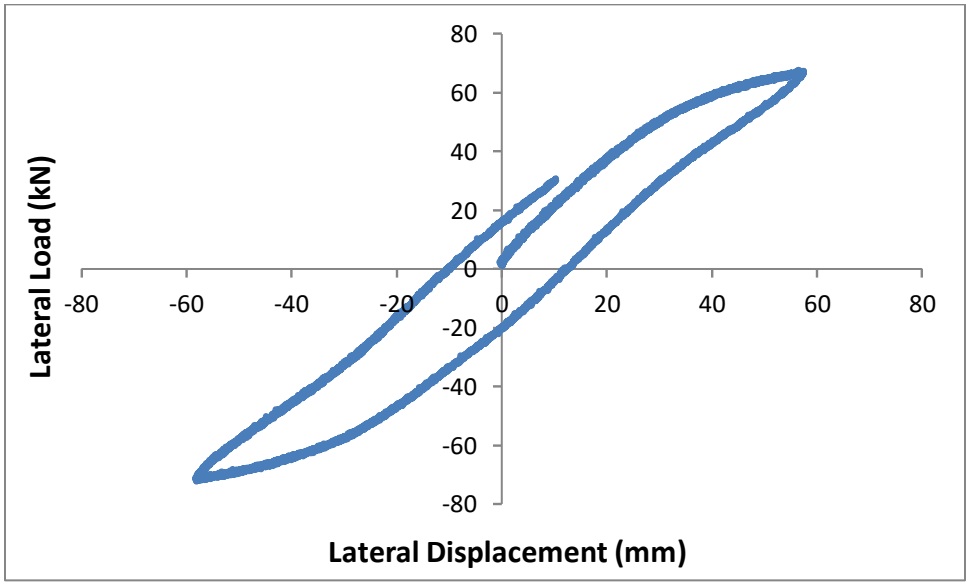

Figure B12-2 B220+B200+B180 SSA= 50%t_r A-SP1 PL =750kN

1-Keff-H($_{SP1)}$ =1198.2N/mm 2-Loop area=2585015N-mm

3-Keef-h= 599.10 N/mm 4-ζ_{SP1}=10.32%

3-Keff-H & ζ by sp2 data:

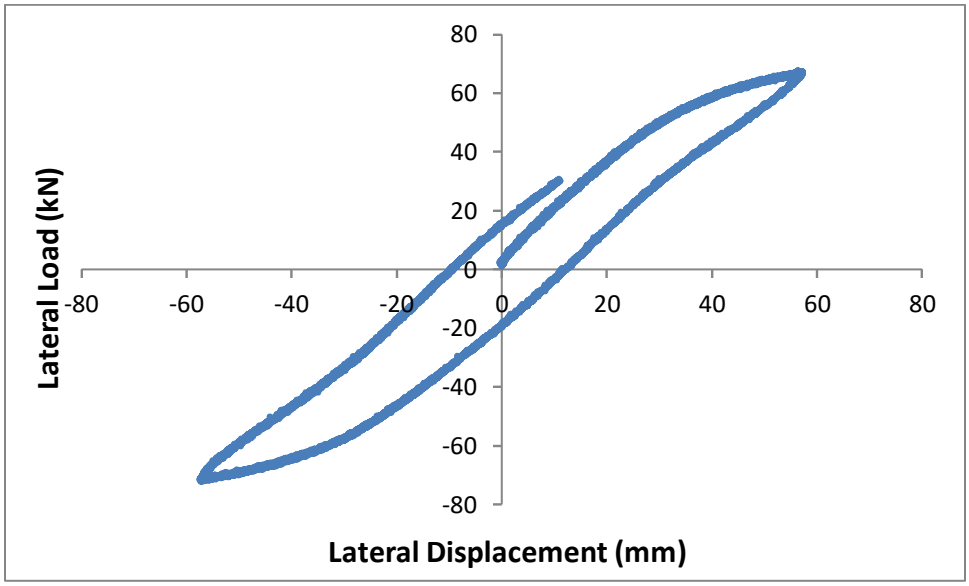

Figure 12-3 B220+B200+B180 SSA=50%t_r A-SP2 ϭ=6.21MPa

1-Keff-H=1203.4 N/mm 2-Loop area=2470158 N-mm

3-Keff-h= 601.7 N/mm 4-ζ_{SP2}= 9.93%

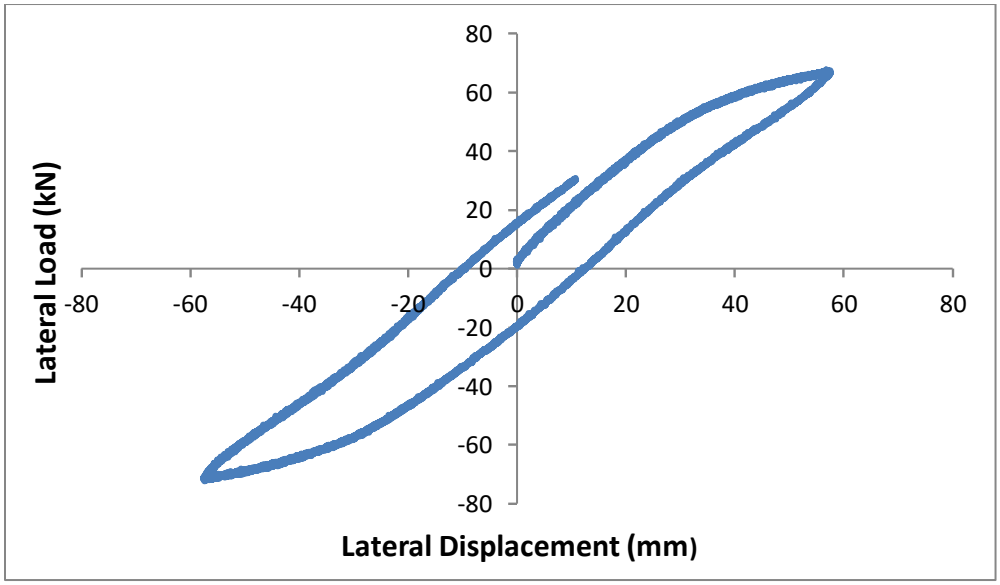

Figure B12-4 B220+B200+B180 SSA=50%t_r - A

1-Keff-H =1210.20 N/mm 2-Keff-h=605.10N/mm

3-Loop Area=2670615.0 N-mm 3-ζ =10.65%

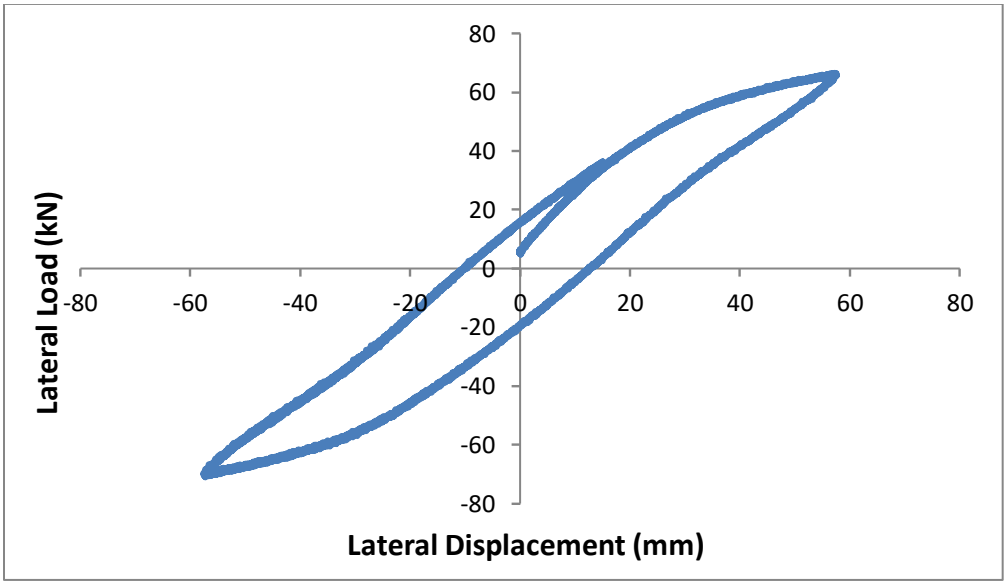

Figure B12-5 B220+B200+B180 SSA=50%t_r -B PL=750kN Ϭ=6.21 MPa

1-Keff-H= 1189.96N/mm 2-Kef-h=594.98 N/mm

3-Hysteresis loop area = 2949244.0 N-mm 4- ζ =12.08%

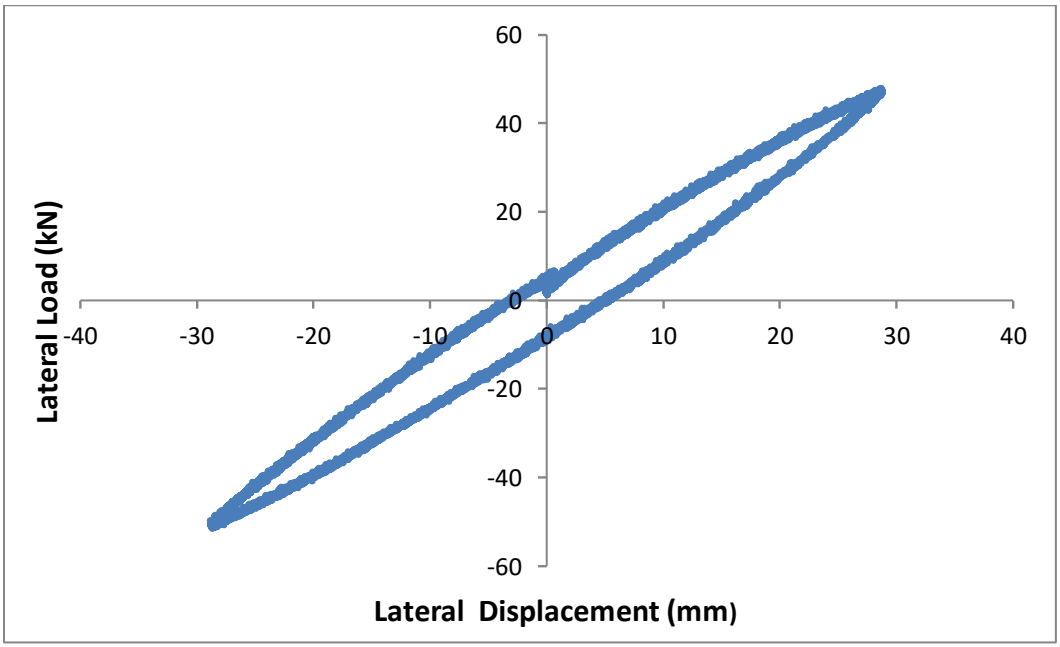

Figure B12-6 B220+B200+B180 SSA= 25%t_r B PL =750kN Ϭ=6.21MPa

1-Keff-H =1709.0 N/mm 2-Keff-h=854.50N/mm

3-Loop Area= 560843.0 N-mm 4- ζ = 6.30%

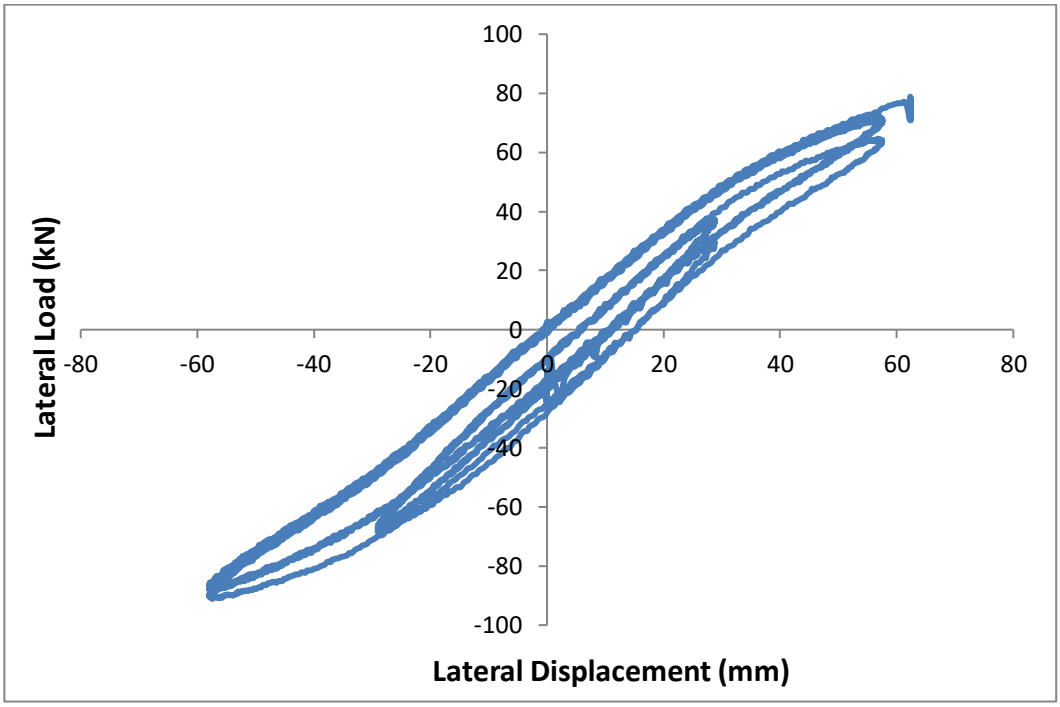

Figure B12-7 Load-Displacement Hysteresis Diagram of B220+B200+B180 Compound Isolator SSA=25-50%t_r (Dynamic Load Profile)

REMARKS:

1- In the table of computation results below, test numbers 1 & 2 are conducted on typical triple compound isolator with relatively high average bonding level (BL= 85.60%), and 3 & 4 on typical low average bonding level (BL= 59.57%).

2- Shear strain amplitude (SSA) is described in terms of $\%t_r$ and t_r is the isolator's total thickness of the rubber layers, which is 115 mm. For example SSA = $50\%t_r$ mean isolator lateral deformation is equal to (50/100) x115= 57.50mm

Compound Triple Isolator CSB-CFREI lateral effective stiffness & damping under PL =750kN constant pre-load.

(Table of computation results)

Compound Triple Isolator CSB-CFREI lateral effective stiffness & damping									
Test #	Test Name	Compound Triple Isolator	Bonding Level BL-%	Axial Load kN	Axial Stress MPa	Shear Strain Ampl. SSA $\%t_r$	Lateral stiff. N/mm Keff-H (2Keff-h)		Damping ζ %
							1^{st} cycle	2^{nd} cycle	2^{nd} cycle
1	Lateral	B260+B240+B220	85.60	750	4.32	25	2701.55	2515.30	3.67
2	lateral	B260+B240+B220	85.60	750	4.30	50	2148.50	2147.00	4.80
3	lateral	B220+B200+B180	59.57	750	6.21	25	1709.00	1674.64	6.30
4	lateral	B220+B200+B180	59.57	750	6.21	50	1212.70	1189.96	12.08